UNIVERSITÀ
DEGLI STUDI
DI PADOVA

Host institution: Università degli Studi di Padova

Dipartimento di Geoscienze

DOCTORAL COURSE IN EARTH SCIENCES
SERIES: XXXI

ANALYSIS OF WIND-WAVE INDUCED EROSIONIN THE VENICE LAGOON IN THE LAST FOUR CENTURIES: FIELD OBSERVATIONS AND MODELLING

Coordinator: Prof. Claudia Agnini
Supervisor: Prof. Andrea D'Alpaos
Co-Supervisor: Prof. Luca Carniello
Prof. Massimiliano Ghinassi

PhD candidate: Laura Tommasini

Università degli Studi di Padova
Department of Geosciences

Ph.D. School in Earth Sciences

Analysis of wind-wave induced erosion in the Venice Lagoon in the last four centuries: field observations and modelling

Ph.D. Candidate:
Laura Tommasini
Matricola 1124825

Thesis advisor:
Prof. Andrea D'Alpaos

Thesis co-advisors:
Prof. Luca Carniello
Prof. Massimiliano Ghinassi

September 2018

To my family
and Nicola

CONTENTS

LIST OF FIGURES

LIST OF TABLES

ABSTRACT

Tidal systems are subjected to a variety of internal and external drivers whose interplay and feedbacks affect the shape and the morphological evolution of typical tidal landforms such as channel networks, salt marshes and tidal flats. Several studies have been carried out describing the various processes that drive the evolution of tidal landforms (e.g., the hydrodynamic circulation, the consequences of tidal currents and wind waves on sediment dynamics, vertical and horizontal dynamics of salt marshes, sea level rise and human interferences). Understanding the positive feedbacks existing between salt-marsh erosion, tidal-flat widening and deepening and more energetic wave generation by means of observational evidence and numerical models is a critical step to predict the response of tidal landforms to future environmental changes. With this aim we first improved current our knowledge on the ancient configurations of the Venice lagoon through the bathymetric reconstruction of the oldest map, dating back to 1611, providing a realistic representation of its morphological features. This furthermore allowed us to gain new insights on the hydrodynamic changes occurred in the last four centuries. We then compared different existing model approaches, in order to unravel the implications of different assumptions and formulations used to model wave dynamics in shallow tidal basins. Subsequently, we analysed the effects of wave action on marsh boundaries and how the wave field has changed in the last four centuries with the aim of further emphasizing the feedbacks existing between the overall erosion of the Venice Lagoon and the increase in wave power density. Finally, we analysed the bottom shear stress distribution obtained for different configurations of the Venice Lagoon, in order to support the possibility of describing wind-wave induced bottom erosion as a marked Poisson process.

The main results from this work highlighted that: I) the most important mophodynamic changes in the Venice Lagoon have started in the last century and were mainly triggered by human interferences; II) the assumptions adopted in different modelling framework strongly influence the computation of the bottom shear stress induced by waves, in particular when very shallow water depths are considered; III) the salt-marsh erosion rate is linearly related to the mean wave power density; IV) the erosive trend of the Venice Lagoon during the last four centuries can be explained also by the increase in wave power density and by the analysis of bottom shear stress distribution; V) wind-wave induced erosion processes over tidal flats can be described as marked Poisson processes for all the past and current lagoon configurations, thus leading important consequences for the prediction of future scenarios and implications for the long-term morphodynamic modelling of tidal environments.

SOMMARIO

I sistemi mareali sono soggetti ad innumerevoli forzanti interne ed esterne, le cui interazioni e feedbacks influenzano l'evoluzione morfologica delle principali strutture morfologiche che caratterizzano gli ambienti a marea:i canali, le barene e i bassifondi. Sono stati svolti innumerevoli studi che descrivono i diversi processi che determinano l'evoluzione degli ambienti lagunari (e.g., l'idrodinamica dei canali a marea, le conseguenze delle correnti di marea e delle onde da vento sulla dinamica dei sedimenti, i meccanismi di evoluzione laterale e orizzontale delle barene, l'incremento del livello del medio mare, gli interventi antropici). Capire i meccanismi di feedback positivi esistenti tra l'erosione delle barene, l'allargamento e approfondimento dei bassifondi e la generazione di moto ondoso più energetico con l'aiuto di dati di campo e di modelli numerici risulta un passo fondamentale per prevedere la risposta delle strutture morfologiche degli ambienti a marea ai futuri cambiamenti ambientali. Al fine di raggiungere questo obiettivo, abbiamo, in primo luogo, ampliato la nostra conoscenza delle configurazioni storiche della Laguna di Venezia attraverso la ricostruzione batimetrica della più antica mappa, risalente al 1611, che forniva una rappresentazione realistica delle strutture morfologiche lagunari. Questo ha consentito di conseguenza di approfondire l'analisi dei cambiamenti idrodinamici che si sono verificati negli ultimi quattro secoli. Abbiamo in seguito confrontato diversi approcci adottati in modelli esistenti, al fine di investigare e comprendere le implicazioni delle diverse assunzioni e formulazioni utilizzate per modellare la dinamica delle onde da vento in bacini a marea poco profondi. Di seguito, abbiamo analizzato gli effetti dell'azione delle onde da vento sui bordi delle barene e il cambiamento del campo di moto ondoso negli ultimi quattro secoli, allo scopo di enfatizzare ulteriormente i feedbacks esistenti tra l'erosione generale della Laguna di Venezia e l'aumento della potenza delle onde. Infine, abbiamo analizzato gli sforzi di attrito al fondo ottenuti per diverse configurazioni della Laguna di Venezia, in modo da supportare la possibilità di descrivere l'erosione del fondo indotta da onde da vento come un processo di Poisson marcato.

I principali risultati di questo lavoro hanno evidenziato che: I) i più gravosi cambiamenti morfodinamici nella Laguna di Venezia sono iniziati nell'ultimo secolo e sono stati innescati principalmente dagli interventi antropici; II) le assunzioni adottate in diversi approcci modellistici fortemente influenzano il calcolo dello sforzo di attrito al fondo dovuto alle onde da vento, in particolare quando si considerano profondità molto ridotte; III) il tasso di erosione delle barene è linearmente correlato alla potenza generata dalle onde da vento; IV) la tendenza erosiva della Laguna di Venezia negli ultimi quattro secoli può essere spiegata dall'aumento della potenza media e dall'analisi della distribuzione dello sforzo di attrito al fondo; V) i processi erosivi

dovuti alle onde da vento in sistemi lagunari possono essere descritti come processi di Poisson marcato in tutte le configurazioni passate e per quella attuale, questo produce importanti conseguenze per quanto riguarda la previsione di scenari futuri e implicazioni per la modellazione morfodinamica a lungo termine degli ambienti a marea.

ACKNOWLEDGMENTS

Firstly and foremost, I would like to thank my advisors Prof. Andrea D'Alpaos, Prof. Luca Carniello and Prof. Massimiliano Ghinassi for the continuous support of my Ph.D study and related research, for their patience, understanding, motivation, and immense knowledge. Their guidance helped me in all the time of research and writing of this thesis.

Besides my advisor, I would like to express my sincere gratitude to my colleagues and co-author, particularly Dr.ssa Marcella Roner, Dr. Alvise Finotello and Dr.ssa Marta Cosma. Besides having assisted me during the writing of this thesis and providing meaningful suggestion for improve this manuscript, they have made this Ph.D. experience worthy, stimulating and above all funny day by day.

My sincere thanks also goes to Prof. Simon Mudd, who provided me the opportunity to join his team at the School of GeoSciences of the University of Edinburgh as visiting student.

Last but not the least, I would like to thank my family: Nicola, my parents, my brother, my aunt Chicca and my grandparents Rosina e Carino for supporting me spiritually throughout writing this thesis and during this three years in general.

Laura Tommasini

1 INTRODUCTION

1.1 OVERVIEW

This study deals with the analysis of wind-wave effects on the long-term evolution of tidal landscapes. Wind waves together with tidal currents, sea level rise, sediment supply and human interferences drive the morphological evolution of shallow tidal basins (e.g., Marani et al., 2007; Carr et al., 2010; Mudd, 2011; Marani et al., 2011; Coco et al., 2013; Mariotti and Carr, 2014; Leonardi et al., 2016b). Improving current understanding of the different interacting processes that act at overlapping spatial and temporal scales in tidal landscapes is a critical step to analyse and predict their response to future environmental changes. In this work, the latter issue is addressed by means of observational evidence and the results of morphodynamic models. In particular, two key mechanisms induced by wind waves were separately analysed: the retreat of salt-marsh boundaries and sediment erosion from the bottom of tidal flats. The Venice Lagoon was considered as a study case, thanks to the unique available dataset of field measurements, maps, satellite and aerial photographs, and bathymetries.

1.2 STATE OF THE ART

Tidal lagoons are transition zones between marine and terrestrial environments. They represent extraordinarily variable and complex environments governed by coupled physical and biological processes and exposed to the effects of climatic changes (e.g., increase in the rate of Relative Sea Level Rise) and to the impact of human activities (e.g., changes in sediment supply and engineering works).

Within shallow tidal environments, from a morphological point of view, one can distinguish four main sub-environments: tidal channel networks, tidal flats, subtidal platforms and salt marshes (Fig. 1.1). Channel networks are the preferential hydrodynamic pathways for tidal wave propagation and sediment fluxes. They cut through salt marshes, tidal flats and subtidal platforms and drain these landforms while increasing their water discharges and size towards the inlets. Tidal flats, with elevations between Minimum Low Water Level (MLWL) and Mean Sea Level (MSL), are characterized by the lack of halophytic vegetation, but can be populated by sea-grass meadows (e.g., Carr et al., 2010). Their elevation is usually such that they are not flooded only in case of exceptionally low tides. Subtidal platforms are located below MLWL and are therefore permanently submerged, they can also host sea-grass meadows (e.g., Carr et al., 2010; Carniello et al., 2014). Fi-

nally, salt marshes are the topographically highest portions of the tidal basin, with elevations between MSL and Mean High Water Level (MHWL). These vegetated platforms are populated by halophytic vegetation, and although they might appear as quite flat structures, they can be characterized by interesting biogeomorphic patterns with a gently sloping surface or a weakly concave-up topography as in the case of the Venice lagoon.

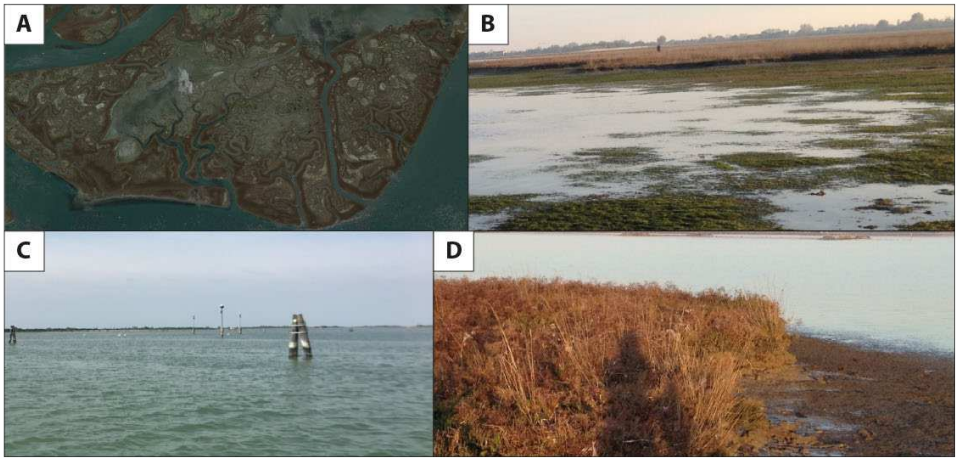

Figure 1.1: Examples of the typical sub-environments that characterize tidal landscapes: (A) channel networks dissecting a salt-marsh platform (©2018 Google); (B) tidal flat; (C) subtidal platform; (D) salt marsh, with a detailed view of its margin.

Several studies, developed especially in the last three decades, describe the various processes that contribute to shape tidal landforms, such as the hydrodynamics of tidal channels and creeks (e.g., Fagherazzi and Sun, 2004; Lawrence et al., 2004; D'Alpaos et al., 2005; Stefanon et al., 2012; Coco et al., 2013; Lanzoni and D'Alpaos, 2015), the effects of tidal currents and their asymmetries on sediment dynamics and other morphological characteristics of tidal channels (e.g., Schuttelaars and Swart, 2000; Lanzoni and Seminara, 2002; Molinaroli et al., 2007; Defendi et al., 2010; Tambroni et al., 2017; Tambroni et al., 2017), morphometric analyses of tidal networks (e.g., Leopold et al., 1993; Rinaldo et al., 1999b; Rinaldo et al., 1999a; Marani et al., 2002; Marani et al., 2003), sedimentation and accretion patterns in tidal systems (e.g., D'Alpaos et al., 2007; Marani et al., 2007; Kirwan et al., 2010; Carniello et al., 2016), the horizontal retreat associated with wave-induced marsh boundary erosion, (e.g., Mariotti and Fagherazzi, 2010; Marani et al., 2011; Mariotti and Carr, 2014; McLoughlin et al., 2015; Bendoni et al., 2016; Leonardi et al., 2016a), ecological dynamics and patterns in salt marshes (e.g., Marani et al., 2004; Pennings et al., 2005; Marani et al., 2013).

In particular, studies related to the survival and disappearance of coastal salt marshes are of relevant interest due to their vital importance from an eco-geomorphological and socio-economical point of view (e.g., Costanza et al., 1997; Zedler and Kercher, 2005; Kirwan and Megonigal, 2013; D'Alpaos and Marani, 2016). Among the several ecosystem services they provide, marshes

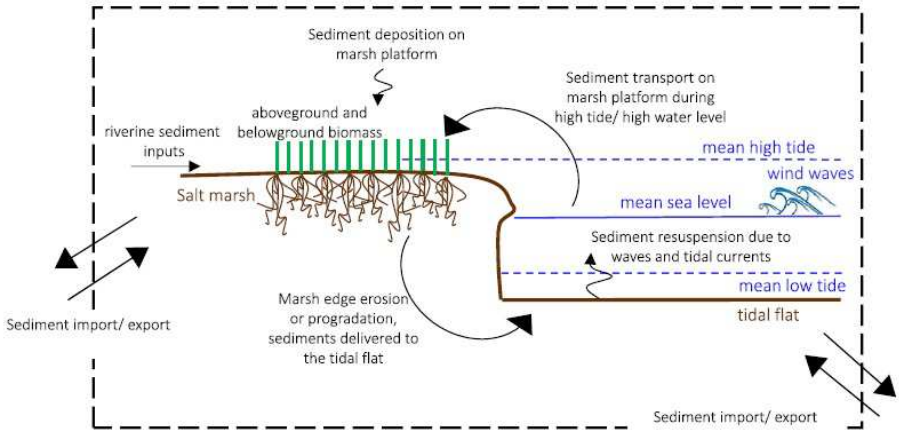

Figure 1.2: Sketch of the possible mechanisms and sediment fluxes driving salt-marsh vertical and horizontal dynamics within an hypothetical control volume (From Leonardi et al., 2018).

dissipate waves and mitigate erosion during storms (e.g., Möller et al., 1999; Howes et al., 2010; Möller et al., 2014), thus reducing the impact on coastal communities (e.g., Möller, 2006; Temmerman et al., 2013; Zhao and Chen, 2014); filter nutrients and pollutants from the water column (Costanza et al., 1997); furnish nursery areas for coastal biota (e.g., Perillo, 2009); and serve as an important organic carbon sink due to their great ability to sequester atmospheric carbon (e.g., Chmura et al., 2003; Barbier et al., 2011; Fourqurean et al., 2012; Kirwan and Mudd, 2012; Roner et al., 2016).

Salt-marsh growth, maintenance, retreat and drowning are governed by a variety of physical and biological processes as well portrayed in Fig. 1.2 (Leonardi et al., 2018). For instance one can list: the exchange of sediments between the tidal-flat and the marsh platforms, biomass production and sediment deposition on the marsh surface promoting vertical accretion, and the possible erosion or progradation of the marsh edge. Marshes may also drown as a consequence of a negative sediment budget when the sediment availability is reduced beyond the threshold required to keep pace with Relative Sea Level Rise (RSLR) (Marani et al., 2007; Kirwan et al., 2010). Tidal marshes can indeed evolve horizontally because of lateral erosional and progradation processes, and vertically, as a net result of organic and inorganic deposition, surface erosion, and RLSR (e.g., Kirwan et al., 2010; D'Alpaos et al., 2011; Marani et al., 2011; Mariotti and Fagherazzi, 2013a; Mariotti and Carr, 2014; Kirwan et al., 2016b; Kirwan et al., 2016a; Leonardi et al., 2016b; Leonardi et al., 2018). If one considers the vertical dynamics of salt marshes and tidal flats, the above recalled processes, often intertwined through non-linear relationships, drive the bifurcation of bottom elevations into two distinct clusters, one above MSL (representing salt-marsh surfaces) and the other below MSL (representing tidal-flat and subtidal platforms) (e.g., Fagherazzi et al., 2006; Defina et al., 2007; Marani et al., 2007; Wang and Temmerman, 2013).

In this context wind-wave attack is usually recognized as one of the main processes leading to marsh horizontal retreat in estuaries and lagoons worldwide (Gedan et al., 2011; Marani et al., 2011; Schwimmer, 2001; Mariotti and Carr, 2014; Leonardi et al., 2016a; Bendoni et al., 2016). This complex phenomenon includes both the continuous removal of small size particles and the sudden collapse of marsh blocks whose size is comparable with the marsh bank height (Bendoni et al., 2014). Salt-marsh lateral erosion is also controlled by the depth and extent of the tidal flats or subtidal platforms in front of the salt-marsh edges, that, together with wind climate, influence the generation and propagation of the impinging wind waves (Mariotti and Fagherazzi, 2013b). Sea level rise can further affect wind-wave climate by causing a more rapid erosion of the marsh boundaries due to the increase in water depth and consequently in the wave height (Mariotti et al., 2010). Tidal range plays also an important role in controlling wave erosion, because due to the increase in the tidal range, the intensity of wind-induced erosive processes over the subtidal platforms and against salt-marsh margins progressively decreases (e.g., Callaghan et al., 2010; D'Alpaos et al., 2012). Furthermore, ship wakes can also promote erosion in proximity of the channel banks (Zaggia et al., 2017).

The presence of vegetation in coastal salt marshes increases their overall resilience, promoting wave dampening and dissipation over the marsh surface (Möller, 2006; Möller et al., 2014) and facilitating sediment deposition (Le Hir et al., 2007). Moreover, vegetation represents an effective shoreline buffer, reducing rates of erosion by stabilizing the soil in the root zone (Gedan et al., 2011).

Average horizontal marsh erosion rates have been estimated, for different observation periods, in the order of 0.4-3.0 m/yr for the Westerschelde (Netherland) (Van der Wal et al., 2008), 0.5-2.0 m/yr in the Virginia Coastal Reserve (Virginia, USA) (McLoughlin et al., 2015), 0.17-7.30 m/yr in the Rehoboth Bay (Delaware, U.S.A) (Schwimmer, 2001), 0.25-2 m/yr in the Barnegat Bay-Little Egg Harbor system (New Jersey, USA) (Leonardi et al., 2016b) and 0.23-2.81 m/yr in the Charleston Sound (South Carolina, USA) (Mariotti and Fagherazzi, 2013a). In the Venice Lagoon (Italy), marsh retreat rates have been estimated around 1.2-2.2 m/yr for the period from 1993 to 1995 in the Southern part of the Lagoon (Day et al., 1998), up to 0.8 m/yr in the Northern Lagoon (Bendoni et al., 2016) and in the order of 0.08-3.3 m^2/yr considering several eroding marshes in the whole Lagoon (Marani et al., 2011).

Several models with different degrees of approximation, and focusing on different spatial and temporal scales, were developed in the last decade in order to describe, and account for, most of the above recalled processes (e.g., Fagherazzi et al., 2012). D'Alpaos et al. (2007) and Kirwan and Murray (2007) developed 3D modelling frameworks to describe tidal marsh accretion and channel network development that couple physical sediment transport processes with biologically-mediated ones. Mariotti and Fagherazzi (2010) presented a one-dimensional model including tidal currents, wind waves,

sediment erosion and deposition, together with vegetation effects to explore the evolution of the marsh boundary under different scenarios of sediment supply and sea level rise. Mariotti and Carr (2014) further developed a three-point dynamic model to predict marsh loss as a function of sea level rise, allochthonous sediment supply, wind regime, tidal range, and marsh bank and mudflat erodability. D'Alpaos et al. (2011) developed a parsimonious analytical model describing salt-marsh vertical evolution, to analyse the dynamic response of marshes to changes in the available sediment concentration, in plant productivity, and in the rate of the RLSR. A cellular automata model was developed by Leonardi and Fagherazzi (2014) to investigate the erosion of marsh boundaries due to wave action, demonstrating that high wave energy conditions promote the uniform erosion of the marsh edge, whereas, if wind waves are weak and the local marsh resistance is strong, jagged marsh boundaries tend to form. D'Alpaos et al. (2013) and Carniello et al. (2016) used the results of a coupled two-dimensional wind-wave tidal model (Carniello et al., 2011) to develop a statistical framework emphasizing that wind-wave induced resuspension events can be modelled as a marked Poisson process, bearing important consequences for the analysis of the long-term morphodynamic evolution of tidal landscapes.

1.2.1 The Venice Lagoon

The Venice Lagoon represents an example of a shallow tidal basin where all the above recalled processes contributing to shape tidal landscapes coexist together with the effects of severe human actions.

The Venice Lagoon, located along the north-western coast of the Adriatic Sea (Italy), forms an elongated water body oriented NE–SW, with a length of about 50 km and width of 10 km, and represents the largest tidal basin in the Mediterranean Sea, with an area of about 550 km^2. The Venice Lagoon is located in the coastal sector of the Venetian Plain, a foreland basin that developed between the Apennine and South-Alpine chains since the late Oligocene (Massari et al., 2004). It is a shallow micro-tidal basin, characterized by a mean water depth of about 1.5 m, excluding the main channels, and a semi-diurnal tidal regime with an average tidal range of about 1.0 m. The Lagoon is connected to the Adriatic Sea through three inlets: Lido, Malamocco and Chioggia (Fig. 1.3).

Since the beginning of the 15th century, the Venice Lagoon has been subjected to severe anthropogenic modifications (Sarretta et al., 2010; D'Alpaos, 2010a; D'Alpaos, 2010b), among which we can list:

- The diversion of the main rivers debouching into the Lagoon (Brenta and Piave rivers), between the 15th and 19th century;

- The construction of the jetties at the inlets, for navigations purposes, between 1808 and 1930;

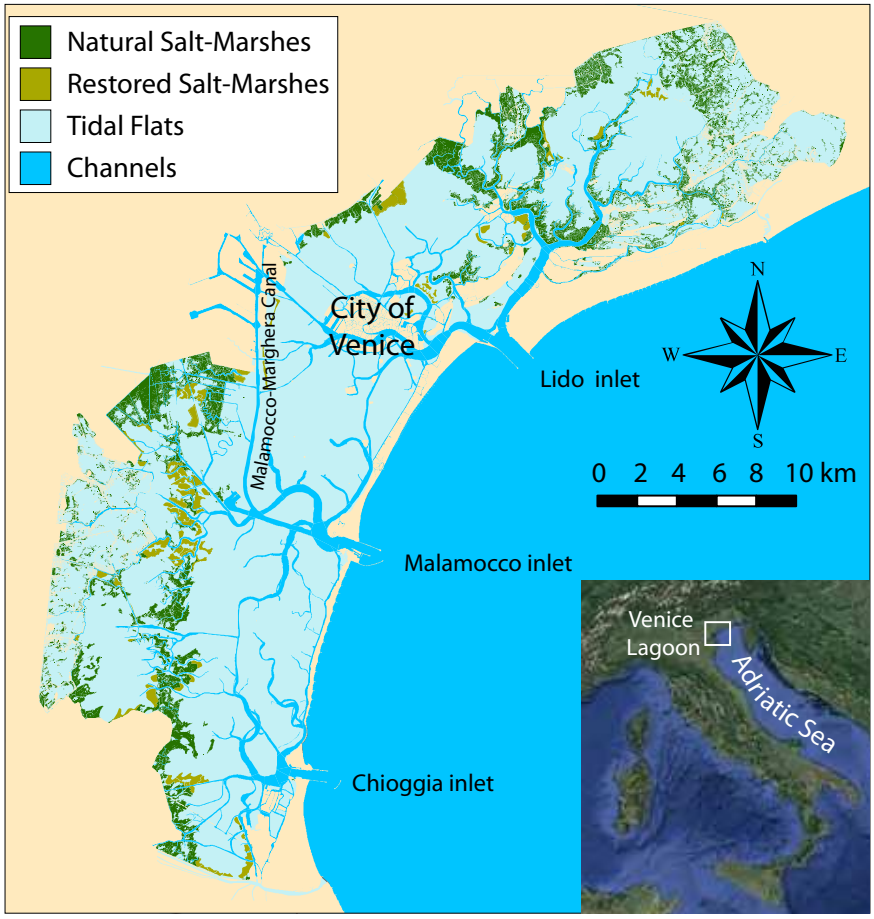

Figure 1.3: Schematic representation of the Venice Lagoon with the spatial distribution of the main morphological features.

- Land reclamations in different periods from 1917 to 1962, in the central and Southern part of the Lagoon between the Chioggia and Malamocco inlets;
- The construction of the fish farming areas separated from the rest of the Venice Lagoon in 1928;
- The excavation of Malamocco-Marghera ship canal, from 1966 to 1969;
- The construction of artificial salt marshes, started in the '90s.

1.2.2 Historical configurations of the Venice Lagoon

Thanks to the great historical relevance of Venice and its lagoon, several historical maps of the Venice lagoon exist (starting from the XVII century, here as an example we report a recent representation of the 1611 configuration – Fig. 1.4). In this context, it is worth recalling some of them, so that the reader can have a preview of the main morphological features character-

izing ancient and recent configurations of the lagoon, that will be described in details within this thesis. The first map of the lagoon reporting bottom elevation data dates back to 1809–1811 (*Augusto Dénaix*, 1810) (Fig. 1.5). Since then, several increasingly accurate and detailed bathymetric surveys have been performed and included in many available maps among which we recall: the 1901 map developed by the Genio Civile (Fig. 1.6); the 1932 map provided by the Ufficio Idrografico (Fig. 1.7); the 1970 map (Fig. 1.8) and the most recent (2012) available map of the lagoon, which integrates the 2003 bottom survey carried out by the Venice Water Authority (Magistrato alle Acque di Venezia) (Fig. 1.9) with the most recent morphological modifications.

Figure 1.4: Representation of the 1611 configuration.

.

Figure 1.5: Representation of the 1810 configuration (from D'Alpaos, 2010b).

As mentioned above, several historical cartographic maps exist older than the Dénaix (1810) map. However, those historical maps only provide planimetric information on ancient morphological configurations of the Venice lagoon. The representation of the lagoon drawn by Cristoforo Sabbadino in

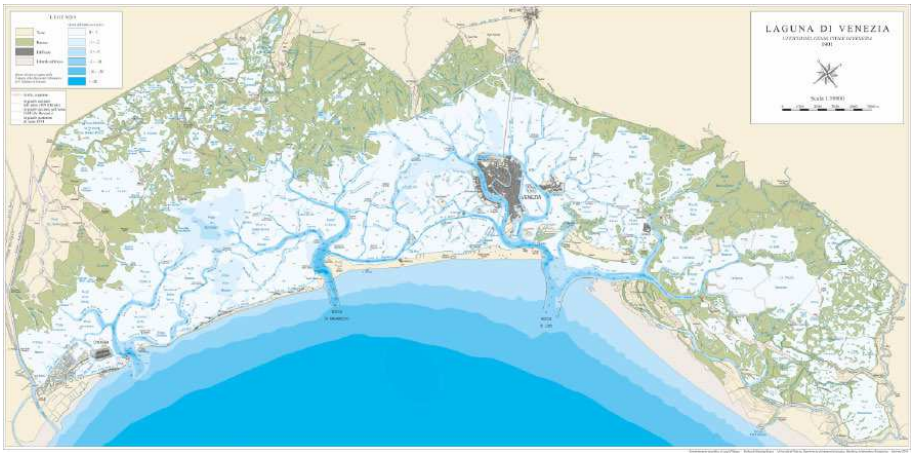

Figure 1.6: Representation of the 1901 configuration (from D'Alpaos, 2010b).

Figure 1.7: Representation of the 1932 configuration (from D'Alpaos, 2010b).

Figure 1.8: Representation of the 1970 configuration (from D'Alpaos, 2010b).

1558 can be considered the most ancient available map that, however, does not reasonably respect the planimetric proportions of the lagoon, thus pre-

Figure 1.9: Representation of the 2003 configuration (from D'Alpaos, 2010b).

venting any reliable georeferentiation. The oldest map providing a realistic representation of the morphological features of the lagoon dates back to the 1611 (*Sebastiano Alberti* 1611) (Fig. 1.4) and was made to officially define the administrative boundaries of the Lagoon.

1.3 GOALS OF THE STUDY

Towards the goal of analysing the effects of the governing processes that control the complex coupled dynamics of salt-marsh and tidal-flat evolution, the present work aims at investigating wind-wave induced erosion processes in the Venice Lagoon during the last four centuries.

We first aim at improving the knowledge of the ancient configurations of the Venice lagoon throughout the bathymetric reconstruction of the Sebastiano Alberti's map (1611). Succesively, we compared different existing model approaches, in order to understand the implications of different assumptions and formulations used to model wave dynamics in shallow tidal basins. Through new simulations with different wave models, we aimed at understanding what simplifications one might use to describe wind-wave propagation and wave-induced bottom shear stress. Subsequently, we focused our analysis on the erosive trend of the Venice Lagoon in the last four centuries, as an important step to provide predictions on possible future scenarios. We analysed the effects of wave action on marsh boundaries and how the wave field has changed through time with the aim of understanding the feedbacks existing between the overall erosion of the Venice Lagoon and the increase in wave power density. Finally, focusing on the bottom shear stresses obtained for different configurations of the Venice Lagoon, we further supported the possibility of describing wind-wave induced bottom erosion as a marked Poisson process, previous studies (D'Alpaos et al., 2013; Carniello et al., 2016) being indeed limited to the analysis of the present configuration of the lagoon.

1.4 THESIS OUTLINE

The present work is organized into five chapters (the first chapter being this very Introduction), whose content is briefly summarised below.

- **Chapter 2**: This chapter describes the construction of a new bathymetric configuration of the Venice Lagoon (the 1611 configuration), in order to increase the number of available configurations to be used in modelling analyses. Among the several existing historical cartographic maps older than the Dénaix 1810 map, the 1611 map by Sebastiano Alberti was selected, being the oldest map capable of providing a realistic representation of the morphological features of the Venice lagoon. This map was drawn to officially define the administrative boundaries of the Venice Lagoon. Starting from the 1611 planar configuration, the 1611 bathymetry was reconstructed by using classical geomorphic relationships. Then, the hydrodynamic behaviour of the Lagoon for the reconstructed morphological configuration was analysed by using a mathematical model (D'Alpaos and Defina, 2007; Carniello et al., 2011). In this chapter the hydrodynamic behavior of the 1611 lagoon is compared with the hydrodynamics of two more recent configurations: i.e., the Dénaix (1810) and the present (2012) configuration revealing interesting differences. This chapter is organized as a journal paper to be submitted to *Geomorphology*.

- **Chapter 3**: The main focus of this chapter is to carry out a detailed scrutiny of different wind-wave models, focusing, in particular, on the different formulations and assumptions adopted for the computation of wave heights and bottom shear stresses. Indeed, when dealing with mathematical models describing wind-wave processes in shallow tidal basins, one might wonder what models can be safely used and what assumptions are permissible compared to fatally flawed ones. This was deemed to be a critical step to address the effects of wind-wave induced erosion processes in shallow tidal basins. We have therefore used different numerical models in order to better highlight their capability to describe wind-wave characteristics (related to wind velocity, water depth and fetch) and their effects on bottom shear stress (BSS), bottom erosion, and on the morphodynamic evolution of salt-marsh and tidal-flat platforms. This chapter is organized as a journal paper to be submitted to *Water Resources Research*.

- **Chapter 4**: This chapter deals with the analysis of the spatial distribution of wave characterisitcs, and in particular of the wave power density, during the last four centuries in the Venice Lagoon (Italy). Recently, Marani et al. (2011) have shown the existence of a linear relationship between incident wave-power density and lateral marsh volumetric erosion rate, on the basis of dimensional analysis and of field observations and simplified wave modelling for the Venice Lagoon. Some authors have then used such a relationship within different modelling

frameworks (Mariotti and Fagherazzi, 2013a; Mariotti and Carr, 2014) while others have further supported its validity by considering different lagoonal systems (e.g., Leonardi et al., 2016b). In this work, building upon analyses from the study case of the Venice Lagoon (Italy), through the application of a fully fledged two-dimensional wind-wave tidal model, we have further tested the validity of the linear relationship between wave power and lateral volumetric erosion rate. In addition, we have also analysed the temporal evolution of wind-wave fields within the lagoon and how their changes have affected the erosional dynamics and the possible evolution of the Lagoon. The results are organized as a journal paper in review on *Earth Surface Processes and Landforms*.

- **Chapter 5**: In this chapter we analysed the temporal evolution (from 1611 to nowadays) of local bottom shear stresses induced by wind waves, and we have also further tested the possibility of describing wind-wave erosion events as marked Poisson processes (D'Alpaos et al., 2013; Carniello et al., 2016). This goal was pursued by applying a fully coupled finite element model accounting for the role of wind waves and tidal currents on the hydrodynamic circulation within the Venice Lagoon from 1611 to 2012 in order to analyse the characteristics of combined current- and wave-induced exceedances in bottom shear stresses over a given threshold for erosion. This chapter is organised as a journal paper to be submitted to *Advances in Water Resources*.

- **Chapter 6** summarizes the main results of this thesis.

Appendix A includes a paper in preparation to which I contributed as co-author. In this work we analysed, by means of field observations and mathematical modelling, the role of soil characteristics on the lateral erosion of salt-marsh margins driven by wind-wave effects.

2 THE VENICE LAGOON CONFIGURATION OF 1611

This chapter is a manuscript that will be submitted to *Geomorphology*. Thanks to the great historical relevance of Venice and its Lagoon, several historical maps and depictions of the lagoon are available. These maps provide information on the different planar configurations of the Venice Lagoon through the centuries. However, when dealing with long-term tidal landscape evolution, particularly through the use of morphodynamic models, bathymetric data are also required to set up computational grids and run numerical simulations. In this study we have used the oldest map of the Venice Lagoon, suitable to provide a realistic representation of the planimetric configuration of its main morphological features, to build the corresponding bathymetry. This map dates back to 1611 and was originally drawn by Sebastiano Alberti to officially define the administrative boundaries of the Lagoon. A classical geomorphic relationship (the width-to-depth ratio) for tidal channels and conceptual models of tidal-flat and salt-marsh coevolution were used to set up the bathymetry, that was then tested by considering another relationship of geomorphic relevance, (i.e. the O'Brien-Jarrett-Marchi law) relating channel cross-sectional area to the flowing tidal prism. The hydrodynamic behaviour of the newly reconstructed configuration was then analysed by using a numerical hydrodynamic model and comparisons were carried out with two more recent configurations (i.e. the Dénaix - 1810 and the present - 2012 configurations), revealing interesting differences.

PAPER

MODELLING THE HYDRODYNAMIC FIELD OF THE VENICE LAGOON IN THE LAST FOUR CENTURIES

Laura Tommasini[1], Andrea D'Alpaos[1], Luca Carniello[2], Luigi D'Alpaos[2] and Andrea Rinaldo[2,3]

[1]Dept. of Geosciences, University of Padova, via G.Gradenigo 6, Padova, Italy

[2]Dept. ICEA, University of Padova, via Loredan 20, Padova, Italy

[3]Laboratory of Ecohydrology ECHO/IEE/ENAC, Ecole Polytechnique Federale Lausanne, 1015 Lausanne (CH)

Abstract

Tidal landforms evolve in response to a variety of natural (tides, waves, sediment supply, sea level rise) and anthropogenic forcing. The Venice Lagoon is a unique example of a tidal system whose evolution has been driven by the intertwined effects of biogeomorphic processes and severe human interventions, that started after the XVI century to prevent the shoaling of the lagoonal bottom and extend the use of navigation channels. These interventions caused significant changes in the amount of freshwater and sediment input into the lagoon, triggering a general degradation trend consisting in both the deepening of the tidal flats and the reduction of salt-marsh areas. Improving current knowledge of the ancient configurations of the Venice lagoon is therefore a critical step to understand the key processes driving hydrodynamic and morphodynamic changes. Towards this goal, we developed and tested a procedure to reconstruct the bathymetric features of the Venice Lagoon starting from planimetric information (the 1611 Alberti's map of the Lagoon) through the use of classical geomorphic relationships for tidal channels and conceptual models of tidal-flat and salt-marsh coevolution. The reconstruction of the XVII century bathymetric configuration allowed us to compare its hydrodynamic and wind-induced wave fields with those characterizing other, more recent Lagoon configurations (namely the 1811 and the 2012 configurations). Our analyses highlight important changes in the hydrodynamics and wave dynamics of the Venice Lagoon through the last four centuries, emphasizing the less dissipative and more erosional character of the current configuration. We deem that the proposed procedure for the reconstruction of ancient bathymetries is a useful tool for the analysis of the morphological evolution of tidal systems.

2.1 INTRODUCTION

Tidal landscapes are complex environments exposed to the effects of climatic changes (e.g., increasing rates of Relative Sea Level Rise - RSLR) and human pressure (e.g., reduction in sediment supply, coastal engineering management, etc). Improving our understanding of the temporal evolution of these systems is a critical step to address related issues of conservation. The analysis of landscape changes through centuries requires data on the planimetric configuration and bathymetry of these systems to be available.

On the basis of the spatial and temporal scales addressed in landscape-evolution studies, different types of data can be required. If one considers relatively recent landscape evolution (going back to a few decades), aerial photographs, satellite images, and digital elevation

models are available (Lambeck et al., 2011; Vende et al., 2017; Da Lio et al., 2018), while ancient landscape evolutions (going back to several centuries ago) can be studied through the soil archive or using geophysical methods (Madricardo et al., 2007; Bates and Bates, 2016).

For mid-term analyses (say from about 1500 to present) we dispose of a valuable and scarcely used (e.g., Madricardo and Donnici, 2014; Jongepier et al., 2016) alternative: the use of historical maps, especially those older than 1800, as sources to reconstruct both the bathymetric and planimetric changes of tidal landscape in the past (Jongepier et al., 2016).

Here we consider the study case of the Venice Lagoon, a large microtidal expansion whose unstable balance in production and degradation of fluvial and marine sediment has been significantly affected by anthropic interventions throughout the last few centuries (Carniello et al., 2009; D'Alpaos, 2010a; D'Alpaos, 2010b; Sarretta et al., 2010). The morphological and bathymetric reconstruction of historical configurations of the Venice Lagoon is a major research topic for the implications on the evolution of the hydrodynamic behaviour of the lagoon itself across different historical periods. This in turn bears noteworthy environmental, social, and economic implications on the design of current interventions properly rooted in the evolutionary history of tidal morphologies (D'Alpaos, 2010a).

Reconstructions of this kind are also important towards the establishment of a sound formulation of mathematical models aimed at predicting the long-term morphological evolution of lagoon environments and for our understanding of the incidence of man-made interventions within a constantly evolving domain – the lagoonal environment, *per se* is a major provider of ecosystem services (e.g., Costanza et al., 1997; Chmura et al., 2003; Möller, 2006; Perillo, 2009; Barbier et al., 2011; Fourqurean et al., 2012; Kirwan and Mudd, 2012; Roner et al., 2016).

The bathymetric surveys of the Venice Lagoon are numerous, owing to the perceived importance of the lagoonal morphologies related to, say, the need to maintain navigability for the evolving ships throughout the centuries and because of military issues. In fact, there exist several bathymetries of the XX and XXI century (1901, 1932, 1970, 2012), while the oldest available today dates back to 1810. This is the first hydrographic map laid down by modern topographic criteria based on the survey carried out by Captain Augusto Dénaix between 1809 and 1811. In this map are well-recognizable from the planimetric point of view salt marshes, tidal flats and channels, and detailed depth data of the main channel networks are reported therein. It should be noted that the Dénaix map had been drafted for navigation purposes and thus no elevation data for salt marshes, tidal flats and in general unchanneled portions of the tidal landscape were available.

Here, we aim at extending the time span of bathymetries available by reconstructing the Venice Lagoon as it appeared in the XVII century. The raw material is the historical map of Sebastiano Alberti (1611) (Fig. 2.1). No altimetric information is available in this historic map. However, the main planar morphological structures of the lagoon are well identifiable: large and small tidal channels with their meandering structure and complex network arrangements; tidal flats, subtidal platforms and other unchanneled landforms such as large salt pans. To that end, for the bathymetric reconstruction of the channel network and its reliability test, we have employed relevant morphometric relationships such as: i) the relationship between channel width and channel depth across scales, observed for the channels of Venice Lagoon in its present configuration (Marani et al., 2002) and for the channels that are spreading from the different inlets of the Dutch Wadden Sea (Marciano et al., 2005); ii) the O'Brien-Jarrett-Marchi's (OBJM) law (D'Alpaos et al., 2009), an empirical and theoretical model (O'Brien, 1969; Jarrett, 1976; Marchi, 1990) providing the link between the cross-sectional area of any tidal channel and the tidal prism that shapes it. The 'law', initially proposed for the tidal inlets open seaward of any lagoons, was subsequently extended to any channel cross section cutting through the tidal landscape (Friedrichs, 1995; Rinaldo et al., 1999a; D'Alpaos et al., 2010).

The paper is organized as follows. In Section 2.2 we provide a brief description of the Venice Lagoon and of all the available cartographic and bathymetric data that were used in our analysis. In the same section we briefly recall the numerical model adopted to describe the lagoon hydrodynamics in all of the considered Venice Lagoon configurations, and the morphometric relationships (width-to-depth ratios and tidal prism-channel area relationship - OBJM) used to reconstruct and to test the XVII century lagoon bathymetric features. More in details, in Section 2.3 we discuss the validity of the width-to-depth relationship and of the OBJM law for the 1810 lagoon configuration. Section 2.4 describes in details the procedure adopted to reconstruct the Alberti's lagoon configuration and the bathymetric information used to implement a two-dimensional computational grid based on the suitably geo-referenced Alberti's map. In the same section we describe the hydrodynamic behaviour of the XVII century lagoon determined on the basis of the results of a two-dimensional hydrodynamic model and compare such results with those of the lagoon in later periods, for which similar types of mathematical modelling were already available (Carniello et al., 2009; D'Alpaos, 2010a). A discussion on the implications of the present work on the evolution of the lagoon hydrodynamics, facing the impacts and scopes across layers of anthropic interventions, and echoing a paradigmatic example of the dilemmas facing the Anthropocene, closes then the paper.

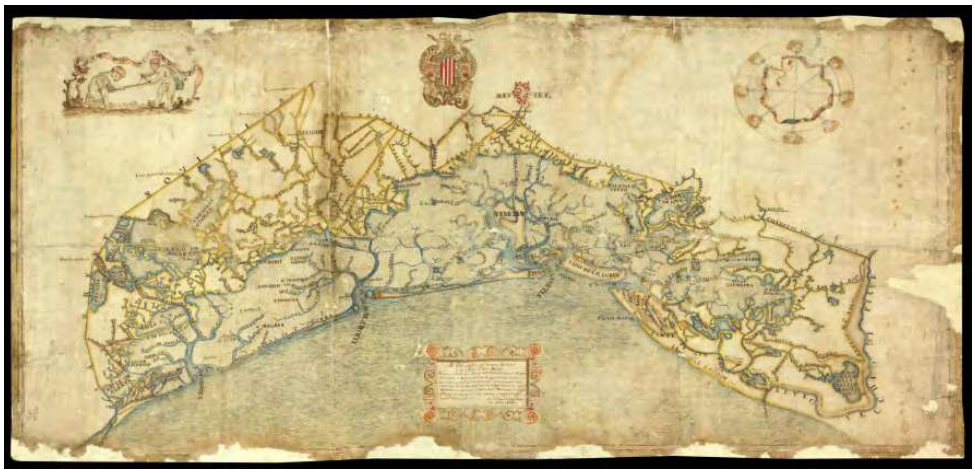

Figure 2.1: Historical map of the Venice lagoon drawn by Sebastiano Alberti in 1611 (Correr Museum, Venice).

2.2 MATERIALS AND METHODS

The Venice lagoon, located along the north-western sector of the Adriatic Sea (Italy), is the largest tidal basin in the Mediterranean, with an area of about 550 km^2. The Venice lagoon is a shallow microtidal basin, characterized by a mean water depth of about 1.5 m, excluding the main channels, and a semidiurnal tidal regime with an average tidal range of about 1.0 m, and maximum astronomical excursions at the inlets of about 0.75 m around Mean Sea Level (MSL). The Lagoon is separated from the Adriatic sea by two barrier islands, and is connected to the sea through three inlets (Lido, Malamocco and Chioggia).

Tidal channel networks, salt marshes, tidal flats, and subtidal platforms are the main ecogeomorphic features that characterize the Lagoon. Branching and meandering tidal channel networks depart from the inlets and cut through the lagoonal basin transporting flood and ebb discharges, sediments and nutrients within the lagoon. Salt marshes, relatively more elevated areas of the tidal basin (with elevations between MSL and Maximum High Water Levels MHWM), are generally the by product of a complex erosional and depositional history. They are regularly flooded by the tide and colonized by halophytic vegetation, and define the transition between permanently emerged and submerged environments. Tidal flats are characterized by lower elevations (between Minimum Low Water Level and MSL), they are not colonized by halophytic plants, and generally lie between salt marshes and the deeper portions of the tidal basin. Subtidal platforms represent the lower unchanneled portion of the tidal landscape (with elevations lower than MLWL) and can host seagrass meadows.

The Venice Lagoon has experienced important morphological transformations as a consequence of human interventions started in the XV century. The first relevant interventions were carried out between the XV and XVII centuries, when the Serenissima Republic of Venice diverted the main rivers (Brenta, Sile and Piave) to the Adriatic Sea with the aim of preventing the Lagoon from silting up with sediments. After these interventions, sediment input to the Venice Lagoon from the watershed almost vanished, thus triggering the progressive erosion of lagoonal morphologies. In the last century, the erosion processes become much more intense due to the construction of the jetties at the inlets and to the excavation of the large navigation channels, such as the Malamocco-Marghera ship canal. In addition, the jetties almost completely prevented any sediment supply from the Adriatic sea (Umgiesser et al., 2006; Defendi et al., 2010).

2.2.1 The Venice lagoon: historical and current configurations

The Sebastiano Alberti map (1611)

Owing to the great historical relevance of Venice and its Lagoon several historical maps and depictions of the lagoon exist. Among these, the map drawn by Sebastiano Alberti in 1611 is the first map in which the planimetric proportions of the lagoon are quite faithfully reproduced and the different morphological features characterizing the lagoon are clearly identified thanks to the accuracy of the depiction (Fig. 2.1): Salt marshes (in yellow in Fig. 2.1), tidal flats (in light blue in Fig. 2.1) and the channel network (in blue in Fig. 2.1) can easily be detected on the map. It should be however noted that the Alberti's map does not provide any altimetric information on the above recalled typical morphological features.

The 1611 Lagoon configuration, unlike the present one, was connected to the Adriatic Sea through five inlets: Chioggia, Malamocco, Venezia (i.e., S. Nicolò), S. Erasmo and Tre Porti. After the construction of the jetties in 1845 the last three inlets were joined together to form the present Lido inlet.

The good quality of the map in reproducing also artificial and stable morphologies (e.g., historical buildings and islands), that can be clearly identified also in the current configuration of the lagoon, allowed us to georeference the 1611 map and set the basis for the reconstruction of XVII century configuration. This was the first step towards the implementation of the computational grid necessary to perform the numerical simulations aimed at reproducing the hydrodynamic behaviour of this ancient lagoon configuration. The reconstruction of the 1611 bathymetry, starting from the georeferenced Al-

berti map and the implementation of the grid, are described in details in Sec. 2.4.

Venice Lagoon bathymetries of 1810 and 2012

Besides the reconstructed 1611 configuration, in the present study we consider other two, more recent, configurations of the lagoon: the 1810 and the present (2012) lagoon configurations, whose computational grids were set up in a previous study (D'Alpaos and Martini, 2005; Carniello et al., 2009). The 1810 configuration derives from the map by the Captain Augusto Dénaix. This is the first historical map providing bathymetric data however available only for the main channels. The map was, in fact, produced for navigation purposes. The bathymetry of the tidal flats was reconstructed (Carniello et al., 2009; D'Alpaos, 2010a) to account for the effects of subsidence and eustatism. The present (2012) configuration of the lagoon was obtained (Carniello et al., 2009) considering the most recent bathymetric survey carried out by the Venice Water Authority using different techniques (multibeam, single beam, GPS, orthophoto restitution, direct topographic survey) in order to obtain accurate results for each range of elevations. The bathymetric survey was actually performed in the period 2000-2003 and then updated in the following years by integrating new surveys for the portions of the lagoon that experienced major modifications. We therefore named 2012 the current configuration of the lagoon as it was updated including the recent modifications introduced at the three inlets by the construction (almost completed in 2012) of the movable gates for protecting Venice by the high tides (Mo.S.E Project). The effect of RSLR is implicitly considered because we referred all the bathymetries to the mean Adriatic Sea level contemporary to each map or survey.

2.2.2 Morphometric relationships

In the procedure (described in detail in Sec. 2.4) we adopted for reconstructing and testing the bathymetry of the 1611 configuration of the Venice lagoon starting form the Sebastiano Alberti map, we used two morphometric relationships derived for characterizing the morphology of tidal environments. These relationships are the width-to-depth ratio derived for the channel cross sections and the OBJM law.

Relationship between channel width and channel depth

The width-to-depth ratio, β, is one of the simplest measures of channels morphology (Allen, 2000; Marani et al., 2002; Solari et al., 2002). Although this ratio is a key factor for characterizing the three-

dimensional morphology of a tidal channel (D'Alpaos et al., 2005), a process-based relationship for predicting β as a function of environmental conditions (such as tidal forcing, sediment features and geometry of the watershed served by a tidal channel) is still missing. Field observations carried out within the Venice lagoon (Marani et al., 2002) indicate that the width-to-depth ratio of salt-marsh channels is usually much smaller than that of tidal-flat channels, owning to the presence of vegetation, cohesive sediments and particular hydrodynamic conditions. This relationship is largely controlled by channel width as suggested by field observations (Garofalo, 1980; Leopold et al., 1993; Gabet, 1998; Marani et al., 2002) and by the results of a recent modelling study (Lanzoni and D'Alpaos, 2015), which describes the morphodynamic evolution and the morphological characteristics of tidal channels. Smaller channels in salt marshes are characterized by more incised cross sections and by nearly constant width-to-depth ratios, whereas larger channels over tidal flats display larger width-to-depth ratios that increase with channel width. Interestingly, the relationship between channel width and channel depth might allow one to determine β values, and therefore channel depths, as soon as channel width is known, e.g., by aerial, satellite images or by historical maps as in the case at hand.

The O'Brien-Jarrett-Marchi law

Another relationship of geomorphic relevance is the relationship between the tidal prism flowing through a given cross section and the cross-sectional area. Long-term tidal morphologies are largely controlled by the net exchange of sediments between the enclosed tidal basin and the adjacent sea. The evaluation of such exchanges has traditionally been carried out by focusing on control sections, typically tidal inlets, where cross-sectional forms adjust to prevailing hydrodynamic and sediment transport conditions.

Eq. 2.1 shows the basic relationship employed for coupling hydrodynamic and morphodynamic processes in an originally empirical linkage of cross-sectional area of a tidal inlet, say Ω, with spring tidal prism, P:

$$\Omega = kP^{\alpha} \tag{2.1}$$

where the scaling coefficient α typically lies in the range 0.85-1.10 (O'Brien, 1931; O'Brien, 1969; Jarrett, 1976; Hughes, 2002). Such a relationship embodies the site-specific feedbacks between tidal-channel morphology and tidal flow properties occurring both in inlet and sheltered channel sections (Friedrichs, 1995; Rinaldo et al., 1999b; D'Alpaos et al., 2009). Various attempts, (e.g., Krishnamurthy, 1977; Marchi, 1990; Hughes, 2002) have been carried out to substantiate,

from a theoretical point of view, the existence of a relationship of the form of the Eq. 2.1 for tidal inlets. All of this approaches assume both a sinusoidal tide, and that at equilibrium the maximum bottom shear stress is represented by the critical threshold for incipient motion of bed sediment. Marchi (1990) tracked the problem by considering the one-dimensional propagation of the tide along a straight rectangular inlet channel connected to the open sea with a schematic tidal basin (Marchi, 1990). In that context, Marchi derived the exact value $\alpha = 6/7$.

In view of the above observation, D'Alpaos et al. (2009) proposed to name Eq. 2.1 as the O'Brien-Jarrett-Marchi (OBJM) "law". Then D'Alpaos et al. (2010) demonstrated the validity of such a relationship, and the consistency of the exponent $\alpha = 6/7$, by considering field observations and modelling analyses both for the sheltered sections of the tidal channel network dissecting the current configuration of the Venice lagoon, and for the corresponding sections on the inlets. Moreover, for the current Venice Lagoon, D'Alpaos et al. (2010) demonstrated that the values of the exponent α in Eq. 2.1 achieves the value $\alpha = 6/7$, which has been empirically observed by O'Brien (1931) and theoretically derived by Marchi (1990). Deviations were observed to occur mainly for small cross sections, less than 20 m large, either undergoing complete drying during the ebb phase, or close to the resolution of geometrical description (Rinaldo et al., 1999b; Lanzoni and Seminara, 2002; D'Alpaos et al., 2009).

2.2.3 Hydrodynamic and advection-diffusion model

The hydrodynamic model (Defina, 2000; D'Alpaos and Defina, 2007) used in the present study to describe the hydrodynamics of different historical lagoon configurations solves the two-dimensional shallow water equations and includes a refined sub-grid modelling of the bathymetry in order to deal with flooding and drying processes in very irregular domains (Defina, 2000; D'Alpaos and Defina, 2007). The two-dimensional shallow water equations are solved using a semi-implicit staggered finite element method based on the Galerkin's approach. The hydrodynamic model, specifically developed for its application in shallow tidal environments, has been widely calibrated and tested by comparison with relevant hydrodynamic data (water levels, flow velocity and flow rates) measured in the Venice lagoon (Carniello et al., 2005; Carniello et al., 2011) and in other lagoons around the world (e.g., Mariotti et al., 2010; Zarzuelo et al., 2016). The hydrodynamic model yields water levels and flow velocities that are used by the advection-diffusion module (Viero and Defina, 2016) to com-

pute the fate of a conservative tracer by solving the depth-averaged conservation equation, described by Eq. 2.2:

$$\frac{\partial C}{\partial t} + \mathbf{U} \cdot \nabla C - \nabla[\mathbf{D}_h \cdot \nabla C] = 0 \tag{2.2}$$

where $C = C(\mathbf{X}, t)$ is the depth-averaged concentration, $\mathbf{X}$ the horizontal position, $\mathbf{U} = \mathbf{U}(\mathbf{U}, t)$ the depth averaged velocity, and $\mathbf{D}_h = \mathbf{D}_h(\mathbf{X,t})$ the two-dimensional diffusivity tensor. In the Eq. 2.2, diffusivity is assumed to be the same as the eddy viscosity computed by the hydrodynamic model.

2.3 APPLICATION OF THE MORPHOMETRIC RELATIONSHIPS TO THE VENICE LAGOON

In order to reconstruct the bathymetry of the 1611 lagoon configuration, we first investigated the validity of the with-to-depth relationship and the OBJM law for the 1810 configuration.

2.3.1 Channel depth versus channel width

We first further investigated the consistency of the relationship between channel width and channel depth by using a wide dataset derived from the 1810 and from present (2012) configurations of the Venice lagoon. We therefore considered about 190 channel cross sections from the 1810 bathymetry and 70 cross sections for the 2012 bathymetry, uniformly distributed across the Lagoon basin. For all these cross sections, we evaluated the maximum channel depth and the channel width at MSL. Fig. 2.2 shows all the selected data (small grey points) and their binning obtained considering a constant interval of width (red points). Channel depth is expressed as a function of channel width on the basis of the following relationship:

$$D = B/(aB^2 + bB + c) \tag{2.3}$$

where a, b and c are constant coefficients whose values read $a = -1,365 \times 10^{-4}$, $b = 0.1646$ and $c = 4.538$ (the coefficients of determination for all the arbitrary sections and for the binned data being equal to $R^2 = 0.54$ and $R^2 = 0.83$, respectively).

In agreement with previous results (Marani et al., 2002; Marani et al., 2004), however based on a smaller dataset, Fig. 2.2 shows that channel depth, D, increases with channel width, B. It clearly emerges that for small channel cross sections ($B <$ 20-30 m), a linear relationship exists between channel width and channel depth, with a width-to-depth ratio of about 8-12. The curve tends to decrease its slope

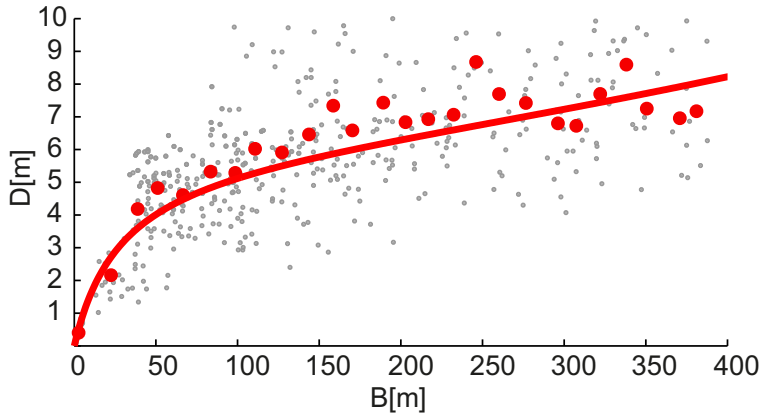

Figure 2.2: Channel depth is plotted versus channel width for arbitrary cross sections within the channel networks of the 1810 and 2012 configurations and for a number of sections surveyed in the Venice Lagoon (Marani et al., 2002) (grey dots). The red line shows the best approximation of the binned data (red dots).

for larger cross sections, and for channels larger than 100-150 m, the width-to-depth ratio is again constant but characterized by smaller values (β= 35-45) thus suggesting that larger channels tend to be proportionally less incised.

2.3.2 OBJM's law

Similarly to the approach adopted for the width-to-depth ratio, we further explored the validity of the OBJM law using data from the 1810 configuration of the Venice lagoon. Specifically, we considered about 190 cross sections belonging to more than 19 tidal channels well distributed within the lagoon, and related their cross-sectional areas to the flowing tidal prism, that we computed, for each cross section, by integrating the discharge obtained from the hydrodynamic model over half of the tidal period (Eq. 2.4):

$$P = \int_0^{T/2} Q(t)dt \tag{2.4}$$

and estimated the cross-sectional area at MSL from the morphology of the 1811 configuration. Following the approach by Krishnamurthy (1977) the flow discharges used in Eq. 2.4 are computed by forcing the hydrodynamic model with a sinusoidal, semi-diurnal tide characterized by an amplitude of 50 cm imposed at the seaward boundary of the computational domain. As a result, we verified the general validity of Eq. 2.1 for the channels of the 1810 configuration (as previously done for the 2012 configuration by D'Alpaos et al. (2010). Fig. 2.3 shows the log-log plot of the data computed for the 190 selected cross sections (blue dots). Our data from the 1810 Venice lagoon, character-

ized by a tidal prism $P > 10^6$ m^3, are well fitted by a power law with exponent $\alpha = 6/7$, in agreement with the theoretical derivation of the OBJM (Marchi, 1990; D'Alpaos et al., 2010). Data from these, large cross sections were integrated with those derived from the four inlets of the 1810 configuration (Chioggia, Malamocco, S. Nicolò and Treporti) and binned considering a constant interval of tidal prism (blue circle):

$$\Omega_{1810} = 1.56 \times 10^{-3} \cdot P_{1810}^{6/7} \tag{2.5}$$

the power-law relationsip being characterized by a coefficient of determination $R^2 = 0.86$. Deviations from the theoretical relationship can be ascribed (see also Rinaldo et al., 1999a; D'Alpaos et al., 2010) to data resolution, the cross sections of the smaller channels ($\Omega < 100$ m^2) being difficult to determine from the historical maps.

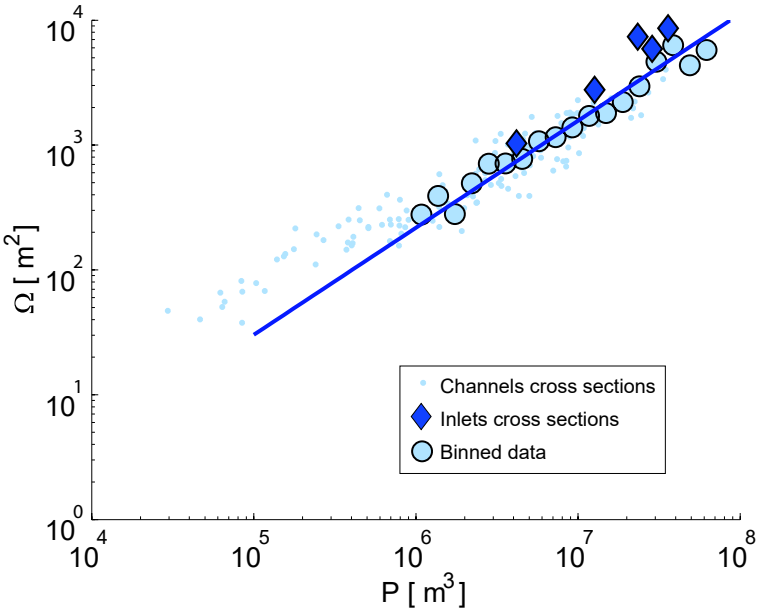

Figure 2.3: The validity of O'Brien-Jarrett-Marchi relationship for arbitrary cross sections within the tidal network (blue dots) and for inlets cross sections (blue diamonds) for the 1810 bathymetry. Tidal prisms are computed by way of a fully equipped finite element model (D'Alpaos and Defina, 2007), whereas cross-sectional areas are calculated with reference to the MSL. Considering the data with tidal prism $P > 10^6$ m^3, the slope fitted to the binned data (blue circle) is the fixed value, i.e., $\alpha = 6/7$, and $k = 1{,}56 \times 10^{-3}$ m$^{2-3\alpha}$ ($R^2 = 0.86$).

2.4 RESULTS AND DISCUSSION

The first goal of the present study was to reconstruct the 1611 Venice lagoon bathymetry and to verify the robustness of the suggested ap-

proach. The 1611 bathymetry was then used to investigate the hydrodynamic behaviour of this ancient lagoon configuration, in order to compare it with those of the 1810 and current (2012) configurations.

2.4.1 Reconstruction of the 1611 bathymetry

We used the Alberti's Historical map as the base for the reconstruction of both the morphology and the bathymetry of the Venice lagoon. Toward this goal we first georeferenced the map and then we created the computational grid for the numerical hydrodynamic model (about 105'000 triangular elements and 54'000 nodes were used). The bathymetry of the 1611 configuration was reconstructed by using different procedures for the different morphological features namely tidal channels, tidal flats and subtidal platforms and salt marshes. Starting from the channels, we measured channel width for several selected cross sections uniformly distributed within the 1611 georeferenced map and we used Eq. 2.3 to define the maximum channel depth. In order to define the cross-sectional shape, we maintained the same cross-sectional shape provided by the corresponding 1810 cross section.

Tidal flat elevations were determined starting from the 1810 bathymetry, reconstructed in previous studies (Carniello et al., 2009; D'Alpaos, 2010a).

As will be detailed in the following, to estimate tidal-flat elevations we assumed a constant rate of RSLR between 1611 and 1810, neglected erosion processes over the tidal flats due to tidal currents and wind waves (Carniello et al., 2011; D'Alpaos et al., 2013; Carniello et al., 2016), and accounted for deposition processes.

Faivre et al. (2012) reconstructed the Sea Level (SL) variations during the past 1500 years based on biological indicators from the Central Adriatic islands, showing that SL was nearly stable during the Little Ice Age, from about 1330 till 1640. Carbognin et al. (2004), analyzing SL records collected at Trieste and Venice, demonstrated that MSL in the Venice lagoon increased at a rate of 1.54 mm/yr from 1896 till 1930 (Carbognin and Taroni, 1996; Carbognin et al., 2004; Carbognin et al., 2010). To determine the rate of SLR between 1810 (Dénaix's map) and 1611 (Alberti's map), we linearly interpolated the rate of SLR at the beginning of the XVII century (0 mm/yr - Faivre et al. (2012)) and at the beginning of the XX century (1.54 mm/yr - Carbognin and Taroni, 1996; Carbognin et al., 2004), obtaining the rate of RSLR for the 200 years between the Alberti's and Dénaix's maps of about 0.50 mm/yr, with a total increase in SL of about 10 cm.

Salt-marsh lateral erosion during the XVII and XVIII centuries made available a non-negligible amount of sediments. By comparing the georeferenced 1611 and 1810 maps we estimated that about 73 km^2 of

salt marshes disappeared in two centuries and we assumed to keep all the volume of sediments eroded from the salt-marsh edges within the lagoon. For the sake of simplicity, we uniformly redistributed such a sediment volume over the tidal flats, neglecting any contribution related sediment transport patterns and to compaction. By assuming an average height of the marsh edge of about 50 cm, the related 0.036 km^3 of sediments were uniformly distributed over the 290 km^2 of tidal flats, thus providing an increase in bottom elevations of about 10 cm over the tidal flats.

Other sources of sediments such as sediment supply from the watershed were assumed to be negligible because main rivers (such as Brenta and Piave), had been already diverted out of the lagoon in 1611, river diversion carried out to prevent the silting up of the lagoon having been performed by the Serenissima Repubblica di Venezia mainly during the XVI century.

Our analysis suggests that the decrease in tidal-flat elevations (compared to the 1810 configuration) due to relative SLR and the increase in bottom elevation due the deposition of former marsh sediments almost compensated, and therefore the same elevation of the 1810 configuration was assigned to the tidal flats in the 1611 configuration. The described sediment transport mechanism according to which salt marsh deterioration feeds the adjacent tidal flats with sediment, tidal flats being therefore to maintain their original elevation counteracting the increase in relative SLR, derives from the conceptual model prosed by Carniello et al. (2009) to describe the long-term evolution experienced by a tidal basin under erosion and agrees with the modelling analyses by Mariotti and Carr (2014).

Salt-marsh elevations were kept constant (same elevations as in 1810 and 1901), by assuming these tidal landforms to be able to keep pace with the rate of RSLR (Mudd et al., 2009; D'Alpaos et al., 2011; Kirwan and Megonigal, 2013) and by neglecting erosion processes over the marsh surface.

Depth [m]	Strickler coefficient [$m^{(1/3)}s^{-1}$]
0.25 — -0.3	15
-0.30 — -1.00	20
-1.00 — -5.00	30
-5.00 — -10.50	35
-10.50 — -44.00	40

Table 2.1: Strickler coefficients assign by using the depth criterion.

The bathymetry of the 1611 configuration used to set up the computational grid was completed, for the sea, by considering the same bathymetry used for the 1810 grid (D'Alpaos, 2010a). Finally, elements of the computational grid representing the 1611 Lagoon, were

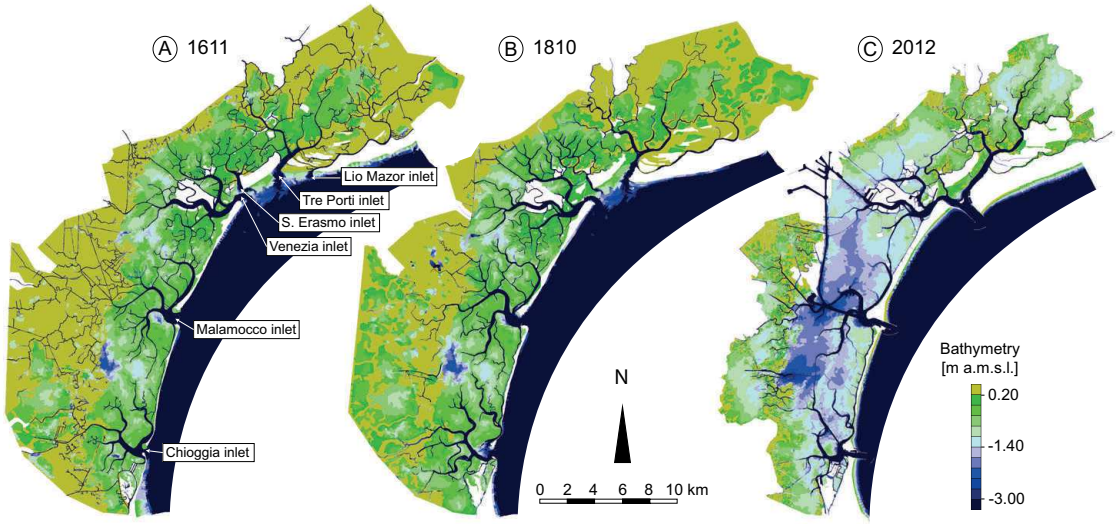

Figure 2.4: Color-coded bathymetry of the Venice lagoon, Italy, in (a) 1611, (b) 1810 and (d) 2012. Elevations are in meters above MSL and they have been referred to the mean Adriatic Sea level recorded when each survey was performed.

assigned a Stickler coefficient depending on depth, following the same approach adopted for the other computational grids (1810 and 2012) (Carniello et al., 2009; D'Alpaos, 2010a). The larger the depths, the larger the assigned coefficients (Tab. 2.1).

2.4.2 Testing the procedure used to build the 1611 configuration

The reconstructed 1611 bathymetry allowed us to set up the computational grid of the corresponding lagoon configuration, a key step to study the hydrodynamic behaviour of the lagoon in the XVII century on the basis of the numerical model proposed by Defina (2000) and D'Alpaos and Defina (2007). The model was forced by a sinusoidal semi-diurnal tide of amplitude 0.5 m, which is typical of the Northern Adriatic Sea. Model results were first used to test the procedure adopted to obtain the 1611 configuration (Fig. 2.4). In addition, the main hydrodynamic features of the 1611 configuration, such as water levels, flow velocities and discharges, were compared with those obtained by performing the same simulations for the 1810 and 2012 configurations of the Venice lagoon.

The procedure was tested by verifying whether or not the OBJM law was observed for the newly reconstructed 1611 configuration. To this end, we considered about 170 cross sections belonging to more than 17 tidal channels (red points in Fig. 2.5) together with the six inlet cross sections for the 1611 configuration. We related the tidal prism flowing through each cross section (determined by integrating water discharges flowing through the section during half of the tidal

cycle) to the cross-sectional areas computed, on the basis of the reconstructed bathymetry, with reference to MSL Eq. 2.4. Fig. 2.5 shows how the binned data at constant intervals (red circles) clearly cluster along the power-law relationship (straight line in the log-log plot) with the theoretical exponent $\alpha = 6/7$, and $k = 1{,}38 \times 10^{-3}\ m^{2-3\alpha}$.

$$\Omega_{1611} = 1.38 \times 10^{-3} \cdot P_{1611}^{6/7} \tag{2.6}$$

When considering only the cross sections characterized by a tidal prism $P > 10^6 m^3$ we obtain a determination coefficient equal to $R^2 = 0.98$. The agreement is remarkable over a wide range of scales, deviations occurring at small scales being dictated by either the resolution of the topography (the dimension of the smaller channels is indeed difficult to determine from the historical maps) or the drying of the entire section during the ebb phase (Fig. 2.5). Our testing experiment suggests that the procedure adopted to reconstruct the 1611 bathymetry allows us to reproduce one of the most relevant geomorphic relationships of tidal landscapes.

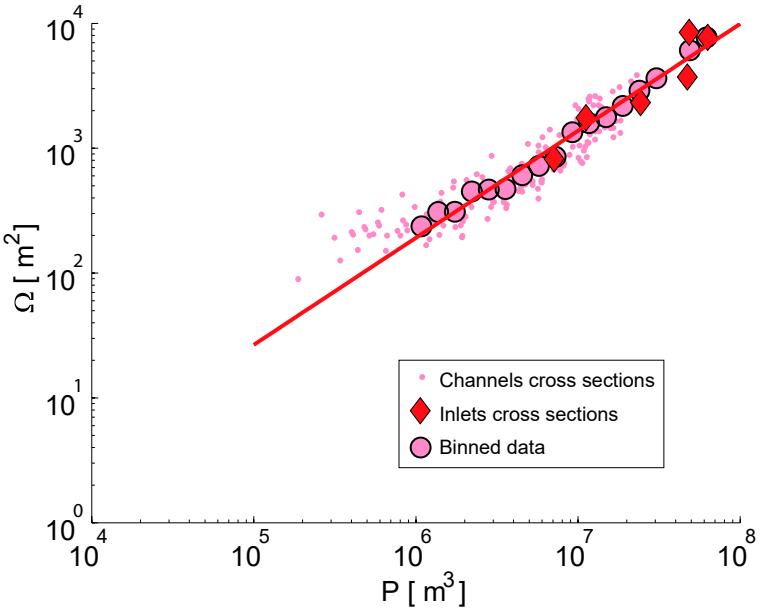

Figure 2.5: The validity of O'Brien-Jarrett-Marchi relationship for arbitrary cross sections within the tidal network (red dots) and for the inlet cross section of 1611 bathymetry (red diamonds). Tidal prisms are computed by way of a fully equipped finite element model (D'Alpaos and Defina, 2007), whereas cross-sectional areas are calculated with reference to the MSL. Considering the data with tidal prism $P > 10^6\ m^3$, the slope fitted to the binned data with a fixed value of the exponent, i.e., $\alpha = 0.857$, and $k = 1{,}38 \times 10^{-3}\ m^{2-3\alpha}$, ($R^2 = 0.97$).

It is worthwhile noting that the validity of the OBJM relationship was not granted by the methodology adopted for reconstructing the

1611 bathymetry, because channel cross sections of the Alberti's configuration were not obtained by using the OBJM law, but rather using the independent empirical relationship between channel width (B) and channel depth (D). The validity of the OBJM relationship for the cross sections of the 1611 lagoon provides evidence of the goodness of the assumptions adopted to reconstruct the bathymetry of the lagoon in the early XVII century.

To further test the consistency of the procedure, we compared the OBJM relationships obtained for the three configurations of the Venice lagoon (1611, 1810, 2012) (Fig. 2.6). It is worth noting that when fitting the data obtained by considering the three configurations of the Venice lagoon (i.e., 1611, 1810 and 2012), with a power law characterized by a fixed value of the exponent $\alpha = 6/7$, we obtain values of the intercept k that are quite similar in all the cases, thus confirming the validity of the framework used to reconstruct the 17^{th} century bathymetry.

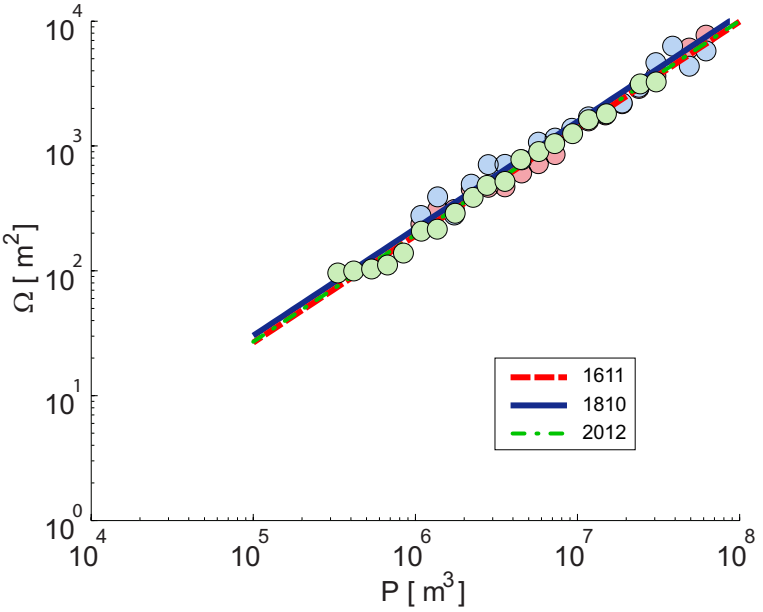

Figure 2.6: The comparison between the OBJM relationships obtained from several cross sections gathered in the whole Venice lagoon of 1611 (red, dashed line), 1810 (blue line), 2012 (green, dashed-dotted line).

As a final, stringent test to analyse the reliability of the adopted methodology and to asses the sensitivity of the OBJM relationship to our assumptions, we calculated the OBJM relationship with other two different bathymetries of 1611 Lagoon, that were built by introducing possible errors in the estimation of the elevation of the different morphological features considered. Bottom elevation, and therefore the local water depth is, in fact, the variable that more influences the computation of the tidal prism and of the channel cross section. The first "incorrect" bathymetry was created by decreasing tidal flat elevations

of 1 m, based on the observation that 1 m might be a reasonable error for the estimation of the elevation of these morphological features. In fact, the frequency area distributions as a function of bottom elevation (Carniello et al., 2009) shows that the relative peaks for the probability distribution of the tidal-flat depths lie in a range between -0.50 m (1901) and -1.5 m (2003) (Fig. 2.7). The best fitting power law for the Ω vs P data obtained by considering this incorrect modified bathymetry of the 1611 configuration reads:

$$\Omega = 12.04 \times 10^{-3} \cdot P^{0.73} \tag{2.7}$$

with α and k coefficients quite different from the actual ones (see Fig. 2.6).

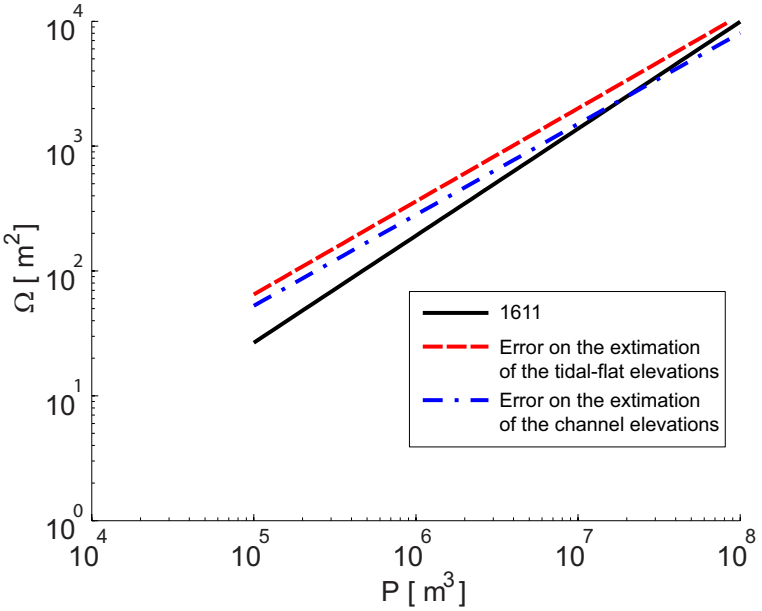

Figure 2.7: The graph compares the OBJM relationships obtained from the modified 1611 bathymery. The blue, dashed line identifies the results related to modifications in the elevations of the tidal flats (α = 0.73, and k = 12.04 $\times 10^{-3}$ $m^{2-3\alpha}$) and the dashed-dotted line identifies the OBJM relationship obtained from the cross sections gathered within an error in channel depths (α = 0.75, and k = 12.18$\times 10^{-3}$ $m^{2-3\alpha}$).

A second incorrect bathymetry was created by assuming an error in the estimation of the channel maximum depth of about 5 m (i.e., by considering channels deeper than those obtained by using the observed width-to-depth ratios). In this case the best fitting power law for the Ω vs P values reads:

$$\Omega = 12.18 \times 10^{-3} \cdot P^{0.75} \tag{2.8}$$

with α and k coefficients that are again quite different from the actual ones (see Fig. 2.6).

Fig. 2.7 shows the comparison between Eq. 2.7, Eq. 2.8 and the OBJM law obtained for the orginal reconstructed 1611 bathymetry (Eq. 2.6), emphasizing that errors in procedure adopted to reconstruct the ancient bathymetry would have produced configurations not capable to satisfy the OBJM law.

2.4.3 Comparison of the Hydrodynamic behaviour of the 1611, 1810 and 2012 configurations

Using the computational grid reproducing the reconstructed morphology and bahymetry of the lagoon at the beginning of the XVII century and the grids reproducing the lagoon in 1810 and 2012, we examined the main modifications occurred in the hydrodynamic behaviour of the Venice Lagoon during the last four centuries. The analysis was carried out by forcing the different configurations with the same sinusoidal semi-diurnal tide oscillating over the contemporary MSL with an amplitude of 0.5 m.

The results obtained by considering the three configurations of the lagoon enabled us to evaluate whether and to what extent humans interventions and the related morphological modifications affected the hydrodynamic behaviour of the Lagoon over time.

In particular, we analysed modifications of the tidal signal along four hydraulic paths departing from the three inlets and reaching the innermost portions of the basin (Fig. 2.8). Comparing water levels in the three configurations along the four hydraulic paths clearly shows (see Fig. 2.8 for the Venice path and Northern path and Fig. 2.9 for Southern path and Central path) that the propagation of the tide in the past configurations of the lagoon was characterized by a significant phase lag and a strong reduction in tidal amplitude with respect to the present lagoon. This is particularly evident when observing the tide propagation along the Venice path (Fig. 2.8) and along the central and southern paths (Fig. 2.9). In the present lagoon, the tidal amplitude even increases, of about 2 cm, while propagating from the open see to Punta della Salute and up to 4 cm when reaching the Porto Marghera (see Venice path Fig. 2.8C). This amplification of the tidal signal in the present lagoon along the hydraulic path cutting through the city of Venice is also documented by the water level data recorded during spring tides from the tide gauge stations. On the contrary, the results obtained when considering the ancient configurations of the lagoon show that, with respect to the tide at the sea, the maximum water levels at Punta della Salute are reduced of about 8 cm in both 1611 and 1810 configurations (see Venice path Fig. 2.8). Proceeding from Punta della Salute towards the Lagoon's boundaries with the

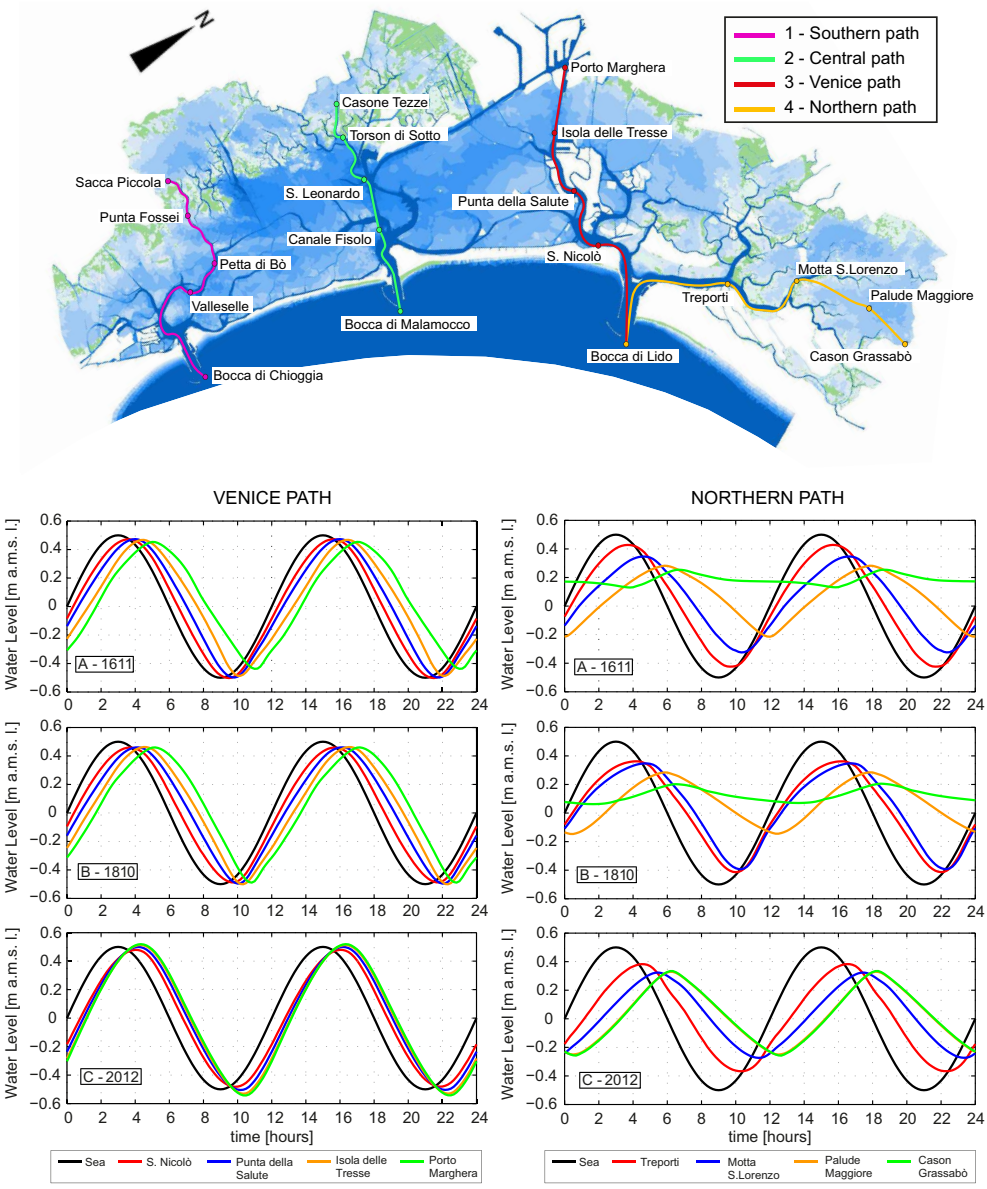

Figure 2.8: Water level trajectory inside the Venice lagoon in the three different configurations following the Venice and the Northern paths.

mainland the attenuation process was negligible in 1810 but further affected the tide propagation in 1611 by reducing the maximum water level of other 2 cm (see Venice path Fig. 2.8A and B).

The hydraulic path along which the dissipative hydrodynamic behaviour of the lagoon has been mostly preserved during the last centuries is the one connecting the Lido inlet to the northernmost part of the lagoon (Northern path in Fig. 2.8). The northern lagoon is, in fact, the portion of the lagoon that has experienced the mildest and slowest erosive trend compared to the central and southern lagoon (Carniello et al., 2009). In all the configurations, the attenuation of the tidal amplitude and the phase lag clearly emerge (in the ancient configu-

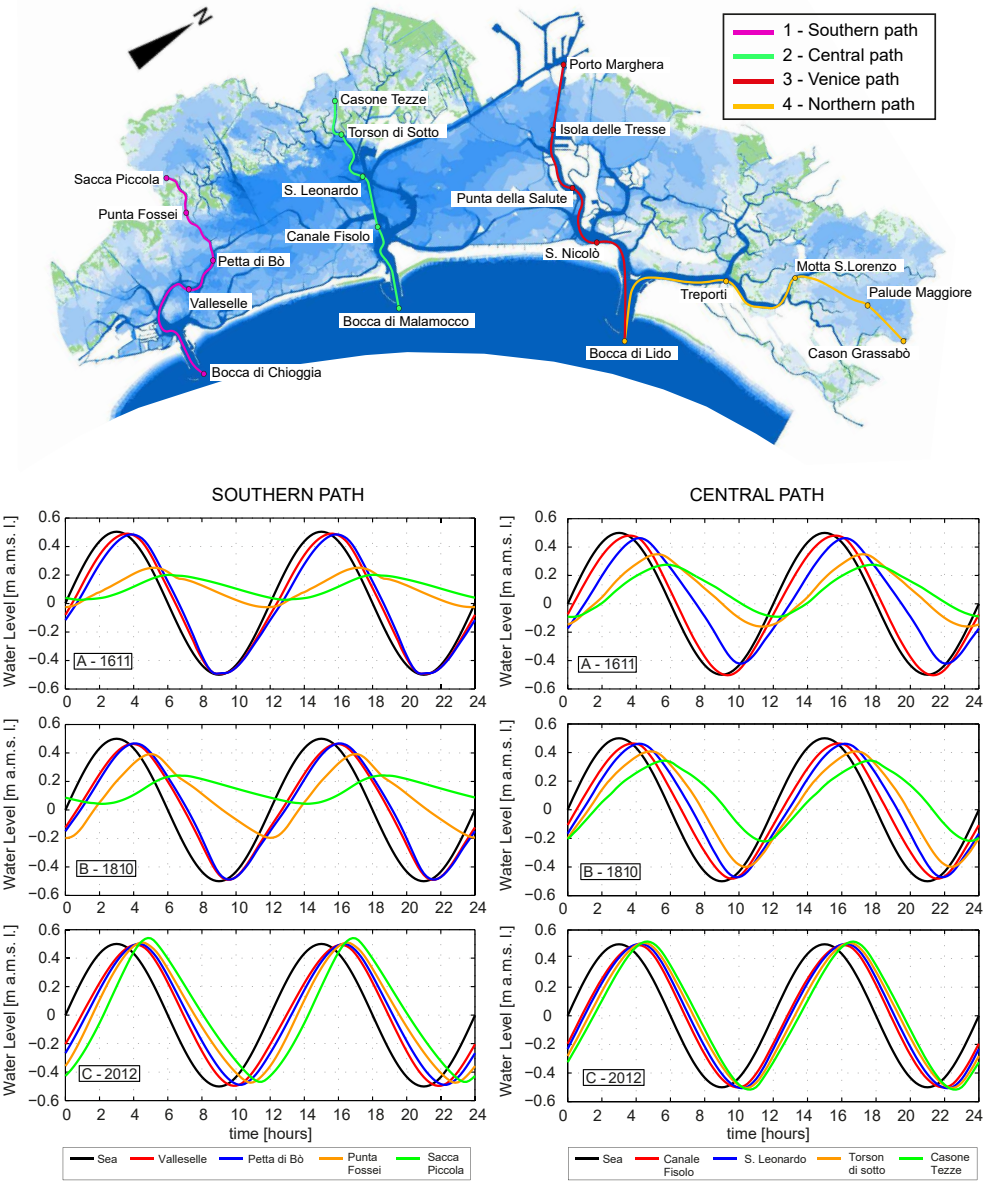

Figure 2.9: Water level within the Venice lagoon in the three different configurations following the Southern and Central paths.

ration the attenuation from the open sea to Cason Grassabò is about 20 cm and the phase lag is about 3.40 hours, while in the present configuration the attenuation is about 16 cm and the phase lag is about 3.20 hours). Interestingly the tidal wave reduction is not symmetrical: along the path, the wave crests decrease less than the wave troughs, as a result of the non-linear relationship between energy dissipation and flow velocity.

We can conclude that the tidal propagation within the Venice lagoon before the construction of the jetties at the three inlets was dominated by dissipative processes, whereas in the present Lagoon inertial forces prevail. In particular, the lower depths of the ancient lagoon

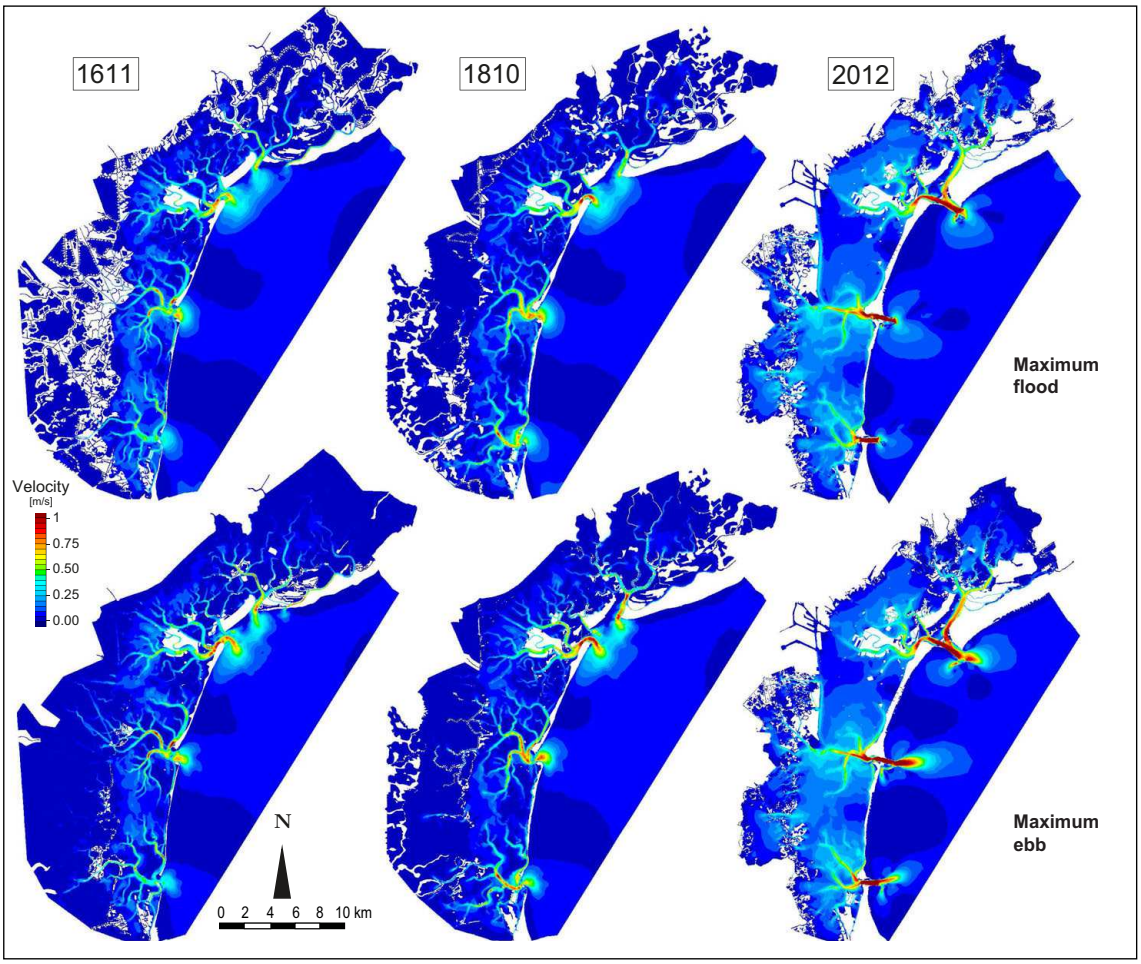

Figure 2.10: Computed flow velocity in the three different configurations of the Venice lagoon.

inlets produced a much higher friction with respect to the deeper actual configuration of the lagoon inlets. A further observation supported by the northern path of Fig. 2.8 A and B and by the central and southern paths of Fig. 2.9 A and B is that the attenuation of the tidal signal suddenly increases when tide propagates across the salt marshes, thus confirming the relevant role exerted by these morphological features on the lagoon hydrodynamics. As a consequence of the different water levels, the discharges and the water volumes flowing through the three inlets during the ebb and flood phases strongly changed during the last four centuries. The discharges at the inlets are much higher for the present Lagoon compared to the ancient ones. The main difference is at the Malamocco inlet, where the maximum discharge during the flood phases was of about 4400 m^3/s in 1611 and 8800 m^3/s in 2012, while during the ebb phase the maximum discharge was of about 4300 m^3/s in 1611 and 8900 m^3/s in 2012 (see Tab. 2.2).

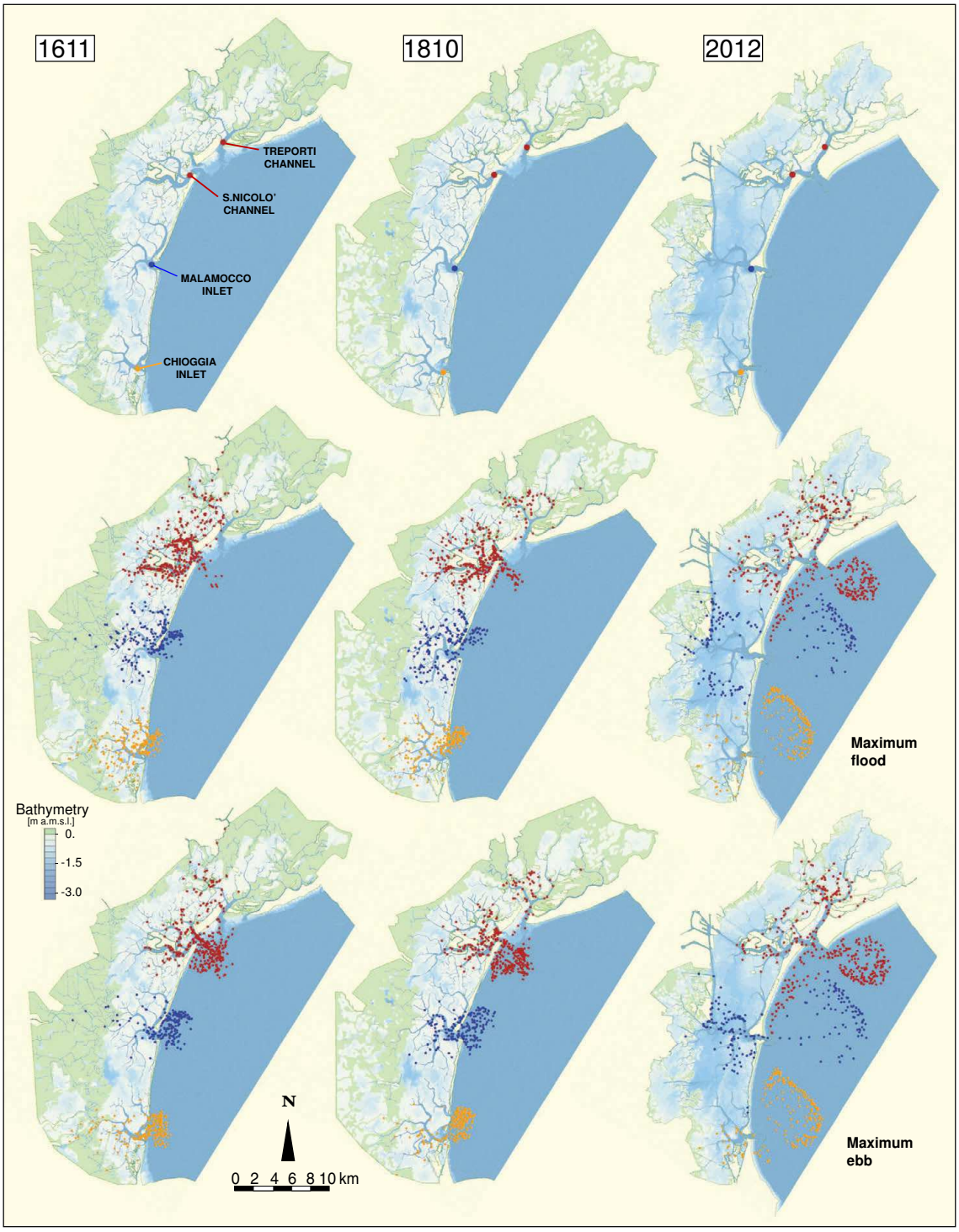

Figure 2.11: Dispersion of particles released at the inlets superimposed on the bathymetry for three different configurations of the Venice lagoon.

Fig. 2.10 shows the spatial distribution of the flow velocities computed with the hydrodynamic model during the flood and ebb phases for the three configurations. The hydrodynamic flow field at the inlets in the ancient configurations of the lagoon was characterized by a

	Water discharge					
	1611		1810		2012	
	Flood [m^3/s]	Ebb [m^3/s]	Flood [m^3/s]	Ebb [m^3/s]	Flood [m^3/s]	Ebb [m^3/s]
Chioggia Inlet	3555	3506	4008	4026	4560	4883
Malamocco Inlet	4453	4386	4963	4942	8822	8909
Venezia Inlet	4375	4267	4447	4510	4740	4820
Tre Porti Inlet	1731	1636	1718	1791	2287	2351

Table 2.2: Maximum values of water discharge during the ebb and the flood phases in the three different configurations.

symmetric behaviour, while in the present lagoon an asymmetric behaviour clearly emerges from Fig. 2.10 with plumes forming during the ebb phase because of the presence of the jetties. This asymmetric hydrodynamic behaviour has been observed (Carniello et al., 2012) to be one of the main processes contributing for the erosive trend the lagoon has been experiencing since the beginning of the last century (the construction of the jetties started in 1839 at the Malamocco inlet and was completed in 1934 with the construction of the jetties at the Chioggia inlet).

As a final analysis we applied the dispersion model (Viero and Defina, 2016) to the three different configurations simulating 6 tidal cycle (72 h), to investigate the dynamics of spots of particles released at different locations close to the inlets within the lagoon (see Fig. 2.11). In the 1611 and 1810 Lagoons the particles were able to travel in and out during the flood and ebb phases while in the present lagoon they are projected far away into the Adriatic sea during the ebb phases and the previously discussed asymmetric behaviour of inlets prevents the re-entry of most of the particles during the subsequent flood phase. From our analysis we conclude that, after the diversion of the main rivers carried out during the XVI ad XVII century, the hydrodinamic behaviour has not significantly changed until the beginning of the XX century, when the construction of the jetties at the three inlets was completed. The historical lagoons were less dynamic compared to the present configuration, nevertheless, with the exception of the navigation problem, from the beginning of the XVII century to the beginning of the XX century the lagoon was kept in more than acceptable environmental conditions, despite the reduced fluxes at the three inlets. In particular, the ancient lagoon has been able to preserve both the strong channel networks and some morphological forms such as salt marshes, which in the present lagoon are disappearing, thus producing a strong modification of the tidal environment.

2.5 CONCLUSIONS

In this work, we developed a procedure to reconstruct the bathymetric features of a tidal system starting from planimetric information. We considered the study case of the Venice Lagoon for which numerous cartographic map exist, owing to the perceived importance of the lagoonal morphologies. Starting from the oldest map (the 1611 Alberti's map) of the Venice Lagoon suitable to provide a realistic representation of the planimetric configuration of its main morphological features, we built the corresponding bathymetry through the use of the classical width-to-depth geomorphic relationships for tidal channels and conceptual models of tidal-flat and salt-marsh coevolution. The newly reconstructed bathymetry was then tested on the basis of another relationship of geomorphic relevance, the O'Brien-Jarrett-Marchi's law, relating channel cross-sectional area to the flowing tidal prism. The reconstruction of the XVII century bathymetric configuration allowed us to compare its hydrodynamic and wind-induced wave fields with those characterizing other, more recent Lagoon configurations. Our analyses highlight important changes in the hydrodynamics and wave dynamics of the Venice Lagoon through the last four centuries, emphasizing the less dissipative and more erosional character of the current configuration. Tidal wave dampening within the lagoon has decreased in the last four centuries, whereas the strength of tidal currents, the discharges flowing through the inlets, the height of wind waves and the intensity of wave- and current- induced bottom shear stresses, together with the amount of sediments lost towards the Adriatic sea, have largely increased. We therefore suggest that the proposed procedure for the reconstruction of ancient bathymetries is a fundamental step for the analysis of the morphological evolution of tidal systems.

3 WIND WAVES AND BOTTOM SHEAR STRESSES IN SHALLOW TIDAL BASINS

This chapter is a manuscript in preparation for *Water Resources Research*, whose primary goal is to improve current knowledge on the theoretical frameworks that can be used by scientists and managers to make predictions on the evolution of estuarine and lagoonal landscapes. Towards this goal, it is critical to better understand the processes responsible for the entrainment and transport of sediments. Modelling frameworks, as long as they reveal to be appropriate for the study cases at hand, provide a useful tool for long-term morphodynamic studies. We are, in particular, interested in modelling frameworks describing the generation and propagation of wind waves that are, indeed, the main natural process responsible for sediment resuspension over shallow unchanneled tidal landforms. In this contribution, we report new simulations exploring the consequences of the possible assumptions embedded in different wave models. We then compare model results with data from the Venice Lagoon and we demonstrate the sensitivity of model results to small changes in the depth of shallow environments. Our analyses suggest that the greatest changes in wave dynamics in the face of sea level rise will potentially occur in areas where field observations are scarce, compared to the abundance of data for deeper areas.

PAPER

CHARACTERISTICS OF WIND WAVES IN SHALLOW TIDAL BASIN AND HOW THEY AFFECT BED SHEAR STRESS, BOTTOM EROSION, AND THE MORPHODYNAMIC EVOLUTION OF MUDFLAT LANDFORMS

Laura Tommasini[1], Luca Carniello[2], Guillaume Goodwin[3], Simon M. Mudd[3], Giovanni Coco[4], Zeng Zhou[5], Ian Townend[6] and Andrea D'Alpaos[1]

[1]Dept. of Geosciences, University of Padova, via G. Gradenigo 6, Padova, Italy

[2]Dept. ICEA, University of Padova, via Loredan 20, Padova, Italy

[3]School of Geosciences, University of Edinburgh, Edinburgh, United Kingdom
[4]Faculty of Science, University of Auckland, Auckland, New Zealand
[5]Jiangsu Key Laboratory of Coast Ocean Resources Development and Environment Security, Hohai University, Nanjing210098, China
[5]Faculty of Engineering and the Environment, University ofSouthampton, Southampton, UK

Abstract

Wind-wave induced erosion is one of the main processes controlling the morphodynamic evolution of shallow tidal basins because wind waves promote the erosion of subtidal platforms, tidal flats and salt marshes. One of the most important questions when dealing with mathematical models describing wind-wave processes in shallow tidal basins is what models can be safely used and what assumptions are permissible compared to fatally flawed ones. In order to answer this question our study considered zero-, one- and two-dimensional wave models and tested their capability in reproducing observed wave characteristics. First, we analysed the relationships between wave parameters, depth and bed shear stress with two zero-dimensional models based on the Young and Verhagen (1996b), and Carniello et al. (2011) approaches. The first one is an empirical method that computes wave height and the variable wave period based on wind velocity, fetch and water depth. The second is based on the solution of wave action conservation equation, and computes the bottom shear stress and wave height considering a wave period related to wind speed and water depth. Second, we compared the wave spectral model SWAN (Simulating WAve Nearshore) with a fully coupled Wind-Wave Tidal Model (WWTM) (Carniello et al., 2011) applied to a 1D rectangular domain. Finally, we applied the two-dimensional WWTM to six different configurations of the Venice lagoon considering the same boundary conditions and we evaluated the spatial variation of mean wave height and mean and maximum wave-induced bottom shear stress. Our results highlight the crucial role that assumptions, made on wind wave modelling, exert when those models are used for investigating the morphodynamic evolution of shallow tidal environments.

3.1 INTRODUCTION

Many middle to high latitude coastlines feature salt marshes, which are particularly prominent along the Atlantic and Gulf coasts of North America, the coastlines of northern Europe, and the Yangtze River Delta in China. Despite the relatively small area occupied by these

ecosystems, they play an outsized role in carbon sequestration: some estimates place their sequestration potential higher than temperate forests (Chmura et al., 2003; Mcleod et al., 2011). Many coastal marshes, which tend to sit in the upper portions of the tidal frame (Allen, 2000), also feature extensive flats that sit below mean sea level (e.g., Fagherazzi et al., 2006; Marani et al., 2007; Zhou et al., 2016). The commonplace bifurcation of elevation and bathymetry into two distinct clusters, one above mean sea level and one below, along coastlines featuring marshes have led many authors to propose feedback mechanisms driving this bifurcation (e.g., Fagherazzi et al., 2006; Defina et al., 2007; Marani et al., 2007; Wang and Temmerman, 2013). These feedback mechanisms are thought to be governed by sediment exchanges between marshes and flats: when marshes accrete to elevations near mean high tide there is insufficient bottom shear stress to erode these vegetated surfaces (Augustin et al., 2009; Möller et al., 2014), whereas subtidal flats can only provide sediment once the water depth is high enough to produce bottom shear stresses that cause sediment resuspension at the bed (e.g., Carniello et al., 2012; D'Alpaos et al., 2013; Carniello et al., 2014; Carniello et al., 2016).

In sheltered estuaries and lagoons, it is primarily waves that promote sediment resuspension, as tidal currents are typically not strong enough to cause sediment entrainment (Amos et al., 2004; Mariotti et al., 2010). In addition, in sheltered systems, wind waves dominate the generation of bottom shear stresses (e.g., Carniello et al., 2005; D'Alpaos et al., 2013; Mariotti and Carr, 2014). The transfer of sediment from tidal flats to marshes is not the only factor controlling the balance of the area that is either marsh or tidal flat: lateral marsh migration also plays a major role in determining marsh extent (Mariotti and Fagherazzi, 2010; Marani et al., 2011; Leonardi et al., 2018). Both sediment resuspension and lateral migration of the marsh edge are closely linked to the depth of the adjacent tidal flat (McLoughlin et al., 2015). These processes are driven by waves, which influence bed shear stress (e.g.,Mariotti et al., 2010; Mariotti and Fagherazzi, 2013b; Leonardi and Fagherazzi, 2014). Recent works have also shown that the rate of marsh edge retreat is closely correlated with wave power (Marani et al., 2011; Leonardi and Fagherazzi, 2015; Leonardi et al., 2016b).

The depth of the tidal flats plays a major role in determining wave heights, wave periods, and by extension wave celerities (Mariotti and Fagherazzi, 2013b). An increase in the depth of the tidal flats leads to larger waves and enhanced wave power, and this, in turn, leads to sediment erosion further increasing the depth of the tidal flats in a positive feedback mechanism. As a consequence, larger depths promote increased wave power at the marsh edge, thus leading to accelerated marsh retreat. These positive feedbacks can be amplified by

relative sea level rise as long as such a process promotes an increase in water depth.

In order to describe the most relevant processes contributing to shape shallow tidal systems and to predict their morphodynamic evolution, one needs to improve the understanding of the processes that promote sediment resuspension and entrainment. Towards this goal, a key issue concerns the possible use of appropriate models for wind-wave generation and propagation. A large number of recent studies have employed numerical models to investigate sediment resuspension and entrainment due to wind waves and the impact that such processes have on the evolution of shallow tidal environments (Mariotti and Fagherazzi, 2010; Carniello et al., 2012; D'Alpaos et al., 2013; Carniello et al., 2014; Leonardi and Fagherazzi, 2014; Zhou et al., 2016). These studies have used a wide range of wave models to obtain estimates of sediment transport and morphological change (Tab.3.1). In this contribution, we report new simulations that explore the consequences of the possible assumptions embedded in different wave models. We then compare model outcomes with data from the Venice Lagoon. We note a marked paucity of appropriate data on waves in shallow (0-1 m deep) environments: a limiting factor to set up and test modelling strategies. We highlight the sensitivity of model results to small changes in the depth of shallow environments, suggesting that the greatest changes in wave dynamics in the face of sea level rise might potentially occur in those portions of the coastline where field observations are scarce, thus calling for new detailed field observations to set up and test mathematical models. We finally applied a fully coupled Wind Wave Tidal Model (WWTM) to six configurations of the Venice Lagoon to compare the related spatial distribution of wave heights and wave-induced bottom shear stresses.

3.2 METHODS

We explore the implications of model assumptions within three frameworks for this study: i) analytical models based primarily on the work of Young and Verhagen (Young and Verhagen, 1996a; Young and Verhagen, 1996b); ii) numerical models such as the Wind Wave Tidal Model (WWTM) (Carniello et al., 2005; Carniello et al., 2011) and the Simulating WAves Nearshore (SWAN) model (Booij et al., 1999).

3.2.1 Young and Verhagen equations (Y&V)

A number of studies exploring how wind waves influence the evolution of marsh and tidal flat systems have done so on the basis of analytical models developed by Young and Verhagen (Young and Verha-

Table 3.1: List of some of the models used to compute the wave height and the bottom shear stress induced by wind in shallow tidal basin and coastal systems.

Wave Model	Model Dim.	T_p	f_w	Grain size	Note	References
WWTM	0D	$T = 2$ s	Soulsby, 1997	D_{50}	-	Fagherazzi et al., 2006; Fagherazzi et al., 2007; Marani et al., 2007; Marani et al., 2010; D'Alpaos et al., 2012
WWTM	0D	T variable	Soulsby, 1997	D_{50}	-	Venier et al., 2014
WWTM	1D	$T = 2$ s	Soulsby, 1997	D_{50}	-	Mariotti and Fagherazzi, 2010
WWTM	2D	$T = 2$ s	Soulsby, 1997	D_{50}	-	Carniello et al., 2005; Defina et al., 2007
WWTM	2D	T variable [a] = 3.5, b = 0.35	Soulsby, 1997	D_{50}	-	Carniello et al., 2011; D'Alpaos et al., 2013; Carniello et al., 2016
WWTM	2D	T variable [a] = 5, b = 0.357	$f_w = 0.04 \left(\frac{U_{ov} T_p}{2\pi k_b} \right)^{-0.25}$	$k_b = 2D_{90}$ [mm]	-	Mariotti et al., 2010
SWAN	1D	T variable	$f_w = 0.015$	–	-	Mariotti and Fagherazzi, 2013b
SWAN	1D	T variable	Soulsby, 1997	D_{50}	-	Hu et al., 2015
SWAN	2D	T variable	Soulsby, 1997	D_{50}	-	Umgiesser et al., 2004
Y&V	0D	T Variable	$f_w = 0.4 \left(\frac{H_s}{k_o \sinh kd} \right)^{0.75}$	$k_0 = 1$ [mm]	-	Mariotti and Fagherazzi, 2013a; Mariotti and Carr, 2014; Kirwan et al., 2016b
Y&V	0D	T Variable	(Soulsby, 1997)	D_{50}	Shallow water	Zhou et al., 2016
Y&V	0D	T Variable	(Soulsby, 1997)	D_{50}	-	Zhou et al., 2015
Y&V	0D	T Variable	$f_w = 0.03$	-	-	Lauzon et al., 2018
Y&V	0D	T Variable	(Swart, 1974)	D_{50}	-	Kakeh et al., 2016
Measured	0D	T Variable	(Soulsby, 1997)	D_{50}	-	Zhang et al., 2016

gen, 1996a; Young and Verhagen, 1996b) (Y&V). These authors, based on wind-wave data from an Lake George in Australia, found a set of equations to predict locally generated wind waves. Their model describes relationships between non-dimensional wave height (ε), non-dimensional wave frequency (ν), non dimensional fetch length (χ), and non dimensional water depth (δ), read:

$$\varepsilon = \frac{gH_s}{U_w^2}, \tag{3.1}$$

$$\nu = \frac{gT_p}{U_w}, \tag{3.2}$$

$$\chi = \frac{gX}{U_w^2}, \tag{3.3}$$

$$\delta = \frac{gd}{U_w^2}, \tag{3.4}$$

where g [ms^{-2}] is the gravitational acceleration, X [m] is the dimensional fetch, H_s [m] is the significant wave height, T_p [s] is the peak wave period and U_w [ms^{-1}] is the wind speed measured at an elevation of 10 meters above still water level. The relationships proposed by Young and Verhagen (Young and Verhagen, 1996a; Young and Verhagen, 1996b) are:

$$\varepsilon = 0.2413 \left\{ \tanh A_1 \tanh \left[\frac{B_1}{\tanh A_1} \right] \right\}^{0.87} \tag{3.5}$$

$$\nu = 7.518 \left\{ \tanh A_2 \tanh \left[\frac{B_2}{\tanh A_2} \right] \right\}^{0.37} \tag{3.6}$$

with the empirical coefficients A_1, A_2, B_1, and B_2 defined as:

$$A_1 = 0.493\,[\delta]^{0.75} \tag{3.7}$$

$$A_2 = 0.331\,[\delta]^{1.01} \tag{3.8}$$

$$B_1 = 3.13 \times 10^{-3}\,[\chi]^{0.57} \tag{3.9}$$

$$B_2 = 5.25 \times 10^{-4}\,[\chi]^{0.73} \tag{3.10}$$

Eq. (3.6) allows one to calculate the wave period and Eq. (3.5) the significant wave height when the analytical model of Y&V is applied.

3.2.2 Wind Wave Tidal Model (WWTM)

The Wind Wave Tidal Model (WWTM) (Carniello et al., 2005; Carniello et al., 2011) is a fully coupled model linking the hydrodynamic flow field and wind-wave properties on a single computational grid.

One-dimensional and two-dimensional implementation

The hydrodynamic module allows for the description of tidally induced variable water levels and currents. It solves the two-dimensional shallow water equations modified to deal with wetting and drying processes in irregular domains. The two-dimensional shallow water equations are solved using a semi-implicit staggered finite element method based on Galerkin's approach and is very suitable to deal with morphologically complex basins such as the Venice lagoon (Defina, 2000; Martini et al., 2004; D'Alpaos and Defina, 2007). The standard two-dimensional equations, averaged over the wet phase of the reference area, are:

$$\frac{\partial q_x}{\partial t} + \frac{\partial}{\partial x}\left(\frac{q_x^2}{d}\right) + \frac{\partial}{\partial y}\left(\frac{q_x q_y}{d}\right) - \left(\frac{\partial R_{xx}}{\partial x} + \frac{\partial R_{xy}}{\partial y}\right) + \frac{\tau_{bx}}{\rho} + \frac{\tau_{wx}}{\rho} + gd\frac{\partial h}{\partial x} = 0 \tag{3.11}$$

$$\frac{\partial q_y}{\partial t} + \frac{\partial}{\partial x}\left(\frac{q_x q_y}{d}\right) + \frac{\partial}{\partial y}\left(\frac{q_y^2}{d}\right) - \left(\frac{\partial R_{xy}}{\partial x} + \frac{\partial R_{yy}}{\partial y}\right) + \frac{\tau_{by}}{\rho} + \frac{\tau_{wy}}{\rho} + gd\frac{\partial h}{\partial y} = 0 \tag{3.12}$$

$$\eta\frac{\partial h}{\partial t} + \frac{\partial q_x}{\partial x} + \frac{\partial q_y}{\partial y} = 0 \tag{3.13}$$

where t is time, q_x, q_y are the flow rates per unit width in the x and y directions respectively, defined on a Cartesian grid. R_{ij} are the Reynolds stresses (with i and j denoting either the x or the y coordinates, respectively), $\tau_{b,curr} = (\tau_{bx}, \tau_{by})$ is the bottom shear stress due to tidal currents, $\tau_w = (\tau_{wx}, \tau_{wy})$ is the shear stress at the free surface due to wind action, ρ is fluid density, h is the free surface elevation, g is gravity, d is the equivalent water depth and η is the local fraction of wetted domain. The hydrodynamic module provides the wind-wave module with the flow field characteristics necessary to compute wind-wave generation and propagation.

The wind-wave module (Carniello et al., 2005; Carniello et al., 2011) computes both the generation and the propagation of waves. It is

based on the conservation of the wave action N, which is defined as the ratio of wave energy, E, to the relative wave frequency, σ. The wave action conservation equation, in the most general spectral formulation, is (Hasselmann et al., 1973):

$$\frac{\partial N}{\partial t} + \frac{\partial}{\partial x} c_{gx} N + \frac{\partial}{\partial y} c_{gy} N + \frac{\partial}{\partial \sigma} c_{\sigma} N + \frac{\partial}{\partial \vartheta} c_{\vartheta} N = \frac{S}{\sigma} \tag{3.14}$$

Wave action, N, is a function of space (x, y), time (t), frequency (σ) and direction (ϑ), i.e., $N = N(x, y, t, \sigma, \vartheta)$. The first term on the left hand side of Eq. (3.14) is the local rate of change of wave action density in time, the second and third terms propagate the wave action density in space (c_{gx} and c_{gy} are the x and y components of the wave group celerity along the x and y directions, respectively); the fourth and fifth terms propagate the wave action density in the space of wave frequency (σ) and direction (ϑ), respectively. The right hand term S of Eq. (3.14) is a source term.

Two key assumptions are made in this model (Carniello et al., 2005; Carniello et al., 2011). First, the model assumes that the direction of wave propagation instantaneously readjusts to match the wind direction (e.g., Lin et al., 2002) meaning that the model implicitly neglects wave refraction. Second, the model uses the zero-order moment of the wave action spectrum in the frequency domain for the parametrization. This reduces Eq. (3.14) to:

$$\frac{\partial N}{\partial t} + \frac{\partial}{\partial x} c_{gx} N + \frac{\partial}{\partial y} c_{gy} N = \frac{S}{\sigma} \tag{3.15}$$

where the wave group celerity c_g is calculated according to linear wave theory as:

$$c_g = \frac{1}{2} \frac{\sigma}{k} \left(1 + \frac{2kd}{\sinh(kd)} \right) \tag{3.16}$$

The wave number, k, is obtained by solving the dispersion equation and the mean wave frequency, σ was computed considering the common JONSWAP spectrum and is related to the peak period, T_p, by (Hasselmann et al., 1973):

$$\sigma = 1.095 \frac{2\pi}{T_p} \tag{3.17}$$

The source term, S, in Eq. (3.15) is described by (Booij et al., 1999; Carniello et al., 2005):

$$S = S_{wg} + S_{bf} + S_{wc} + S_{br} \tag{3.18}$$

The wind generation term S_{wg} (Eq. 3.19) describes the linear growth of wave energy in time through resonance between free surface and

turbulent pressure fluctuations (Willmarth and Wooldridge, 1962; Cavaleri and Malanotte Rizzoli, 1981) (Eq. 3.20), and the exponential growth of wave energy in time through the transfer of energy from the wind to the disturbed water surface (Barnett, 1968) (Eq. 3.21).

$$S_{wg} = \alpha + \beta E \tag{3.19}$$

where E is the wave energy, and the term α is determined by:

$$\alpha = \frac{80\rho_a^2 \sigma C_d^2 U_w^4}{\rho_w^2 g^2 k^2} \tag{3.20}$$

where C_d = 0.0012 is a drag coefficient, ρ_a is the air density and ρ_w is the water density. The term β in Eq. (3.19) is solved using:

$$\beta = max\left\{\left[\frac{\rho_a}{T_p \rho_w}\left(\frac{U_w k}{\sigma} - 0.9\right)\right], 0\right\} \tag{3.21}$$

The bottom friction term, S_{bf}, (Collins, 1972) describes the wave energy dissipation at the bed:

$$S_{bf} = -\frac{4C_{bf} U_{bf} k}{\sinh(2kd)} E \tag{3.22}$$

where C_{bf} is a dissipation coefficient equal to 0.015 (Collins, 1972) and

$$U_{bf} = \sqrt{\frac{2gkE}{\sinh(2kd)}} \tag{3.23}$$

The white capping (Hasselmann et al., 1973; Komen et al., 1984) term, S_{bf}, describes the dissipative process related to wave breaking when the wave exceeds the limit steepness during propagation:

$$S_{wc} = -3.33 \times 10^{-5} \sigma \left(\frac{\gamma_{wc}}{\gamma_{PM}}\right)^2 E \tag{3.24}$$

where $\gamma_{PM} = 0.0045$ is the theoretical value of γ for a Pearson-Moskowitz spectrum and the integral wave steepness parameter $\gamma_{wc} = E\sigma^4/g^2$.

The breaking term, S_{br}, accounts for depth-induced breaking:

$$S_{br} = \frac{2Q_b}{T_p}\left(\frac{H_{MAX}}{H_{rms}}\right)^2 E \tag{3.25}$$

where Q_b is the probability that a wave of height H_{rms} will break, H_{rms} is the parameter of the Rayleigh-type distribution in the model assumed to be equal to the wave height computed by the model in each grid element. The model uses the expression for Q_b suggested by Battjes and Janssen (1978):

$$\frac{1-Q_b}{\ln Q_b} = -\left(\frac{H_{rms}}{H_{MAX}}\right) \tag{3.26}$$

The maximum wave height before breaking, H_{MAX}, for transition water is (Miche, 1944):

$$H_{MAX} = \frac{1.1}{k}\tanh\left(\frac{0.8kd}{1.1}\right) \tag{3.27}$$

The solution of the parametric wave-action conservation (Eq. 3.15) for the zero-order moment, m_0, provides the significant wave height, H_s:

$$H_s = 4\sqrt{m_0} = \sqrt{16E} \tag{3.28}$$

where the zero order moment, m_0, is calculated as (Holthuijsen et al., 1989):

$$m_0 = E = \int_0^\infty E(f)\,df \tag{3.29}$$

In the most recent version of the WWTM (Carniello et al., 2011), the peak wave period T_p is computed at each time step and at each grid point through an empirical equation relating the wave period to the local water depth and wind speed (e.g., Young and Verhagen, 1996a; Breugem and Holthuijsen, 2007):

$$T_p = a\frac{U_w}{g}\left(\frac{gd}{U_w^2}\right)^b \tag{3.30}$$

The two parameters a and b have been calibrated using data collected from two stations within the Venice Lagoon (stations 1BF and 2BF) (Fig. 3.2), yielding $a = 3.5$ and $b = 0.35$ (Carniello et al., 2011).

Eq. (3.30) assumes fetch unlimited conditions, and its validity is confirmed by the comparison between the measured and the modelled peak wave period (Fig. 3.1). The calibration data only include meteorological conditions characterized by wind speeds larger than 3 m/s, because weaker wind conditions do not generate significant wave height (Carniello et al., 2011).

Zero-dimensional implementation

Fully coupled two-dimensional models are computationally expensive, and may not be adequate to evaluate long-term morphological changes. For this reason, a zero-dimensional version of the WWTM is examined here, with the assumption that waves are fully grown. In this situation, Eq. (3.15) becomes:

$$\frac{\Delta E}{\Delta t} = S \tag{3.31}$$

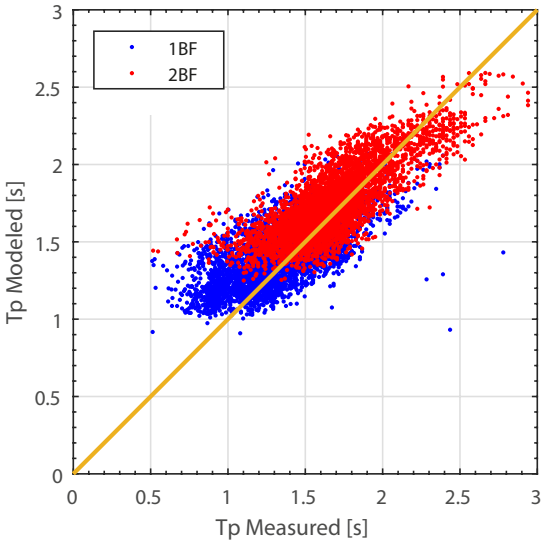

Figure 3.1: Computed versus observed peak wave period at the 2BF and 1BF station within the Venice Lagoon from October 2002 to May 2003. The solid line represents the perfect agreement.

and Eq. (3.31) is solved iteratively by discretizing Eq. (3.32):

$$E_{n+1} = E_n + (\alpha + \beta E_n + S_{bf} + S_{wc} + S_{br})\,\Delta t \tag{3.32}$$

We performed our computations using a time step Δt = 10 s until reaching the conditions of fully developed wave field considering different values of the water depth and wind speed.

3.2.3 Simulating WAve Nearshore (SWAN)

The SWAN model (Booij et al., 1999) does not contain a hydrodynamic module, and is used to calculate exclusively wave parameters, assuming the free surface to be horizontal. Like WWTM, SWAN computes wind wave generation based on Eq. (3.14) and the source terms are written as:

$$S = S_{wg} + S_{bf} + S_{wc} + S_{br} + S_{nl} \tag{3.33}$$

where S_{nl} is the non-linear transfer of wave energy.

For the wind generation term S_{wg}, the linear growth of Cavaleri and Malanotte Rizzoli (1981) and the exponential growth of Komen et al. (1984) were used in our simulations. The process of bottom friction S_{bf} was represented by the drag law model of (Collins, 1972) (Eq. 3.22) considering the dissipation coefficient $C_{bf} = 0.015$. The dissipative process of whitecapping, S_{wc}, is represented by the pulse-

based model of Hasselmann et al. (1973) and applied to finite water depth (Komen et al., 1984):

$$S_{wc} = \Gamma \sigma \frac{k}{\tilde{k}} \tag{3.34}$$

$$\Gamma = C_{ds} \left((1-\delta) + \delta \frac{k}{\tilde{k}} \right) \left(\frac{\gamma_{wc}}{\gamma_{PM}} \right)^{p} E \tag{3.35}$$

where we set the theoretical value of γ for a Pearson-Moskowitz spectrum ($\gamma_{PM} = 0.0000208$) and the tunable coefficients ($C_{ds} = 0.00302$, $p = 2$ and $\delta = 0$). The depth-induced breaking source term, S_{br}, in SWAN is computed by the Battjes and Janssen (1978) model and we consider a constant breaking parameter equal to 0.78. The non-linear wave-wave interactions S_{nl} were disabled because, as demonstrated by Mariotti and Fagherazzi (2013b), the formulation produced changes in wave height and wave period less than 0.01% and for very shallow water depth we did not find any influence. A spectral discretization of $\Delta\sigma/\sigma = 0.1$ and $\Delta\theta = 10^{\circ}$ are used and at the boundary, the significant wave height and the wave period were set equal to zero.

3.2.4 Analysis of the bed shear stresses

The wave properties calculated by the considered wind-wave models are then used to compute the bed shear stress induced by wind waves τ_b [Pa]. τ_b (BSSw) is the quantity that geomorphic models compare to the critical bed shear stress, τ_c, to determine whether sediment is resuspended and reads:

$$\tau_b = \frac{1}{2} \rho f_w U_{ov}^2 \tag{3.36}$$

where ρ is the is water density (1027 kg/m^3), f_w is the friction factor and U_{ov} is the wave orbital velocity at the bed computed as:

$$U_{ov} = \frac{\pi H_s}{T_p \sinh(kd)} \tag{3.37}$$

In Eqs. (3.36) and (3.37), the quantities H_s, k, T_p are dependent on the outputs of wind-wave models. However, the friction factor f_w is independently determined. U_{ov} in the SWAN model (Eq. 3.36) equals the root-mean-square value (in m/s) of the maxima of the orbital motion near the bottom (U_{bot}), the latter being directly computed by SWAN.

Friction factor

The friction factor, f_w, may be computed following different approaches. One of the approaches (Mariotti and Fagherazzi, 2013b) sets the wave friction factor f_w equal to the bed friction coefficient C_{bf} (i.e., $f_w = 0.015$) of the Collins's equation (Eq. 3.22).

Some other equations were used for the computation of friction factor, such as:

$$f_w = 0.04 \left(\frac{U_{ov} T_p}{2\pi k_b} \right)^{-0.25} \tag{3.38}$$

$$f_w = 0.4 \left(\frac{H_s}{k_o \sinh kd} \right)^{0.75} \tag{3.39}$$

$$f_w = exp \left(5.213 \left(\frac{2.5 D_{50}}{\frac{T_p U_{ov}}{2\pi}} \right)^{0.194} - 5.977 \right) \tag{3.40}$$

Eq. (3.38) with $k_b = 2D_{90}$ [mm] is used by Mariotti et al. (2010), Eq. (3.39) with $k_0 = 1$ [mm] by Mariotti and Fagherazzi (2013a), Mariotti and Carr (2014), and Kirwan et al. (2016b) and Eq. (3.40) by Swart (1974) and Kakeh et al. (2016).

In other approaches, the calculation of f_w is based on the wave Reynolds number, Re_w (Soulsby, 1997; Soulsby and Whitehouse, 2005).

$$Re_w = \frac{U_{ov}^2 T_p}{2\pi\nu} \tag{3.41}$$

where ν is the kinematic viscosity and U_{ov} is the wave orbital velocity at the bottom.

Some studies systematically calculate f_w in rough turbulent flow conditions (Fagherazzi et al., 2006; Fagherazzi et al., 2007; Marani et al., 2007; Marani et al., 2010; D'Alpaos et al., 2012). In this case f_w reads:

$$f_{wr} = 1.39 \left(\frac{U_{ov} T_p}{2\pi \frac{2.5 D_{50}}{30}} \right) \tag{3.42}$$

However, other authors (e.g., Carniello et al., 2011; D'Alpaos et al., 2013; Carniello et al., 2016) calculate f_w in smooth turbulent flow conditions and laminar flow, employing the following relationships:

$$\text{If} \qquad Re_w > 150000 \qquad f_{ws} = 0.0521 Re_w^{-0.187} \tag{3.43}$$

$$\text{If} \qquad Re_w \leqslant 150000 \qquad f_{ws} = 2Re_w^{-0.5} \qquad (3.44)$$

The friction factor is then calculated as the maximum of these two values, i.e., $f_w = max(f_{wr}, f_{ws})$. In our analyses and simulations we applied the latter described procedure.

3.3 DATA SET AND STUDY AREA

The Venice Lagoon is the largest lagoon within the Mediterranean Sea. Due to the rich maritime history of the area, and its commercial importance over the last half millennium, the Lagoon has one of the richest worldwide datasets of bathymetry, wind, and waves (D'Alpaos, 2010a; D'Alpaos, 2010b; Carniello et al., 2011). The Lagoon is currently characterized by a mean water depth of 1.5 m, excluding channel networks dissecting tidal and subtidal platforms. The maximum tidal excursion around Mean Sea Level (MSL) is ± 0.70 meters.

In this study we used wind speeds, wind directions, wave periods, wave heights and water depths recorded from October 2002 to May 2003 at two stations within the Lagoon. The first station (1BF) is located on a shoal in the northern part of the lagoon where the tidal flat has a depth of -1.10 a. MSL. The second station (2BF) is located in a deeper area in the central-southern part of the lagoon (Fondo dei Sette Morti) with the tidal flat depth of -2.10 a. MSL (Fig. 3.3). The wind climate of the Venice Lagoon features two winds: the most frequent and intense wind is Bora which blows from North-East. The the second most frequent wind is the Sirocco, blowing from South-East (Fig. 3.2). In our analyses we only considered winds whose directions are included in the range 0°–90° (i.e., North-East quadrant) which is representative of the predominant wind of the Venice Lagoon.

Beside the application of the different numerical models presented before, carried out considering simplified domains and synthetic boundary conditions performed for investigating the effect of the different approaches, the full fladged bi-dimensional model (WWTM) was applied to six different configurations of the Venice Lagoon described in details in the second and third chapters of the present thesis. In particular, we compute the wind-wave field by considering: a) the configuration of 1611 reconstructed from the historical map by Sebastiano Alberti (Tommasini et al., 2017); b) the configuration surveyed at the beginning of the 19th century by the Napoleonic Captain A. Dènaix (1809-1811) (D'Alpaos and Martini, 2005; D'Alpaos, 2010a); c) the configuration dating back to the beginning of the 20^{th} century (1901) (Carniello et al., 2009; D'Alpaos, 2010a) ; the configurations derived from the surveys carried out by the Venice Water Authority in

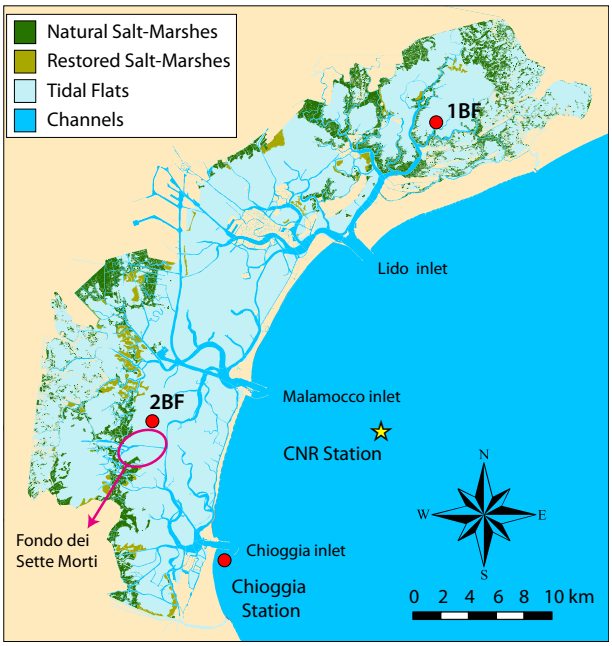

Figure 3.2: Spatial distribution of the main morphological features characterizing the Venice Lagoon. The location of the two stations (1BF and 2BF) within the Lagoon and of the anemometric (Chioggia) and mareographic (CNR Oceanographic Platform) stations are also shown.

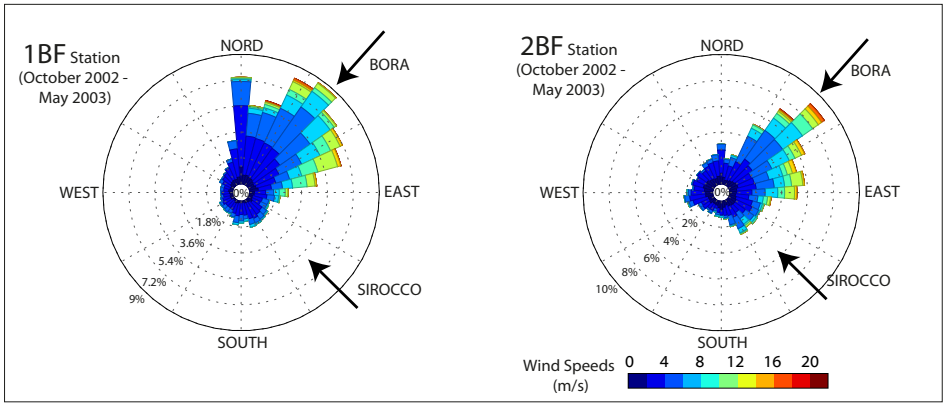

Figure 3.3: Wind rose of 1BF and 2BF stations in the period October 2002 - May 2003

1932 (d) and in 1970 (e) (Carniello et al., 2009; D'Alpaos, 2010a); and the present (2012) configuration (f) (Carniello et al., 2009; D'Alpaos, 2010a) updated by including the recent morphological modifications (almost completed in 2012) introduced at the three inlets by the construction of the movable gates for protecting Venice from high tides (Mo.S.E Project).

3.4 RESULTS AND DISCUSSIONS

The models considered in this study range in complexity and have been variously used by numerous authors. We wish to explore how the wave predictions, and ultimately predictions of bottom shear stress, differ between these models. We therefore run models (both numerical and analytical) over a range of parameter values. We used two different values of the median grain size D_{50} (i.e., 20 and 600 μm), a range of water depths between 0 to 3 m typical of the tidal flats in shallow tidal systems, and a set of wind velocities between 4 to 16 m/s that are characteristic for the Venice Lagoon (Fig. 3.3). We also run a one-year-long complete simulation using the fully coupled bidimensional model (WWTM) for the whole Venice lagoon in six different configurations, in order to evaluate the evolution of the mean wave height and of the mean and maximum bottom shear stresses induced by wind waves (τ_b).

3.4.1 Zero-dimensional simulations

We compare the results retrieved from two zero-dimensional models (see Fig. 3.4): the Young and Verhagen equations (Y&V) as described in Sec. (3.2.1) and the WWTM used zero-dimensional implementation (0D WWTM) described in Sec. (3.2.2). Model results are compared to the measured data collected in the two stations within the Venice Lagoon, 1BF and 2BF (Fig. 3.2). We recall that the 0D WWTM assumes that waves are fully developed so the fetch length is not considered in the equations, whereas the empirical equations of Y&V consider the fetch length. In the Y&V equations we used the fetch length retrieved considering the direction of the Bora wind (i.e., North-East), that is 4,5 km for the 1BF station and 12,5 km for the 2BF station.

Model results and field observations show (Fig. 3.4) that the wave height increases with the water depth and wind velocity for small (1BF) and greater (2BF) fetches. The wave height obtained with Y&V equations is generally higher than the wave height obtained with the 0D WWTM for water depths lower than 1 m, while for water depths larger than 1 m the wave heights tend to reach a constant value, irrespective of the water depth and lower than the value obtained with 0D WWTM. The different behaviour is due to the equations employed in the two different models and to the different simplifications. For lower water depth the white capping term prevents the wave growth in the WWTM, while for larger water depth the fetch unlimited condition allows the formation of higher waves. On the contrary the imposed fetch length limits the wave growth in the Y&V equations. Moreover the Y&V equations were developed specifically for water

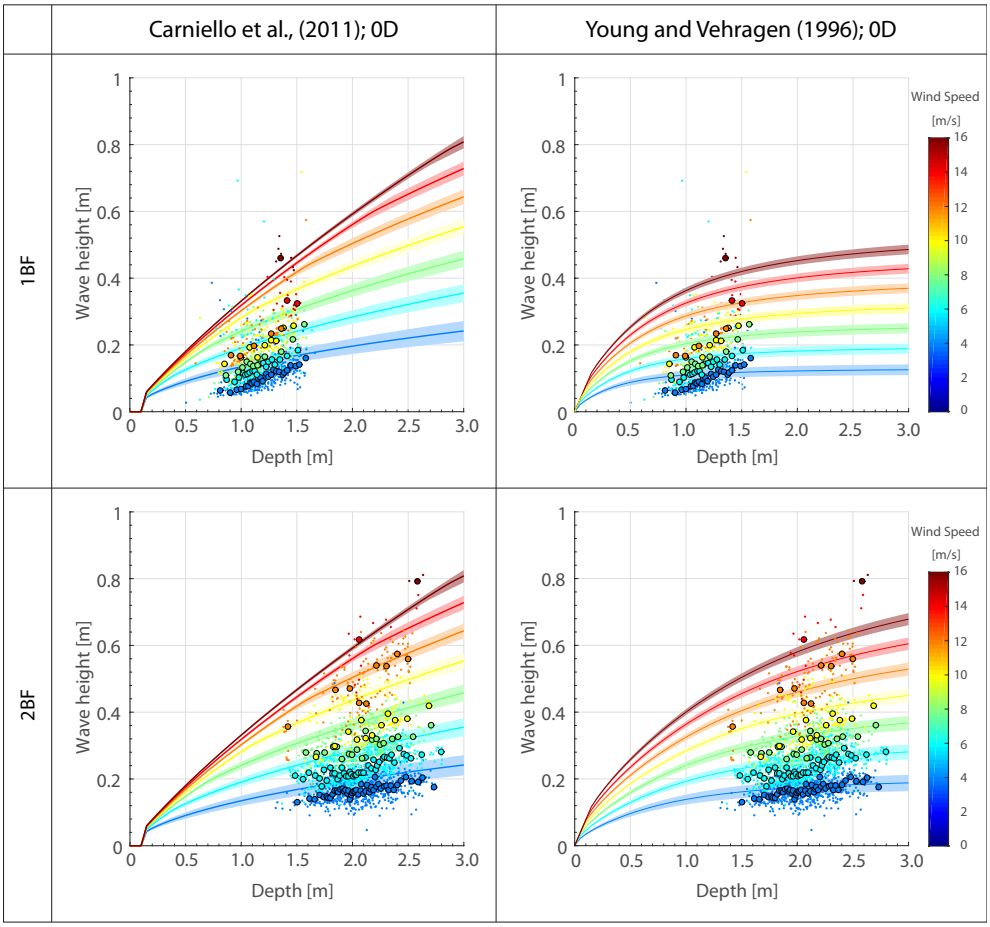

Figure 3.4: Wave height computed with the zero-dimensional version of WWTM (Carniello et al., 2011) (on the left) and with Young and Verhagen equations (Young and Verhagen, 1996a; Young and Verhagen, 1996b) (on the right) for different wind velocities and water depths. In the 0D version of WWTM the fetch in both the station is unlimited and the wave period depends from the depth and the wind velocity (Eq.3.30). Young and Verhagen equations consider limited fetch length 4.5 km for 1BF and 12.5 for 2BF and the period is computed with Eq. 3.6. The shaded areas define an interval of $\pm 0,5$ m/s around the selected wind velocity. The small dots are all the measured data while the circles indicate values obtained by averaging data points over intervals of 15 data to emphasize the overall trend.

depth of 2 m and the applications for other water depth is an extrapolation.

In both zero-dimensional models the results show that the significant wave heights are easier to capture for the 2BF than the 1BF station. Indeed, the first station (2BF) is located in a deeper area in the Southern part of the lagoon (Fondo dei Sette Morti) (Fig. 3.2) where fetch unlimited conditions occurr, while the second one (1BF) is located on a shoal in the Northern part of the lagoon (San Felice marsh) (Fig. 3.2) with irregular fetch and bathymetry.

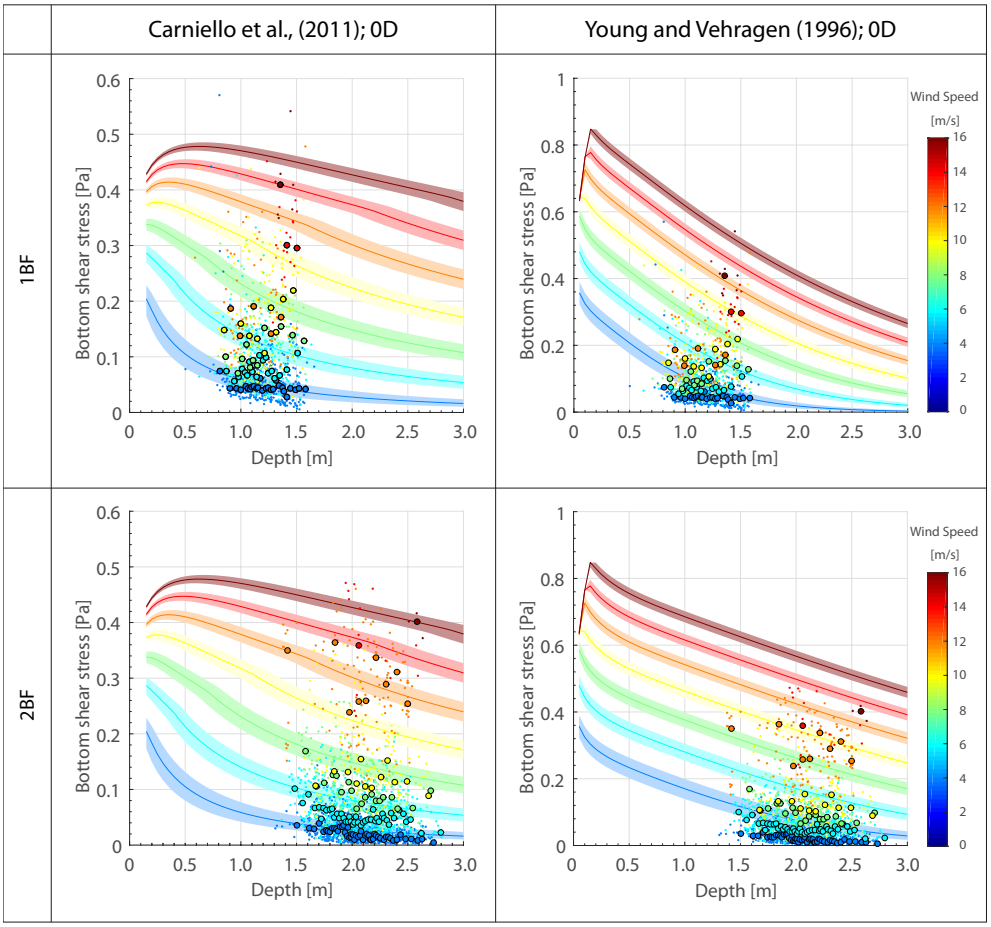

Figure 3.5: Bottom shear stress induced by wind waves computed with the zero-dimensional version of WWTM (Carniello et al., 2011) (on the left) and with Young and Verhagen equations (Young and Verhagen, 1996a; Young and Verhagen, 1996b) (on the right) for different wind velocities and water depths. The shaded areas define an interval of $\pm 0,5$ m/s around the selected wind velocity. The small dots are all the measured data while the circles indicate values obtained by averaging data points over intervals of 15 data to emphasize the overall trend. The bottom shear stress both for models and data was calculated with $D_{50} = 20\mu m$.

We used the wave height obtained from the two zero-dimensional models to calculate the bottom shear stress induced by waves, BSSw. We tested two different values of medium grain size D_{50} of tidal flats, i.e., 20 µm and 600 µm. For both cases we evaluated the BSSw by using the Soulsby and Whitehouse (2005) approach described in Sec. (3.2.4). We chose D_{50} = 20 µm that is a typical value for the tidal flats of the Venice Lagoon (Venier et al., 2014). Then we selected a higher value of D_{50} equal to 600 µm with the aim of accounting for the presence of bedforms, vegetation, shell fragments and for the effects of bioturbation. In the first case (Fig. 3.5), due to the lower Reynolds number, we always fall in the laminar flow condition (Eq. 3.44), while in the second case (Fig. 3.6), due to the increase in friction factor,

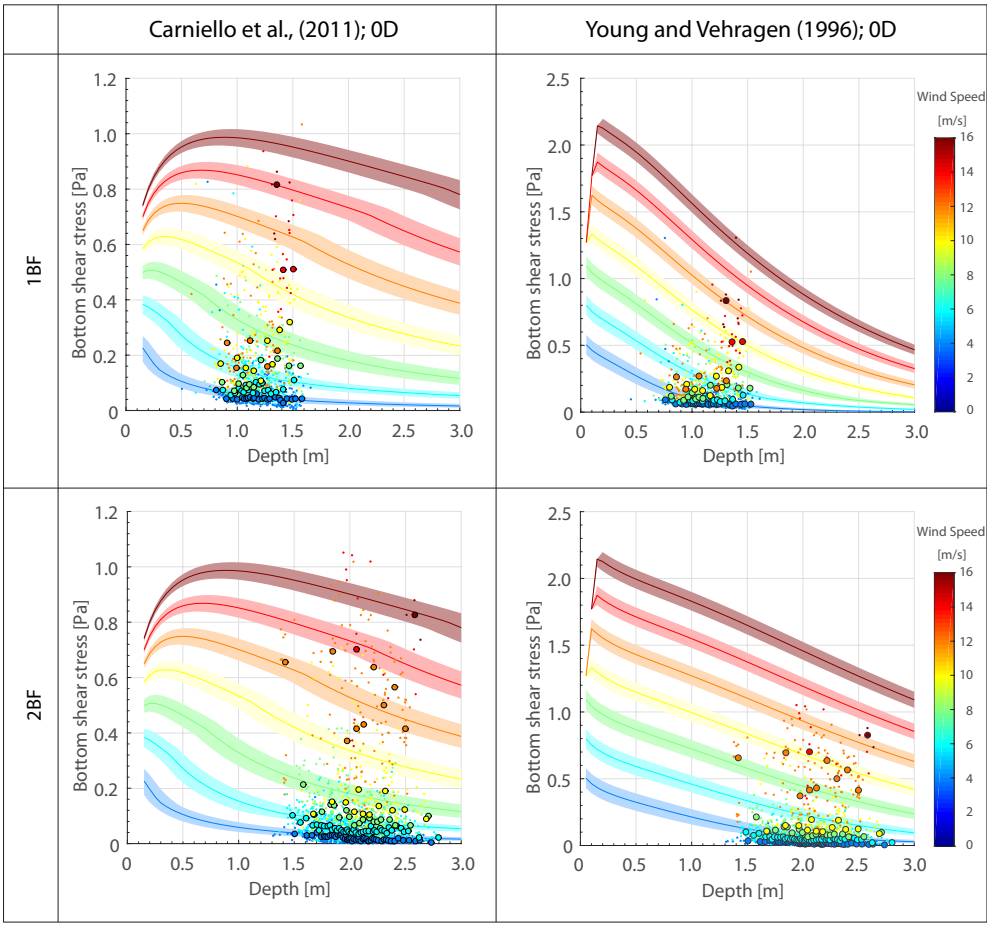

Figure 3.6: Bottom shear stress induced by wind waves computed with the zero-dimensional version of WWTM (Carniello et al., 2011) (on the left) and with Young and Verhagen equations (Young and Verhagen, 1996a; Young and Verhagen, 1996b) (on the right) for different wind velocities and water depths. The shaded areas define an interval of $\pm 0,5$ m/s around the selected wind velocity. The small dots are all the measured data while the circles indicate values obtained by averaging data points over intervals of 15 data to emphasize the overall trend. The bottom shear stress both for models and data was calculated with D_{50} = 600 µm.

rough turbulent flow conditions occur and the Eq. (3.42) is applied. It is worth noting that the value of 600 µm was selected also to allow the transition between laminar to rough turbulent flow, that was prevented when we considered $D_{50} < 600$ µm.

It is important to remind that measured BSSw was, indeed, calculated through the Eq. 3.36 on the basis of the measured water depths, wave periods, wave heights and wind velocities, because no direct measures of BSSw are available. The friction factor f_w is the maximum between f_{wr} (Eq. 3.42) and f_{ws} (Eqs. 3.44 and 3.43) (Soulsby and Whitehouse, 2005).

Considering the results illustrated in Figs. 3.5 and 3.6, the analysis with zero-dimensional models shows that the effects of the different model assumptions on the computation of wave periods and heights cannot be neglected. In particular, the relationship between BSSw and water depth presents different behaviours when different models are considered. Two results emerge: first, differences are higher for small depths; second the maximum values reached with the Y&V equations are usually larger than the maximum values obtained with 0D WWTM approach. Moreover with the variable wave period and friction factor considered herein, we did not retrieve the same relationschip between BSSw and depth obtained in previous studies, where the wave-induced shear stresses peaks at a specific water depth which is a function of the local wave climate and fetch distance. Unlike our analysis, those studies considered a constant peak wave period (Fagherazzi et al., 2006; Fagherazzi et al., 2007; Marani et al., 2010) or a constant friction factor (Mariotti and Fagherazzi, 2013b; Lauzon et al., 2018). In particular, we only obtained the decreasing branch with Y&V (Figs. 3.5 and 3.6). This means that, applying these empirical equations to determine the wave height and period, wind-waves might induce erosion also for very low depths, thus artifically deepening tidal flat bottoms (with consequences on wave generation and propagation, and on wave characteristics) and preventing the transition from tidal-flat to salt-marsh equilibrium states. With the 0D WWTM we obtained a curve that peaks between 0 and 0,5 m for wind velocities greater than 10 m/s (Fig. 3.5) and D_{50} = 20 μm, while the curve reaches the maximum between 0 and 1 m for wind velocities greater than 8 m/s and D_{50} = 600 μm. The BSSw is more than doubled by the increase in median grain size (from D_{50} = 20μm to D_{50} = 600μm), according to both the 0D WWTM and Y&V approaches. In our view, the results obtained with D_{50} = 600 μm seem to be more realistic: in fact, if one considers the results of 0D WWTM (Fig. 3.5) and a critical bottom shear stress typical of the Venice Lagoon or other lagoons worldwide (τ_c = 0,3 - 0,4 Pa) (Amos et al., 2004; Marani et al., 2010; Mariotti et al., 2010; D'Alpaos et al., 2013) the erosion of tidal-flat surfaces could be triggered by wind velocities larger than 8 m/s.

Finally, the comparison between data and model results shows that 0D WWTM allows one to obtain a better agreement with the observations, in particular when low wind velocities (4 and 6 m/s) and larger fetches, close to the fetch unlimited conditions are considered, as for the 2BF station. It is indeed worthwhile to point out that data are only available for water depths in the range 0.7-2.8 m. In our view, the relationship between BSS and water depth for very shallow water depths (i.e. < 0.5 m), and therefore the shape of the rising branch

of the curve, deserves further investigation possibly once additional field data are available.

3.4.2 One-dimensional simulations

We run several simulations within a schematic one-dimensional rectangular computational grid to compare the previously described bi-dimensional models WWTM (Sec. 3.2.2) and SWAN (Sec. 3.2.3), considering controlled and simplified conditions.

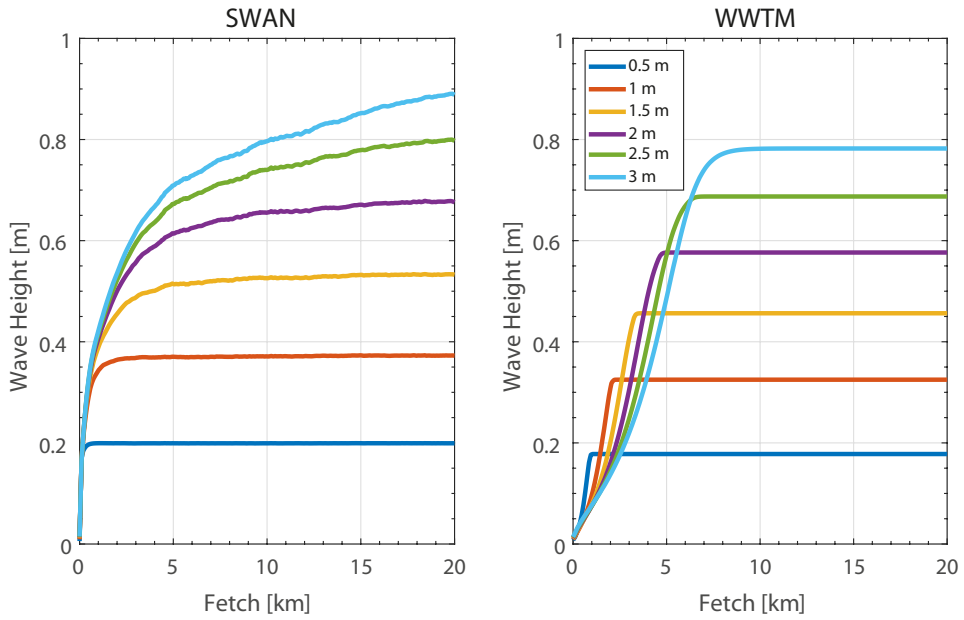

Figure 3.7: Wave height for different water depth and constant wind velocity of 15 m/s obtained applying SWAN (on the right panel) and WWTM (on the left panel) on a 1D rectangular domain.

In order to compare the two models we considered a computational grid consisting in a 20 km long and 10 km wide rectangular basin and characterized by a constant water depth, forced with a spatially uniform wind of 15 m/s blowing along the main axis of the domain, with no currents, and we computed the wave height along the domain. In both models, wave height increases with fetch and water depth (Fig. 3.7). The comparison shows that, at the end of the computational grid when fully developed conditions are likely to occur, the wave height reaches similar values (Fig. 3.8), although the SWAN model always provides the highest value. The main differences between the two models occur before the fetch unlimited condition is reached, and in particular, in the first 7 km of the domain. With a wind velocity of 15 m/s, the WWTM suggests that fully developed conditions are reached, for all the analysed water depths, at the end of the domain, whereas SWAN suggests that, for water depths greater than 2 m, the

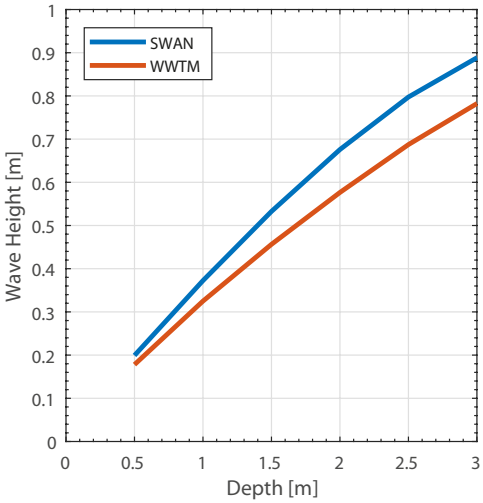

Figure 3.8: Wave height for different water depth and constant wind velocity of 15 m/s obtained at the end of the one-dimensional rectangular domain (20 km) applying SWAN and WWTM.

wave height keeps growing also after 20 km. Furthermore, SWAN model suggests that, for the different water depths considered, when the wind starts blowing, the waves grow and wave heights resemble the same path. On the contrary, the WWTM suggests wave growth to be faster for low water depth. This means that small fetches cause the wave height to increase as the water depth decreases (Fig. 3.7), and that the fetch unlimited condition is reached first in shallower areas and later in higher depth regions. This behaviour could be ascribed to the fact that, overall, the inertia of the system increases with water depth and, as a result, the fetch length needed for waves to grow is larger for high water depths relatively to low depths. In the wave action conservation equation, this behaviour depends on the wind generation term and on the related parameters.

We also compare the wave height obtained for different wind speeds with the two one-dimensional models (Figs. 3.9 and 3.10). Fig. 3.9 shows the wave height reached at the end of the computational domain (20 km). The results show that wave heights predicted by the WWTM are higher than those obtained with SWAN when one considers low velocities of 4 and 6 m/s, and that when we apply higher values of wind speed of 8, 10, 12, 14 and 16 m/s the SWAN model provides higher wave heights than the WWTM. In general, however, differences are quite limited and never exceed 10 cm.

With the aim of comparing the modelled wave heights with the data in Fig. 3.10, we compared model results with the data recorded in the 1BF and 2BF stations. In this case, we have considered the actual fetches (calculated from the North-East direction) of the two

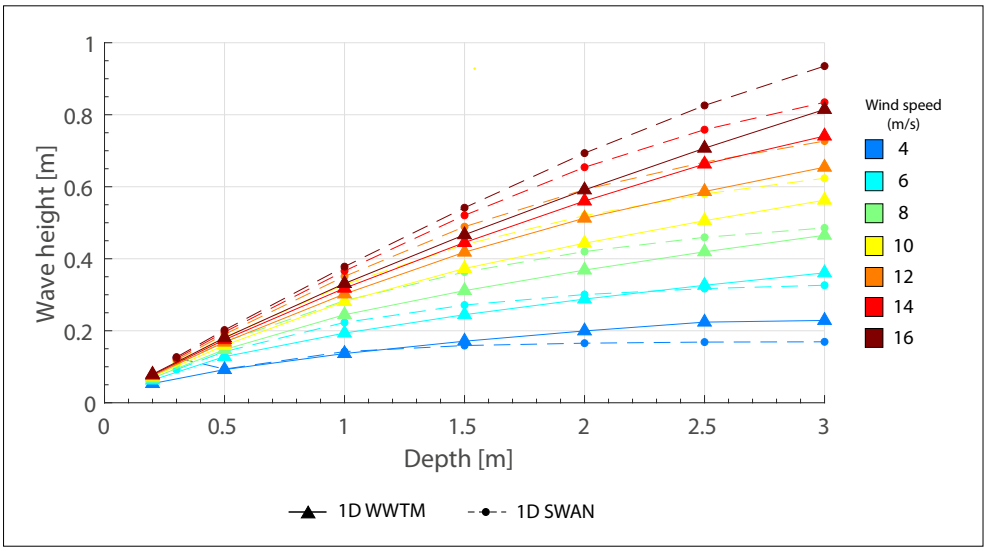

Figure 3.9: Comparison of the wave height at the end of the computational domain (fetch = 20 km) with the 1D WWTM and 1D SWAN models. The results were obtained with different water depths and wind speeds.

stations (4,5 km for 1BF and 12,5 for 2BF) and have applied the bi-dimensional models to two rectangular grids, 4,5 and 12,5 km long, respectively. The wave height measured at 2BF station, close to the fetch unlimited condition, is well described by both the models (bottom plot in Fig. 3.10) except for wave heights obtained with WWTM, for water depths between 2,5 and 3 m and wind speed of 4 m/s. Both SWAN and WWTM seem to be unable to capture wave heights measured at the 1BF station (Fig. 3.10, top plot). In particular, for wind speeds of 10, 12 and 14 m/s the SWAN and WWTM models overestimate the wave height. We speculate this can be ascribed to the highly irregular morphology of the northern lagoon, where the 1BF station was located, compared to the central-southern part. The morphological characteristics of the northern lagoon are indeed likely to affect the wind field and making it difficult to estimate a correct fetch length for any single location. We further observe that the wave height computed with the WWTM for a constant wind speed decreases with the increasing of water depth, as it also emerges from Fig. 3.7 for a wind speed of 15 m/s. In fact, the fetch unlimited condition is reached first for lower depths and later for higher water depths. This behaviour is emphasized as wind speed decreases.

We computed the BSSw for two different median grain sizes, in fetch unlimited conditions (Fig. 3.11) and we compared model results with field data (Figs. 3.12, 3.13). Using D_{50} = 20 µm we always fall in the laminar flow regime, either we consider fetch unlimited conditions (top plots in Fig. 3.11) or fetch limited ones (top plots in Figs. 3.12 and 3.13). When we apply the two models with a higher value of median grain size, in order to use Eq. 3.42 we need D_{50} = 600

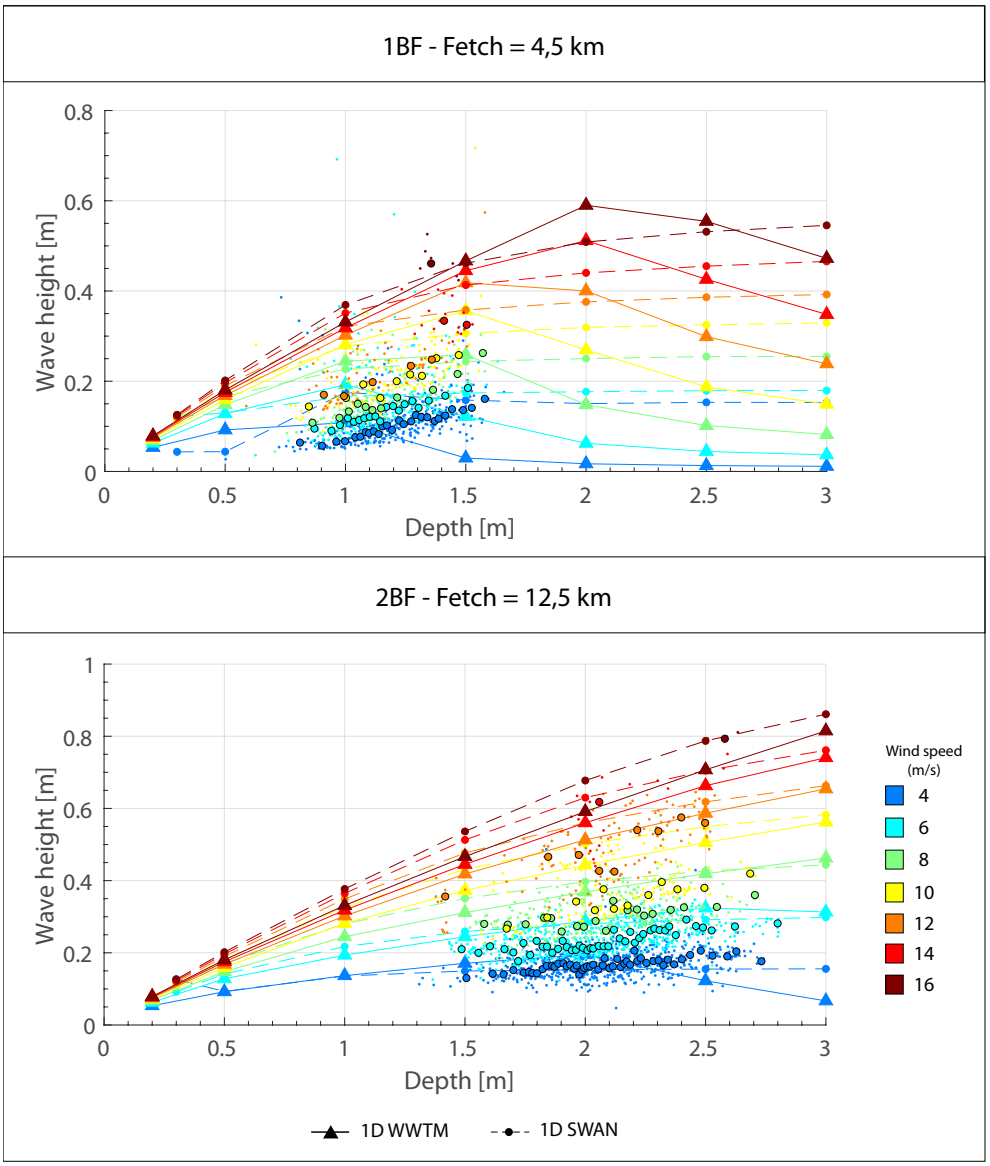

Figure 3.10: Comparison of measured wave height with predictions of the 1D WWTM model and the 1D SWAN model. Different fetch lengths were considered, namely 4,5 km (1BF station) and 12,5 km (2BF station).

μm for the WWTM and D_{50} = 2000 μm for SWAN model (Figs. 3.11 and 3.13). Despite the artificial increase in D_{50} in SWAN, which can hardly be associated to the presence of any realistic bedform, the BSSw computed with WWTM are always higher than those obtained from SWAN. This is partially due to the different ways the wave peak period T_p is computed and partially to the wave orbital velocity at the bed U_{ov}. It is worth noting that the two models produce more similar results when the water depth increases (Figs. 3.11, 3.12 and 3.13).

With the fetch unlimited condition (Fig. 3.11), both for greater and lower D_{50}, the BSSw decreases when the depth increases for wind speeds of 4, 6 and 8 m/s, while with strong wind conditions (>12

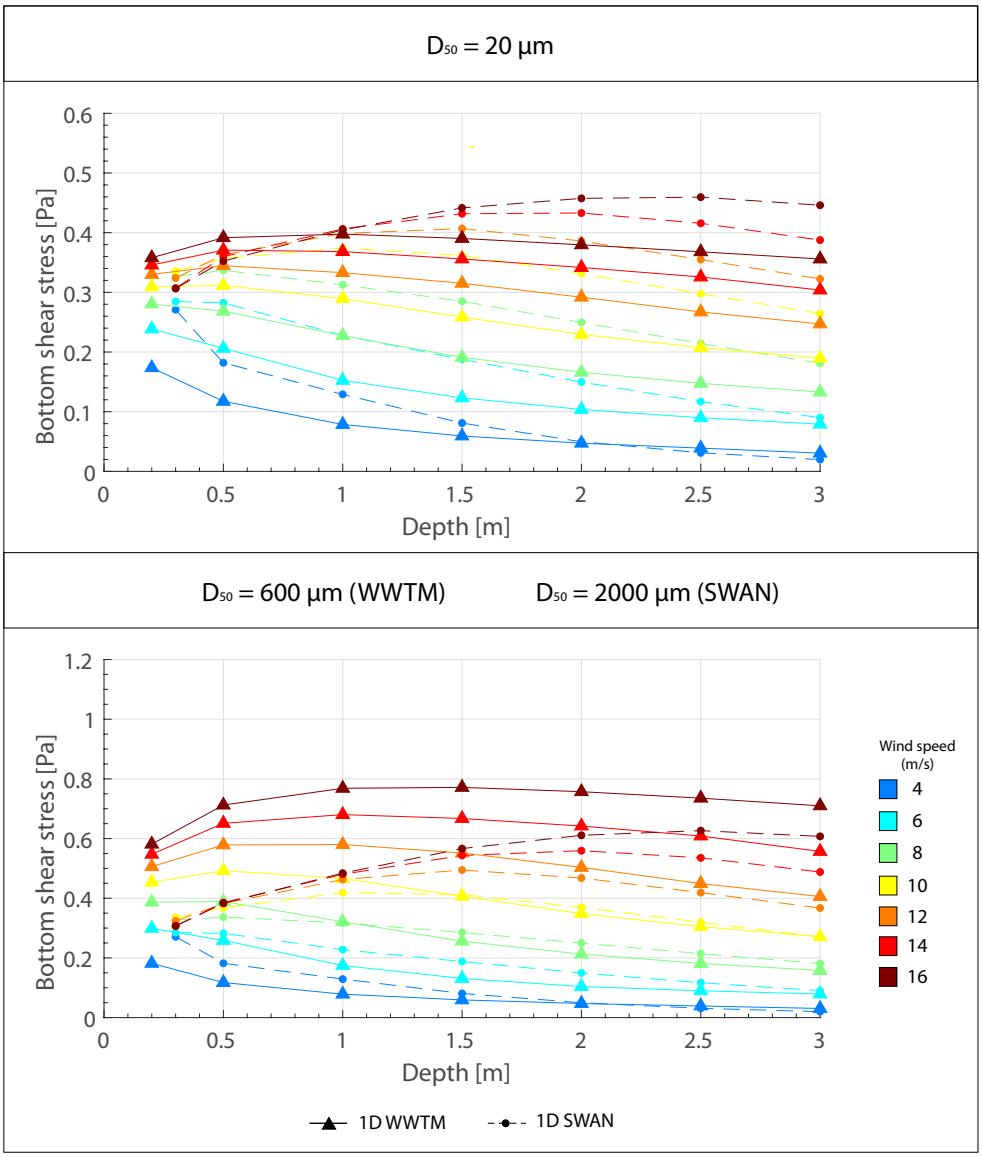

Figure 3.11: Comparison of bottom shear stresses at the end of the computational domain (fetch = 20 km) with the 1D WWTM and 1D SWAN models. The results were obtained with different water depths and wind speeds. Two values of medium grain size were considered: a lower value of 20 µm (top) and a higher value (bottom).

m/s) the BSSw peaks at some intermediate water depths between 0.5 and 1 m with WWTM and between 2 and 2.5 m with SWAN. Fig. 3.12 shows the comparison between the data and the BSSw computed with the two models and D_{50} = 20 µm. Model results from both models fit quite well the data when one considers low wind speeds (4 and 6 m/s) and higher water depths. Moreover, model results for the 2BF station, that approximates the fetch unlimited condition, better fit field observations. We observe the same behaviour in Fig. 3.13 with a higher median grain size. In this case, for a lower fetch (top

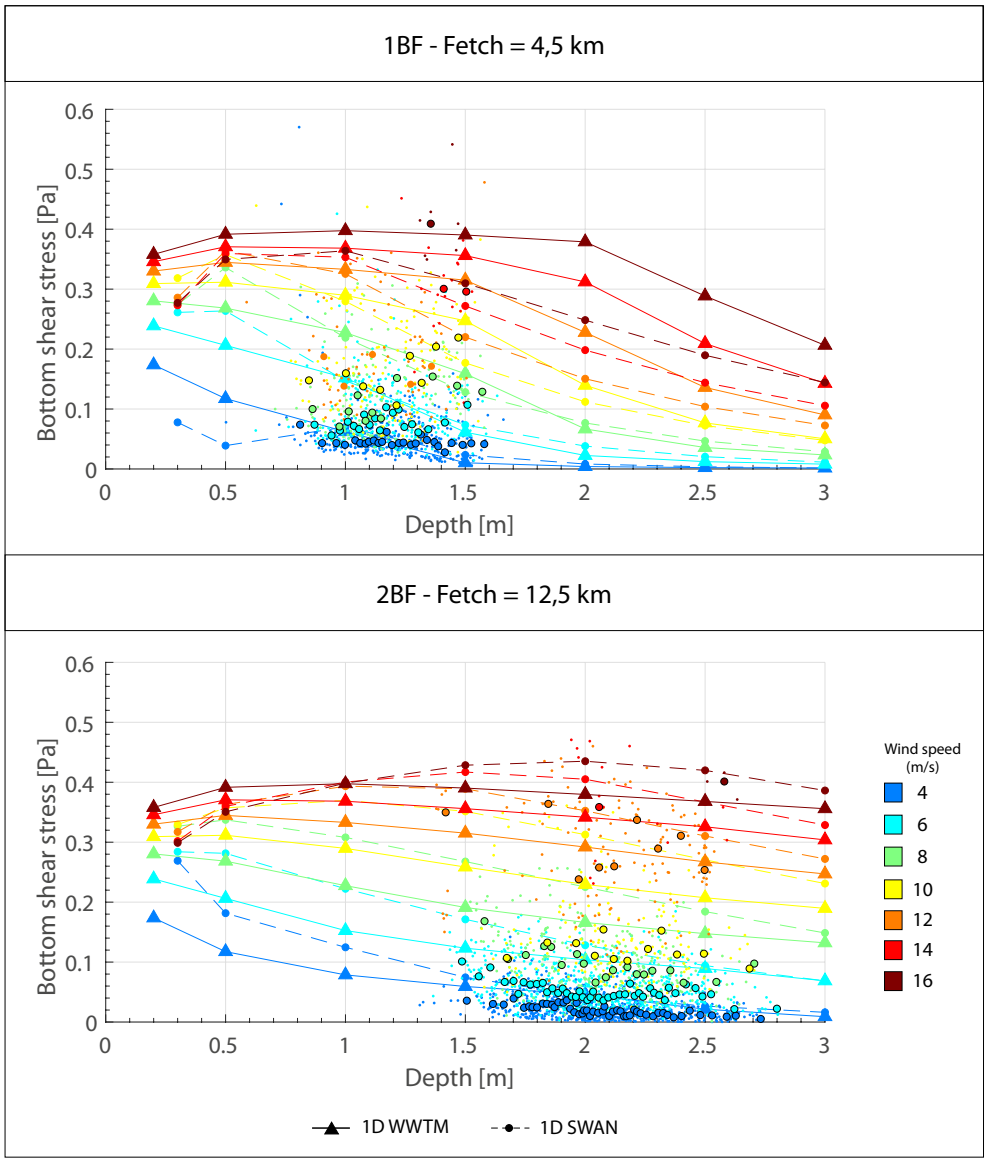

Figure 3.12: Comparison of measured bottom shear stress with the results of the 1D WWTM model and the 1D SWAN model. Different fetch lengths were considered, namely 4,5 km (1BF station) and 12,5 km (2BF station). D_{50} = 20 µm was used as the medium grain size.

plot in Fig. 3.13) the bottom shear stress increases with the deepening, peaks at some point between 0.5 and 1.5 m and then starts to decrease. On the contrary, when close to the fetch unlimited condition (bottom plot in Fig. 3.13) the BSSw seems to be quite independent from the water depth.

3.4.3 Two-dimensional simulations

We finally extended our analysis to the actual two-dimensional domain of the Venice Lagoon. We applied the fully coupled Wind-Wave

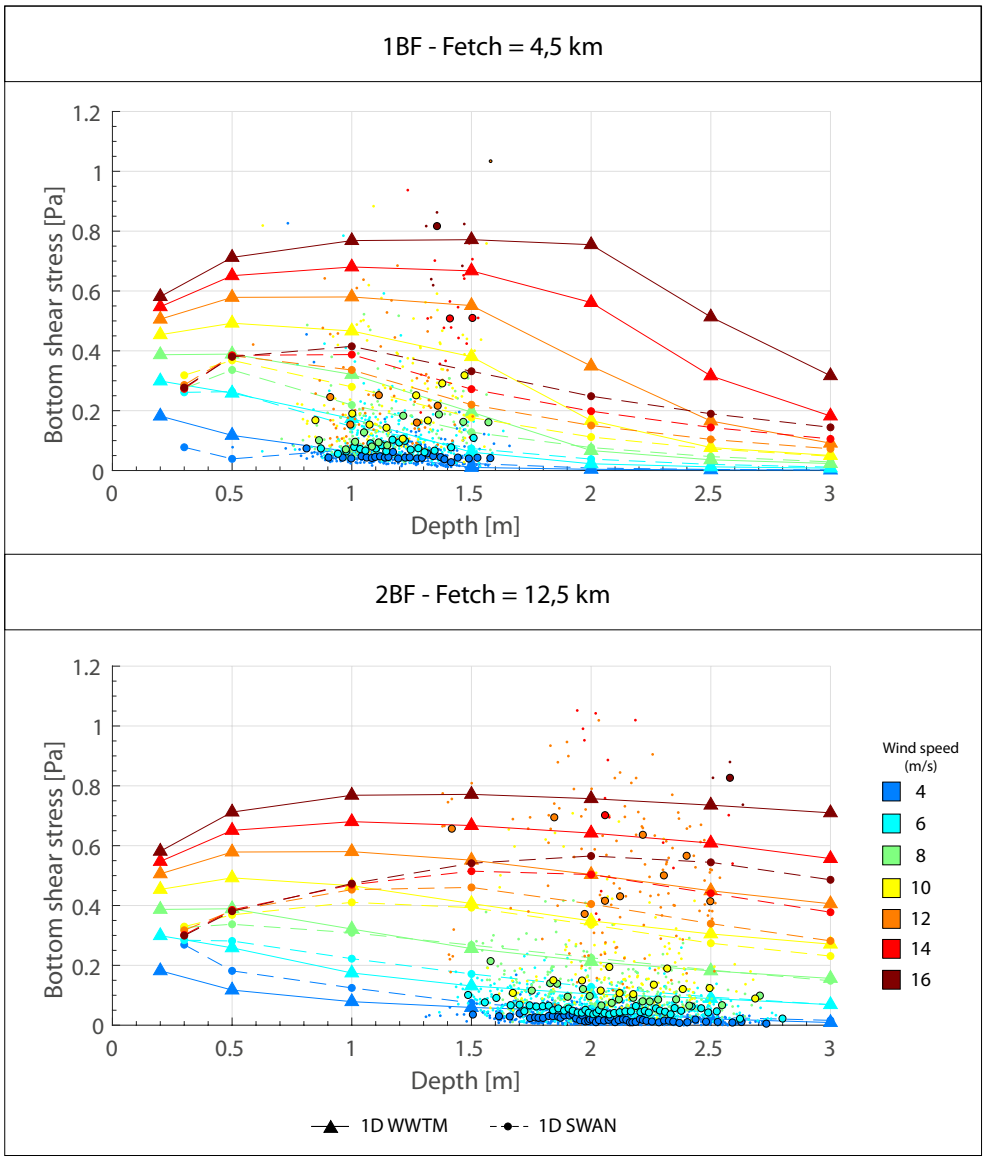

Figure 3.13: Comparison of measured bottom shear stress with predictions of the 1D WWTM model and the 1D SWAN model. Different fetch lengths were considered, namely 4,5 km (1BF station) and 12,5 km (2BF station). D_{50} = 600 µm was used as the medium grain size in WWTM, while D_{50} = 2000 µm was used in SWAN model.

Tidal Model (WWTM) to evaluate the wind-wave field and the related bottom shear stress (BSSw) for the six selected configurations of the lagoon (namely 1611, 1810, 1901, 1932, 1970 and 2012), thus covering a time span of four centuries.

The numerical simulations were carried out by imposing as boundary conditions tidal levels (measured at the CNR station, see Fig. 3.2) at the inlets and wind velocities and directions (measured at the Chioggia Station) collected in the Venice Lagoon in 2005, a representative year in terms of wind forcings for the period between 2000 and 2008

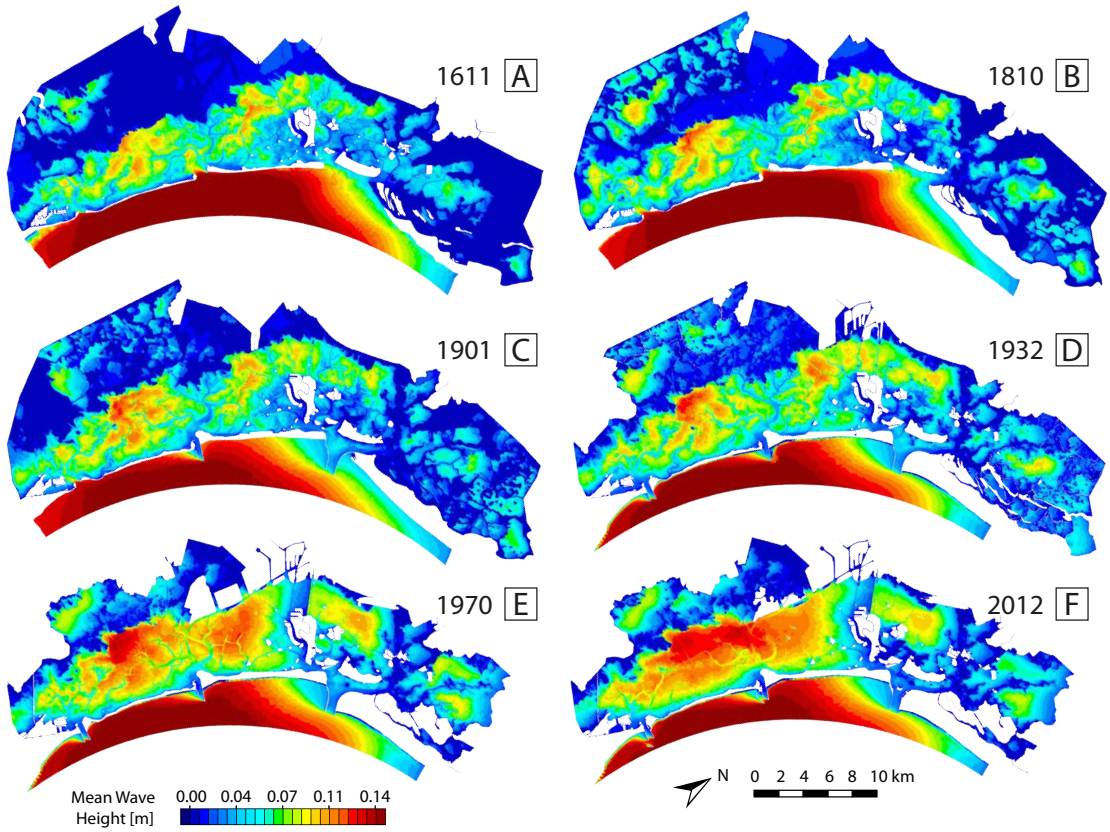

Figure 3.14: Color-coded representation of the mean wave height for the different configurations of the Venice Lagoon 1611 (A), 1810 (B), 1901 (C), 1932 (D), 1970 (E), and 2012 (F).

(D'Alpaos et al., 2013; Carniello et al., 2016). The WWTM provides, at each location within the Venice Lagoon, the temporal evolution (time interval: thirty minutes) of significant wave heights and bottom shear stresses induced by wind waves. The friction factor at each location of the Lagoon, such as in previous works (e.g., D'Alpaos et al., 2013), were calculated by using D_{50} = 600 μm and the method proposed by Soulsby and Whitehouse (2005) in order to account for bottom irregularities.

Fig. 3.14 shows the mean wave height averaged over the one-year simulation. We see a slow increase in wave height from 1611 to 1932, while the two most recent Lagoons are characterize by a rapid increase in wave height. In agreement with the results of zero and one dimensional models, the higher wave height are located were fetch is larger and tidal flats are deeper, i.e., in the central southern part of the lagoon between the Lido and Chioggia inlets. On the contrary the northern part of the lagoon, protected by salt marshes and by the mainland, displayed lower wave heights.

Before evaluating the mean bottom shear stress induced by wind waves (Fig. 3.15), it is worthwhile recalling the relationship between

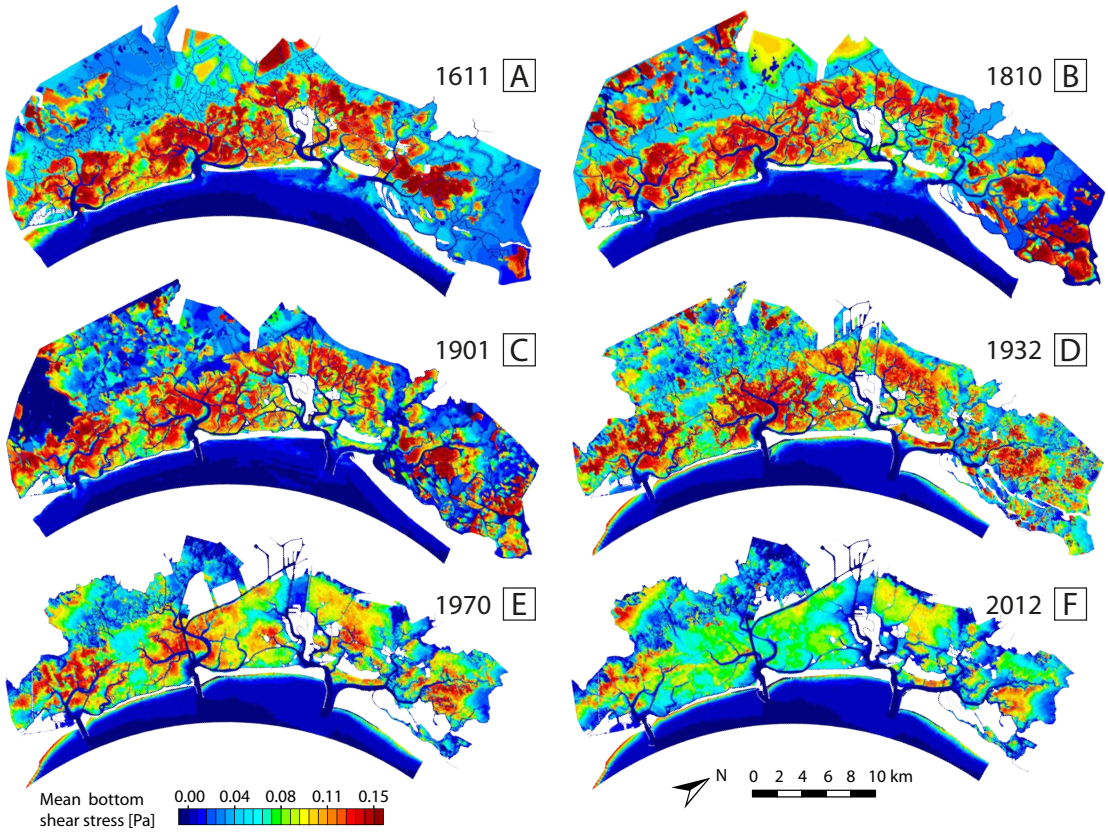

Figure 3.15: Color-coded representation of the mean bottom shear stress induced by waves for the different configurations of the Venice Lagoon 1611 (A), 1810 (B), 1901 (C), 1932 (D), 1970 (E), and 2012 (F).

BSSw, water depth and wind velocity obtained with the zero-dimensional version of WWTM. The mean BSSw increases until 0.5 m and then starts to decrease again. In other words the BSSw deceases for water depth higher than 0.5 m, regardless of the considered wind speed. The above mentioned relationship leads to the temporal and spatial pattern of the mean bottom shear stress observed for the six bathymeries. On average, in the ancient lagoons, the shear stress at the bottom was more intense respect to the most recent configurations, due to the shallower tidal flats. It is interesting to observe that the tidal flat area in the middle of the central-southern Lagoon, characterized by quite low bottom elevations, called "Fondo dei Sette Morti", display a negligible variation in the mean BSSw because bottom elevations in this area is maintained quite constant over time. Nowadays the erosion process develops horizontally through a progressive expansion of the deepest areas and the BSSw of the southern lagoon is becoming close to the equilibrium value characteristic of the "Fondo dei Sette Morti". If, on the other hand we analyse the maximum shear stress (Fig. 3.16), we find the highest value, around 1 Pa, in the central-southern Lagoon and for the configurations of 1970 and

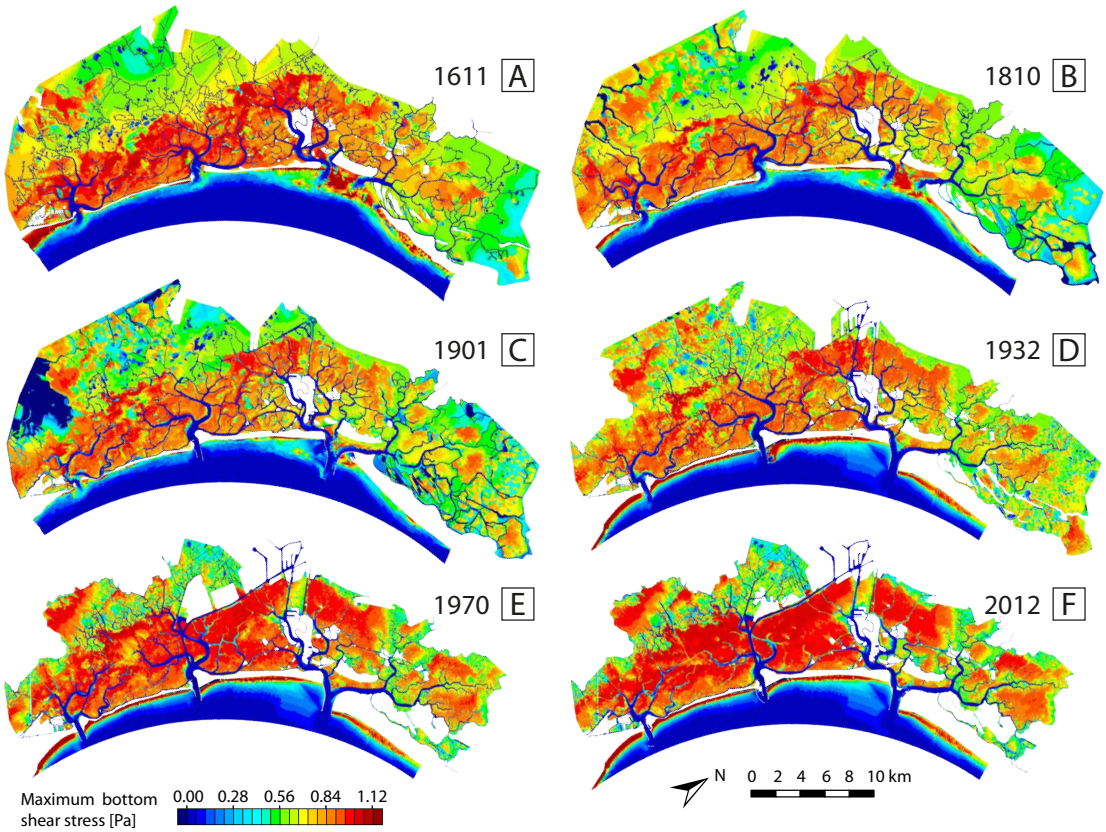

Figure 3.16: Color-coded representation of the maximum bottom shear stress induced by waves for the different configurations of the Venice Lagoon 1611 (A), 1810 (B), 1901 (C), 1932 (D), 1970 (E), and 2012 (F).

2012 because of the larger fetches. Moreover because of the overall retreat of salt-marsh boundaries and to the tidal-flat flattening, the recent configurations display a more uniform pattern both for the mean and the maximum BSSw. We can conclude by observing that tidal-flat evolution is the result by a combination of the effects of both strong, less frequent and lower, but more frequent events. We also note that if, on the one hand, the mean bottom shear stress induced by waves is controlled by the water depth and as a consequence, the tidal flat deepening over a specific depth seems to reach a temporary equilibrium condition, on the other hand, the maximum BSSw depends on the site morphology (i.e., the distribution of salt marshes and the width of the tidal flats).

3.5 CONCLUSIONS

We applied several models, aimed at reproducing wind-wave effects in shallow tidal environments, in order to provide new insights on the influence that the different assumptions embedded in the models

have on the results. Our results suggest that all the models need to be applied with awareness of the implications introduced by the simplifications, in particular when addressing the study of long-term erosion of tidal landscape. We compared the data recorded within the Venice lagoon with zero and one-dimensional models and then we used a full fledged two-dimensional model to simulate the wind wave field in the Venice Lagoon considering different configurations over the past four centuries.

Our results show that different model assumptions and empirical formulations strongly influence the computation of the bottom shear stress, whereas modeled wave heights seem to be consistent among different models and display better agreement with field observations. We found a strong sensibility of the computed bottom shear stress and, as a result of possible erosion processes governing morphodynamic evolution, to changes in sediment grain size, friction factor, fetch length and wave period.

The following conclusions are drawn from the analysis carried out herein:

- We do not retrieve the bell-shape relationship between depth and wave-induced bottom shear stress obtained in previous studies with a constant wave period, or a constant friction. In particular, we show that when using the Young and Verhagen empirical formulation, the BSSw is quite large for very shallow water depths, and it then decreases with depth thus leading to a possible overestimation of erosion for shallow depths and important consequences on the study of long-term morphology. Indeed overestimation of BSSw for small depths might inhibit salt-marsh growth in the vertical plane.

- The application of the two one-dimensional models shows different results when short fetches are considered. The SWAN model simulates a wave that constantly increases with the fetch and water depth, while the WWTM simulates a rapid wave growth for lower water depths and a slower growth for larger water depths.

- The comparison with field data shows that the the BSSw generated with larger fetches is easier to capture than the BSSw of more complex bathymetries and water depths lower than 1 m. Moreover the lack of data for water depths lower than 1 m leads to a difficult prediction of BSSw in very shallow water conditions, which are very important for sediment transport. Further investigations possibly supported by new field data are necessary for better understanding wind-wave dynamics and the related BSSw in super shallow water conditions.

- The application of the two-dimensional WWTM model enabled us to investigate the variability in time and space of the mean wave height and mean and maximum bottom shear stress induced by wind waves. Our results show the strong increase in the wave height after 1970, strongly intertwined to the tidal-flat deepening in the southern lagoon. The mean bottom shear stress decreases the past to the present towards an equilibrium value, however the maximum bottom shear stress occurs in the most recent configuration characterized by larger fetches.

4 MODELLING THE WIND-WAVE FIELD WITHIN THE VENICE LAGOON

This chapter is a manuscript submitted to Earth Surface *Processes and Landforms*. The paper deals with the analysis of the spatial distribution of wave power density in the last four centuries in the Venice Lagoon (Italy) and with the study of the relationship between incident wave power density and salt-marsh erosion rate. In this work, by analysing the study case of the Venice Lagoon, we aim at evaluating, through the application of a two-dimensional Wind Wave Tidal Model (WWTM), the effects of the impinging wind wave on marsh boundaries and how the temporal evolution of wind-wave fields affects erosional dynamics. Model results show that on the one hand the mean wave power density has not significantly changed from 1611 to 1901, on the other hand in the last century (1901-2012) a rapid increase in wave power densities was observed leading to strong erosion processes. Moreover, our new analyses, based on the results of a complete WWTM, show that the volumetric erosion rate computed for several areas of the Venice Lagoon is linearly related to wave power density.

PAPER

MODELLING CHANGES IN THE WIND–WAVE FIELD WITHIN THE VENICE LAGOON IN THE LAST FOUR CENTURIES

Laura Tommasini[1], Luca Carniello[2], Marcella Roner[1], Massimiliano Ghinassi[1] and Andrea D'Alpaos[1]

[1]Dept. of Geosciences, University of Padova, via G. Gradenigo 6, Padova, Italy

[2]Dept. ICEA, University of Padova, via Loredan 20, Padova, Italy

Abstract

Salt marshes are crucially important ecosystems at the boundary between the land and the sea, that are experiencing significant losses worldwide mainly dictated by the erosion of their margins. Improv-

ing our understanding of the mechanisms controlling marsh edge erosion is a key step to address conservation issues and salt-marsh response to changes in the environmental forcing. Here we have employed a complete, coupled Wind-Wave Tidal Model (WWTM) to analyse the temporal evolution of the wave field, and in particular of the mean wave power density, in the Venice Lagoon over the past four centuries (from 1611 to 2012). We have then related wave-field changes to the observed erosion patterns determined by comparing recent aerial photographs (1978-2010) and historical bathymetric data. The results of our analyses from the Venice Lagoon show that, while wave-fields did not significantly change from 1611 to 1901, a rapid increase in wave power densities occurred in the last century with important morphodynamic implications. We also emphasize the existence of a strong positive linear relationship between the volumetric marsh erosion rate and wave power density. We thus suggest that relating salt-marsh lateral erosion rates to properly computed mean wave power densities provides a valuable tool to address long-term tidal morphodynamics.

4.1 INTRODUCTION

Coastal salt marshes, located at the interface between marine and terrestrial environments, are systems of vital importance from the eco-geomorphological and socio-economical point of view (e.g., Costanza et al., 1997; Zedler and Kercher, 2005; Kirwan and Megonigal, 2013; D'Alpaos and Marani, 2016). Among the several ecosystem services they provide, marshes dissipate waves and mitigate erosion during storms (e.g., Möller et al., 1999; Howes et al., 2010; Möller et al., 2014), thus reducing the impact on coastal communities (e.g., Möller, 2006; Temmerman et al., 2013; Zhao and Chen, 2014); filter nutrients and pollutants from the water column (Costanza et al., 1997); furnish nursery areas for coastal biota (e.g., Perillo, 2009); and serve as an important organic carbon sink due to their great ability to sequester atmospheric carbon (e.g., Chmura et al., 2003; Barbier et al., 2011; Fourqurean et al., 2012; Kirwan and Mudd, 2012; Roner et al., 2016).

Despite the ecological and socio-economical value of salt marshes, these critically important ecosystems are currently being lost at large rates, threatened as they are by a combination of natural and anthropogenic processes that have triggered a large decrease in their extent worldwide in the last century (Day et al., 2000; Gedan et al., 2009; Marani et al., 2010), furthermore promoted by the increasing rates of relative sea level rise and by the limited sediment supply (e.g., Day et al., 2000; Marani et al., 2010; Mariotti and Fagherazzi, 2010; D'Alpaos

et al., 2011; Gedan et al., 2011; Mudd, 2011; Mariotti and Carr, 2014; Silvestri et al., 2018).

As an example, the marsh erosion in Essex (England) between 1973 and 1993 was estimated to lead to the loss of around 25% of the total salt-marsh area originally present (Cooper et al., 2001). Over the last century, in the San Francisco Bay, the amount of salt-marsh loss has been documented to be around 200 km^2 (Gedan et al., 2009), while in the Mississippi Delta plain about 4800 km^2 of wetlands disappeared (Day et al., 2009). In the Venice Lagoon (Italy), salt-marsh extent has faced a reduction of 76% in the last two centuries, decreasing from about 180 km^2 in 1811 to 43 km^2 in the present days (Carniello et al., 2009; D'Alpaos, 2010a).

Salt-marsh growth, maintenance and/or disappearance are governed by a variety of physical and biological processes that drive their evolution both in the vertical and in the horizontal directions. Tidal marshes can indeed evolve horizontally because of lateral erosional and progradation processes, and vertically, as a net result of organic and inorganic deposition, surface erosion, and relative sea level rise (Kirwan et al., 2010; D'Alpaos et al., 2011; Marani et al., 2011; Carr et al., 2012; Mariotti and Fagherazzi, 2013a; Leonardi and Fagherazzi, 2014; Mariotti and Carr, 2014; Kirwan et al., 2016a; Kirwan et al., 2016b; Leonardi et al., 2016a; Leonardi et al., 2016b; Leonardi et al., 2018).

Decades of research on marsh vertical dynamics have addressed the processes leading to the formation of salt-marsh equilibria and the related ecogeomorphic patterns (e.g., Bricker-Urso et al., 1989; Allen, 1990; D'Alpaos et al., 2005; Van de Koppel et al., 2005; D'Alpaos et al., 2007; Kirwan and Murray, 2007; Marani et al., 2007; Mudd et al., 2009; Marani et al., 2010; D'Alpaos et al., 2011). Accretion rates have been shown to vary in space and time (Delaune et al., 1978; Day et al., 1998; Allen, 2000; Friedrichs and Perry, 2001; Temmerman et al., 2005; D'Alpaos et al., 2007) and, under certain circumstances, marshes can keep pace with sea level rise and reach equilibrium conditions (Temmerman et al., 2005; French, 2006; Kirwan et al., 2010; D'Alpaos et al., 2011; Kirwan et al., 2016a) characterized by the formation of distinctive ecogeomorphic patterns (Reed, 1989; Silvestri et al., 2005; Marani et al., 2013; D'Alpaos and Marani, 2016).

Only relatively recently, researchers have analysed the erosion processes leading to the horizontal evolution of salt-marsh systems (e.g., Schwimmer, 2001; Van de Koppel et al., 2005; Gedan et al., 2009; Mariotti and Fagherazzi, 2010; Marani et al., 2011; McLoughlin et al., 2015; Bendoni et al., 2016; Leonardi et al., 2016b; Mariotti and Carr, 2014; Carr et al., 2018; Donatelli et al., 2018). In the horizontal plane, salt marshes are suggested to be inherently weak and unstable (Mariotti et al., 2010; Mariotti and Fagherazzi, 2013a), because of the action of

waves impacting the salt-mash edge where bare sediment below the vegetation layer can be easily mobilized thus promoting bank retreat triggered by cantilever failure mechanisms (Mariotti and Fagherazzi, 2010; Bendoni et al., 2014; Leonardi and Fagherazzi, 2014; Leonardi et al., 2016a).

Average horizontal erosion rates have been estimated, for different observation periods, in the order of 0.4-3.0 m/yr for the Westerschelde (Netherland) (Van der Wal et al., 2008), 0.5-2.0 m/yr in the Virginia Coastal Reserve (Virginia, USA) (McLoughlin et al., 2015), 0.17-7.30 m/yr in the Rehoboth Bay (Delaware, U.S.A) (Schwimmer, 2001), 0.25-2 m/yr in the Barnegat Bay-Little Egg Harbor system (New Jersey, USA) (Leonardi et al., 2016b) and 0.23-2.81 m/yr in the Charleston Sound (South Carolina, USA) (Mariotti and Fagherazzi, 2013a).

In the Venice Lagoon (Italy), marsh retreat rates have been estimated around 1.2-2.2 m/yr for the period from 1993 to 1995 in the Southern part of the Lagoon (Day et al., 1998), up to 0.8 m/yr in the Northern Lagoon (Bendoni et al., 2016) and in the order of 0.08-3.3 m^2/yr per unit area considering several eroding marshes in the whole Lagoon (Marani et al., 2011).

Unravelling the main processes responsible for marsh boundary erosion is a difficult task, particularly in rapidly eroding environments subjected to climate changes and anthropogenic pressures, where salt-marsh loss may be triggered by different hydrodynamic forces acting at different spatial and temporal scales, frequently affected by human interference (e.g., Costanza et al., 1997; Day et al., 2000; Carniello et al., 2009; D'Alpaos, 2010a; Fagherazzi et al., 2013).

Wind-wave attack is usually recognized as one of the main processes leading to marsh horizontal retreat in estuaries and lagoons worldwide (Schwimmer, 2001; Gedan et al., 2011; Marani et al., 2011; Mariotti and Carr, 2014; Bendoni et al., 2016; Leonardi et al., 2016a). This complex phenomenon includes both the continuous removal of small size particles and the sudden detachment of marsh portions whose size is comparable to the marsh bank height (Bendoni et al., 2014). Salt-marsh lateral erosion is also controlled by the depth and extent of the tidal flats or subtidal platforms in front of the salt-marsh boundary, that, together with wind climate, influence the characteristics of the impinging wind waves (Mariotti and Fagherazzi, 2013b). Sea level rise can further affect wind-wave climate by causing a more rapid erosion of the marsh boundaries due to the increase in water depth and consequently in the wave height (Mariotti et al., 2010). Tidal range plays also an important role in controlling wave erosion, because as the tidal range increases, the intensity of wind-induced erosive processes over the subtidal platforms and against salt-marsh margins progressively decreases (e.g., Callaghan et al., 2010; D'Alpaos et al., 2012). Furthermore Leonardi and Fagherazzi (2014) demonstrated

that the lateral erosion mechanism depends on the wave climate and the marsh properties, they found that salt marshes boundaries erode uniformly when are exposed to high wave energy conditions, while when wind waves are weak and the local marsh resistance is strong, jagged marsh boundaries are formed.

When analysing salt-marsh lateral erosion, bank instability due to water table fluctuations forced by the tide and erosion associated with tidal currents are thought to be negligible in microtidal systems, whereas ship wakes can promote erosion in proximity of the channel banks (Zaggia et al., 2017).

The presence of vegetation in coastal salt marshes increases their overall resilience, promoting wave dampening over the marsh surface (Möller et al., 2014) and facilitating sediment deposition. Moreover, vegetation represents an effective shoreline buffer, reducing rates of erosion by stabilizing the soil in the root zone (Gedan et al., 2011). In addition, the stabilization effect of vegetation was found to be more pronounced in sandy soils, where erosion was reduced by 80% compared to 17% in silty soils (Lo et al., 2017). Because the impinging of wind waves strongly contributes to salt-marsh horizontal erosion (e.g., Schwimmer, 2001; Marani et al., 2011; Mariotti and Fagherazzi, 2013a; Leonardi et al., 2016b; Leonardi et al., 2018), understanding the relationship between erosion rate and impacting wave-power density is critical also for the maintenance and management of marsh ecosystems.

In view of the chief role of wind waves in driving salt-marsh loss worldwide, Schwimmer (2001) related salt-marsh margin retreat rate, R_M (e.g., in m/yr), to the the mean power density of incident waves, P_w, on the basis of an empirical power law of the type $R_M = aP_w^b$, whereas Mariotti and Fagherazzi (2010) proposed another non-linear relationship, of the type $R_M = c(P_w - P_c)$, where P_c is a critical threshold for lateral erosion. The existence of a linear relationship between wind-wave power density and the volumetric lateral erosion rate has recently been proved on theoretical and empirical grounds by Marani et al. (2011), receiving further empirical support by other studies on marsh lateral erosion (McLoughlin et al., 2015; Bendoni et al., 2016; Leonardi et al., 2016b; Leonardi et al., 2016a). Bendoni et al. (2016) explored the erosion of marsh boundaries on the basis of a systematic field monitoring at small spatial and temporal scales, whereas other studies (e.g., Marani et al., 2011; McLoughlin et al., 2015; Leonardi et al., 2016b; Leonardi et al., 2016a) analysed field data collected over larger spatial (kilometres) and temporal (decades) scales. When analysing marsh erosion at large temporal scales, a common assumption is to relate the wind-wave field associated to the most recent bathymetric and morphologic data to the erosion rate determined by analysing morphological changes occurred over decades. However, it

should be emphasized that the wind-wave field responsible for the erosion evolves in response to these bathymetric and morphological modifications in a positive feedback. In order to account for the above recalled morphodynamic changes, in this manuscript we analyse the temporal morphological evolution of the Venice Lagoon (Italy) and of the related wind-wave fields, using a full-fledged numerical Wind Wave Tidal Model (WWTM) (Carniello et al., 2011) applied to different historical configurations. In particular, we compute the wind-wave field by considering: a) the configuration of 1611 reconstructed from the historical map by Sebastiano Alberti (see the second chapter); b) the configuration surveyed at the beginning of the 19^{th} century by the Napoleonic Captain A. Dènaix (1809-1811); c) the configuration dating back to the beginning of the 20th century (1901); the configurations derived from the surveys carried out by the Venice Water Authority in 1932 (d) and in 1970 (e); and the present (2012) configuration (f).

We first explore, at the scale of the whole Lagoon, the temporal evolution of the wave field determined by performing 1-year-long simulations obtained by forcing the numerical model with the time series (of water levels, wind velocities and directions) recorded in 2005, for each of the above mentioned historical configurations of the Venice Lagoon. The use of the same forcings for all the configurations aimes at disclosiong the effect of bathymetric and morphological changes alone. We then use model results and field observations, retrieved from the analysis of remotely sensed data, to investigate the relationship between incident wave-power density and salt-marsh volumetric erosion rates (e.g., Marani et al., 2011). For the latter analysis, we considered 18 km of salt-marsh boundaries in the southern part of the Venice Lagoon where quite intense morphological deterioration, due to both marsh lateral retreat and tidal flat erosion, was observed during the last century.

4.2 MATERIALS AND METHODS

4.2.1 Morphological and bathymetric configurations

The Venice Lagoon, whose area is of about 550 km^2, is the largest lagoon in the Mediterranean sea. The Lagoon is connected to the Adriatic Sea by three inlets (Lido, Malamocco and Chioggia – see Fig. 4.1) and it is characterized by a semidiurnal microtidal regime, with an average tidal range of about 1.0 m and maximum tidal excursions at the inlets of about ± 0.75 m around Mean Sea Level (MSL). Bora wind, blowing from North-East at speeds that can exceed 20 m/s, is the most intense and morphologically significant wind in the Venice

Lagoon, and is quite frequent from October to March. Sirocco wind blows from South-West and dominates the summer season, being less intense than Bora wind as it rarely exceeds 10 m/s (Fig. 4.1).

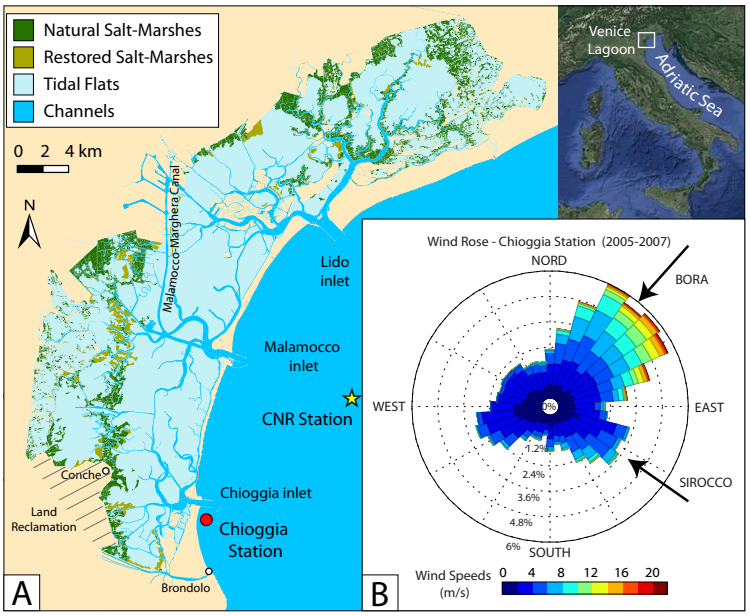

Figure 4.1: (A) Spatial distribution of the main morphological features characterizing the Venice Lagoon. The locations of the anemometric (Chioggia) and mareographic (CNR Oceanographic Platform) stations are also shown. (B) Wind rose obtained on the basis of the data recorded in the Chioggia station in the period 2005–2007

The Venice Lagoon has experienced important morphological transformations due to human intervention started in the XV century. In the last century, in particular, the increasing anthropogenic pressure has deeply accelerated the morphological deterioration process. The first relevant human interventions were carried out between the XV and XVII centuries, when the Serenissima Republic of Venice (an ancient Venetian State) diverted the main rivers (Brenta, Sile and Piave) to the Adriatic Sea to prevent the lagoon from silting up. Due to these interventions, sediment input in the Venice Lagoon from the watershed almost vanished thus rapidly turning the silting up process into the progressive erosion that actually characterizes the present morphological trend of the basin. In the southern lagoon, the Brenta river was diverted to the sea at Brondolo in 1540 but it was temporarily reintroduced into the lagoon at Conche (see Fig. 4.1) from 1858 to 1896 (D'Alpaos, 2010a). In these 56 years, the Brenta river provided a large sediment input, and sediment accumulation at the outlet promoting the infilling with sediments of an area of about 24 km^2 (D'Alpaos, 2010b; Roner et al., 2017), thus highlighting the crucial role of sediment supply on marsh formation.

In the last century, the erosion processes become much more intense (Fig. 4.2) due to the construction of the jetties at the inlets and the excavation of the big navigation channels, such as the Malamocco-Marghera ship canal (Sarretta et al., 2010). The jetties, in fact, completely modified the hydrodynamic field at the inlets, establishing an asymmetric behaviour characterized by the formation of huge plumes during the ebb phase of the tide, responsible for a net export of sediments especially during intense storm events, capable of resuspending large amounts of sediments within the lagoon (Carniello et al., 2012; D'Alpaos and Martini, 2005). Moreover the construction of the jetties, completed in the 1934 with the jetties at the Chioggia inlet, almost entirely stopped any sediment supply from the sea (Umgiesser et al., 2006; Defendi et al., 2010).

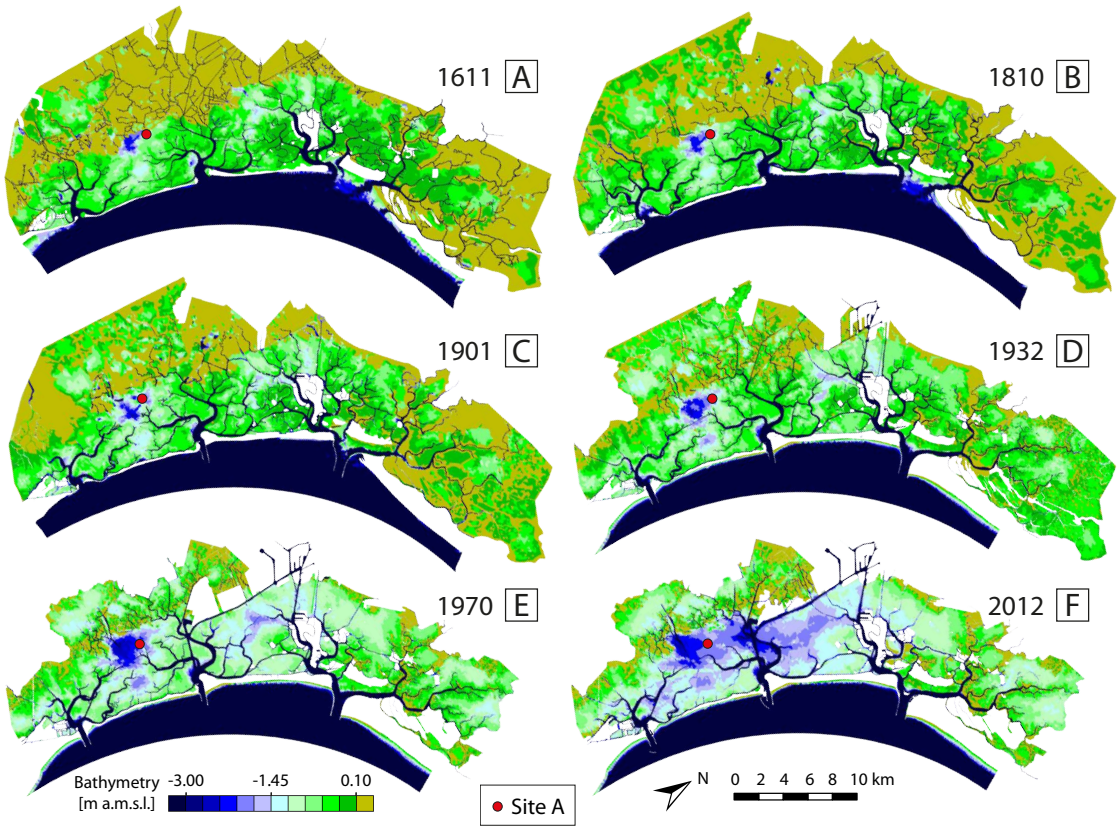

Figure 4.2: Color-coded bathymetries of the Venice lagoon, Italy, in (A) 1611, (B) 1810, (C) 1901, (D) 1932, (E) 1970, (F) 2012. Elevations are in meters above mean sea level (m a.m.s.l.) and they have been referred to the mean Adriatic Sea level recorded when each survey was performed, therefore accounting for the effect of sea level rise (e.g., Carniello et al., 2009). The red solid dot in the different bathymetries represents the Site A considered to analyse the wave power density one year of simulation (see Fig. 4.7)

We considered six different lagoon configurations in order to access and quantify the morphological changes in the Venice Lagoon during

the last five centuries. We reconstructed these configurations by using historical maps (1611, 1810 and 1901), and more recent topographic surveys carried out by the Venice Water Authority (Magistrato alle Acque di Venezia) in 1932, 1970 and 2003. The computational grids reproducing all the six configurations of the lagoon were realized in previous studies: 1611 by Tommasini et al. (2017); 1810 by D'Alpaos and Martini (2005) and D'Alpaos (2010a); 1901, 1932, 1970 and 2003 by Carniello et al. (2009) and D'Alpaos (2010a).

In the following we briefly summarize the techniques adopted for reconstructing the oldest three configurations and provide information on the available bathymetric data. The 1611 configuration of the lagoon was reconstructed by Tommasini et al. (2017) on the basis of the morphology depicted in the historical map by Sebastiano Alberti (1611), which mainly portrays the planimetric features of lagoonal morphologies, integrated by bathymetric information retrieved on the basis of morphometric relationships between relevant geomorphic quantities such as channel width-to-depth ratios and considering the effects of relative sea level rise (RSLR).

The first map of the lagoon reporting bottom elevation data dates back to 1809–1811 (Dènaix, 1810) and was realized by the Captian Augusto Dénaix for navigation purposes. In this map, the planimetric description of salt marshes, tidal flats and channel networks is quite detailed, although elevation data are provided only within the main channels. The bathymetry was integrated over the tidal flats and salt marshes by Carniello et al. (2009) based on more recent (1901) bathymetric data and accounting for subsidence and eustatism effects (Carbognin et al., 2004). The 1901 bathymetry, reconstructed from the survey carried out by the Genio Civile di Venezia, is actually the first complete set of data with accurate elevations, in particular for the central southern portion of the Lagoon.

The 1932, 1970, and 2003 bathymetries were created by means of the data surveyed by the Venice Water Authority (Carniello et al., 2009). No error estimation is available for the 1932 bathymetry. The 1970 bathymetry was gathered by Theodolite on land and stadia rod on shallow flats and the Venice Water Authority estimate an error of ± 10 cm for subtidal flat elevations. The standard errors for the bottom elevation data in the more recent 2003 bathymetric survey are in the range (Consorzio Venezia Nuova, 2007): ± 5 cm for salt marshes, ± 5 cm for subtidal flats and, ± 10 cm for tidal channels (Consorzio Venezia Nuova, 2007).

We updated the 2003 configuration, and the related computational grid, by including the recent morphological modifications (almost completed in 2012) introduced at the three inlets by the construction of the movable gates for protecting Venice from high tides (Mo.S.E

Project). For this reason we refer to this configuration as the 2012 configuration.

4.2.2 Aerial Photographs and Erosion Rates

We carried out detailed analyses of salt-marsh lateral erosion in the period between 1978 and 2010. We focused on the salt marshes located in the southern part of the lagoon between the Malamocco and Chioggia inlets (Fig. 4.3). In this portion of the lagoon, salt marshes are characterized by different bank heights in the range 0.05-2.27 m, from the top to the toe. The higher cliffs, mainly located in front of the "Fondo dei Sette Morti" salt marshes, are characterized by steep slope, whereas the "Conche" salt marshes are characterized by a more gentle slope toward the adjacent tidal flat (see Fig. 4.3). These salt marshes are mainly distributed along the landward boundary of the lagoon and their seaward boundaries are mainly exposed to Bora wind conditions (i.e., the geomorphologically dominant wind blowing from Norh-East). Fetch exceeds 10 km, thus producing fetch-unlimited wave fields in front of the marshes. Moreover, the considered salt marshes are located in front of large tidal flats and subtidal platforms and far from the main channels, and are therefore poorly affected by boat traffic effects that might strongly influence the erosion of channel edges (Zaggia et al., 2017).

We evaluated marsh boundary erosion by means of aerial photographs that were downloaded from the official Geoportale of the Veneto Region for the selected sites, on the basis of image availability and quality. Photographs were obtained for 1978 and 2010; the 1978 photographs are in black and white with a ground resolution of 0.96 m produced at a scale of 1:20'000, while the 2010 photographs are in natural colours with ground resolution of 0.32 m. Both the photograph data sets were georectified using ArcGIS georeferencing tools and by considering ground control points such as buildings or streets recognized in the most recent cartographic survey (Carta Tecnica Regionale - 2005) (Fig. 4.3). Using the two data sets of aerial photographs we digitalized about 18 km of marsh edges in the southern lagoon, selected by excluding the artificial marshes (Fig. 4.3) restored by the Venice Water Authority since the early 1990s. We digitalized the salt marsh edge on the aerial photographs by identifying the vegetation limit. We subdivided the 2010 edge in 100-m-long segments measured by considering the along-edge coordinate. For each point separating two adjacent segments in the 2010 boundary, we identified the closest corresponding point in the 1978 edge boundary (Fig. 4.4). The adopted procedure is described in Fig. 4.4a and enabled us to divide the whole marsh area eroded in between 1978 and 2010 in 191 sub-areas (A_i).

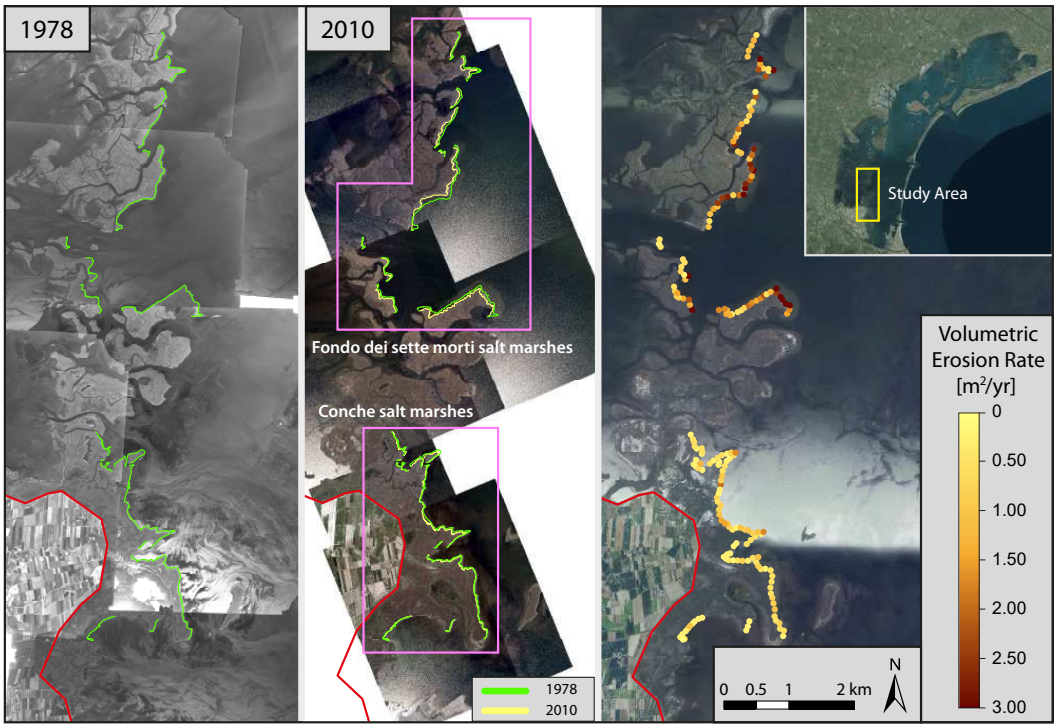

Figure 4.3: Digitalized marsh boundaries in 1978 and 2010 (left panels) and color coded representation of the volumetric erosion rate determined between 1978 and 2010 (right panel).

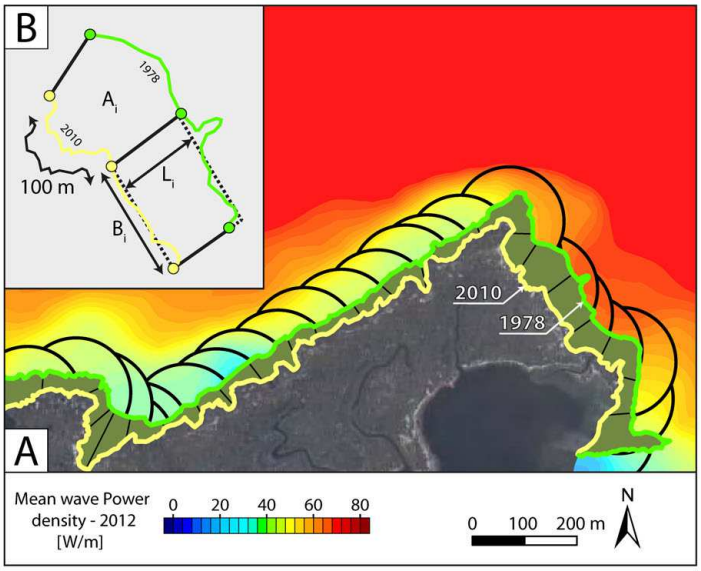

Figure 4.4: Sketch to explain how the volumetric erosion rate was computed. (A) Example of the subdivision of the eroded area in different segments. The black circles represent the area in which the mean wave power density was averaged. (B) Example of the procedure adopted to evaluate the volumetric erosion rate.

For each segment we computed the linear retreat (L_i) as the ratio between the eroded sub-area and the segment length in 2010 (B_i) and the lateral erosion rate (l_i) dividing L_i by the considered time interval (i.e., 32 years). We then determined the height of the marsh edge scarp for each segment by means of the most recent 2003 bathymetry and computed the volumetric erosion rate (i.e., expressed in (m^2/yr) for each sub-area as the lateral erosion rate (l_i) times the corresponding scarp height (a_i). We applied the same methodology for evaluating the long-term erosion rate between 1611 and 1810 and between 1810 and 1901. The digitalized shorelines were obtained from the historical maps. For both periods, we analysed the portions of salt-marsh edges in the southern lagoon characterized by the larger erosion and not affected by the reintroduction (from 1840 to 1896) of the Brenta River. In view of the lower accuracy of the historical maps, compared to the aerial photographs, the segment length was assumed equal to 500 m. We identified and analysed 21 segments for the first time interval (1611 – 1810) and 25 segments for the second interval (1810 – 1901).

4.2.3 Numerical model

We used the two-dimensional fully coupled Wind-Wave Tidal Model (WWTM) (Carniello et al., 2005; Carniello et al., 2011) to evaluate the hydrodynamic and the wind-wave fields in the six selected configurations of the lagoon (namely 1611, 1810, 1901, 1932, 1970 and 2012). The numerical model consists of two modules: the hydrodynamic module coupled with the wind-wave module. The hydrodynamic module solves the 2-D shallow water equations, properly modified for reproducing flooding and drying processes in very shallow and irregular domains, using a semi-implicit staggered finite element method based on Galerkin's approach (Defina, 2000; Martini et al., 2004; D'Alpaos and Defina, 2007). The hydrodynamic module provides the wind-wave module with the flow field characteristics, which are used by the wind-wave module to assess wave group celerity c_g and bottom influence on wave propagation. The wind-wave module (Carniello et al., 2005; Carniello et al., 2011) is based on the solution of the wave action conservation equation parameterized using the zero-order moment of the wave action spectrum. The spatial and temporal distribution of the wave period is calculated through an empirical function relating the peak wave period to the local wind speed and water depth following the approach suggested by (Young and Verhagen, 1996a; Breugem and Holthuijsen, 2007) and verified using wind wave data from the Venice Lagoon by Carniello et al. (2011). The WWTM has been widely tested by comparing model results to hydrodynamic and wind-wave data collected not only in the Venice Lagoon (Carniello et al., 2005; D'Alpaos and Defina, 2007; Carniello et

al., 2011) but also in other lagoons worldwide (Mariotti and Fagherazzi, 2010; Zarzuelo et al., 2016). In the present study we applied the numerical model to perform a one-year-long simulations considering the computational domains reproducing the six configurations of the Venice Lagoon and a portion of the Adriatic Sea in front of it (Fig. 4.2). The numerical simulations were run imposing as boundary conditions the time records of tidal levels (measured at the CNR station, (see Fig. 4.1) and wind velocities and directions (measured at the Chioggia Station, see Fig. 4.1) collected in the Venice Lagoon in 2005. The 2005 is a representative year in terms of wind forcings, being the probability distribution of wind velocities in that year the closest to the average distribution observed between 2000 and 2008 (D'Alpaos et al., 2013; Carniello et al., 2016). The WWTM provides, at each location within the Venice Lagoon, the temporal evolution (time interval: thirty minutes) of significant wave height (H) and wave group celerity (c_g). These quantities allow us to calculate the wave power density (Eq. 4.1) per unit length of the wavefront (Mariotti et al., 2010; Marani et al., 2011):

$$P_w = \frac{H^2 \rho g c_g}{8} \tag{4.1}$$

where ρ is water density and g is gravitational acceleration. In each element of the computational grid we calculate the mean wave power density (MWPD) averaging P_w over the one-year-long simulations (Fig. 4.5) and the maximum wave power density (MaxWPD) (Fig. 4.6).

4.3 RESULTS

We start analysing the volumetric erosion rate for each segment of the considered marsh boundary in the period 1978–2010 (Fig. 4.3). We observe that the "Fondo dei Sette Morti" salt marshes are those characterized by the highest erosion rates that reach values of 4.8 m^2/yr (mean erosion rate equal to 1.36 m^2/yr, median erosion rate equal to 1.16 m^2/yr). This can be ascribed to the fact that those salt marshes are directly exposed to Bora wind and face quite wide and deep tidal flats, their edges being characterized by relatively high scarps. As to the "Conche" salt marshes, our analyses suggest volumetric erosion rates lower than 2 m^2/yr (mean erosion rate equal to 0.55 m^2/yr, median erosion rate equal to 0.78 m^2/yr). Although the "Conche" salt marshes are also exposed to Bora wind, the reduced erosion rates can be explained by the shallower tidal flats located in front of those marshes, which promote wave attenuation and reduce the height of waves impacting the salt marsh edge. In order to improve our under-

standing of the processes responsible for the observed lateral erosion rates, we analysed the wave-field characteristics, and in particular the spatial distribution of the Mean Wave Power Density (MWPD), for the most recent configurations (1970 and 2012) and furthermore extended our analyses to previous configurations going back to 1611. Before analyzing the spatial distribution of MWPD, it is worthwhile recalling that wave power density increases with the second power of wave height, H, which in turn increases with wind velocity and duration, fetch, and water depth. For any prescribed wind intensity and duration (the considered lagoonal configurations are indeed forced by the same wind and tidal forcing), wave height increases with fetch length and with the depth of the platforms over which waves propagate. Fetch depends on basin morphology, whereas the water depth is a function of basin bathymetry and local tidal levels. Fig. 4.5 shows the spatial distribution of MWPD, computed for all the selected configurations of the lagoon.

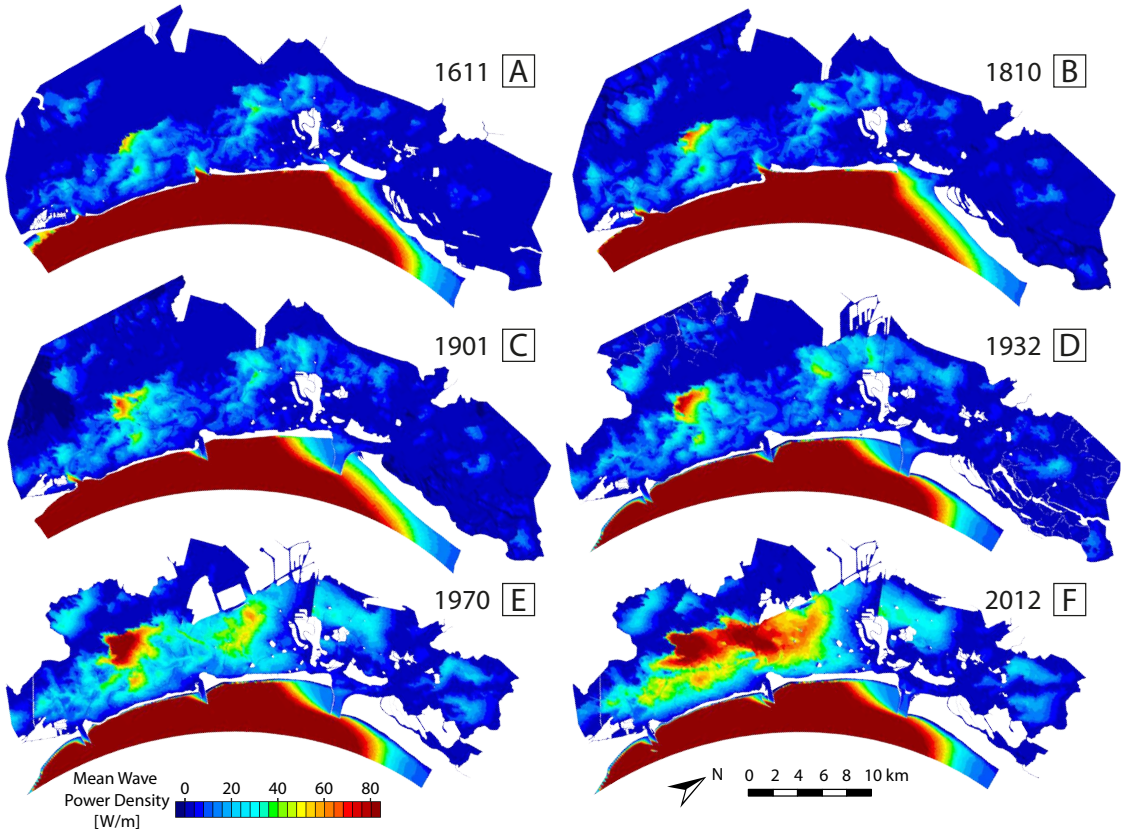

Figure 4.5: Color-coded representation of the mean wave power density for the different configurations of the Venice Lagoon 1611 (A), 1810 (B), 1901 (C), 1932 (D), 1970 (E), and 2012 (F).

It clearly emerges that a general increase in the MWPD can be observed from 1611 to 2012. The spatial distribution of the MWPD does not display strong changes between 1611 and 1932, while MWPD val-

ues increased from 1932 to 2012. The lagoon configurations in 1611, 1810 and 1901 are almost uniformly characterized by small values of the MWPD mainly because of the very shallow water depths (see the color-coded bathymetries of the Venice lagoon configurations in Fig. 4.2) and also because of the presence of large salt-marsh areas that limit fetch extension in the southern lagoon and continuously interrupt the fetch, thus preventing the growth of high waves. More in general, in all configurations, small MWPD values are observed seeward of mainland, natural and artificial marshes (in the north-eastern part of the Venice Lagoon), islands and spits, providing a sheltering effect particularly to Bora wind that is observed to be the most intense and morphologically significant wind in the Venice Lagoon (see the wind rose in Fig. 4.1). On the contrary, the larger values of the local MWPD, in all configurations, occur in the central and southern parts of the Venice Lagoon. In particular, between the Chioggia and Malamocco inlets, where deeper subtidal platforms in the "Fondo dei Sette Morti" area (elevations ranging from 1.37 m in 1611 to 2.23 m in 2012) are constantly observed in all the considered lagoonal configurations (Fig. 4.2), MWPD values are much higher than in the northern part, that is sheltered from Bora winds by the mainland and large salt marsh portions, and is characterized by very shallow flats. This finding in general agrees with recent observations emphasizing a strong erosive trend for salt-marsh edges and for the tidal flats and subtidal platforms in the central-southern part of the Venice Lagoon (e.g., Carniello et al., 2009; D'Alpaos, 2010a). Fig. 4.6 shows the computed Maximum Wave Power Density (MaxWPD) for the six configurations. Model results emphasize that if on the one hand, the maximum values occur approximately where also the MWPD displays its highest values, on the other hand quite high values of the MaxWPD are also observed at locations characterized by few, strong wind events that are not representative of the local morphologically significant wind-wave field. This is particularly evident in the configurations of 1970 and 2012, over the tidal flats located in the central part of the lagoon, southern of the city of Venice, and close to the barrier islands. These areas are characterized by high values of MaxWPD, probably due to Sirocco wind conditions, while the MWPD is smaller compared to other locations within the lagoonal basin (see e.g., the "Fondo dei Sette morti" area, see Fig. 4.3).

In order to provide a more quantitative description of the computed wave power density fields for the different configurations, we selected a site (Site A in Fig. 4.2), located close to the "Fondi dei Sette Morti" subtidal platform, where the lagoonal bottom elevations experienced the less important modifications (e.g., Marani et al., 2007; Carniello et al., 2009) between 1611 and 2012. Fig. 4.7 shows the temporal evolution of the computed wave power density during the entire year of

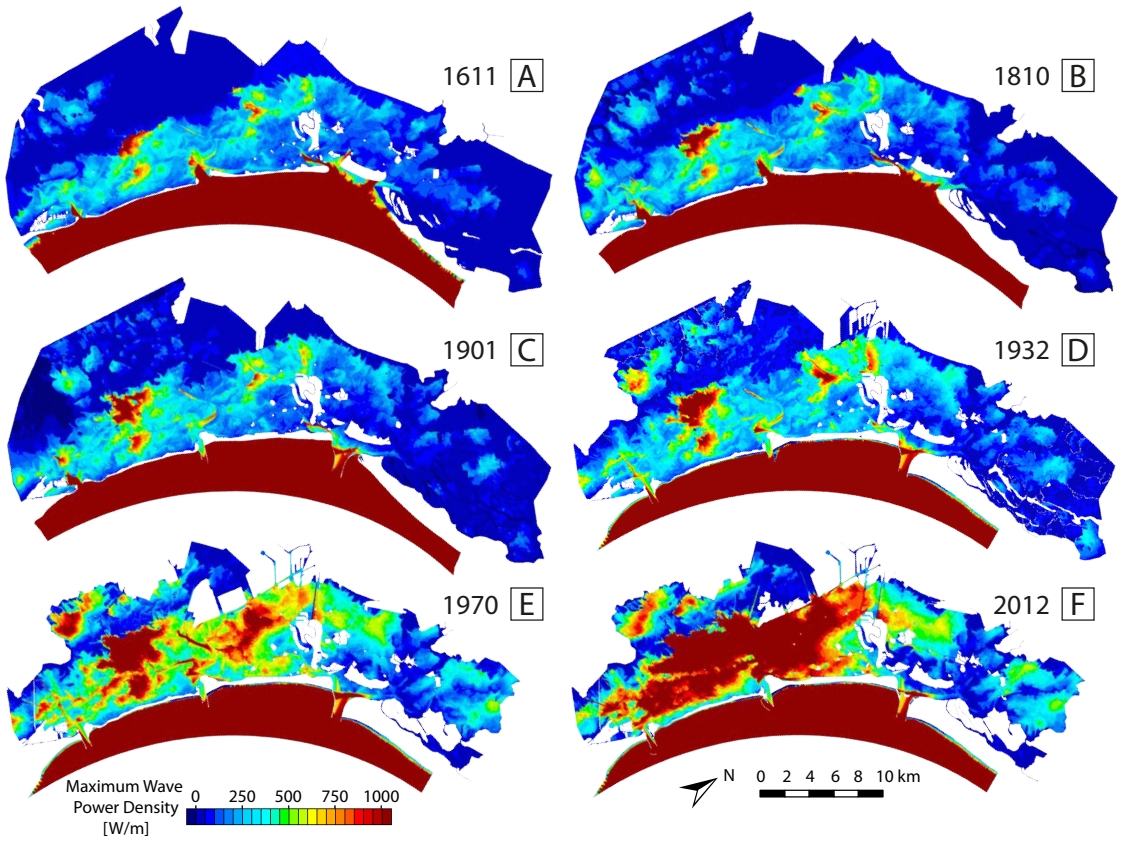

Figure 4.6: Color-coded representation of the maximum wave power density for the different configurations of the Venice Lagoon 1611 (A), 1810 (B), 1901 (C), 1932 (D), 1970 (E), and 2012 (F).

simulation for all of the considered lagoon configurations. Our results clearly show that both the MWPD and MaxWPD increased from 1611 to 2012. In particular, the stronger events (e.g., 10-11 April and 22-24 November) in the most recent configurations (1970 and 2012) were able to produce much higher values of wave power density (see Fig. 4.7) compared to MWPD values obtained for the other historical configurations (1611, 1810, and 1900).

We also selected four sites next to salt-mash edges (Fig. 4.8) for which we provide the temporal evolution of the computed P_w for the more recent 2012 configuration, in order to provide more quantitative information on the difference between MWPD and MaxWPD. Two of the selected sites are located in the northern part (site 1 and site 2) whereas the other two are located in the southern portion (site 3 and site 4). Sites 1 and 3 are mainly exposed to Sirocco wind blowing from south-west, while sites 2 and 4 are mainly exposed to Bora wind blowing from north-east. Sites 1 and 2 are characterized by the same MWPD (2.81 W/m and 2.02 W/m, respectively), whereas the MaxWPD at site 2 (247.78 W/m) is more than double compared to the MaxWPD at site 1 (116.35 W/m) due to a single event occurred

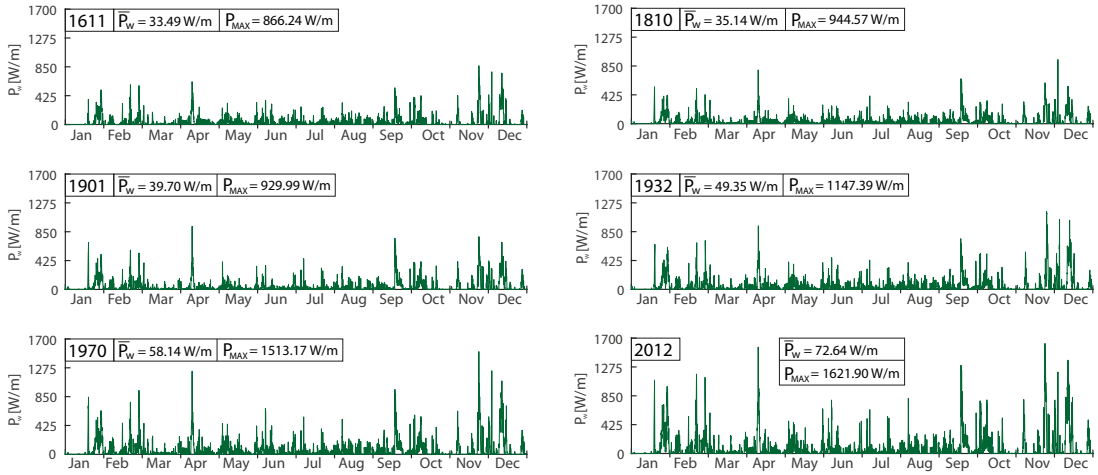

Figure 4.7: Evolution in time of the computed wave power densities at site A (see Fig. 4.2) in the six considered configurations.

between November and December. In addition, we note that sites 3 and 4, located in the southern portion of the lagoon, display a similar MWPD values (29.58 W/m vs 28.50 W/s, respectively), whereas the MaxWPD at site 4 (1213.11 W/m) is almost 50% larger than the MaxWPD at site 3 (820.03 W/m). Also in this case, one single, quite intense event made the difference.

We then focused our attention on the central-southern portion of the lagoon, the area characterized by the largest increase in MWPD through the centuries. We computed the probability density function of MWPD over the "Fondo dei Sette Morti" subtidal platform for all the configurations (Fig. 4.9), furthermore excluding the areas dissected by tidal channels and covered by salt marshes. The results highlight that the more ancient configurations (1611, 1810 and 1901) were characterized by higher probability values for lower MWPD (smaller than 10 W/m in 1611 and 1810, and around 12 W/m in 1901). In 1932, the peak of the probability distribution started to move toward higher values of MWPD, and in addition the probability of very high MWPD increased. The same trend is much more evident when considering the two most recent configurations. Our results show that the MWPD peak was about 22 W/m in 1970 and about 42 W/m in 2012, with a widening of the probability distribution in particular for high values of MWPD. Interestingly the 2012 probability distribution displays a bimodal shape, with a second peak characterized by MWPD values of about 70 W/m.

We finally analysed the possible linear relationship between the computed MWPD and the observed volumetric erosion rates originally proposed by Marani et al. (2011), evaluated by comparing the position of salt-marsh edges between 1978 and 2010 for each of the 100 m long segments considered in the analysis. We have previously shown

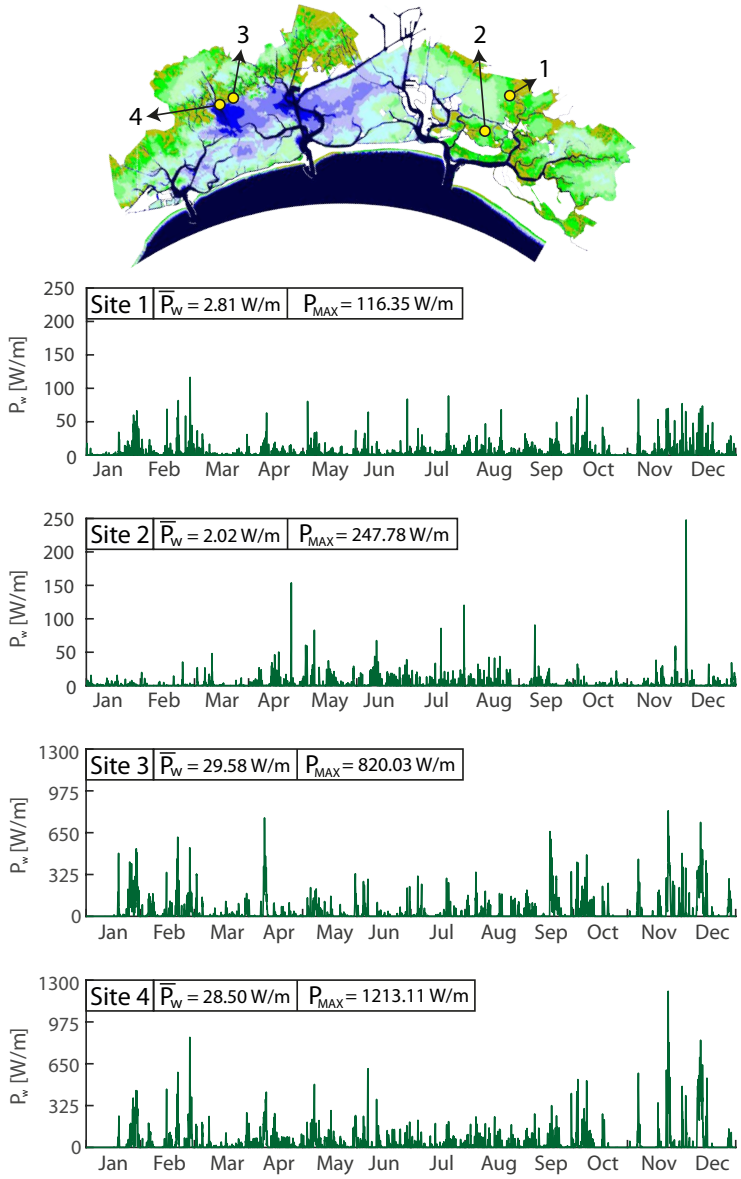

Figure 4.8: Evolution in time of the computed wave power density at four sites in the present configuration of the Venice Lagoon. Two sites are located within the northern Lagoon (1 and 2) and two sites in the southern Lagoon (3 and 4).

that (Fig. 4.5) the spatial distribution of MWPD can strongly change in time in relation to changes in the morphological configuration of the tidal system (and viceversa). As a consequence, in order to estimate the spatial distribution of MWDP in 1994, which represents the middle of the time interval between the two sets of aerial photographs (1978 and 2010), we linearly interpolated the MWDP computed for the 1970 and 2012 configurations. To estimate the 1994 MWPD impacting each 100m long segment of the considered salt marsh edge, we first evaluated the MWPD impacting each segment by averaging the

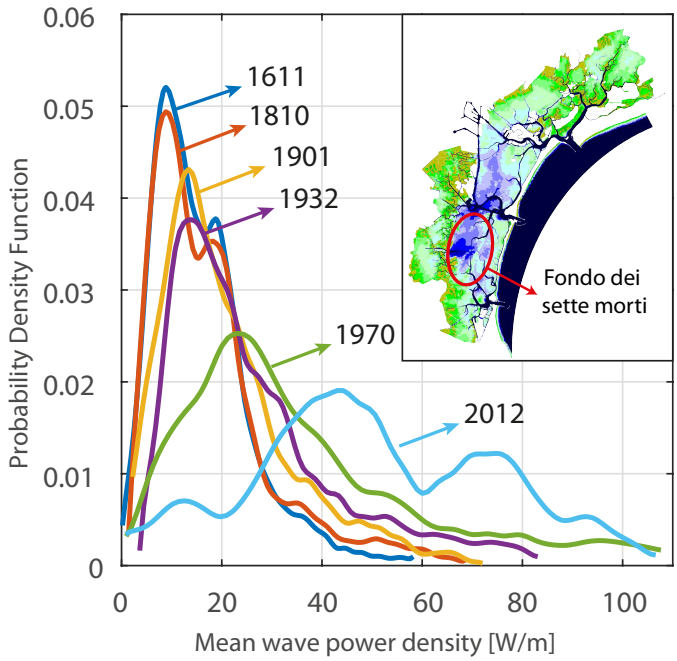

Figure 4.9: Evolution in time of the probability density function of the mean wave power density in the central-southern part of the Venice Lagoon.

modelled MWPDs over the tidal flats in front of the considered mash edges within a radius of 100 m (see Fig. 4.4A), for both the 1970 and 2012 configurations. We then computed the 1994 MWPD by linearly interpolating the data obtained for the 1970 and the 2012 configurations. Fig. 4.10 shows, for each of the considered segments (light blue points), the 1994 MWPDs [W/m] and the corresponding 1978-2010 Volumetric Erosion Rates (VERs) [m^2/y]. Solid red circles represent suitably binned MWPDs and VERs from observational data (i.e., average MWPDs and VERs computed over non-overlapping subintervals defined every 20 points counted along the x axis - standard deviations for every bin are also shown). The red line in Fig. 4.10, fitted to the binned data (R^2 = 0.96), emphasizes the noteworthy overall validity of a linear relationship between MWPDs and VERs (Marani et al., 2011 - blue line in Fig. 4.10) and bears important long-term morphodynamic inferences, as we will discuss in the following. Single MWPD and VER values (light blue points) do exhibit a larger scatter (R^2 = 0.57) around the linear relationship, that can be ascribed to the uncertainties involved in the estimation of both the volumetric erosion rates and the MWPD values. A similar procedure applied to relate the VERs to the MWPD computed for the 1970 (Fig. 4.11) and 2012 (Fig. 4.12) configurations, provides lower regression coefficients (R^2 = 0.89 and R^2 = 0.84 for the 1970 and 2012 configurations, respectively), thus suggesting that the use of an averaged MWPD for the considered

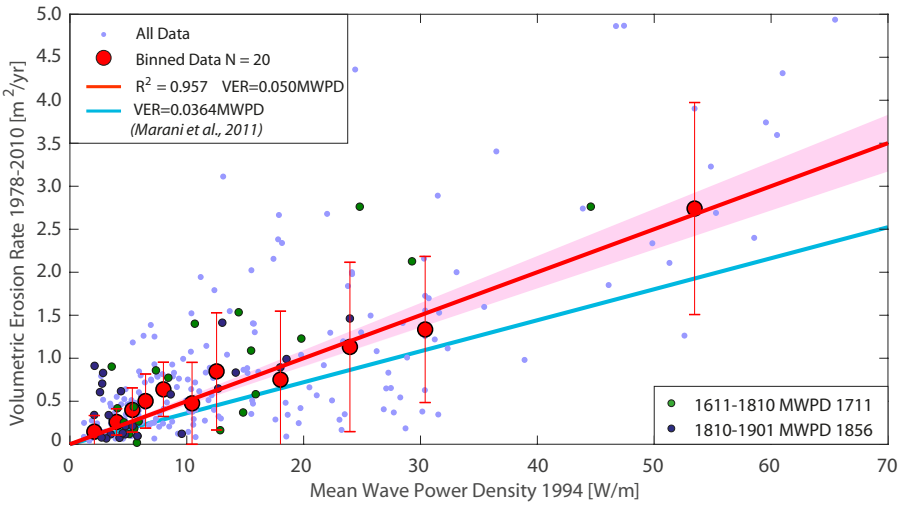

Figure 4.10: Relationship between the volumetric erosion rate and the incident wave power density. Red circles indicate values obtained by averaging data points over intervals of 20 data to emphasize the overall linear trend, whereas each red vertical line represents the standard deviation for the considered bin. The pink shaded area portrays the uncertainty of the prediction of the volumetric erosion rate over a range of coefficients with 95% bounds. The blue line represents the relationship obtained by Marani et al. (2011). The long-term volumetric erosion rates, between 1611 and 1810 (green dots) and between 1810 and 1901 (blue dots) are also shown in the plot.

interval (1978-2010) provides a better description of the geomorphic relationship. Fig. 4.10 further shows the long-term Volumetric Erosion Rates estimated considering the ancient configurations of the lagoon in the interval 1611-1810 and 1810-1901. Those estimated VERs were associated to intermediate MWPDs computed for 1711, by linearly interpolating the data form 1611 and 1810 (green dots), and for the 1856, by interpolating the data from 1810 and 1901 (dark blue dots). Interestingly the two more ancient datasets nicely meet the regression line obtained considering the dataset for the period 1978-2010.

4.4 DISCUSSION

In this study we compared six historical configurations of the Venice Lagoon (namely 1611, 1810, 1901, 1932, 1970 and 2012 - Fig. 4.2) whose bathymetric and planimetric features retain the signatures of the different processes that, acting at overlapping spatial and temporal scales, drive the morphological evolution of the tidal basin, such as tidal fluctuations, relative sea level rise, wind waves and human interferences. Our analyses concerning the temporal evolution

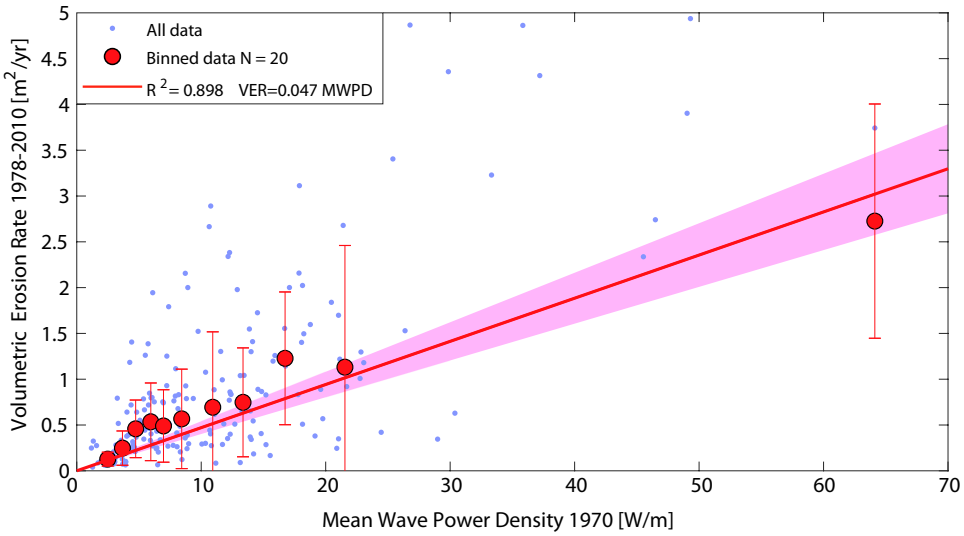

Figure 4.11: Relationship between the volumetric erosion rate and the incident wave power density of 1970. Red circles indicate values obtained by averaging data points over intervals of 20 data to emphasize the overall linear trend, whereas each red vertical line represents the standard deviation for the considered bin. The pink shaded area portrays the uncertainty of the prediction of the volumetric erosion rate over a range of coefficients with 95% bounds.

of the MWPD, computed for the six configurations, allow us to emphasize the mutual relationship and adjustment between wind-wave forcing and tidal morphologies. Wind-wave induced processes, mediated by tidal fluctuations, play a key role on sediment erosion and transport thus driving morphological changes. These changes, in turn, affect the characteristics of the hydrodynamic and wind-wave field in a positive feedback mechanism that can lead to abrupt morphological changes (e.g., Mariotti and Fagherazzi, 2010; Mariotti and Fagherazzi, 2013a; Mariotti and Fagherazzi, 2013b; Leonardi et al., 2016a; Leonardi et al., 2016b; McLoughlin et al., 2015). In the case at hand, the construction of the jetties at the inlets of the Lagoon, completed at the beginning of the 20th century, the excavation of the Malamocco-Marghera navigable channel (Fig. 4.1), completed in 1969, and the increase in relative sea level rise, enhanced the intensity and frequency of wind-wave induced bottom erosion (e.g., D'Alpaos et al., 2013; Carniello et al., 2016) and lateral marsh retreat (Marani et al., 2011). These erosion processes triggered a net and intense sediment export from the lagoon (order of magnitude 106 m^3 per year) towards the Adriatic sea (D'Alpaos and Martini, 2005; Carniello et al., 2012) not counteracted by the almost negligible sediment supply from the watershed and the sea (D'Alpaos and Martini, 2005; Tambroni and Seminara, 2006; D'Alpaos, 2010a). Such a net sediment loss clearly

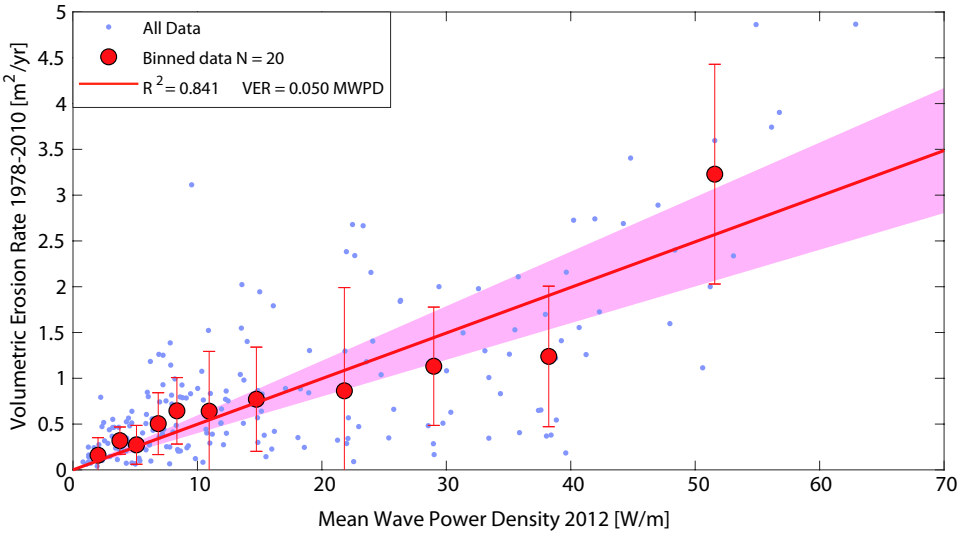

Figure 4.12: Relationship between the volumetric erosion rate and the incident wave power density of 2012. Red circles indicate values obtained by averaging data points over intervals of 20 data to emphasize the overall linear trend, whereas each red vertical line represents the standard deviation for the considered bin. The pink shaded area portrays the uncertainty of the prediction of the volumetric erosion rate over a range of coefficients with 95% bounds.

emerges both from the decrease in salt-marsh extent and from the deepening of tidal flats and subtidal platforms (Fig. 4.13). Indeed, in the last century salt-marsh extent decreased from 164.36 km^2 to 42.99 km^2, while the average tidal-flat bottom elevation decreased from -0.51 m a.m.s.l. to -1.49 m a.m.s.l..

Our modelling analyses clearly show how these trends characterize the behaviour of the averaged MWPD generated over the tidal flats that increased in the last century from 10.33 W/m to 23.64 W/m with a rapid acceleration starting from 1932, when tidal flat deepening experienced a strong acceleration. The increase in fetch length due to salt-marsh loss and the deepening of the tidal flats led to an increase in wave height impacting the marsh edge and consequently to a higher rate of salt-marsh erosion (Fig. 4.10). This accelerated salt-marsh loss triggered a positive feedback among salt-marsh erosion, fetch increase and more energetic wave generation, thus leading to strong changes at the tidal basin scale. Our analyses, based on a unique record of lagoonal morphological configurations, support previous findings that highlighted the existence of the above recalled positive feedbacks (Mariotti and Fagherazzi, 2010; D'Alpaos et al., 2013; Mariotti and Fagherazzi, 2013a; Leonardi et al., 2016a). Interestingly, in the ancient configurations that were not affected by human interferences, wave growth was prevented by the lower depths of tidal flats

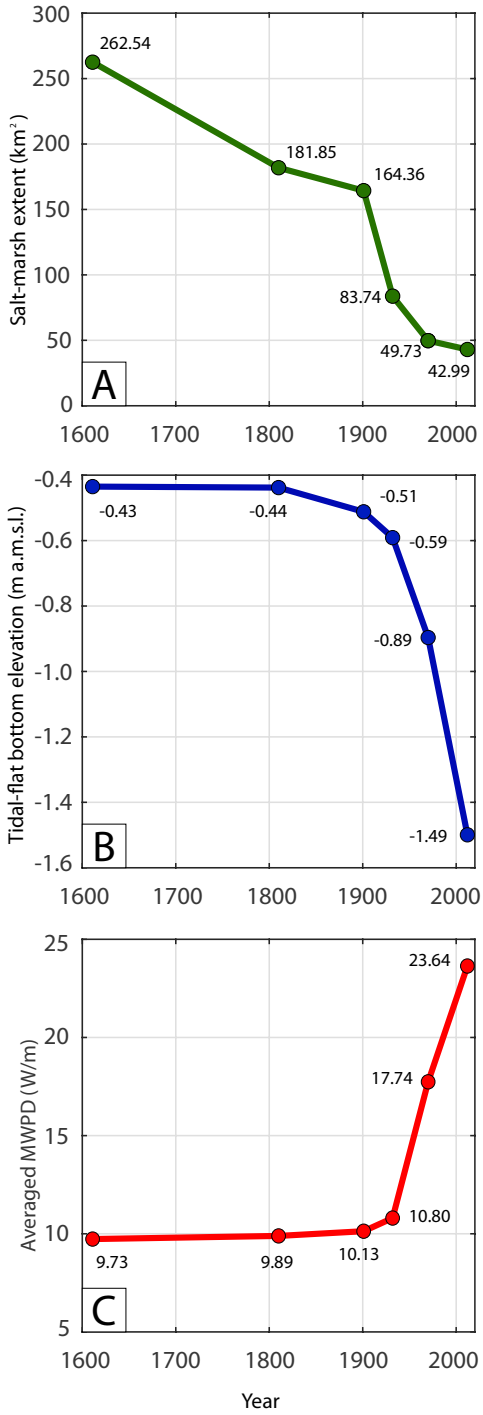

Figure 4.13: Temporal variation of (A) salt-marsh extent during the last four centuries, (B) spatially averaged bottom elevation of the tidal flats during the last four centuries; and (C) averaged mean wave power density in correspondence of the tidal flats within the Venice Lagoon.

and by the widespread presence of salt marshes that reduced fetch length. The enlargement and deepening of tidal flat areas, quite evident starting from 1932 (Fig. 4.2), promoted both an increase in the

MWPD and an increase in the extent of the portion of the lagoon characterized by high MWPD values (Fig. 4.5).

In addition we observe that wave and morphological dynamics might be site specific, displaying important differences within the same system. The central-southern portion of the lagoon is characterized by large tidal-flat and sub-tidal platforms with greater depths and with salt marshes mainly distributed along the landward boundary. In the case of Bora winds, therefore, fetch unlimited conditions are likely to occur. On the contrary, in the northern lagoon, the increase in the MWPD during the last centuries is much less evident. The presence of large salt-marsh areas and islands distributed throughout the northern basin does not allow large fetches to develop, and fetch unlimited conditions are rare. The positive feedback between wave growth and morphological degradation cannot be triggered, thus leading to a much smaller erosive trend (Fig. 4.2), as confirmed also by Carniello et al. (2009). Our analysis suggests that even in the absence of significant changes in the meteorological conditions (e.g., without an increase in storminess), increases in the MWPD would have been observed and will likely be observed in the future, particularly in the absence of sediment supply.

Our results show that particular attention should be paid to the selection of the time interval over which the P_w is computed (or measured) and averaged. Short time intervals that consider only a single or few intense storm events lead to an over estimation of the wave power density (Figs. 4.6 and 4.7) and therefore of the erosion rate (Fig. 4.10). This clearly emerges when comparing the distribution of the mean (Fig. 4.5) and of the maximum wave power densities (Fig. 4.6). We carried out one-year long simulations because this allows us to consider all the wind conditions that typically occur in the Venice Lagoon, and furthermore allows us to consistently relate the MWPD to erosion rates evaluated over a long time period. In agreement with other studies that show how long-term salt-marsh deterioration is dictated by average wave conditions, and not by single strong storm events (Leonardi and Fagherazzi, 2014; Leonardi et al., 2016a), we chose to relate the erosion rate to the MWPD. The MaxWPD might indeed be representative of a single (or a few) strong events that may occur with low frequency. On the contrary, the MWPD describes the overall wave power conditions. Marsh erosion rate is usually evaluated either as a linear erosion rate (Schwimmer, 2001; Leonardi et al., 2016b) or as a volumetric erosion rate (Marani et al., 2011; Bendoni et al., 2016). Here we decided to consider a volumetric erosion rate (m^2/yr), by assuming to neglect changes in the cliff height, h, in agreement with other studies (Marani et al., 2011; Bendoni et al., 2016). The positive linear correlation between the MWPD and the volumetric erosion rate agrees with previous studies carried out considering

data from the Venice Lagoon (Marani et al., 2011) and other lagoons worldwide (Leonardi et al., 2016a). We emphasize that the use of a fully-coupled 2D wave model, compared to the 0D model adopted by Marani et al., 2011, suggests that wind wave power is one of the main factors controlling the erosion of salt marsh edges, and that the above recalled linear relationship might safely be used for long-term morphodynamic studies. The relationship proposed by (Marani et al., 2011), respect to our relationship overestimates the mean wave power density needed to produce the same erosion (see Fig. 4.10). The scatter of the experimental points from the regression line can be ascribed to errors in image rectification and digitalization, image discretization errors, errors associated with the spatial heterogeneity of the wind field, wave model approximations, as well as to the spatial variability of sediment properties and vegetation cover, and to boat-induced waves that were not accounted for in our simulations. We deem important to recall that we considered the average MWPD impinging marsh edges between 1978 and 2010. To this end we linearly interpolated the MWPD computed for the 1970 and the 2012 configurations of the lagoon, and estimated the MWPD in 1994, that is in the middle year between the two available aerial photos (1978 and 2010). We adopted this methodology in order to account for the morphological changes between the two configurations of 1970 and 2012, that strongly affected the spatial distribution of the MWPD. Considering the P_w of the 1970 configuration would have led to an underestimation of the MWPD, whereas considering the 2012 P_w would have led to an overestimation of the wave field in the considered period. We investigated the validity of the suggested linear relationship between MWPD and Volumetric Erosion Rate also by analysing data from two different and longer periods considering the more ancient configurations of the lagoon (namely 1611-1810 and 1810-1901). Observed erosion rates and the computed MWPD were found to nicely agree with the relationship obtained considering the more recent data (Fig. 4.10), thus further supporting the validity and the importance of the linear geomorphic relationship.

4.5 CONCLUSIONS

Wind-wave erosion is one of the main mechanisms that control the morphological evolution of shallow tidal environments, affecting the equilibrium elevation and dynamics of subtidal and tidal-flat surfaces, and the stability of salt marsh margins. We have used a widely tested Wind-Wave Tidal Model (WWTM) and field observations retrieved from remotely sensed images, to analyse and interpret changes in the morphological features of lagoonal systems and their relationship

with the hydrodynamic and wave fields. The WWTM was applied to six historical configurations of the Venice Lagoon (namely 1611, 1810, 1901, 1932, 1970, 2012), marsh lateral erosion was determined by comparing recent aerial photos (1978, 2010), and morphological changes at the whole system scale were obtained by comparing the six available bathymetries. The main results of our analyses can be summarised as follows.

- Model results suggest that while the spatial distribution of the Mean Wave Power Density has not significantly changed from 1611 to 1901, a rapid, dramatic increase in the MWPD was observed in the last century (1901 - 2012).
- Our results also emphasize the different evolutionary trends experienced by the northern and southern part of the lagoon: erosion and deposition dynamics are strongly site specific also within the same tidal system. While the northern part of the lagoon was subjected to a slow erosive trend mitigated by the shallow water depths and the short fetches that limit wind-wave erosion, a strong increase in the erosive trend of salt-marsh areas and tidal-flat/subtidal platforms was observed in the central-southern part of the Venice Lagoon.
- As to the erosion trends at the lagoonal scale, the elevation of the tidal flats decreased from -0.51 m (a.m.s.l.) to -1.50 m (a.m.s.l.) in the last century, whereas salt-marsh extent decreased from about 164 km^2 to about 43 km^2. Erosion processes were driven by the increase in wave height and power, the MWPD having increased from 10 W/m to 23.6 W/m in the same time interval. The unique dataset of bathymetries and maps from the Venice Lagoon allowed us to highlight the positive feedbacks between the vertical and lateral erosion of lagoonal bottoms and the increase in wave height and power.
- Finally we quantitatively investigated the relationship between wave power density (for two most recent configurations of the lagoon, 1970 and 2012) and the retreat rate of salt-marsh margins (determined by comparing aerial photographs in 1978 and 2010). Our analyses support the existence of a strong linear relationship between the volumetric marsh lateral erosion rate and the incident mean wave power density, thus confirming previous findings based on theoretical grounds and tested by considering the results of a simplified point wave model (Marani et al., 2011). The use of a full-fledged widely WWTM further supports the possibility of adopting such a linear relationship for long-term morphodynamic analyses. Our results thus suggest that relating salt-marsh retreat rates to properly computed mean wave

power densities is a valuable morphological tool for long-term morphodynamics. The quality and nature of the theoretical and empirical validations, coupled with the breadth and importance of the implications, reinforce earlier proposals to use such a relationship for long-term morphodynamic issues.

5 STATISTICAL MECHANICS OF WIND WAVE-INDUCED EROSION

This chapter is a manuscript in preparation that will be submitted to *Advances in Water Resources*, whose main goal is to unravel wind-wave erosional effects within the Venice Lagoon in the last four centuries by means of a statistical framework originally proposed by D'Alpaos et al. (2013) and later adopted by Carniello et al. (2016). Wind wave-induced erosion is one of the main landscape-forming processes in tidal biomorphodynamics. Indeed, wave-driven bottom erosion controls the equilibrium elevation and dynamics of subtidal and tidal-flat surfaces, and the impinging of wind-waves against salt marsh boundaries is one of the main factors responsible for marsh retreat. Here we have applied a fully-coupled finite element model accounting for the role of wind waves and tidal currents to six configurations of the Venice Lagoon, ranging from 1611 to 2012, in order to analyse the characteristics of combined current- and wave-induced exceedances in bottom shear stress. The results of our analyses suggest that wind wave-induced resuspension events can be modelled as a marked Poisson process consistently for all the six considered configurations. This result will allow us to set up a theoretical framework which can be used to model wind-wave resuspension effects during a time span of centuries, through the use of Monte Carlo realizations, thus bearing important applications for quantitative analyses on the long-term morphodynamic evolution of shallow tidal systems.

PAPER

STATISTICAL MECHANICS OF WIND WAVE–INDUCED EROSION WITHIN THE VENICE LAGOON IN THE LAST FOUR CENTURIES

Laura Tommasini[1], Luca Carniello[2], Luigi D'Alpaos[2], Andrea Rinaldo[2], and Andrea D'Alpaos[1]

[1]Dept. of Geosciences, University of Padova, via G. Gradenigo 6, Padova, Italy

[2]Dept. ICEA, University of Padova, via Loredan 20, Padova, Italy

Abstract

The long-term evolution of tidal landscapes is strongly influenced by wind-wave induced erosion events and by the related dynamics of suspended sediments. Improving our knowledge on the characteristics of such events is a key point to address tidal-landscape long-term evolution, particularly through the use of effective simplified theoretical frameworks. Here we employed a widely tested bi-dimensional mathematical model that describes the spatial and temporal dynamics of bottom shear stress (BSS) induced by tidal currents and wind waves. By forcing the model with a one-year long time series of observed water levels and wind data from the Venice lagoon, we analysed the characteristics of combined current- and wave-induced exceedances in bottom shear stress over a given threshold for erosion. The same forcings were used to analysed BSS dynamics for six different configurations of the Venice Lagoon, from 1611 to 2012, on the basis of the "Peak Over Threshold" theory. Our analysis suggests that erosion events can be modelled as a marked Poisson process over most of the Lagoon for all of the considered historical lagoon configurations. In addition, our study suggests that intensity and duration of overthreshold events are temporally correlated, while almost no correlation exists between interarrival times and both duration and intensities. Finally, our analyses will be useful in that they allow one to provide predictions on future erosive scenarios for the Venice Lagoon, in particular, and to discuss implications for long-term morphodynamic modelling of tidal environments, in general.

5.1 INTRODUCTION

Subtidal platforms, tidal flats and salt marshes are vitally important morphological features of tidal landscapes that can be strongly eroded and impacted by wind-wave induced processes. Indeed, the equilibrium elevation and dynamics of subtidal platforms and tidal flats is driven by sediment deposition, wave-induced erosion and by the rate of relative sea level rise (RSLR) (e.g., Fagherazzi et al., 2006; Callaghan et al., 2010; Marani et al., 2010; D'Alpaos et al., 2012; Green and Coco, 2014). Moreover, with their erosive action wind waves dictate the horizontal progradation or retreat of salt-marsh margins, thus affecting the position of salt-marsh boundaries (e.g., Möller et al., 1999; Schwimmer, 2001; Marani et al., 2010; Mariotti and Fagherazzi, 2010; Marani et al., 2011; McLoughlin et al., 2015; Bendoni et al., 2016; Leonardi et al., 2018). In addition, temporal and spatial patterns of wind-wave induced bottom shear stresses can influence the morphological and biological features of the tidal landscape (e.g., Carniello

et al., 2005; Fagherazzi and Wiberg, 2009; Mariotti et al., 2010). Wind-wave induced bottom shear stresses can in fact promote the disruption of the polymeric microphytobenthic biofilm (MPB) typically colonizing the bed sediment in shallow tidal environments (Amos et al., 2004; Mariotti and Fagherazzi, 2012; Pivato et al., under review on Earth Surface Processes and Landforms) and lead to the erosion of tidal-flat surfaces. The related increase in suspended sediment concentration can trigger a negative feedback by promoting the decrease of light availability in the water column and thus limiting the sea grass and MPB proliferation (Lawson et al., 2007; Carr et al., 2010; Chen et al., 2017).

As an example, the Venice Lagoon has experienced strong erosion processes in the last centuries, which progressively deepened the lagoonal bottoms, promoted the loss of fine cohesive sediments through the main channels and the inlets after storms, and led to the loss of extensive salt-marsh areas (Carniello et al., 2009; D'Alpaos, 2010a; D'Alpaos, 2010b). Furthermore wave-induced erosion processes control the size of the tidal prism and as a consequence the related morphological features of tidal networks, such as channel cross-sectional area (e.g., D'Alpaos et al., 2009; D'Alpaos et al., 2010) and drainage density (Marani et al., 2003; Stefanon et al., 2012).

Several numerical models exist that describe the hydrodynamic and wind-wave fields in shallow tidal basins (e.g., Umgiesser et al., 2004; Carniello et al., 2011) and their influence on the morphodynamic evolution of tidal landscapes (e.g., Marani et al., 2010; D'Alpaos et al., 2012; Mariotti and Fagherazzi, 2013a).

Modelling the morphodynamic evolution over time scales of centuries using fully-fledged models is a difficult task due to the numerical burdens involved. The use of simplified approaches is therefore more and more frequently adopted (e.g., Murray, 2007). Towards the goal of further developing a synthetic theoretical framework to represent wind wave-induced resuspension events and accounting for their erosional effects on the long-term morphodynamic evolution of tidal systems, we applied a two dimensional finite element model reproducing the role of wind waves and tidal currents on the hydrodynamic circulation to several bathymetric configurations of the Venice Lagoon. More precisely, in the present study we used the fully coupled wind wave-tidal model developed by D'Alpaos and Defina (2007) and Carniello et al. (2011) to investigate the hydrodynamic behaviour of six different configurations of the Venice Lagoon (namely the 1611, 1810, 1901, 1932, 1970 and 2012 configurations). For each configuration we run a one-year-long simulation considering representative tidal and meteorological boundary conditions. The resulting spatial and temporal dynamics of Bottom Shear Stresses (BSSs) for the six configurations have been analyzed on the basis of the peak over

threshold theory once a critical shear stress for the erosion of cohesive sediments was chosen, in the framework used by D'Alpaos et al. (2013) for the analysis of the wave-induced BSSs and by Carniello et al. (2016) for the analysis of suspended sediment concentrations for the present configuration. The main goal of the present analysis is to find whether, in line with previous results, wave-induced resuspension events can be modeled as marked Poisson processes also for the historical configurations of the Venice Lagoon. This is particularly relevant because the possibility of describing those erosion processes as a Poisson process represents a promising framework for long-term studies. Indeed, the analytical characterization of the long-term behaviour of geophysical processes is becoming increasingly popular in hydrology and geomorphology (e.g., Rodriguez-Iturbe et al., 1987; D'Odorico and Fagherazzi, 2003; Botter et al., 2007; Park et al., 2014), although the applications to tidal landscape are still quite rare (D'Alpaos et al., 2013; Carniello et al., 2016). Our analyses provide a temporally and spatially explicit characterization of wind-induced erosion events for the Venice Lagoon starting from the beginning of the XVII century, thus allowing us to investigate and understand the main features of the erosive trends the lagoon has been experiencing and to provide predictions on future scenarios.

5.2 METHODS AND DATA

We considered six different configurations of the Venice Lagoon, covering a time span of four centuries, in order to access the feedbacks existing between morphology and wind waves action that controls the evolution of the tidal landscape. These configurations were reconstructed by using historical maps (1611, 1810 and 1901), and the more recent topographic surveys carried out by the Venice Water Authority (Magistrato alle Acque di Venezia) in 1932, 1970 and 2003. For a complete description of the Lagoon bathymetries we refer the reader to the second and fourth chapters of the present work. The computational grids reproducing all the six configurations of the lagoon were already used in previous studies: the 1611 by Tommasini et al. (2017); the 1810 by D'Alpaos and Martini (2005) and D'Alpaos (2010a); the 1901, 1932, 1970 and 2003 by Carniello et al. (2009) and D'Alpaos (2010a).

5.2.1 Numerical Model and Numerical Simulations

The Wind Wave Tidal Model (WWTM) applied herein consists of two modules: the hydrodynamic module coupled with the wind-wave module. The WWTM describes, on the same computational

grid, the hydrodynamic flow field together with the generation and propagation of wind waves (Carniello et al., 2005; Carniello et al., 2011).

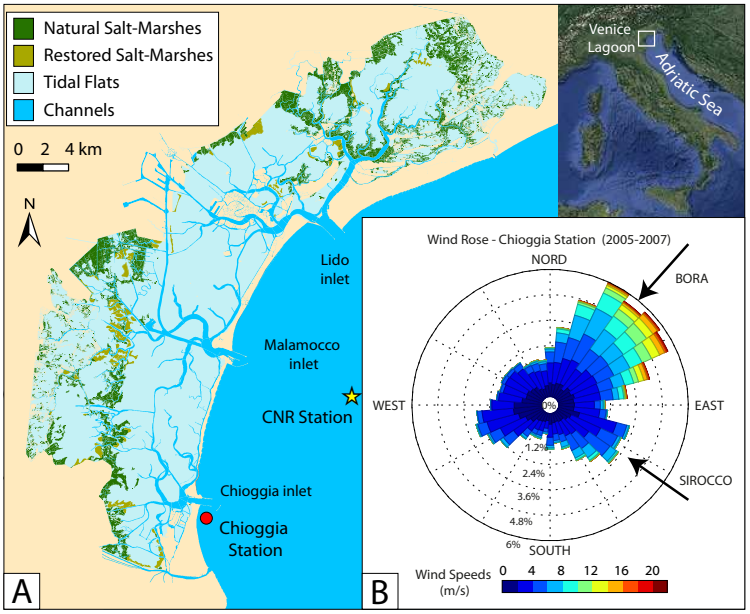

Figure 5.1: (A) Spatial distribution of the main morphological features characterizing the actual Venice Lagoon. The locations of the anemometric (Chioggia) and mareographic (CNR Oceanographic Platform) stations are also shown. (B) Wind rose obtained on the basis of the data recorded in the Chioggia station in the period 2005–2007

The hydrodynamic module solves the 2-D shallow water equations using a semi-implicit staggered finite element method based on Galerkin's approach (Defina, 2000; D'Alpaos and Defina, 2007). Considering the case of a turbulent flow over a rough wall, the bottom shear stress induced by currents, τ_{tc}, is evaluated using the Strickler equation (Defina, 2000). The hydrodynamic module provides the water levels that are used by the wind wave module to assess the wave group celerity and the bottom influence on wind wave propagation.

The wind wave model is based on the solution of the wave action conservation equation, parameterized using the zero-order moment of the wave action spectrum in the frequency domain (Carniello et al., 2005; Carniello et al., 2011). The spatial and temporal distribution of the wave period is determined through an empirical correlation function relating the peak wave period to the local wind speed and water depth (Young and Verhagen, 1996a; Breugem and Holthuijsen, 2007; Carniello et al., 2011). The wind-wave module computes the bottom shear stress induced by wind waves, τ_{ww}, as a function of the maximum horizontal orbital velocity at the bottom, which is related to the significant wave height through the linear theory. The total bottom shear stress, τ_{wc}, resulting from the combined effect of tidal currents

and wind waves, is greater than the sum of the two contributions, because of the nonlinear interaction between the wave and the current boundary layer. In the WWTM this is accounted for by using the empirical formulation suggested by (Soulsby and Whitehouse, 2005):

$$\tau_{wc} = \tau_{tc} + \tau_{ww}\left[1 + 1.2\left(\frac{\tau_{ww}}{\tau_{ww} + \tau_{tc}}\right)\right] \tag{5.1}$$

The WWTM has been largely tested against field observations in the Venice Lagoon and in other lagoons wordwide (e.g., D'Alpaos and Defina, 2007; Mariotti et al., 2010; Carniello et al., 2011; Zarzuelo et al., 2018), thus suggesting that the model is suited to determine temporal and spatial variations of BSSs in shallow microtidal basins. Numerical simulations were carried out using the six computational grids described above and representing the Venice Lagoon and a portion of the Adriatic Sea.

The model was forced by using hourly tidal levels measured at the Consiglio Nazionale delle Ricerche (CNR) Oceanographic Platform, located in the Adriatic Sea in front of the lagoon, and wind velocities and directions measured at the Chioggia anemometric station, where a quite long data set was available which enabled us also to analyse the wind climate over the lagoon (Fig. 5.1). We forced the model with the time series recorded in 2005, which was shown to be a representative year for the wind characteristics in the Venice Lagoon (D'Alpaos et al., 2013).

5.2.2 Peak Over Threshold Analysis

The hydrodynamic, biologic and geomorphologic processes, which include deterministic and stochastic components control the sediment transport dynamics in tidal environments. The morphological evolution of the Venice Lagoon is related to some limited and intense resuspensions events induced by wind waves (Carniello et al., 2011) whose dynamics are marked stochastic in the present configuration of the Venice Lagoon (D'Alpaos et al., 2013; Venier et al., 2014; Carniello et al., 2016). In the present work, at any location within the Venice lagoon, we analyzed the temporal and spatial evolution of the τ_{wc} using the peak over threshold theory (POT) (Balkema and De Haan, 1974). We carried out a statistical analysis of the interarrival times, durations and intensities of the exceedences of the selected threshold. The POT method allowed us to identify (i) the interarrival time, as the time elapsed between two consecutive upcrossings of the threshold; (ii) the duration of the events, that is the time elapsed between any upcrossing and the subsequent downcrossing of the threshold, and (iii) the intensity, calculated as difference between the maximum value of τ_{wc} in the time elapsed between the upcrossing and the downcross-

ing, and the threshold $\tau_c = 0.4$Pa (Amos et al., 2004; Marani et al., 2010). These variables could be illustrated by their probability density functions and the corresponding moments. The analysis is performed pointwise and in all the configurations and repeated for each location of the Venice lagoon in order to provide an accurate description of the spatio-temporal patterns of τ_{wc}. This adopted methodology resembles that used by D'Alpaos et al. (2013) to characterize the patterns of bottom shear stresses in the present configuration of the lagoon and later applied by Carniello et al. (2016) to analyse suspended sediment dynamics. Importantly, in this paper the statistical analysis is extended to six different configurations of the Venice Lagoon. We performed a Kolmogorov-Smirnov (KS) goodness of fit test to test the hypothesis that the interarrival time of resuspension events is an exponentially distributed random variable. The distribution intervals play an important role, because if the interarrival times between subsequent exceedances of τ_{wc} are independent and exponentially distributed random variables, τ_{wc} dynamics can be mathematically described as a marked Poisson process, where a vector of random marks (intensity and duration of each over threshold event) is associated to a sequence of random events that define a 1-D Poisson process along the time axis. Poisson processes are characterized by mathematical features such as the memoryless property. Owning to this property the probability of observing a certain number of events in a pre-established time interval is independent of the position of the latter, depending only on its duration. The Poisonnianity of the BSSs would therefore allow one to immediately identify the probabilities of observing a certain number of resuspension events in a year or during a season, because all the sources of stochasticity in the physical drivers are described by a single parameter (the mean frequency of the process).

5.3 RESULTS AND DISCUSSIONS

In order to provide a statistical characterization of wave-induced resuspension events, we have analysed the time series of computed total BSSs, on the basis of a POT method. For all the six configurations we set the critical shear stress equal to 0.4 Pa (Amos et al., 2004). Over the tidal flats current-induced BSSs are typically below the critical value, while wind wave-induced BSSs give the main contribution to the total BSS (D'Alpaos et al., 2013). Moreover the non-linear interaction effect between currents and wind waves can be as large as 10% of the total BSS. In order to remove short-term fluctuation and spurius upcrossing and downcrossing of the fixed threshold, the time series of BSSs were filtered by applying a moving average with a time window of 6 hours.

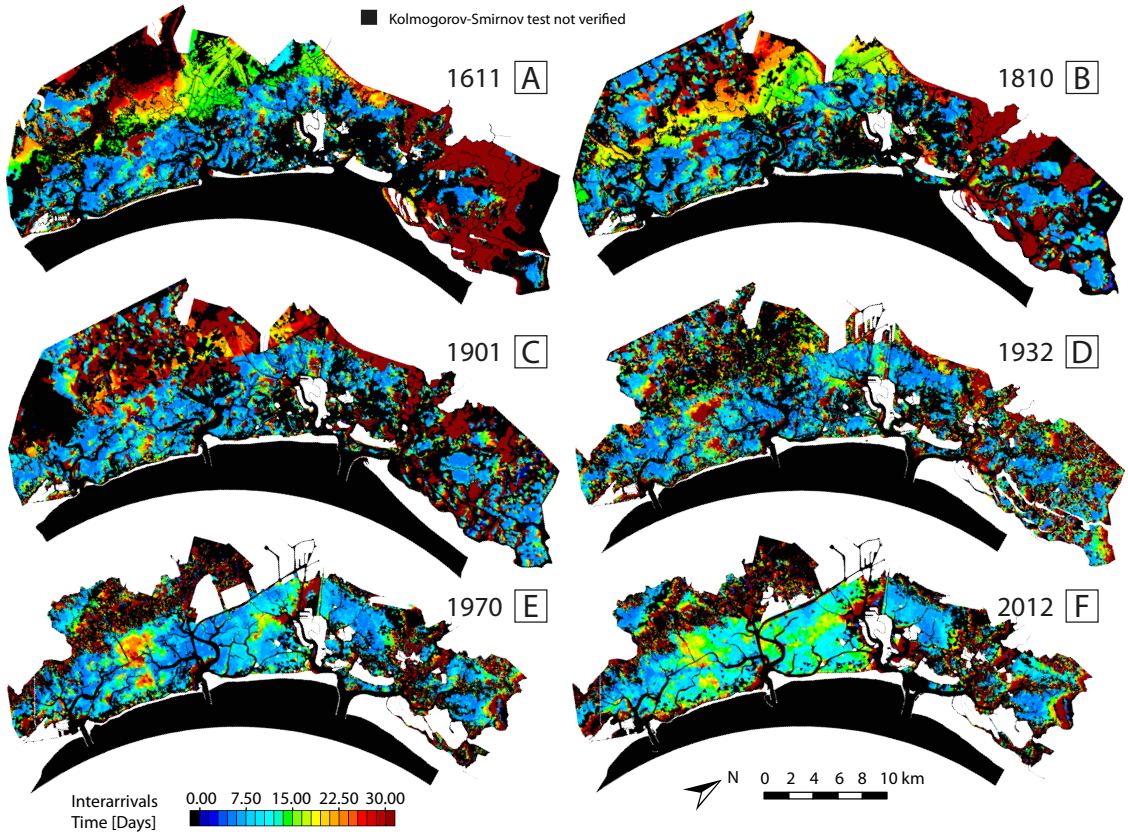

Figure 5.2: Spatial distributions of mean interarrival times where the probability distributions of local interarrival times of overthreshold events are exponential, as confirmed by the KS test (α = 0.05) for the six different configurations of the Venice Lagoon: 1611 (A), 1810 (B), 1901 (C), 1932 (D), 1970 (E), and 2012 (F).

We analysed the spatial variability of mean interarrival times (Fig. 5.2), peak excesses (Fig. 5.3) and durations (Fig. 5.4) in the six configuration of the Venice Lagoon. Due to the BSS variation, that depends on wind velocity, fetch length, and water depth, the characteristics of the resuspension events display a complex spatial pattern in particular for the ancient configurations. For each configuration we portrayed the mean interarrival time, peak excess and duration of overthreshold events at any location whitin the Venice Lagoon in which the KS test, made in order to verify that the mentioned variables are exponentially distributed random variables, is satisfied at significance level $\alpha = 0.05$. Fig. 5.5 shows the spatial distribution of the results of the KS test. In particular we distinguished: (i) the blue area where the KS is not verified for the interarrival time, i.e., resuspension events can not be described as a Poisson process; (ii) the red area where the KS test is verified for all the three stochastic variables we considered, namely interarrival times, intensity, and duration, i.e., resuspension events are indeed a marked Poisson process where also intensity and duration

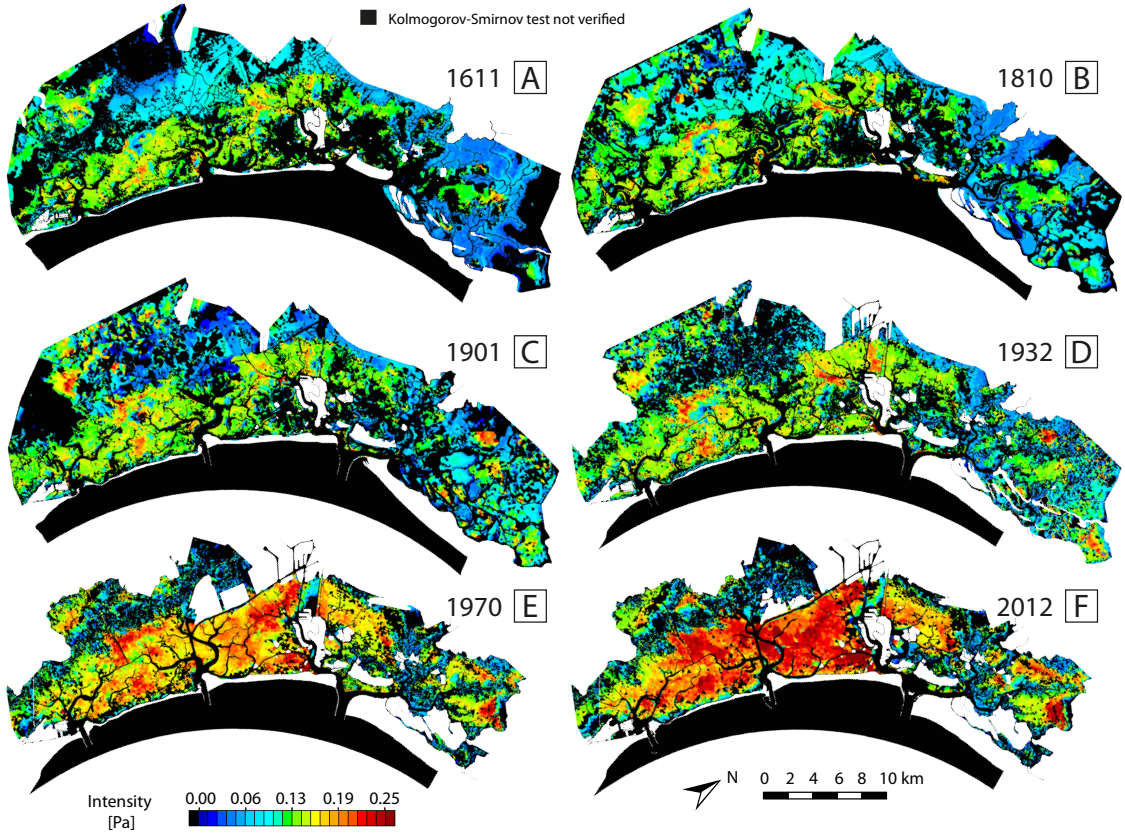

Figure 5.3: Spatial distributions of mean intensities of peak excesses where the probability distributions of mean intensities of peak excesses are exponential, as confirmed by the KS test (α =0.05) for the six different configurations of the Venice Lagoon: 1611 (A), 1810 (B), 1901 (C), 1932 (D), 1970 (E), and 2012 (F).

are exponentially distributed random variables; (iii) the yellow area where the KS test is verified for the interarrival time but not for the intensity and/or duration, i.e., resuspension events are a marked Poisson process but at least one between intensity and duration is not an exponentially distributed random variable.

In all the configurations we note that the portions of the lagoon where resuspension events cannot be modelled as a Poisson process (blue area in Fig. 5.5) are mostly represented by salt marshes and tidal channels. Over salt marsh platforms no exceedencances of the fixed threshold tend to occur because of the lower water depth (e.g., Möller et al., 1999). Along the channels the exceedences are mostly related to peak excesses promoted by tidal currents, which cannot be modelled as a Poisson process. Moreover comparing the results obtained for the six configurations we note that the present Lagoon is characterized by wider areas where the KS is verified respect to the historical configurations, this happens for interarrival times as well as for intensities and durations. This is mainly due to the complex distribution of salt

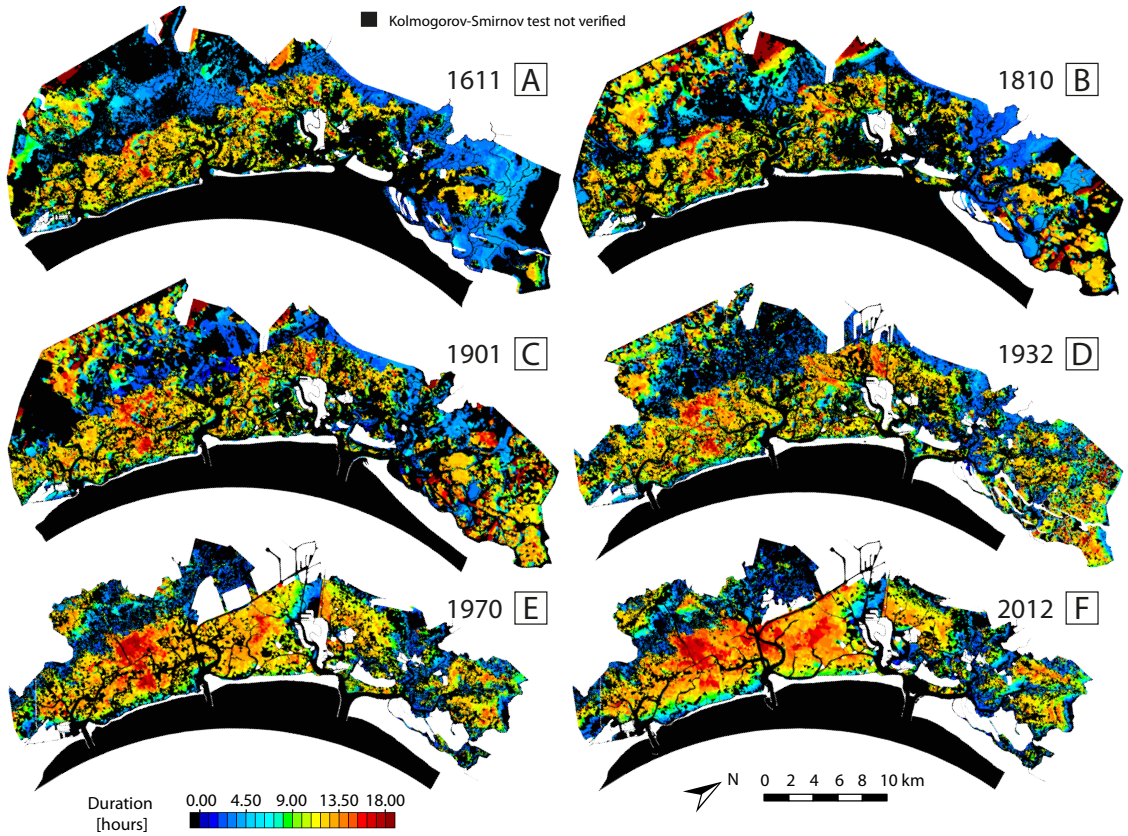

Figure 5.4: Spatial distributions of mean durations of overthreshold exceedances where the probability distributions of mean durations of overthreshold exceedances are exponential, as confirmed by the KS test (α =0.05) for the six different configurations of the Venice Lagoon 1611 (A), 1810 (B), 1901 (C), 1932 (D), 1970 (E), and 2012 (F).

marshes that characterized the historical configurations, as a consequence in some sheltered tidal flat the resuspension events were more modest and only few events exceeded the critical threshold of 0.4 Pa (Fig. 5.5). We found large interarrival times in the area sheltered from the Bora wind, blowing from North-East. A clear example is provided by the area protected by marsh platforms and by the mainland in the northeastern and in the western portion of the lagoon as well as the areas located downwind of islands and artificial structures (Fig. 5.2). This pattern becomes more evident in the configurations of 1611, 1810 and 1901 where larger portions of the lagoon were occupied by salt marshes. In the area between the Chioggia and the Malamocco inlets the interarrival times decreased from the past to the present (i.e., resuspension events are more frequent) due to the generalized deepening experienced by this part of the lagoon. Furthermore in the ancient configurations we found shorter interarrival times spread all around the lagoon basin, while the present configuration, characterized by a more constant and larger water depth (in some areas grater than 1.5

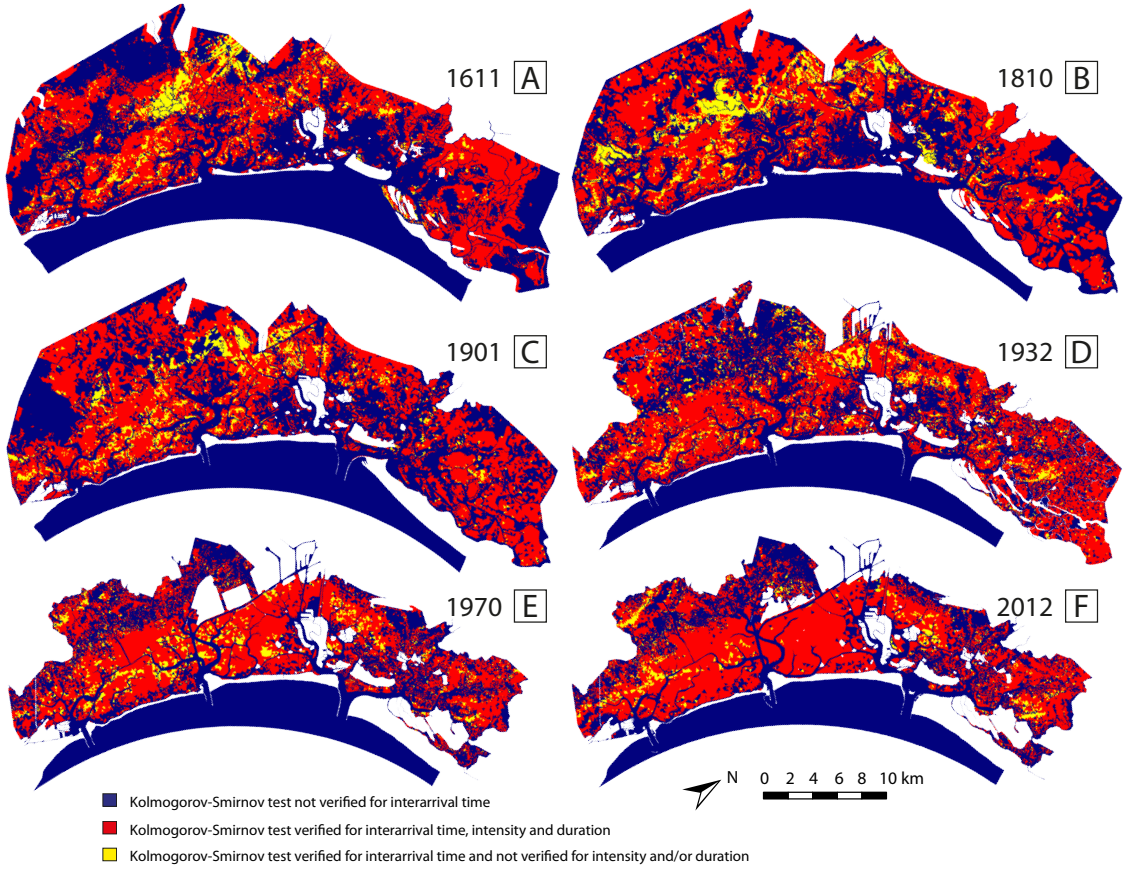

Figure 5.5: Maps providing the spatial distribution of Kolmogorov-Smirnov test (KS) at significance level (α =0.05) for the six different configurations of the Venice Lagoon 1611 (A), 1810 (B), 1901 (C), 1932 (D), 1970 (E), and 2012 (F). In the maps we distinguish areas where the KS test is: not verified (blue); verified for all the considered stochastic variables (interarrival time, intensity over the threshold and duration) (red) ; verified for the interarrival time and not for intensity and/or duration (yellow).

m), displays intermediate interarrival times between 7 and 10 days for the entire portion between Lido and Chioggia inlets (Fig. 5.2). This is mainly due to the relationship existing between τ_{ww} and water depth that, for a fixed wind velocity, decreases as the water depth increases (see the third chapter). Indeed, in the historical configurations large areas covered by tidal flats are characterized by lower water depth ($\leqslant$ 0.5 m), as a result the τ_{ww} are higher also for weak wind speeds, thus increasing the number of exceedances of the threshold.

The over threshold peak intensities (Fig. 5.3) strongly increased during the last four centuries. As one might expect, or all the configurations intensities are much larger in the central and southern portion of the Lagoon, than in its northern part, which is sheltered by the mainland from Bora wind conditions and is characterized by the presence of very shallow flats and large salt-marsh portions which also provide

a protection and interrupt the fetch. In the central part of the lagoon, where the lagoon experienced the flattening and the deepening of tidal flats, the mean intensities have increased from around 0.13 Pa to around 0.25 Pa over the threshold, while in the northern portion the increase is less evident due to the salt-marsh conservation.

The durations of events, likewise intensities, increased in particular in the central-southern portion. We observed short durations for all the configurations in the area sheltered by the mainland and salt marshes.

The larger overthreshold peak intensities, as well as the longer durations characterizing the central-southern portion of the lagoon and increasing from the past to the present, are in agreement with recent observations emphasizing a critical erosive trend for the tidal flats and subtidal platforms in this area (e.g., D'Alpaos, 2010b; Defendi et al., 2010; Sarretta et al., 2010; Carniello et al., 2009).

Fig. 5.6, 5.7 and 5.8, show for the six configurations, the temporal cross correlation between the three random variables, computed for each point within the Lagoon. The results underline that the intensity of peak excesses and the duration of over threshold exceedances are highly correlated, thus suggesting a pseudo-deterministic link between peak intensities and the corresponding durations (Fig. 5.6). On the other hand, almost no correlation exists between durations and interarrival times (Fig. 5.7), as well as between intensities and interarrival times (Fig. 5.8). These results, in line with the correlation obtained for the statistical characteristics of suspended sediment concentration by Carniello et al. (2016), suggest that resuspension events can be modelled as a 3-D Poisson process in which the marks (duration and intensity of events) are mutually dependent but independent from the the interarrival times.

In order to provide a more quantitative estimation of the spatial heterogeneity of interarrival times, durations and intensities we computed the erosion work (Marani et al., 2010; Mariotti and Fagherazzi, 2013b) along the simulation (Fig. 5.9). The mean values of the characteristics of the resuspension events (i.e., interarrival times, durations and intensities), were used to compute the average erosion in each grid element $[E_w]$, as:

$$[E_w] = \int_{t_1}^{t_2} \frac{e}{\rho_s} \left(\frac{\tau_{wc} - \tau_c}{\tau_{wc}} \right) dt. \tag{5.2}$$

where e is the value of the erosion coefficient which depends on the sediment properties and ρ_s is the sediment density. We set e equal to 0.00001 $kgm^{-2}s^{-1}$, as suggested for sand-mud mixtures (Van Ledden et al., 2004) and ρ_s 2650 kg/m^2.

We can simplify the Eq. (5.2) as follows:

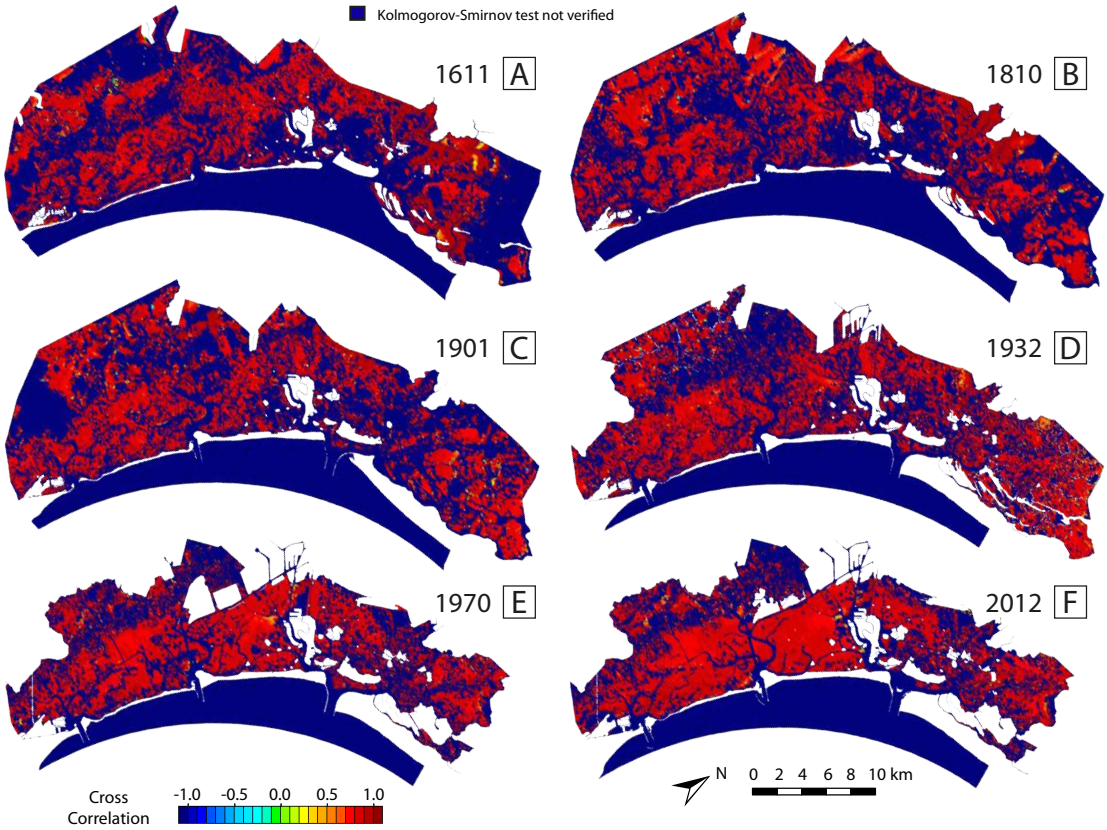

Figure 5.6: Spatial distribution of temporal cross-correlation between intensity of peak excesses and duration of over threshold exceedence for the different configurations of the Venice Lagoon 1611 (A), 1810 (B), 1901 (C), 1932 (D), 1970 (E), and 2012 (F). Dark blue identifies sites where the bottom shear stress cannot be modelled as a marked Poisson process (i.e., the KS test is not verified for the interarrival time).

$$[E_w] = \frac{e}{\rho_s}\left(\frac{\tau_{wc} - \tau_c}{\tau_{wc}}\right)(t_2 - t_1) \tag{5.3}$$

where we assume $(t_2 - t_1)$ to be the mean duration of the event and $(\tau_{wc} - \tau_c)$ the mean intensity. In order to obtain the erosion in the entire year of simulation we multiplied the result obtained with the Eq. (5.3) for the number of events computed as 365 (days per year) divided by the mean interarrival time of each element.

Fig. 5.9 provides the spatial distribution of the erosion work, E_w, for the six configurations of the lagoon and clearly shows that the erosion work is constant between 1611 and 1932, it reaches its maximum in the 1970 and then it decreases again in the present configuration. We refer the reader to the third chapter where the variation of the bottom shear stress according with depth, fetch, and wind velocity is described in details. We recall here only that for any prescribed wind intensity, the relationship between BSS and water depth is rep-

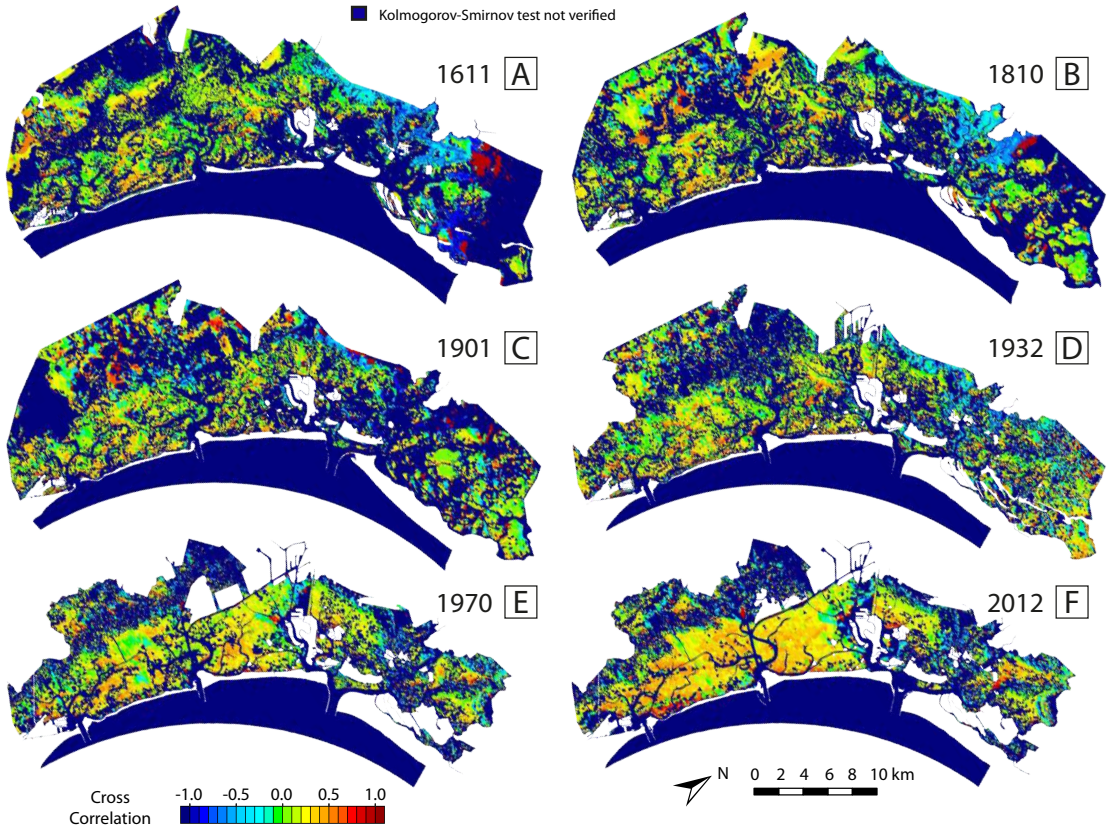

Figure 5.7: Spatial distribution of temporal cross-correlation between intensity of peak excesses and interarrival time for the different configurations of the Venice Lagoon 1611 (A), 1810 (B), 1901 (C), 1932 (D), 1970 (E), and 2012 (F). Dark blue identifies sites where the bottom shear stress cannot be modelled as a marked Poisson process (i.e., the KS test is not verified for the interarrival time).

resented by a curve peaking, for strong wind speed, around -0.5/-0.8 m a. MSL. The average elevation of the tidal flats in the central southern part of the 1970 configuration of the lagoon is quite close to that characterizing the maximum in the BSS curve, thus explaining the trend previously described. The ancient configurations (i.e., 1611, 1810, 1901 and 1932) display a complex spatial pattern because of the presence of salt marshes and islands distributed throughout the basin and the shallower tidal flats. This morphology is such that the fetch is continuously interrupted, thus preventing the erosion that is located only in some tidal flats, while in the area sheltered by mainland and salt marshes the erosion is negligible. The erosion strongly increases in the with a peak of 2.5 cm/year, thus leading to the present morphology and bathymetry characterized by less complex erosion pattern and a roughly constant erosion rate, around 1.5 cm/year, in the central-southern part due to the enlargement and flattening of tidal flats. Our results further support previous studies (e.g.,

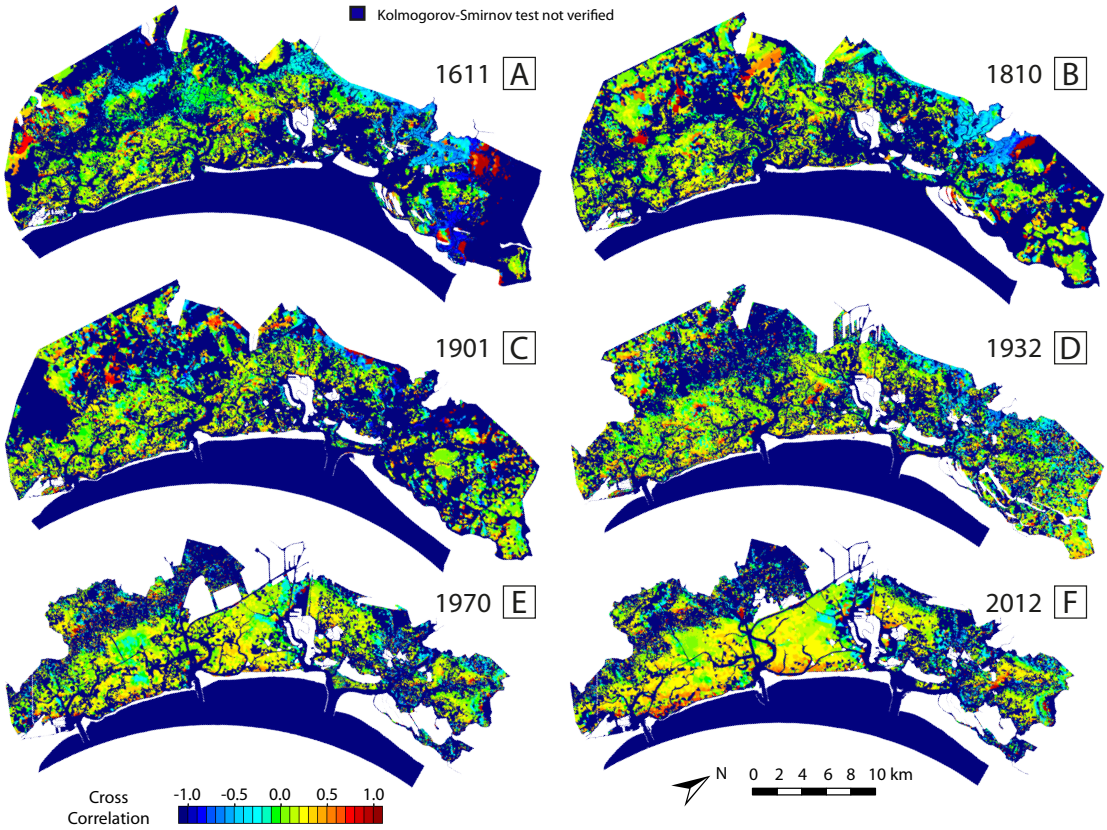

Figure 5.8: Spatial distribution of temporal cross-correlation between duration of over threshold exceedence and interarrival time for the different configurations of the Venice Lagoon 1611 (A), 1810 (B), 1901 (C), 1932 (D), 1970 (E), and 2012 (F). Dark blue identifies sites where the bottom shear stress cannot be modelled as a marked Poisson process (i.e., the KS test is not verified for the interarrival time).

Carniello et al., 2009) that identified two different evolutionary trend in the northern lagoon and in the central-souther part. The northern lagoon displays, on average, a very low erosion rate. The same behaviour is found also in the areas adjacent to the landward boundary of the central-southern lagoon, sheltered from wave action by the salt marshes aligned parallel to the land. On the contrary, high erosion rates are observed in the central-southern part of the lagoon and close to the city of Venice: in particular very high erosion rates affect the area located in the proximity of the S. Leonardo harbour and near the Malamocco-Marghera ship canal.

5.4 CONCLUSIONS

Our analyses integrate previous studies on the statistical mechanics of wind wave-induced erosion (D'Alpaos et al., 2013) and on statistical

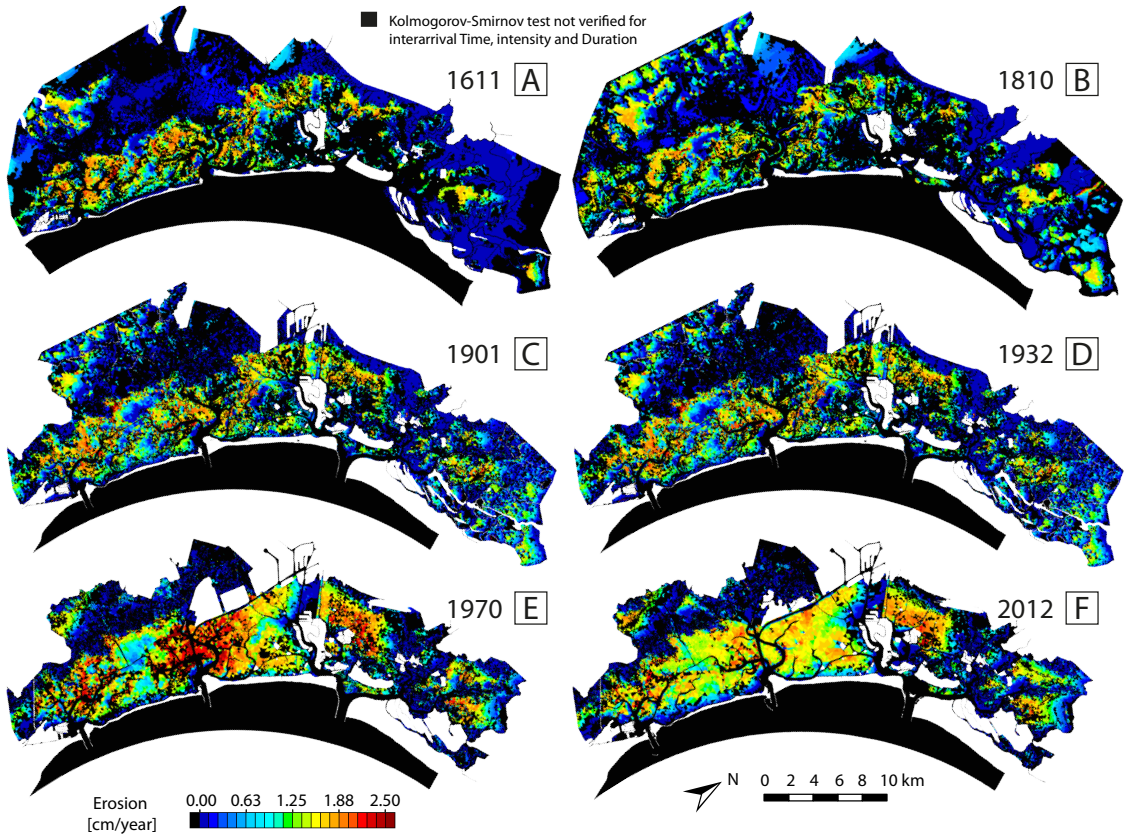

Figure 5.9: Color-coded representation of erosion work for the six different configurations of the Venice Lagoon 1611 (A), 1810 (B), 1901 (C), 1932 (D), 1970 (E), and 2012 (F).

characterization of spatio-temporal suspended sediment dynamics in the present configuration of the Venice Lagoon (Carniello et al., 2016). We extended the investigation of the temporal evolution of the BSS on the basis of the "Peaks Over Threshold" (POT) analysis to other five configurations of the Venice Lagoon, covering a time span of four centuries. In this additional configurations we also verified whether or not wind wave resuspension events could be modelled as a marked Poisson process. To this end we performed the Kolmogorov-Smirnov (KS) goodness of fit to verify the hypothesis that the interarrival time of resuspension events together with the durations and intensities are exponentially distributed random variables. The main results of our study can be summarized as follows:

- Statistical analyses suggest that the interarrival time between two consecutive resuspension events, their durations and intensities, for all the analysed configurations of the Venice lagoon are exponentially distributed random variables and thus resuspension events can be modelled as a marked Poisson processes over wide areas of Venice Lagoon.

- We show that through the last four centuries the interarrival times of erosion events have increased, as well as their intensities and durations, thus leading to less frequent but stronger erosion events. The computations of the erosion work show a peak erosion in 1970 and then a slow decreasing with a more uniform pattern in the present configuration.
- Furthermore, we observed that the intensity of peak excesses and duration of overthreshold exceedances are highly correlated, while almost no correlation exists between duration and interarrival time and between intensity and interarrival time.

Our results improve current understanding on the effects of wave driven erosion processes on the morphodynamic evolution of tidal landscapes, demonstrating that these processes in the Venice Lagoon and for the last four centuries can be described as marked Poisson process over the last centuries. This approach is important for long term morphodynamic studies in order to generate Poissonian sequences of forcings through which Monte Carlo realizations of relevant morphological evolution can be performed.

6 CONCLUSIONS

Towards the goal of improving current understanding of the processes that drive the long-term morphodynamic evolution of tidal systems in general, and, in particular, of the Venice Lagoon during the last four centuries, this thesis focused on wind-wave induced erosion processes. More in detail, in this work we addressed: i) the bathymetric reconstruction of an ancient configuration of the Venice Lagoon (dating back to 1611) and the comparison of its hydrodynamic and wind-wave fields with those characterizing more recent (1810 and 2012) configurations; ii) the implications of the different assumptions and formulations embedded in currently used wave models to evaluate wind-wave characteristics and to determine wind wave-induced bottom shear stresses, that are agreed to be of critical importance to determine erosion processes in shallow tidal systems; iii) the effects of wave action on marsh boundaries and how changes in the wave field are intertwined with morphological changes in tidal landscapes, in general, and in the Venice lagoon during the last four centuries, in particular; iv) the statistical mechanics of wind wave-induced erosion events in shallow tidal basins and the possibility of modelling wind wave-induced erosion processes as marked Poisson processes.

The main results of this thesis can be summarized as follows:

- We developed and tested a procedure to reconstruct the bathymetric features of the Venice Lagoon starting from planimetric information (the 1611 Alberti's map of the Lagoon) through the use of classical geomorphic relationships for tidal channels and conceptual models of tidal-flat and salt-marsh coevolution. The reconstruction of the 1611 bathymetric configuration allowed us to compare its hydrodynamic and wind-induced wave fields with those characterizing other, more recent Lagoon configurations. This comparison made it possible to highlight important changes in the hydrodynamics and wave dynamics of the Venice Lagoon through the last four centuries, emphasizing the less dissipative and more erosional character of the current configuration. We deem that the proposed procedure for the reconstruction of ancient bathymetries is a fundamental step for the analysis of the morphological evolution of tidal systems.
- Through a detailed scrutiny of different wave models we observed that the assumptions adopted in different modelling frameworks strongly influence the computation of wave characteristics

and of the wave-induced bottom shear stress. This is particularly relevant when very shallow water depths are involved, because non-accurate model descriptions of BSSw might lead one to overestimate wave-induced erosion processes in shallow tidal landscapes. As recalled above, differences in BSSw evaluation become particularly evident when depths lower than 0.5 m are considered.

- Our analysis of the spatial distribution of wave characteristics, and in particular of the Mean Wave Power Density (MWPD), during the last four centuries in the Venice Lagoon suggests that while the spatial distribution of MWPD did not significantly changed from 1611 to 1901, a rapid, dramatic increase in the MWPD was observed in the last century (1901 - 2012). Such an increase is strongly related with the erosion of tidal landforms in a positive feedback that drives landscape evolution. In addition, through the application of a two-dimensional wind-wave tidal model (WWTM), we have further tested the validity of the linear relationship between MWPD and lateral volumetric erosion rate, originally developed on the basis of dimensional analysis and supported by the results of a simplified wave model. The use of a full-fledged WWTM further supports the possibility of adopting such a linear relationship for long-term morphodynamic analyses. Our results thus suggest that relating salt-marsh retreat rates to properly computed mean wave power densities is a valuable morphological tool for long-term morphodynamics.

- The statistical analysis performed on the bottom shear stress distribution resulting from the combined effect of tidal currents and wind waves suggests that wave-induced erosion processes can be modelled as marked Poisson processes. Indeed, the interarrival times between two consecutive resuspension events, as well as the intensities and the durations, for the six configurations of the Venice Lagoon analysed in this work (1611, 1810, 1901, 1932, 1970, 2012) are exponentially distributed random variables. We also observed that the intensity of peak excesses and duration of overthreshold excedances are highly correlated, while almost no correlation exists between durations and interarrival times and between intensities and interarrival times. Furthermore, we have also shown that, in the last four centuries, the interarrival times of erosion events have decreased, whereas their intensities and durations have largely increased in the central and southern parts of the Lagoon, thus leading to more frequent and stronger erosion events.

BIBLIOGRAPHY

Allen, J. R. L. (1990). "Salt-marsh growth and stratification: A numerical model with special reference to the Severn Estuary, southwest Britain". In: *Marine Geology* 95.2, pp. 77–96.

Allen, JRL (2000). "Morphodynamics of Holocene salt marshes: a review sketch from the Atlantic and Southern North Sea coasts of Europe". In: *Quaternary Science Reviews* 19, pp. 1155–1231.

Amos, C. L., A. Bergamasco, G. Umgiesser, S. Cappucci, D. Cloutier, L. DeNat, M. Flindt, M. Bonardi, and S. Cristante (Nov. 2004). "The stability of tidal flats in Venice Lagoon - The results of in-situ measurements using two benthic, annular flumes". In: *Journal of Marine Systems* 51.1-4. WOS:000225327300015, pp. 211–241. DOI: 10.1016/j.jmarsys.2004.05.013.

Augustin, L. N., J. L. Irish, and P. Lynett (2009). "Laboratory and numerical studies of wave damping by emergent and near-emergent wetland vegetation". In: *Coastal Engineering* 56.3. Cited By :149, pp. 332–340.

Balkema, August A and Laurens De Haan (1974). "Residual life time at great age". In: *The Annals of probability*, pp. 792–804.

Barbier, Edward B., Sally D. Hacker, Chris Kennedy, Evamaria W. Kock, Adrian C. Stier, and Brian R. Sillman (2011). "The value of estuarine and coastal ecosystem services". In: *Ecological Monographs* 81.2, pp. 169–193.

Barnett, T. P. (1968). "On the generation, dissipation, and prediction of ocean wind waves". In: *Journal of Geophysical Research* 73.2, pp. 513–529.

Bates, Charles R. and Martin R. Bates (2016). "Palaeogeographic Reconstruction in the Transition Zone: The Role of Geophysical Forward Modelling in Ground Investigation Surveys". In: *Archaeological Prospection* 23, pp. 311–323. DOI: 10.1002/arp.1546.

Battjes, Jurjen A and J.P.F.M. Janssen (1978). "Energy loss and set-up due to breaking of random waves". In: *Proceedings of 16th International Conference Conference on Coastal Engineering*. New York: Am. Soc. of Civ. Eng., pp. 569–587.

Bendoni, Marco, Stefania Francalanci, Luca Cappietti, and Luca Solari (2014). "On salt marshes retreat: Experiments and modeling toppling failures in-

duced by wind waves". In: *Journal of Geophysical Research: Earth Surface* 119, pp. 603–620. DOI: 10.1002/2013JF002967.

Bendoni, Marco, Riccardo Mel, Luca Solari, Stefano Lanzoni, Stefania Francalanci, and Hocine Oumeraci (2016). "Insights into lateralmarsh retreat-mechanism through localized field measurements". In: *Water Resources Research* 52. DOI: 10.1002/2015WR017966.

Booij, N., R. C. Ris, and Leo H. Holthuijsen (1999). "A third-generation wave model for coastal regions: 1. Model description and validation". In: *Journal of Geophysical Research* 104.C4, pp. 7649–7666.

Botter, Gianluca, A Porporato, I Rodriguez-Iturbe, and A Rinaldo (2007). "Basin-scale soil moisture dynamics and the probabilistic characterization of carrier hydrologic flows: Slow, leaching-prone components of the hydrologic response". In: *Water resources research* 43.2.

Breugem, W. A. and Leo H. Holthuijsen (2007). "Generalized Shallow Water Wave Growth from Lake George". In: *Journal of waterway, port, and ocean engineering* 133.3, pp. 173–182. DOI: 10.1061/(ASCE)0733-950X(2007)133:3(173).

Bricker-Urso, S., S. W. Nixon, J. K. Cochran, D. J. Hirschberg, and C. Hunt (1989). "Accretion Rates and Sediment Accumulation in Rhode Island Salt Marshes". In: *Estuaries* 12.4, pp. 300–317.

Callaghan, D. P., Tjeerd J. Bouma, P. Klaassen, Daphne Van der Wal, M. J F Stive, and P. M J Herman (2010). "Hydrodynamic forcing on salt-marsh development: Distinguishing the relative importance of waves and tidal flows". In: *Estuarine, Coastal and Shelf Science* 89.1, pp. 73–88. DOI: 10.1016/j.ecss.2010.05.013.

Carbognin, Laura and Giancarlo Taroni (1996). "Eustatismo a Venezia e Trieste nell'ultimo secolo". In: *Atti Istituto Veneto di Scienze Lettere ed Arti* 154, pp. 281–298.

Carbognin, Laura, Pietro Teatini, and Luigi Tosi (2004). "Eustacy and land subsidence in the Venice Lagoon at the beginning of the new millennium". In: *Journal of Marine Systems* 51, pp. 345–353. DOI: 10.1016/j.jmarsys.2004.05.021.

Carbognin, Laura, Pietro Teatini, Luigi Tosi, Tazio Strozzi, and Alberto Tomasin (2010). "Present Relative Sea Level Rise in the Northern Adriatic Coastal Area". In: *Marine research at CNR*, pp. 1–10.

Carniello, Luca, Andrea D'Alpaos, Gianluca Botter, and Andrea Rinaldo (2016). "Statistical characterization of spatio-temporal sediment dynamics

in the Venice lagoon". In: *Journal of Geophysical Research: Earth Surface* 121, pp. 1049–1064. DOI: 10.1002/2015JF003793.

Carniello, Luca, Andrea D'Alpaos, and Andrea Defina (2011). "Modeling wind waves and tidal flows in shallow micro-tidal basins". In: *Estuarine, Coastal and Shelf Science* 92.2, pp. 263–276. DOI: 10.1016/j.ecss.2011.01.001.

Carniello, Luca, Andrea Defina, and Luigi D'Alpaos (2009). "Morphological evolution of the Venice lagoon: Evidence from the past and trend for the future". In: *Journal of Geophysical Research* 114. DOI: 10.1029/2008JF001157.

Carniello, Luca, Andrea Defina, and Luigi D'Alpaos (2012). "Modeling sand-mud transport induced by tidal currents and wind waves in shallow microtidal basins: Application to the Venice Lagoon (Italy)". In: *Estuarine, Coastal and Shelf Science* 102-103, pp. 105–115. DOI: 10.1016/j.ecss.2012.03.016.

Carniello, Luca, Andrea Defina, Sergio Fagherazzi, and Luigi D'Alpaos (2005). "A combined wind wave-tidal model for the Venice lagoon, Italy". In: *Journal of Geophysical Research* 110, F04007. DOI: 10.1029/2004JF000232.

Carniello, Luca, Sonia Silvestri, Marco Marani, Andrea D'Alpaos, Vincenzo Volpe, and Andrea Defina (2014). "Sediment dynamics in shallow tidal basins: In situ observations, satellite retrievals, and numerical modeling in the Venice Lagoon". In: *Journal of Geophysical Research: Earth Surface* 119.4, pp. 802–815. DOI: 10.1002/2013JF003015.

Carr, J., P. D'Odorico, K. McGlathery, and P. Wiberg (2010). "Stability and bistability of seagrass ecosystems in shallow coastal lagoons: Role of feedbacks with sediment resuspension and light attenuation". In: *Journal of Geophysical Research: Biogeosciences* 115.3, pp. 1–14. DOI: 10.1029/2009JG001103.

Carr, Joel A., Paolo D'Odorico, Karen J. McGlathery, and Patricia L. Wiberg (2012). "Modeling the effects of climate change on eelgrass stability and resilience: Future scenarios and leading indicators of collapse". In: *Marine Ecology Progress Series* 448, pp. 289–301. DOI: 10.3354/meps09556.

Carr, Joel Adam, Giullio Mariotti, Sergio Fagherazzi, Karen McGlathery, and Patricia Wiberg (2018). "Exploring the impacts of seagrass on coupled marsh-tidal flat morphodynamics". In: *Frontiers in Environmental Science* 6.September, p. 92. DOI: 10.3389/FENVS.2018.00092.

Cavaleri, Luigi and Paola Malanotte Rizzoli (1981). "Wind wave prediction in shallow water: Theory and applications". In: *Journal of Geophysical Research* 86.C11, pp. 10961–10973.

Chen, X. D., C. K. Zhang, Z. Zhou, Z. Gong, J. J. Zhou, J. F. Tao, D. M. Paterson, and Q. Feng (2017). "Stabilizing Effects of Bacterial Biofilms: EPS Penetration and Redistribution of Bed Stability Down the Sediment Profile". In: *Journal of Geophysical Research: Biogeosciences* 122.12, pp. 3113–3125. DOI: 10.1002/2017JG004050.

Chmura, G. L., S. C. Anisfeld, D. R. Cahoon, and J. C. Lynch (Dec. 2003). "Global carbon sequestration in tidal, saline wetland soils". In: *Global Biogeochemical Cycles* 17.4, p. 1111. DOI: 10.1029/2002GB001917.

Coco, Giovanni, Z. Zhou, B. van Maanen, M. Olabarrieta, Rafael Tinoco, and Ian Townend (2013). "Morphodynamics of tidal networks: Advances and challenges". In: *Marine Geology* 346, pp. 1–16. DOI: 10.1016/j.margeo.2013.08.005.

Collins, J. Ian (1972). "Prediction of shallow-water spectra". In: *Journal of Geophysical Research* 77.15, pp. 2693–2707.

Consorzio Venezia Nuova (2007). *Studio C.2.10/III: Attività di aggiornamento del piano degli interventi per il recupero morfologico in applicazione della delibera del Consiglio dei Ministri del 15.03.01, Rapporto finale—Modello morfologico a maglia curvilinea: Relazione tecnica*. Tech. rep. Magistrato alle Acque di Venezia, Venice, Italy, p. 129.

Cooper, N. J., T. Cooper, and F. Burd (2001). "25 years of salt marsh erosion in Essex: Implications for coastal defence and nature conservation". In: *Journal of Coastal Conservation* 7, pp. 31–40. DOI: 10.1007/BF02742465.

Costanza, Robert, Ralph D'Arge, Rudolf de Groot, Stephen Farber, Monica Grasso, Bruce Hannon, Karin Limburg, Shahid Naeem, Robert V. O'Neill, Jose Paruelo, Robert G. Raskin, Paul Sutton, and Marjan van den Belt (1997). "The value of the world's ecosystem services and natural capital". In: *Nature* 387, pp. 253–260.

D'Alpaos, A., L. Carniello, and A. Rinaldo (2013). "Statistical mechanics of wind wave-induced erosion in shallow tidal basins: Inferences from the Venice Lagoon". In: *Geophysical Research Letters* 40.13, pp. 3402–3407.

D'Alpaos, A., C. Da Lio, and M. Marani (2012). "Biogeomorphology of tidal landforms: Physical and biological processes shaping the tidal landscape". In: *Ecohydrology* 5.5, pp. 550–562.

D'Alpaos, Andrea, Stefano Lanzoni, and Marco Marani (2010). "On the tidal prism-channel area relations". In: *Journal of Geophysical Research* 115, F01003. DOI: 10.1029/2008JF001243.

D'Alpaos, Andrea, Stefano Lanzoni, Marco Marani, Sergio Fagherazzi, and Andrea Rinaldo (2005). "Tidal network ontogeny: Channel initiation and early development". In: *Journal of Geophysical Research* 110, F02001. DOI: 10.1029/2004JF000182.

D'Alpaos, Andrea, Stefano Lanzoni, Marco Marani, and Andrea Rinaldo (2007). "Landscape evolution in tidal embayments: Modeling the interplay of erosion, sedimentation, and vegetation dynamics". In: *Journal of Geophysical Research* 112, F01008. DOI: 10.1029/2006JF000537.

D'Alpaos, Andrea, Stefano Lanzoni, Marco Marani, and Andrea Rinaldo (2009). "On the O'Brien-Jarrett-Marchi law". In: *Rend. Fis. Acc. Lincei* 20, pp. 225–236. DOI: 10.1007/s12210-009-0052-x.

D'Alpaos, Andrea and Marco Marani (2016). "Reading the signatures of biologic-geomorphic feedbacks in salt-marsh landscapes". In: *Advances in Water Resources* 93, pp. 265–275. DOI: 10.1016/j.advwatres.2015.09.004.

D'Alpaos, Andrea, Simon Marius Mudd, and Luca Carniello (2011). "Dynamic response of marshes to perturbations in suspended sediment concentrations and rates of relative sea level rise". In: *Journal of Geophysical Research* 116, F04020. DOI: 10.1029/2011JF002093.

D'Alpaos, Luigi (2010a). *Fatti e misfatti di idraulica lagunare. La laguna di Venezia dalla diversione dei fiumi alle nuove opere delle bocche di porto*. Istituto Veneto di Scienze, Lettere e Arti.

D'Alpaos, Luigi (2010b). *L'evoluzione morfologica della laguna di Venezia attraverso la lettura di alcune mappe storiche e delle sue mappe idrografiche*. Istituto Veneto di Scienze, Lettere e Arti.

D'Alpaos, Luigi and Andrea Defina (2007). "Mathematical modeling of tidal hydrodynamics in shallow lagoons: A review of open issues and applications to the Venice lagoon". In: *Computers and Geosciences* 33, pp. 476–496. DOI: 10.1016/j.cageo.2006.07.009.

D'Alpaos, Luigi and Paolo Martini (2005). "The influence of inlet configuration on sediment loss in the Venice lagoon". In: *Flooding and Environmental Challenges for Venice and its Lagoon: State of Knowledge*. Ed. by C. A. Fletcher and T. Spencer. Cambridge, U. K.: Cambridge Univ. Press, pp. 419–430.

D'Odorico, Paolo and Sergio Fagherazzi (2003). "A probabilistic model of rainfall-triggered shallow landslides in hollows: A long-term analysis". In: *Water Resources Research* 39.9, pp. 1–14. DOI: 10.1029/2002WR001595.

Da Lio, Cristina, Pietro Teatini, Tazio Strozzi, and Luigi Tosi (2018). "Understanding land subsidence in salt marshes of the Venice Lagoon from SAR

Interferometry and ground-based investigations". In: *Remote Sensing of Environment* 205.September 2017, pp. 56–70. DOI: 10.1016/j.rse.2017.11.016.

Day, John W., Louis D. Britsch, Suzanne R. Hawes, Gary P. Shaffer, Denise J. Reed, and Donald Cahoon (2000). "Pattern and rocess of land loss in the Mississippi Delta: A spatial and temporal analysis of wetland habitat change". In: *Estuaries* 23.4, pp. 425–438.

Day, John W., J. E. Cable, J. H. Cowan, R. DeLaune, K. de Mutsert, B. Fry, H. Mashriqui, D. Justic, P. Kemp, R. R. Lane, J. Rick, S. Rick, L. P. Rozas, G. Snedden, E. Swenson, R. R. Twilley, and B. Wissel (2009). "The Impacts of Pulsed Reintroduction of River Water on a Mississippi Delta Coastal Basin". In: *Journal of Coastal Research* 54, pp. 225–243. DOI: 10.2112/SI54-015.1.

Day, John W., F. Scarton, A. Rismondo, and D. Are (1998). "Rapid deterioration of a salt marsh in Venice Lagoon, Italy." In: *Journal of Coastal Research*, pp. 583–590.

Defendi, V., V. Kovačević, F. Arena, and L. Zaggia (2010). "Estimating sediment transport from acoustic measurements in the Venice Lagoon inlets". In: *Continental Shelf Research* 30, pp. 883–893. DOI: 10.1016/j.csr.2009.12.004.

Defina, A., L. Carniello, S. Fagherazzi, and L. D'Alpaos (July 2007). "Self-organization of shallow basins in tidal flats and salt marshes". In: *Journal of Geophysical Research-Earth Surface* 112.F3, F03001. DOI: 10.1029/2006JF000550.

Defina, Andrea (2000). "Two-dimensional shallow flow equations for partially dry areas". In: *Water Resour. Res.* 36, (11), pp. 3251–3264.

Delaune, R. D., W. H. Patrick, and R. J. Buresh (1978). "Sedimentation rates determined by137Cs dating in a rapidly accreting salt marsh [12]". In: *Nature* 275.5680, pp. 532–533. DOI: 10.1038/275532a0.

Dènaix, A. (1810). *Carta Topografica Idrografica Militare della Laguna di Venezia e del Littorale compreso tra l'Adige e la Piave eseguita sotto i Ministeri de' Signori Generali Divisionarj Conti Caffarelli e Fontanelli negli anni 1809–10 e 11, Map, 36 sheets, scale, 1:150*. Castello 5252, 30122 Venice, Italy.

Donatelli, Carmine, Neil Kamal Ganju, Sergio Fagherazzi, and Nicoletta Leonardi (2018). "Seagrass Impact on Sediment Exchange Between Tidal Flats and Salt Marsh, and The Sediment Budget of Shallow Bays". In: *Geophysical Research Letters*, pp. 4933–4943. DOI: 10.1029/2018GL078056.

Fagherazzi, Sergio, Luca Carniello, Luigi D'Alpaos, and Andrea Defina (2006). "Critical bifurcation of shallow microtidal landforms in tidal flats and salt marshes". In: *Proceedings of the National Academy of Sciences* 103.22, pp. 8337–8341. DOI: 10.1073/pnas.0508379103.

Fagherazzi, Sergio, Matthew L. Kirwan, Simon Marius Mudd, Glenn R. Guntenspergen, Stijn Temmerman, Andrea D'Alpaos, Johan Van de Koppel, John M. Rybczyk, Enrique Reyes, Chris Craft, and Jonathan Clough (2012). "Numerical models of salt marsh evolution: ecological, geomorphic, and climatic factors". In: *Reviews of Geophysics* 50.RG1002. DOI: 10.1029/2011RG000359.1.

Fagherazzi, Sergio, Giulio Mariotti, P. L. Wiberg, and K. J. McGlathery (2013). "Marsh collapse does not require sea level rise". In: *Oceanography* 26.3, pp. 70–77. DOI: 10.5670/oceanog.2011.65.

Fagherazzi, Sergio, C. Palermo, M. C. Rulli, L. Carniello, and A. Defina (2007). "Wind waves in shallow microtidal basins and the dynamic equilibrium of tidal flats". In: *Journal of Geophysical Research: Earth Surface* 112.2, F02024. DOI: 10.1029/2006JF000572.

Fagherazzi, Sergio and Tao Sun (2004). "A stochastic model for the formation of channel networks in tidal marshes". In: *Geophysical Research Letters* 31.21, pp. 1–4. DOI: 10.1029/2004GL020965.

Fagherazzi, Sergio and P. L. Wiberg (2009). "Importance of wind conditions, fetch, and water levels on wave-generated shear stresses in shallow intertidal basins". In: *Journal of Geophysical Research: Solid Earth* 114.3, pp. 1–12. DOI: 10.1029/2008JF001139.

Faivre, Sanja, Tatjana Bakran-Petricioli, Nada Horvatinčić, and Andreja Sironić (2012). "Distinct phases of relative sea level changes in the central Adriatic during the last 1500 years — influence of climatic variations?" In: *Palaeogeography, Palaeoclimatology, Palaeoecology* 369, pp. 163–174. DOI: 10.1016/j.palaeo.2012.10.016.

Fourqurean, James W., Carlos M. Duarte, Hilary Kennedy, Núria Marbà, Marianne Holmer, Miguel Angel Mateo, Eugenia T. Apostolaki, Gary A. Kendrick, Dorte Krause-Jensen, Karen J. McGlathery, and Oscar Serrano (2012). "Seagrass ecosystems as a globally significant carbon stock". In: *Nature Geoscience* 5.7, pp. 505–509. DOI: 10.1038/ngeo1477.

French, Jon (2006). "Tidal marsh sedimentation and resilience to environmental change: Exploratory modelling of tidal, sea-level and sediment supply forcing in predominantly allochthonous systems". In: *Marine Geology* 235, pp. 119–136. DOI: 10.1016/j.margeo.2006.10.009.

Friedrichs, Carl T (1995). "Stability shear stress and equilibrium cross-sectional geometry of sheltered tidal channels". In: *Journal of Coastal Research*, pp. 1062–1074.

Friedrichs, Carl T and James E Perry (2001). "Tidal Salt Marsh Morphodynamics: A Synthesis". In: *Journal of Coastal Research* 27, pp. 7–37.

Gabet, Emmanuel J. (1998). "Lateral migration and bank erosion in a saltmarsh tidal channel in San Francisco Bay, California". In: *Estuaries* 21.4B, pp. 745–753.

Garofalo, Donald (1980). "The Influence of Wetland Vegetation on Tidal Stream Channel Migration and Morphology". In: *Estuaries* 3.4, pp. 258–270.

Gedan, Keryn B., Matthew L. Kirwan, Eric Wolanski, Edward B. Barbier, and Brian R. Silliman (2011). "The present and future role of coastal wetland vegetation in protecting shorelines: Answering recent challenges to the paradigm". In: *Climatic Change* 106, pp. 7–29. DOI: 10.1007/s10584-010-0003-7.

Gedan, Keryn B., B.R. Silliman, and M.D. Bertness (2009). "Centuries of Human-Driven Change in Salt Marsh Ecosystems". In: *Annual Review of Marine Science*, pp. 117–141. DOI: 10.1146/annurev.marine.010908.163930.

Green, Malcolm O. and Giovanni Coco (2014). "Review of wave driven sediment resuspension and transport in estuaries". In: *Reviews of Geophysics* 52.1, pp. 77–117. DOI: 10.1002/2013RG000437.Received.

Hasselmann, K., T.P. Barnett, E. Bouws, H. Carlson, D.E. Cartwright, K. Enke, J.A. Ewing, H. Gienapp, D.E. Hasselmann, P. Kruseman, A. Meerburg, P. Müller, D.J. Olbers, K. Richter, W. Sell, and H. Walden (1973). *Measurements of wind-wave growth and swell decay during the Joint North Sea Wave Project (JONSWAP)*, pp. 1–95.

Holthuijsen, L. H., N. Booij, and T. H.C. Herbers (1989). "A prediction model for stationary, short-crested waves in shallow water with ambient currents". In: *Coastal Engineering* 13, pp. 23–54.

Howes, Nick, D. M. FitzGerald, Z. J. Hughes, I. Y. Georgiou, M. A. Kulp, M. D. Miner, J. M. Smith, and J. A. Barras (2010). "Hurricane-induced failure of low salinity wetlands". In: *Proceedings of the National Academy of Sciences* 107.32, pp. 14014–14019. DOI: 10.1073/pnas.0914582107.

Hu, Z., Z. B. Wang, T. J. Zitman, M. J. F. Stive, and Tjeerd J. Bouma (2015). "Predicting long-term and short-term tidal flat morphodynamics using a

dynamic equilibrium theory". In: *Geophysical Research: Earth Surface* 120, pp. 1803–1823. DOI: 10.1002/2015JF003486.

Hughes, Steven A. (2002). "Equilibrium cross-sectional area at tidal inlets". In: *Journal of Coastal Research* 18(1), pp. 160–174.

Jarrett, James T (1976). *Tidal prism-inlet area relationships*. Tech. rep. General investigation of tidal inlets, report 3. U.S. Army Coastal Engineering Research Center, Fort Belvoir, VA. U.S. Army Engineers Waterways Experiment Station, Vicksburg, MS., 32 pp.

Jongepier, Iason, Tim Soens, Stijn Temmerman, and Tine Missiaen (2016). "Assessing the Planimetric Accuracy of Historical Maps (Sixteenth to Nineteenth Centuries): New Methods and Potential for Coastal Landscape Reconstruction". In: *The Cartographic Journal* 53.2, pp. 114–132. DOI: 10.1179/1743277414Y.0000000095.

Kakeh, Nabil, Giovanni Coco, and Marco Marani (2016). "Advances in Water Resources On the morphodynamic stability of intertidal environments and the role of vegetation". In: *Advances in Water Resources* 93, pp. 303–314. DOI: 10.1016/j.advwatres.2015.11.003.

Kirwan, Matthew L., Glenn R. Guntenspergen, Andrea D'Alpaos, James T. Morris, Simon M. Mudd, and Stijn Temmerman (2010). "Limits on the adaptability of coastal marshes to rising sea level". In: *Geophysical Research Letters* 37, p. L23401. DOI: 10.1029/2010GL045489.

Kirwan, Matthew L. and J .Patrick Megonigal (2013). "Tidal wetland stability in the face of human impacts and sea-level rise." In: *Nature* 504, pp. 53–60. DOI: 10.1038/nature12856.

Kirwan, Matthew L. and Simon Marius Mudd (2012). "Response of salt-marsh carbon accumulation to climate change". In: *Nature* 489, pp. 550–553. DOI: 10.1038/nature11440.

Kirwan, Matthew L. and A. B. Murray (2007). "A coupled geomorphic and ecological model of tidal marsh evolution". In: *Proceedings of the National Academy of Sciences* 104.15, pp. 6118–6122. DOI: 10.1073/pnas.0700958104.

Kirwan, Matthew L., Stijn Temmerman, Emily E. Skeehan, Glenn R. Guntenspergen, and Sergio Fagherazzi (2016a). "Overestimation of marsh vulnerability to sea level rise". In: *Nature Climate Change* 6, pp. 253–260. DOI: 10.1038/nclimate2909.

Kirwan, Matthew L., David C. Walters, William G. Reay, and Joel A. Carr (2016b). "Sea level driven marsh expansion in a coupled model of marsh

erosion and migration". In: *Geophysical Research Letters* 43, pp. 4366–4373. DOI: 10.1002/2016GL068507.

Komen, G. J., K. Hasselmann, and K. Hasselmann (1984). "On the Existence of a Fully Developed Wind-Sea Spectrum". In: *Journal of Physical Oceanography* 14.8, pp. 1271–1285.

Krishnamurthy, Muthusamy (1977). "Tidal prism of equilibrium inlets". In: *Journal of the Waterway Port Coastal and Ocean Division* 103.4, pp. 423–432.

Lambeck, K., F. Antonioli, M. Anzidei, L. Ferranti, G. Leoni, G. Scicchitano, and S. Silenzi (2011). "Sea level change along the Italian coast during the Holocene and projections for the future". In: *Quaternary International* 232.1-2, pp. 250–257. DOI: 10.1016/j.quaint.2010.04.026.

Lanzoni, Stefano and Andrea D'Alpaos (2015). "On funneling of tidal channeling". In: *J. Geophys. Res. Earth Surf.* 120, pp. 433–452. DOI: 10.1002/2014JF003203.

Lanzoni, Stefano and Giovanni Seminara (2002). "Long-term evolution and morphodynamic equilibrium of tidal channels". In: *Journal of Geophysical Research* 107.C1. DOI: 10.1029/2000JC000468.

Lauzon, Rebecca, A Brad Murray, Laura J Moore, Matthew L Kirwan, and Sergio Fagherazzi (2018). "Effects of Marsh Edge Erosion in Coupled Barrier Island-Marsh Systems and Geometric Constraints on Marsh Evolution Journal of Geophysical Research : Earth Surface". In: 123. DOI: https://doi.org/10.1029/2017JF004530.

Lawrence, D. S. L., J. R. L. Allen, and G. M. Havelock (2004). "Salt marsh morphodynamics: An investigation of tidal flows and marsh channel equilibrium". In: *Journal of Coastal Research* 20.1, pp. 301–316.

Lawson, S.E., Patricia L. Wiberg, Karen J. McGlathery, and D.C. Fugate (2007). "Wind-driven sediment suspension controls light availability in a shallow coastal lagoon". In: *Estuaries Coasts* 30.1, pp. 102–112.

Le Hir, P, Y Monbet, and F Orvain (2007). "Sediment erodability in sediment transport modelling: can we account for biota effects?" In: *Continental Shelf Research* 27.8, pp. 1116–1142. DOI: https://doi.org/10.1016/j.csr.2005.11.016.

Leonardi, Nicoletta, Iacopo Camacina, Carmine Donatelli, Neil Kamal Ganju, Andrew James Plater, Mark Schuerch, and Stijn Temmerman (2018). "Dynamic interactions between coastal storms and salt marshes: A review". In: *Geomorphology* 301, pp. 92–107. DOI: 10.1016/j.geomorph.2017.11.001.

Leonardi, Nicoletta, Zafer Defne, Neil K Ganju, and Sergio Fagherazzi (2016a). "Salt marsh erosion rates and boundary features in a shallow Bay". In: *Journal of Geophysical Research: Earth Surface* 121. DOI: 10.1002/2016JF003975.

Leonardi, Nicoletta and Sergio Fagherazzi (2014). "How waves shape salt marshes". In: *Geology* 42.10, pp. 887–890. DOI: 10.1130/G35751.1.

Leonardi, Nicoletta and Sergio Fagherazzi (2015). "Effect of local variability in erosional resistance on large-scale morphodynamic response of salt marshes to wind waves and extreme events". In: *Geophysical Research Letters* 42.14, pp. 5872–5879. DOI: 10.1002/2015GL064730.

Leonardi, Nicoletta, Neil K. Ganju, and Sergio Fagherazzi (Jan. 2016b). "A linear relationship between wave power and erosion determines salt-marsh resilience to violent storms and hurricanes". In: *Proceedings of the National Academy of Sciences of the United States of America* 113.1, pp. 64–68. DOI: 10.1073/pnas.1510095112.

Leopold, L.B., J.N. Collins, and L.M. Collins (1993). "Hydrology of some tidal channels in estuarine marshland near San Francisco". In: *CATENA* 20, pp. 469–493.

Lin, Weiqi, Lawrence P. Sanford, and Steven E. Suttles (2002). "Wave measurement and modeling in Chesapeake Bay". In: *Continental Shelf Research* 22, pp. 2673–2686.

Lo, V. B., T. J. Bouma, J. van Belzen, C. Van Colen, and L. Airoldi (2017). "Interactive effects of vegetation and sediment properties on erosion of salt marshes in the Northern Adriatic Sea". In: *Marine Environmental Research* 131, pp. 32–42. DOI: http://dx.doi.org/10.1016/j.marenvres.2017.09.006.

Madricardo, Fantina and S. Donnici (2014). "Mapping past and recent landscape modifications in the Lagoon of Venice through geophysical surveys and historical maps". In: *Anthropocene* 6, pp. 86–96. DOI: 10.1016/j.ancene.2014.11.001.

Madricardo, Fantina, Sandra Donnici, Alberto Lezziero, Federica De Carli, Silvano Buogo, Paola Calicchia, and Emiliano Boccardi (2007). "Palaeoenvironment reconstruction in the Lagoon of Venice through wide-area acoustic surveys and core sampling". In: *Estuarine, Coastal and Shelf Science* 75, pp. 205–213. DOI: 10.1016/j.ecss.2007.02.031.

Marani, M., A. D'Alpaos, S. Lanzoni, L. Carniello, and A. Rinaldo (2010). "The importance of being coupled: Stable states and catastrophic shifts in tidal biomorphodynamics". In: *Journal of Geophysical Research* 115.F04004. DOI: doi:10.1029/2009JF001600.

Marani, Marco, Enrica Belluco, Andrea D'Alpaos, Andrea Defina, Stefano Lanzoni, and Andrea Rinaldo (2003). "On the drainage density of tidal networks". In: *Water Resources Research* 39.2, p. 1040. DOI: 10.1029/2001WR001051.

Marani, Marco, Andrea D'Alpaos, Stefano Lanzoni, Luca Carniello, and Andrea Rinaldo (June 2007). "Biologically-controlled multiple equilibria of tidal landforms and the fate of the Venice lagoon". In: *Geophysical Research Letters* 34.11. WOS:000247368400007, p. L11402. DOI: 10.1029/2007GL030178.

Marani, Marco, Andrea D'Alpaos, Stefano Lanzoni, and Marco Santalucia (2011). "Understanding and predicting wave erosion of marsh edges". In: *Geophysical Research Letters* 38, p. L21401. DOI: 10.1029/2011GL048995.

Marani, Marco, Cristina Da Lio, and Andrea D'Alpaos (2013). "Vegetation engineers marsh morphology through multiple competing stable states." In: *Proceedings of the National Academy of Sciences of the United States of America* 110.9, pp. 3259–3263. DOI: 10.1073/pnas.1218327110.

Marani, Marco, Stefano Lanzoni, Sonia Silvestri, and Andrea Rinaldo (2004). "Tidal landforms, patterns of halophytic vegetation and the fate of the lagoon of Venice". In: *J. Marine Systems* 51, pp. 191–210. DOI: 10.1016/j.jmarsys.2004.05.012.

Marani, Marco, Stefano Lanzoni, Diego Zandolin, Giovanni Seminara, and Andrea Rinaldo (2002). "Tidal meanders". In: *Water Resources Research* 38, p. 1225. DOI: 10.1029/2001WR000404.

Marchi, Enrico (1990). "Sulla stabilità delle bocche lagunari a marea". In: *Rend Fisici Accad Lincei* 9, pp. 137–150.

Marciano, Raffaele, Zheng Bing Wang, Anneke Hibma, Huib J. De Vriend, and Andrea Defina (2005). "Modeling of channel patterns in short tidal basins". In: *Journal of Geophysical Research: Earth Surface* 110.1, pp. 1–13. DOI: 10.1029/2003JF000092.

Mariotti, G. and J. Carr (2014). "Dual role of salt marsh retreat: Long-term loss and short-term resilience". In: *Water Resources Research* 50, pp. 2963–2974. DOI: doi:10.1002/2013WR014676.

Mariotti, G. and S. Fagherazzi (2010). "A numerical model for the coupled long-term evolution of salt marshes and tidal flats". In: *Journal of Geophysical Research: Earth Surface* 115.1.

Mariotti, G. and S. Fagherazzi (2012). "Modeling the effect of tides and waves on benthic biofilms". In: *Journal of Geophysical Research G: Biogeosciences* 117.4, pp. 1–14. DOI: 10.1029/2012JG002064.

Mariotti, G. and S. Fagherazzi (2013a). "Critical width of tidal flats triggers marsh collapse in the absence of sea-level rise". In: *Proceedings of the National Academy of Sciences of the United States of America* 110.14, pp. 5353–5356.

Mariotti, G. and S. Fagherazzi (2013b). "Wind waves on a mudflat: The influence of fetch and depth on bed shear stresses". In: *Continental Shelf Research* 60, S99–S110.

Mariotti, Giulio, Sergio Fagherazzi, P. L. Wiberg, K. J. McGlathery, Luca Carniello, and Andrea Defina (2010). "Influence of storm surges and sea level on shallow tidal basin erosive processes". In: *Journal of Geophysical Research: Oceans* 115, F01004. DOI: 10.1029/2009JC005892.

Martini, Paolo, Luca Carniello, and C. Avanzi (2004). "Two dimensional modelling of flood flows and suspended sediment transport: the case of the Brenta River, Veneto (Italy)". In: *Natural Hazards and Earth System Science* 4, pp. 165–181.

Massari, F., D. Rio, R. Serandrei Barbero, A. Asioli, L. Capraro, E. Fornaciari, and P. P. Vergerio (2004). "The environment of Venice area in the past two million years". In: *Palaeogeography, Palaeoclimatology, Palaeoecology* 202.3-4, pp. 273–308. DOI: 10.1016/S0031-0182(03)00640-0.

Mcleod, Elizabeth, Gail L. Chmura, Steven Bouillon, Rodney Salm, Mats Bjork, Carlos M. Duarte, Catherine E. Lovelock, William H. Schlesinger, and Brian R. Silliman (2011). "A blueprint for blue carbon: toward an improved understanding of the role of vegetated coastal habitats in sequestering CO2". In: *Frontiers in Ecology and the Environment* 9.10. WOS:000297824500018, pp. 552–560. DOI: 10.1890/110004.

McLoughlin, Sean M., Patricia L. Wiberg, Ilgar Safak, and Karen J. McGlathery (2015). "Rates and Forcing of Marsh Edge Erosion in a Shallow Coastal Bay". In: *Estuaries and Coasts* 38, pp. 620–638. DOI: 10.1007/s12237-014-9841-2.

Miche, A. (1944). "Mouvements ondulatoires de la mer en profondeur croissante ou décroissante. Première partie. Mouvements ondulatoires périodiques et cylindriques en profondeur constante". In: *Ann. Ponts Chaussées* 114, pp. 42–78.

Molinaroli, Emanuela, Stefano Guerzoni, Alessandro Sarretta, Andrea Cucco, and Georg Umgiesser (2007). "Links between hydrology and sedimentology in the Lagoon of Venice, Italy". In: *Journal of Marine Systems* 68, pp. 303–317. DOI: 10.1016/j.jmarsys.2006.12.003.

Möller, I., M. Kudella, F. Rupprecht, T. Spencer, M. Paul, B. K. Van Wesenbeeck, G. Wolters, K. Jensen, T. J. Bouma, M. Miranda-Lange, and S. Schimmels (2014). "Wave attenuation over coastal salt marshes under storm surge conditions". In: *Nature Geoscience* 7.10. Cited By :135, pp. 727–731.

Möller, Iris (2006). "Quantifying saltmarsh vegetation and its effect on wave height dissipation: Results from a UK East coast saltmarsh". In: *Estuarine, Coastal and Shelf Science* 69, pp. 337–351. DOI: 10.1016/j.ecss.2006.05.003.

Möller, Iris, T. Spencer, J.R. French, D.J. Leggett, and M. Dixon (1999). "Wave transformation over saltmarshes: a field and numerical modelling study from North Norfolk, England." In: *Estuarine, Coastal and Shelf Science* 49, pp. 411–426. DOI: 10.1006/ecss.1999.0509.

Mudd, Simon M., Susan M. Howell, and James T. Morris (2009). "Impact of dynamic feedbacks between sedimentation, sea-level rise, and biomass production on near-surface marsh stratigraphy and carbon accumulation". In: *Estuarine, Coastal and Shelf Science* 82, pp. 377–389. DOI: 10.1016/j.ecss.2009.01.028.

Mudd, Simon Marius (2011). "The life and death of salt marshes in response to anthropogenic disturbance of sediment supply". In: *Geology* 39.5, pp. 511–512. DOI: 10.1130/focus052011.1.

Murray, A Brad (2007). "Reducing model complexity for explanation and prediction". In: *Geomorphology* 90.3-4, pp. 178–191.

O'Brien, Morrough P. (1931). "Estuary tidal prisms related to entrance areas". In: *Civ. Eng.* 1, pp. 738–739.

O'Brien, Morrough P. (1969). "Equilibrium flow areas of inlets in sandy coasts". In: *ASCE j. Waterways Harbors Div.* 95, pp. 43–52.

Park, Jeryang, Gianluca Botter, James W Jawitz, and P Suresh C Rao (2014). "Stochastic modeling of hydrologic variability of geographically isolated wetlands: Effects of hydro-climatic forcing and wetland bathymetry". In: *Advances in Water Resources* 69, pp. 38–48.

Pennings, Steven C., Mary Bestor Grant, and Mark D. Bertness (2005). "Plant zonation in low-latitude salt marshes: Disentangling the roles of flooding, salinity and competition". In: *Journal of Ecology* 93.1, pp. 159–167. DOI: 10.1111/j.1365-2745.2004.00959.x.

Perillo, Gerardo M E (2009). "Tidal Courses: Classification, Origin and Functionality". In: *COASTAL WETLANDS: An Integrated Ecosystem Approach*. First edit. Elsevier, pp. 185–210.

Pivato, Mattia, Luca Carniello, Isabella Moro, and Paolo D'Odorico (under review on Earth Surface Processes and Landforms). "On the feedback between water turbidity and microphytobenthos growth in shallow tidal environments". In:

Reed, Denise J. (1989). "Patterns of sediment deposition in subsiding coastal salt marshes, Terrebonne Bay, Louisiana: The role of winter storms". In: *Estuaries* 12.4, pp. 222–227. DOI: 10.1007/BF02689700.

Rinaldo, Andrea, Sergio Fagherazzi, Stefano Lanzoni, Marco Marani, and William E Dietrich (1999a). "Tidal networks 3. Landscape-forming discharges and studies in empirical geomorphic relationships". In: *Water Resources Research* 35.12, pp. 3919–3929.

Rinaldo, Andrea, Sergio Fagherazzi, Stefano Lanzoni, Marco Marani, and William E. Dietrich (1999b). "Tidal networks 2. Watershed delineation and comparative network morphology". In: *Water Resources Research* 35, pp. 3905–3917.

Rodriguez-Iturbe, Ignacio, David Roxbee Cox, and Valerie Isham (1987). "Some models for rainfall based on stochastic point processes". In: *Proc. R. Soc. Lond. A* 410.1839, pp. 269–288.

Roner, Marcella, Andrea D'Alpaos, Massimiliano Ghinassi, Marco Marani, Sonia Silvestri, E. Franceschinis, and N. Realdon (2016). "Spatial variation of salt-marsh organic and inorganic deposition and organic carbon accumulation: Inferences from the Venice lagoon, Italy". In: *Advances in Water Resources* 93, pp. 276–287. DOI: https://doi.org/10.1016/j.advwatres.2015.11.011.

Roner, Marcella, Massimiliano Ghinassi, Mariaelena Fedi, Lucia Liccioli, Luca Giorgio Bellucci, Lara Brivio, and Andrea D'Alpaos (2017). "Latest Holocene depositional history of the southern Venice Lagoon, Italy". In: *Holocene*, pp. 1731–1744. DOI: 10.1177/0959683617708450.

Sarretta, Alessandro, S. Pillon, Emanuela Molinaroli, Stefano Guerzoni, and G. Fontolan (2010). "Sediment budget in the Lagoon of Venice, Italy". In: *Continental Shelf Research* 30, pp. 934–949. DOI: 10.1016/j.csr.2009.07.002.

Schuttelaars, H M and H E De Swart (2000). "Multiple morphodynamic equilibria in tidal embayments". In: *Journal of Geophysical Research* 105, pp. 24, 105–24, 118.

Schwimmer, Reed A (2001). "Rates and Processes of Marsh Shoreline Erosion in Rehoboth Bay, Delaware, U.S.A." In: *Journal of Coastal Research* 17.3, pp. 672–683.

Silvestri, Sonia, Andrea D'Alpaos, Giovanna Nordio, and Luca Carniello (2018). "Anthropogenic Modifications can Significantly Influence the Local Mean Sea Level and Affect the Survival of Salt Marshes in Shallow Tidal Systems." In: *Journal of Geophysical Research: Earth Surface* 123. DOI: https://doi.org/10.1029/2017JF004503.

Silvestri, Sonia, Andrea Defina, and Marco Marani (2005). "Tidal regime, salinity and salt marsh plant zonation". In: *Estuarine, Coastal and Shelf Science* 62.1-2, pp. 119–130. DOI: 10.1016/j.ecss.2004.08.010.

Solari, L, G Seminara, S Lanzoni, M Marani, and A Rinaldo (2002). "Sand bars in tidal channels Part 2. Tidal meanders". In: *Journal of Fluid Mechanics* 451, pp. 203–238. DOI: 10.1017/S0022112001006565.

Soulsby, Richard (1997). *Dynamics of marine sands: a manual for practical applications*.

Soulsby, Richard L and Richard JS Whitehouse (2005). "Prediction of ripple properties in shelf seas-Mark 2 Predictor". In:

Stefanon, Luana, Luca Carniello, Andrea D'Alpaos, and Andrea Rinaldo (2012). "Signatures of sea level changes on tidal geomorphology: Experiments on network incision and retreat". In: *Geophysical Research Letters* 39.12, p. L12402. DOI: 10.1029/2012GL051953.

Swart, D.H. (Dec. 1974). *Offshore sediment transport and equilibrium beach profiles*.

Tambroni, N., R. Luchi, and G. Seminara (2017). "Can tide dominance be inferred from the point bar pattern of tidal meandering channels?" In: *Journal of Geophysical Research: Earth Surface* 122.2, pp. 492–512. DOI: 10.1002/2016JF004139.

Tambroni, Nicoletta and Giovanni Seminara (2006). "Are inlets responsible for the morphological degradation of Venice Lagoon?" In: *Journal of Geophysical Research* 111, F03013. DOI: 10.1029/2005JF000334.

Temmerman, Stijn, Tjeerd J. Bouma, G. Govers, Z. B. Wang, M. B. De Vries, and P. M J Herman (2005). "Impact of vegetation on flow routing and sedimentation patterns: Three-dimensional modeling for a tidal marsh". In: *Journal of Geophysical Research: Earth Surface* 110, F04019. DOI: 10.1029/2005JF000301.

Temmerman, Stijn, Patrick Meire, Tjeerd J. Bouma, Peter M J Herman, Tom Ysebaert, and Huib J. De Vriend (2013). "Ecosystem-based coastal defence in the face of global change". In: *Nature* 504, pp. 79–83. DOI: 10.1038/nature12859.

Tommasini, Laura, Andrea D'Alpaos, Luca Carniello, Luigi D'Alpaos, and Andrea Rinaldo (2017). "Ricostruzione morfologica della Laguna di Venezia ai tempi dell'Alberti (1611)". In: *La laguna di Venezia e le nuove opere alle bocche*. Vol. III. Venice: Istituto Veneto di Scienze, Lettere e Arti, pp. 29–60.

Umgiesser, Georg, Francesca De Pascalis, Christian Ferrarin, and Carl L. Amos (2006). "A model of sand transport in Treporti channel: Northern Venice lagoon". In: *Ocean Dynamics* 56, pp. 339–351. DOI: 10.1007/s10236-006-0076-z.

Umgiesser, Georg, M. Sclavo, S. Carniel, and A. Bergamasco (2004). "Exploring the bottom stress variability in the Venice Lagoon". In: *Journal of Marine Systems* 51.1-4 SPEC. ISS. Pp. 161–178. DOI: 10.1016/j.jmarsys.2004.05.023.

Van de Koppel, Johan, D. Van der Wal, J.P. Bakker, and P.M.J. Herman (2005). "Self-Organization and Vegetation Collapse in Salt Marsh Ecosystems". In: *The American Naturalist* 165.1.

Van der Wal, Daphne, Annette Wielemaker-Van den Dool, and P. M J Herman (2008). "Spatial patterns, rates and mechanisms of saltmarsh cycles (Westerschelde, The Netherlands)". In: *Estuarine, Coastal and Shelf Science* 76, pp. 357–368. DOI: doi:10.1016/j.ecss.2007.07.017.

Van Ledden, Mathijs, Zheng Bing Wang, Han Winterwerp, and Huib De Vriend (2004). "Sand-mud morphodynamics in a short tidal basin". In: *Ocean Dynamics* 54.3-4, pp. 385–391. DOI: 10.1007/s10236-003-0050-y.

Vende, Myriam, Pascal Dumas, and Marianne Bricquir (2017). "Comptes Rendus Geoscience Wave forcing and morphological changes of New Caledonia lagoon islets : Insights on their possible relations". In: *Comptes Rendus Geoscience* 349, pp. 248–259. DOI: 10.1016/j.crte.2017.09.003.

Venier, C., A. D'Alpaos, and M. Marani (2014). "Evaluation of sediment properties using wind and turbidity observations in the shallow tidal areas of the Venice Lagoon". In: *Journal of Geophysical Research: Earth Surface* 119.7. Cited By :9, pp. 1604–1616.

Viero, Daniele Pietro and Andrea Defina (2016). "Water age, exposure time, and local flushing time in semi-enclosed, tidal basins with negligible freshwater inflow". In: *Journal of Marine Systems* 156, pp. 16–29. DOI: 10.1016/j.jmarsys.2015.11.006.

Wang, Chen and Stijn Temmerman (Mar. 2013). "Does biogeomorphic feedback lead to abrupt shifts between alternative landscape states?: An empirical study on intertidal flats and marshes". In: *Journal of Geophysical Research-Earth Surface* 118.1. WOS:000318271200017, pp. 229–240. DOI: 10.1029/2012JF002474.

Willmarth, W. W. and C.E. Wooldridge (1962). "Measurements of the correlation between the fluctuating velocities and the fluctuating wall pressure in a thick turbulent boundary layer". In: *Journal of Fluid Mechanics* 14, pp. 187–210.

Young, Ian R. and L. A. Verhagen (1996a). "The growth of fetch limited waves in water of finite depth. Part 1. Total energy and peak frequency". In: *Coastal Engineering* 29, pp. 47–78.

Young, Ian R. and L. A. Verhagen (1996b). "The growth of fetch limited waves in water of finite depth. Part 2. Spectral evolution". In: *Coastal Engineering* 29, pp. 79–99.

Zaggia, Luca, Giuliano Lorenzetti, Giorgia Manfe, Gian Marco Scarpa, Emanuela Molinaroli, Kevin Ellis Parnell, John Paul Rapaglia, Maria Gionta, and Tarmo Soomere (2017). "Fast shoreline erosion induced by ship wakes in a coastal lagoon : Field evidence and remote sensing analysis". In: *PLoS ONE* 12(10), e0187210. DOI: https://doi.org/10.1371/journal.pone.0187210Editor:.

Zarzuelo, Carmen, Manuel Diéz-Minguito, Andrea D'Alpaos, Luca Carniello, J. Rosal-Salido, and M. Ortega-Sánchez (2016). "Morphodynamic response to human activities in the bay of Cádiz (2012-2015)". In: *ICCE 2018*, pp. 1–11.

Zarzuelo, Carmen, Alejandro López-Ruiz, Andrea D'Alpaos, Luca Carniello, and Miguel Ortega-Sánchez (2018). "Assessing the morphodynamic response of human-altered tidal embayments". In: *Geomorphology*. DOI: https://doi.org/10.1016/j.geomorph.2018.08.014.

Zedler, J. and S. Kercher (2005). "Wetland resources: status, trends, ecosystem services, and restorability". In: *Annual Review of Environment and Resources* 30.39-74. DOI: https://doi.org/10.1146/annurev.energy.30.050504.144248.

Zhang, Qian, Zheng Gong, Changkuan Zhang, Zeng Zhou, and Ian Townend (2016). "Hydraulic and Sediment Dynamics at times of Very Shallow Water on Intertidal Mudflats: The Contribution of Waves". In: *Journal of Coastal Research* 75, pp. 507–511. DOI: 10.2112/SI75-102.1.

Zhao, Haihong and Qin Chen (2014). "Modeling attenuation of storm surge over deformable vegetation: parametric study". In: *Journal of Engineering Mechanics* 140.12. DOI: 10.1061/(ASCE)EM.1943-7889.0000704.

Zhou, Z., G. Coco, M. van der Wegen, Z. Gong, C. Zhang, and I. Townend (2015). "Modeling sorting dynamics of cohesive and non-cohesive sediments on intertidal flats under the effect of tides and wind waves". In: *Continental Shelf Research* 104, pp. 76–91.

Zhou, Zeng, Qinghua Ye, and Giovanni Coco (2016). "A one-dimensional biomorphodynamic model of tidal flats: Sediment sorting, marsh distribution, and carbon accumulation under sea level rise". In: *Advances in Water Resources* 93. WOS:000377934400012, pp. 288–302. DOI: 10.1016/j.advwatres.2015.10.011.

A | APPENDIX

This appendix is a manuscript in preparation for *Geophysical Research Letters*. I actively contributed to this study in the frame of fieldwork activities and computation of the volumetric erosion rate of salt marshes and mean wave power density with numerical simulations. In this work, by means of core collection in different areas of the Venice Lagoon, we aim at understanding the contribution of different soil properties in increasing or decreasing marsh lateral resistance under the effect of the impinging wind waves.

WHAT DRIVES SALT–MARSH RETREAT?

Roner, Marcella[1], Laura Tommasini[1], Massimiliano Ghinassi[1], Alvise Finotello[1], Marco Marani[2,3], Andrea D'Alpaos[1]

[1]Dept. of Geosciences, University of Padova, via G. Gradenigo 6, Padova, Italy
[2]Dept. ICEA, University of Padova, via Loredan 20, Padova, Italy
[3]Nicholas School of Environment, Duke University, Durham, NC 27708

Abstract

Most of the modern salt-marsh systems are exposed to possibly irreversible transformations due to the effect of climate changes and human pressure. Marsh extent has dramatically decreased worldwide over the last centuries but, although for decades the disappearance of marshes has been ascribed to the effect of the rising sea level and sediment starvation, more recent studies have been carried out considering the erosion triggered by wind waves as one of the primary driver for salt-marsh retreat. In this work we analyse the contribution of different soil sediment properties (e.g., water content, dry bulk density, organic matter content, inorganic grain size) and vegetation cover in increasing, or decreasing, the resistance of salt-marsh margins to erosional processes. The results suggest that the lateral erosion rate is strongly correlated with the mean power density of the waves impact-

ing marsh edges, while soil properties do not influence marsh lateral retreat.

Introduction

Salt marshes are typical morphological features of the higher portions of the intertidal zone. Covered by halophytic vegetation, they provide valuable ecosystem services offering coastal protection, erosion controls, water purification, maintenance of fisheries and serving as important carbon sequestration areas (e.g., Barbier et al., 2011; Möller et al., 2014). Marshes can both accrete vertically and laterally, but while they appear to be resilient in the vertical direction, they seem to be weak in the horizontal one (e.g., Fagherazzi et al., 2013). Much attention has been paid to salt-marsh capability in terms of facing sea level rise through vertical accumulation of organic and inorganic sediments (Marani et al., 2007; Kirwan & Megonigal, 2013; Kirwan et al., 2016). Relatively less research has been focused on the temporal shift of marsh margins even though these processes, possibly driven by both extrinsic (wind exposure and foreshore morphology) and intrinsic (soil and vegetation properties) factors (Wang et al., 2017), are key factors determining the survival or disappearance of salt marshes.

Wind exposure affects marsh erosion rate at large, intermediate and local scales (Wang et al., 2017) through the development of wind waves which, impinging marsh edges, promote their lateral retreat (Schwimmer, 2001; van der Wal & Pye, 2004; Marani et al., 2011; Francalanci et al., 2013; McLoughlin et al., 2015; Bendoni et al., 2016; Leonardi et al., 2016a). Wind-wave propagation strongly depends on water depth and extent of tidal flats facing marsh boundaries (Mariotti & Fagherazzi, 2013; Wang et al., 2017) although the incoming waves on the marsh scarp are also controlled by tidal level and marsh edge geometry (Tonelli et al., 2010). Marsh bank retreat involves a variety of processes including particle erosion, cantilever and slide failures. Mass failures, which are not necessarily correlated to the instantaneous wave forcing (Bendoni et al., 2014), are triggered by the presence of tension cracks at the bank top (Francalanci et al., 2013). A positive strong relationship between erosion rates of marsh edges and wave power density has been recognized (Schwimmer, 2001; Marani et al., 2011; ; McLoughlin et al., 2015; Bendoni et al., 2016) and it has been demonstrated that the long-term marsh deterioration is dictated by average wave conditions, because salt marshes are more susceptible to variations in mean wave energy rather than changes in the extremes (Leonardi et al., 2016b; see also Leonardi et al., 2018).

Beyond the role of wind waves, different vegetation cover and soil properties control the rate of marsh retreat (e.g., Ford et al., 2016; Lo

et al., 2017; Wang et al., 2017). Vegetated salt marshes are more resistant to lateral erosion compared to bare marshes, especially in sandy soils (Lo et al., 2017) and in presence of pioneer vegetation in front of the marsh edge (Wang et al., 2017). Also, increasing plant biodiversity reduces soil erosion rates, and this buffering effect is more important in erosion-prone sandy, rather than in erosion-resistant clay soils (Ford et al., 2016). Moreover, halophytic plants populating the marsh delay mass failure, since rooting provides an overall stabilizing effect (Francalanci et al., 2013). Feagin et al. (2009) suggested that soil type is the most important variable influencing the marsh retreat, and that vegetation may only indirectly reduce erosion via modification of soil properties. Wang et al. (2017) found that sediment erodibility is determined by soil properties and belowground biomass.

The issue concerning marshland disappearance has been globally recognized for decades (e.g., Day et al., 2000, 2009; Davidson, 2014; Jankowski et al., 2017). In the Venice Lagoon (Italy), the most severe and rapid decline in salt-marsh area has occurred over the past century, with a decrease of about 70% (Carniello et al., 2009), mainly because of the interplay between anthropic interventions and natural changes (e.g., Silvestri et al., 2018). In this work we analyse the retreat of salt marshes around the Venice Lagoon. We interpret a large set of observations of marsh retreat rates unravelling the contribution of different sediment types, through a comparison between solid properties and vegetation cover and marsh resistance to waves.

The Venice Lagoon

The Venice Lagoon, our study case, located in the NE sector of Italy (Fig. A.1), is situated in the Venetian foreland basin, which developed between the South-Alpine and the Apennine chains since the Late Oligocene (Massari et al., 2009; Zecchin et al., 2017). The modern Venice Lagoon (Fig. A.1) forms an elongated, NE-SW oriented basin, which represents the largest Mediterranean brackish water body (roughly 550 km^2). The lagoon, with an average depth of about 1.5 m, is subjected to a semidiurnal tidal regime, with astronomical tidal peak oscillations of about 0.75 m (D'Alpaos et al., 2013) around Mean Sea Level (MSL). In winter, the Lagoon is intensely winnowed by wind waves generated by intense storm events, among which the most intense and morphologically significant ones are those triggered by Bora wind blowing up to 20 m/s from NE (Carniello et al., 2011; Marani et al., 2011). During these storms, waves are characterized by a height and wave length of ca. 1 and 8 m, respectively (Carniello et al., 2011).

Materials and Methods

Core collection and lab analyses

We collected 20 undisturbed sediment cores along marsh boundaries at different sites in the Venice Lagoon (Fig. A.1) in the summer 2015 and 2016. Study sites face shallow tidal flats and are away from navigation areas, in order to exclude the contribute of vessel-generated waves to marsh erosion (e.g., Houser, 2010; Silinski et al., 2015; Zaggia et al., 2017).

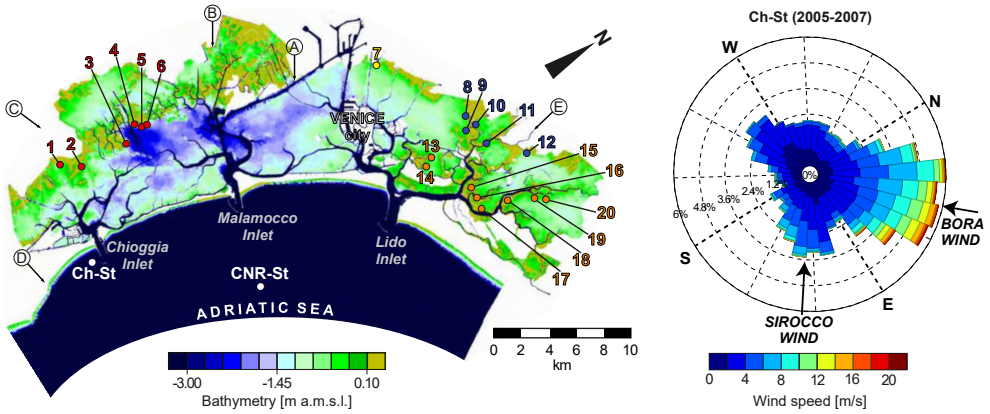

Figure A.1: On the right, color-coded bathymetric map of the Venice Lagoon (Italy) built up on the basis of the most recent (2003) and accurate bathymetric data. The locations of Chioggia anemometric station (Ch-St) and of mareographic CNR Oceanographic Platform station (CNR-St) are shown. The colored dots indicate the core sites and the origin of the salt marsh: red indicates salt marshes originated from the alternation of fresh water inputs and sea water; yellow is for salt marshes originated on continental ground; blue indicates salt marshes at the borders of fluvial water still entering the Lagoon; orange is for "lagoon canal" salt marshes (Bonometto, 2005). Circled letters from (A) to (D) indicate the position of the Brenta River mouth in the last millennium: (A) up to 1457; (B) from 1457 to 1507; (C) from 1507 to 1540 and from 1840 to 1896; (D) from 1540 to 1840 and from 1896 to nowadays, flowing the River directly into the Adriatic Sea. Circled letter (E) indicates the mouth of a branch of the Sile River still entering the Venice Lagoon. On the left, wind rose built up from the Chioggia anemometric station data collected from 2005 to 2007. Blowing from NE, Bora is the predominant wind in the area, followed by Sirocco wind, from SE.

Cores have been gathered on different marshes (Bonometto, 2005): i) salt marshes derived from salinized wetlands, located in the southern part of the Venice Lagoon and dominated at different times by fresh water inputs (cores in red in Fig. A.1) 1); ii) salt marshes originated on continental ground (core in yellow in Fig. A.1); iii) salt marshes in the NW sector of the Lagoon, located at the borders of fluvial waters, as the Sile River branch (cores in blue in Fig. A.1; iv) salt marshes, developed on areas with no freshwater input and flanking the main

tidal channels located in the NE sector close to the Lido Inlet (cores in orange in Fig. A.1). Sediment cores have been recovered through a steel frame 50x10x10 cm horizontally pushed into the vertical marsh edge cliff to avoid sediment compaction. At each sampling site we also took a 14 MP resolution picture, covering an area of 80x80 cm^2. The vegetation density in each photo, a proxy for the above-ground biomass, was evaluated through the superimposition of a regularly spaced grid. For each grid node (225 total nodes) the occurrence of plants or soil was evaluated, providing a percentage of vegetation cover for each sampling site. Because of the decadal time span we considered with the aerial photographs (1978-2010) for determining marsh lateral erosion rate (see Subsection *Aerial photography*), we decided to analyse soil properties along different soil depths for each core in order to consider the most realistic marsh soil thickness deposited between 1978 and 2015 or 2016 (37 or 38 years, respectively). These depth intervals were calculated on the basis of marsh accretion rates documented in different areas of the Venice Lagoon (Day et al., 1998; Bellucci et al., 2007; Roner et al., 2017). We sampled the cores every 5 cm from the top recovering 1 cm thick slices (i.e. 1X10X10 cm). For each slice, 3 samples of about 4 cm^3 were analysed to estimate: i) the percentage of water (WP) [(1 - dry weight/wet weight) x 100]; ii) the dry bulk density (DBD), calculated from the water and mineral contents as used in Kolker et al. (2009) because of the uncertainty on the final volume of each sediment sample; iii) the organic matter content (OM) through a Loss On Ignition (LOI) technique following the method described in Roner et al. (2016). A fourth sample from each slice was analysed in order to estimate the grain size (GS) of the inorganic fraction through laser diffraction technique (Mastersizer 2000, Malvern Instruments) after removal of the organic component with hydrogen peroxide (H_2O_2). For every slice, we calculated representative values of percentage of water, dry bulk density and organic matter content averaging the results obtained from the 3 samples. Finally, we calculated an average value for each core on the basis of the considered marsh thickness.

Aerial photography

To determine the marsh lateral retreat, we used two sets of aerial photographs acquired in 1978 (flight "Reven", black and white images) and in 2010 (flight "Reven area Venezia volo alto", coloured images) available and downloaded from the Geoportale of the Veneto Region. The aerial photographs which cover a circular area of ca. 100 m around each study site, were georectified using the ArcGIS software by considering ground control points on the most recent (2005) cartographic survey of the Venice Lagoon.

For each site, we digitized approximately 200 m of the marsh edge centred on the marsh retrieval point in the 2010 image. We subdivided the 2010 digitalized boundary in 20 m long segments measured considering the along edge coordinates. For each segment terminations, we identified the corresponding point in the 1978 digitalized boundary by the minimum distance criterion. Then, we computed the linear retreat (m) as the ratio between the eroded sub-area and the segment length in 2010, while the linear retreat rate (m/yr) was determined as the ratio between the linear retreat and the corresponding time interval (i.e., 32 years). The height (m) of the marsh scarp in front of each segment was calculated by means of the most recent 2003 bathymetry, and this procedure assumes that scarp height and morphology for each study area have been roughly constant during the considered period (1978 – 2010). For each sub-area, the volumetric erosion rate (m^2/yr) is the result of the lateral erosion rate times the corresponding scarp height. Finally, the retreat rate for each study site has been obtained by averaging the volumetric erosion rate values measured.

Numerical Model

In this study we used the two-dimensional fully coupled Wind-Wave Tidal Model (WWTM) (Carniello et al., 2005, 2011) on two different configurations of the Venice Lagoon (1970 and 2012). This model, largely tested in the Venice Lagoon (Carniello et al., 2005, 2011; D'Alpaos & Defina, 2007) and in other lagoons worldwide (e.g., Mariotti et al., 2010; Zarzuelo et al., 2016) comparing model results with hydrodynamic and wind-wave data, was applied to perform a one-year-long simulation within the two computational grids that reproduce the configurations of the Venice Lagoon. The same boundary conditions and forcing terms were used in the two different configurations to consider the influence of bathymetry and morphology. The model was forced with tidal levels and wind velocities and directions recorded in CNR and Chioggia Stations, respectively (Fig. A.1) for the whole 2005, which is a representative year in terms of wind forcings (D'Alpaos et al., 2013; Carniello et al., 2016). The WWTM provides, at each location within the Venice Lagoon, the temporal evolution of the wave height (H) and wave group celerity (c_g). The wave power density (P_w) associated with the wave front (Mariotti et al., 2010; Marani et al., 2011) reads:

$$P_w = \frac{H^2 \rho g c_g}{8} \tag{A.1}$$

where ρ is water density and g is gravitational acceleration. In each element of the two numerical grids, the mean wave power density (MWPD) has been computed averaging P_w over the one-year long simulations. Finally, we estimate the 1994 MWPD impacting each site

by: i) evaluation of the MWPD for the two configurations dated 1970 and 2012 by averaging the MWPD data over the tidal flat in front of each core within a radius of 200 m; ii) computation of the 1994 MWPD by linear interpolation of the data obtained for the 1970 and 2012 configurations.

Results

Sediment properties in the 20 study cores show both inter- and intra-group variability. Cores from marshes dominated at different times by fresh water inputs (cores 1 – 6, Figs. A.2 and A.3) shows the most intra-group variable distribution within each analysed soil property. On average, in this marsh group WP is 53%, DBD is 0.69 gcm^{-3}, OM is 10.7% and the median GS is 36 μm. Cores from marshes affected by freshwater inputs (cores 8 – 12, Figs. A.2 and A.3) show more homogeneous soil properties, although core 12 appear to be an exception (highest WP and OM; lowest DBD) probably due to its closeness to the mouth of a branch of the Sile River. This marsh group exhibits soil property values similar to the cores of the southern Lagoon (i.e., salt marshes with fresh water inputs), being WP of 67%, DBD of 0.41 gcm^3, OM of 8.4% and median GS of 30 μm. Core 7, located on a marsh originated on continental ground, shows soil characteristics similar both to those from marshes which were affected by freshwater inputs. Differently, cores from salt marshes flanking the main tidal channel (cores 13 – 20 in the northern part of the Lagoon, Figs. A.2 and A.3) show WP lower than the other groups (average of 38.5%), display the highest DBD values (average of 1 gcm^3) and show the lowest organic content (average OM less than 5%). Only the average median GS is comparable with the values of the other groups (27 μm). The halophytic vegetation cover (Fig. A.3e), shows overall values ranging from 37.3% to 100%, but no specific distribution can be recognized. In terms of retreat rate (Fig. A.3f), the marshes in the southern lagoon are the most variables. The volumetric retreat rate ranges between 0.44 up to 4.38 m^2yr^{-1} and the highest values occur in marshes located in front of a tidal-flat area of about 3 m deep (cores 3 – 6, Fig. A.1). Marshes located in the central-north part of the Venice lagoon (cores 7 – 20, Fig. A.3f) exhibit more uniform volumetric erosion rates ranging between 0.01 up to 0.55 m^2yr^{-1}. The WWTM outcomes (Fig. A.3g) indicate that the highest mean wave power density impacting the marshes occurs in the southern portion of the Venice Lagoon. Specifically, the maximum values are registered for cores 3 – 6 with values ranging from 16.12 to 65.96 Wm^{-1}. Moving toward the central-northern part of the lagoon, the mean wave power densities are much lower and comparable to the values obtained in the southernmost lagoon (cores 1 and 2, Fig. A.3g).

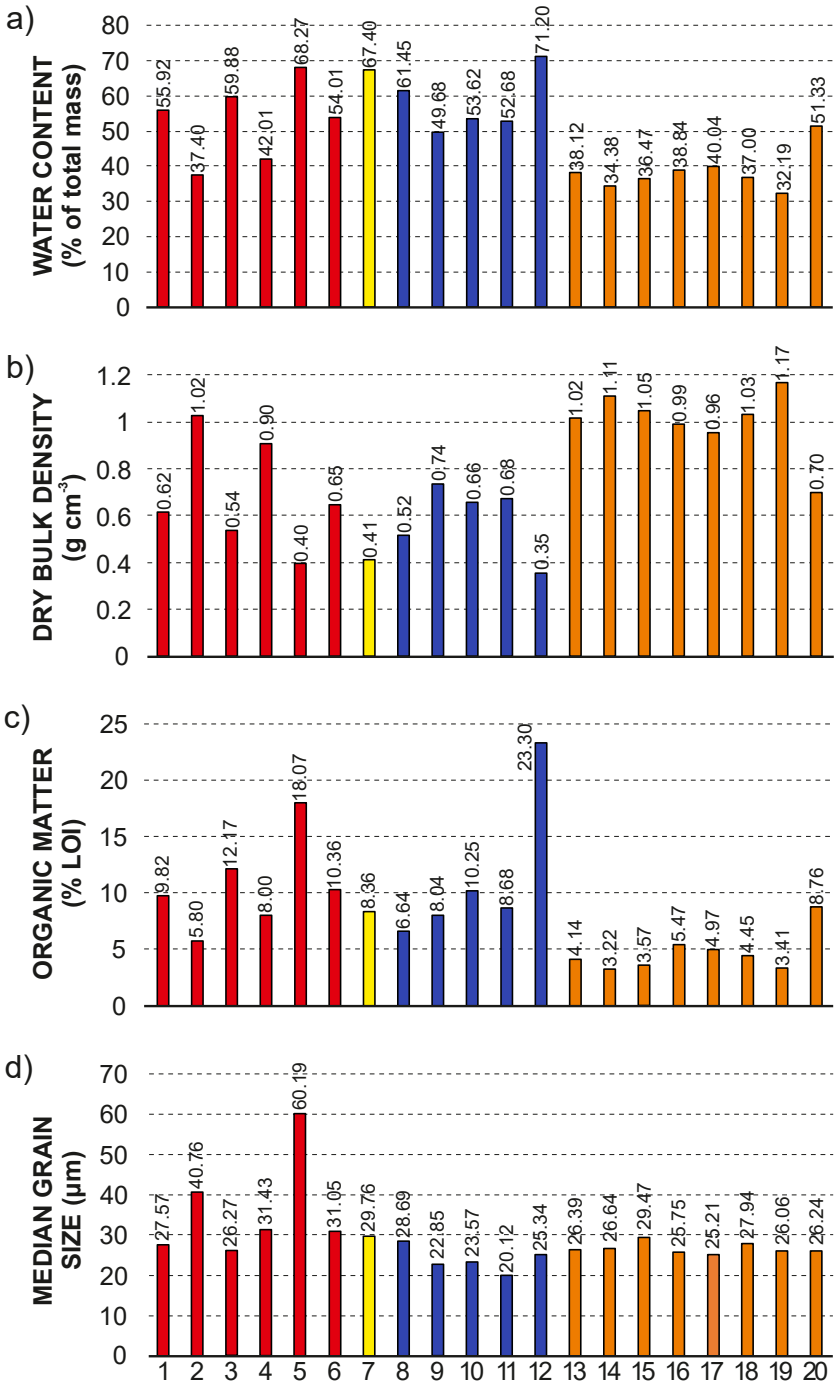

Figure A.2: Distribution of Properties in the 20 cores. a) Water content; b) Dry bulk density; c) Organic matter content; d) D50 grain size. Colors indicate the origin of the salt marsh: red indicates salt marshes originated from the alternation of fresh water inputs and sea water; yellow is for salt marshes originated on continental ground; blue indicates salt marshes at the borders of fluvial water still entering the Lagoon; orange is for "lagoon canal" salt marshes (Bonometto, 2005).

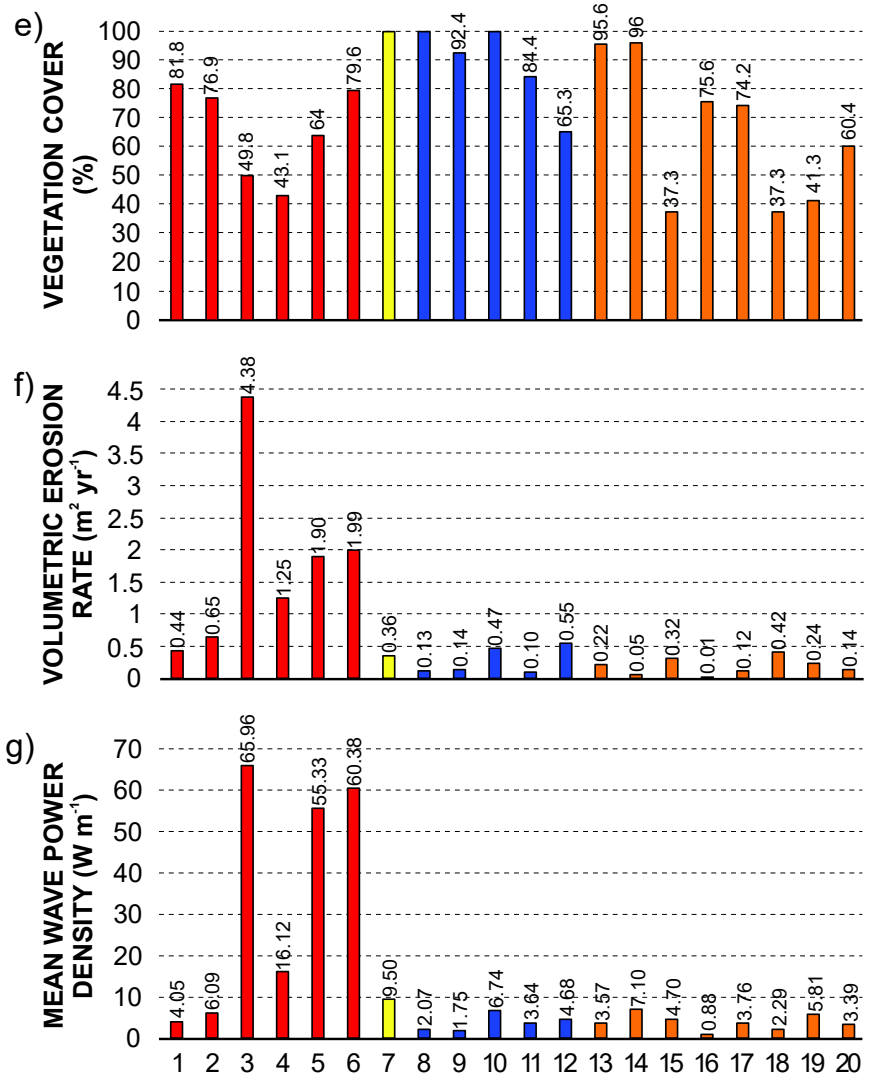

Figure A.3: Properties distribution in the 20 cores. e) Percentage of vegetation cover; f) Volumetric erosion rate; g) Mean wave power density.The colors indicate the origin of the salt marsh: red indicates salt marshes originated from the alternation of fresh water inputs and sea water; yellow is for salt marshes originated on continental ground; blue indicates salt marshes at the borders of fluvial water still entering the Lagoon; orange is for "lagoon canal" salt marshes (Bonometto, 2005).

Discussions

Although salt marshes considered in this study are characterized by different origins, our results firstly suggest that soil properties cannot be used as proxies to discriminate the survey area, except for the "lagoon canal salt marshes", where WP, OM and DBD are significantly different in respect to the other groups. This result is not unexpected since no significant anthropic pressure was exerted on these marshes

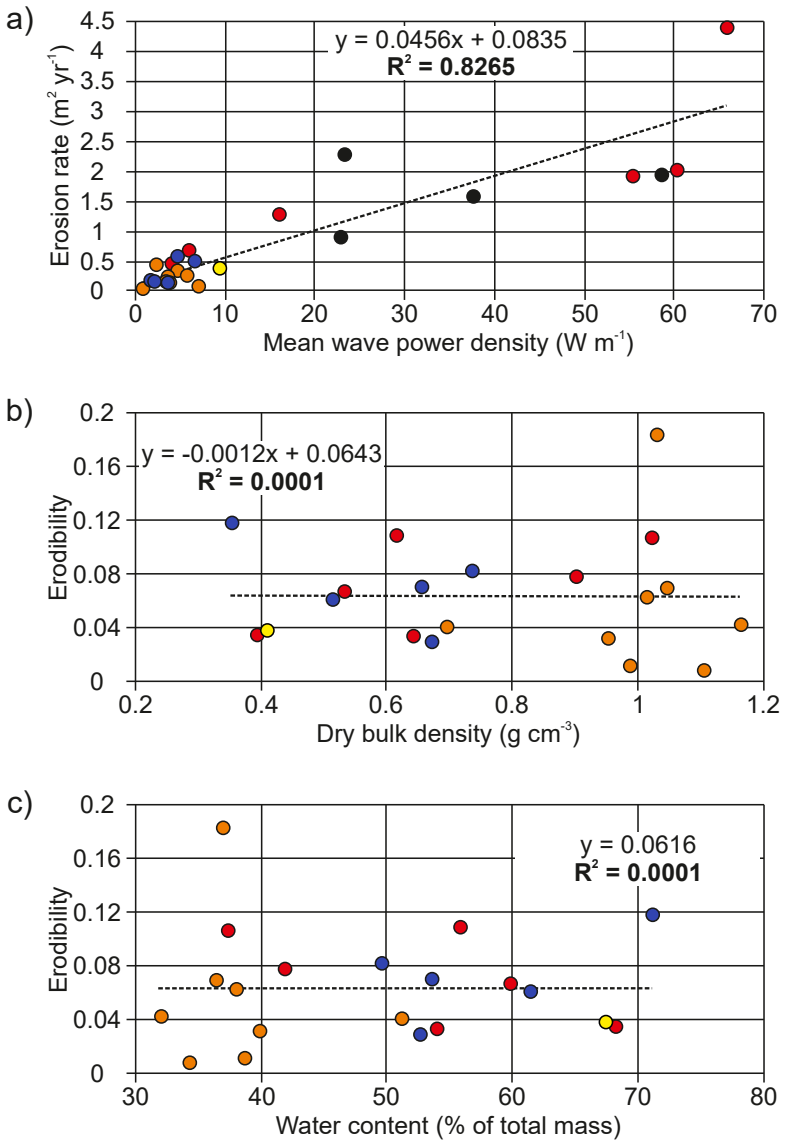

Figure A.4: a) The strong linear correlation between volumetric erosion rate and mean wave power density supports the idea that one of the main mechanisms responsible for the reduction of salt-marsh areas is the attack by wind waves which, impinging the marsh edges, promote their lateral retreat. b) the correlations between the erodibility (i.e., the ratio between the volumetric erosion rate and mean wave power density) and the dry bulk density. c) Correlation between erodibility and the water content. The colors indicate the origin of the salt marsh: red indicates salt marshes originated from the alternation of fresh water inputs and sea water; yellow is for salt marshes originated on continental ground; blue indicates salt marshes at the borders of fluvial water still entering the Lagoon; orange is for "lagoon canal" salt marshes (Bonometto, 2005).

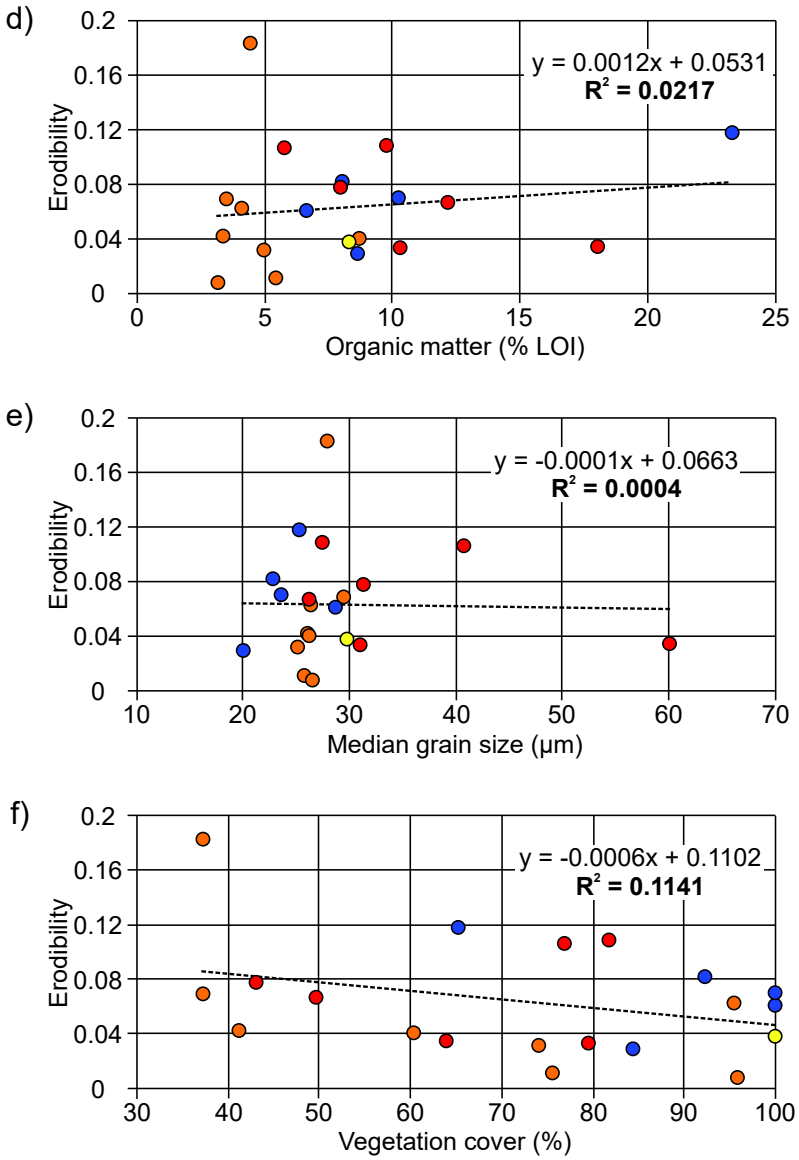

Figure A.5: d) Correlation between erodibility and the organic matter. e) Correlation between erodibility and the median grain size. f) Correlation between erodibility and vegetation cover. The colors indicate the origin of the salt marsh: red indicates salt marshes originated from the alternation of fresh water inputs and sea water; yellow is for salt marshes originated on continental ground; blue indicates salt marshes at the borders of fluvial water still entering the Lagoon; orange is for "lagoon canal" salt marshes (Bonometto, 2005).

over the past decades. In these areas, the role of tidal channels in supplying a remarkable amount of inorganic sediment to the marshes clearly emergse. These marshes managed to face the sea level rise with a minimum accumulation of organic deposits. Inorganic sediment supply from the channels is evident along the marsh margins, where OM is never higher than 8.76 %. The limited presence of OM

leads to a lower retain of water, and consequently the DBD of the soil increases.

The possible dependence of salt-marsh lateral erosion rates on soil properties is shown by plots linking erodibility and (i.e., the volumetric erosion rate per unit of wave power) WP, DBD, OM and GS. Results clearly show that there is no correlation between the erodibility and the considered soil properties (Figs. A.4b, A.4c, A.5d and A.5e). In our study, the marsh erodibility is completely independent from DBD (R^2 = 0.0001, P = 0.9758), WP (R^2 = 0.0001, P = 0.9660), OM (R^2 = 0.0217, P = 0.5351), and median GS of the inorganic fraction (R^2 = 0.0004, P = 0.9323). Our results do not support the outcomes obtained by Feagin et al. (2009), and they cannot help to explain the equation proposed by Marani et al., (2011), in which the specific value of the proportionality constant linking power density and retreat is suggested to be site-dependent and function of sediment properties, at least for the four properties we observed. Also the relationship between the erodibility and the vegetation cover (Fig. A.5f) results very weak (R^2 = 0.1141, P = 0.145). We therefore cannot neither confirm nor discredit the vegetation ability to contrast the marsh lateral erosion.

Our results confirm a strong linear positive correlation between the retreat rate and the mean power density of the waves impacting marsh edges (Fig. A.4a), as initially proposed by Marani et al. (2011) and later considered in a number of studies (McLoughlin et al., 2015; Bendoni et al., 2016; Leonardi et al., 2016a, 2016b). Our results clearly suggest that as the mean wave power increases, the associated erosion rate increases as well (R^2 = 0.827, P < 0.001). Accordingly, the maximum marsh retreat rates are measured where marshes face a widespread, 1.5 - 2 m deep tidal flat (see cores 2, 5, 6 in Fig. A.3g), where the Bora wind (i.e., the geomorphologically dominant wind, see Fig. A.1) is free to generate fetch unlimited wave conditions, with fetches reaching lengths of 12-14 km.

Because of the missing information in the window from 20 to 60 Wm^{-1} from our experimental data, we added 4 data (black dots in Fig. A.4a) to verify if the proportionality relationship still works. This 4 data, which have not been analysed in terms of soil properties because of the complex recovery of cores in that specific sites, fits well with the other 20 data (erosion rate = 0.0423 MWPD + 0.1299; R_2 = 0.775; P < 0.001; results not showed). Moreover, the calculation of a volumetric erosion rate, which accounts also of the depth of the tidal flat in front of the marsh, instead of a linear erosion rate (e.g., Schwimmer, 2001), allows one to obtain a more precise estimate of the volume of marsh eroded over a short-term (decadal) time scale. We find that the slope of the regression line is 0.046, in agreement with the value obtained by Marani et al. (2011), who found a linear regression between the same two variables with a slope of 0.0364.

Conclusions

We conducted a combined study integrating sedimentological and numerical analyses on salt marshes to test the contribution of different soil sediment properties and vegetation cover in increasing, or decreasing, the resistance of salt-marsh margins to erosional processes. Our results suggest that the main forcing affecting marsh horizontal retreat is the mean power density of the waves impacting marsh edges: longer fetches and deeper tidal flats in front of marshes lead to stronger wind waves which, in turn, lead to higher lateral erosion rates. Although several studies demonstrated the marsh horizontal erosion to be correlated with sediment properties, our findings cannot provide insights into the interactive effect of soil characteristics on the ability of salt marshes to resist to lateral erosion. Water content, dry bulk density, organic matter content and grain size of the inorganic fraction, together with percentage of vegetation cover, do not appear to be correlated with the behaviour of salt marshes in the horizontal plane.

References for Appendix A

Barbier, E.B., Hacker, S.D., Kennedy, C., Koch, E.W., Stier, A.C., & Silliman, B.R. (2011). The value of estuarine and coastal ecosystem services. Ecological Monographs, 81(2), 169–193. doi:10.1890/10-1510.1.

Bellucci, L.G., Frignani, M., Cochran, J. K., Albertazzi, S., Zaggia, L., Cecconi, G., & Hopkins, H. (2007). 210Pb and 137Cs as chronometers for salt marsh accretion in the Venice Lagoon – links to flooding frequency and climate change. Journal of Environmental Radioactivity, 97, 85–102. doi:10.1016/j.jenvrad.2007.03.005.

Bendoni, M., Francalanci, S., Cappietti, L., & Solari, L. (2014). On salt marsh retreat: Experiments and modeling toppling failures induced by wind waves. Journal of Geophysical Research: Earth Surface, 119, 603–620. doi:10.1002/2013JF002967.

Bendoni, M., Mel., R., Solari, L., Lanzoni, S., Francalanci, S., & Oumeraci, H. (2016). Insights into lateral marsh retreat mechanism through localized field measurements. Water Resources Research, 52, 1446–1464. doi:10.1002/2015WR017966.

Bonometto, L. (2005). Functional characteristics of salt marshes in the Venice lagoon and environmental restoration scenarios. In Fletcher, C.A., Spencer, T. (Eds.), Flooding and environmental challenges for Venice and its Lagoon, Cambridge University Press, 473–486.

Carbognin, L., Teatini, P., Tomasin, A., & Tosi, L. (2010). Global change and relative sea level rise at Venice: what impact in term of flooding. Climate Dynamics, 35, 1039–1047. doi:10.1007/s00382-009-0617-5.

Carniello, L., & Defina, A. (2005). A combined wind-wave tidal model for the Venice lagoon, Italy. Journal of Geophysical Research, 110, F04007. doi:10.1029/2004JF000232.

Carniello, L., Defina, A., & D'Alpaos, L. (2009). Morphological evolution of the Venice lagoon: Evidence from the past and trend for the future. Journal of Geophysical Research,

114, F04002. doi:10.1029/2008JF001157.

Carniello, L., D'Alpaos, A., & Defina, A. (2011). Modeling wind waves and tidal flows in shallow micro-tidal basins. Estuarine, Coastal and Shelf Science, 92, 263–276.

Carniello, L., D'Alpaos, A., Botter, G., & Rinaldo, A. (2016). Statistical characterization of spatiotemporal sediment dynamics in the Venice lagoon. Journal of Geophysical Research: Earth Surface, 121, 1049–1064. doi:10.1002/2015JF003793.

D'Alpaos, L., & Defina, A. (2007) Mathematical modeling of tidal hydrodynamics in shallow lagoons: A review of open issues and applications to the Venice lagoon. Computers & Geosciences, 33, 476-496. doi:10.1016/j.cageo.2006.07.009.

D'Alpaos, A., Carniello, L., & Rinaldo, A. (2013). Statistical mechanics of wind wave-induced erosion in shallow tidal basins: Inferences from the Venice Lagoon. Geophysical Research Letters, 40, 3402–3407. doi:10.1002/grl.50666.

Davidson, N.C. (2014). How much wetland has the world lost? Long-term and recent trends in global wetland area. Marine and Freshwater Research, 65, 934-941. doi:10.1071/MF14173.

Day, J.W.Jr., Rismondo, A., Scarton, F., Are, D., & Cecconi, G. (1998). Relative sea level rise and Venice lagoon wetlands. Journal of Coastal Conservation, 4, 27–34.

Day, J.W.Jr., Shaffer, G.P., Britsch, L.D., Reed, D.J., Hawes, S.R., & Cahoon, D. (2000). Pattern and process of land loss in the Mississippi Delta: A spatial and temporal analysis of wetland habitat change. Estuaries, 23(4), 425–438.

Fagherazzi, S., Mariotti, G., Wiberg, P.L., & McGlathery, K.J., (2013). Marsh collapse does not require sea level rise. Oceanography, 26(3), 70–77. doi:10.5670/oceanog.2013.47.

Feagin, R.A., Lozada-Bernard, S.M., Ravens, T.M., Möller, I., Yeager, K.M., & Baird, A.H. (2009). Does vegetation prevent wave erosion of salt marsh edges? Proceedings of the National Academy of Sciences of the United States of America, 106, 10109–10113.

Francalanci, S., Bendoni, M., Rinaldi, M., & Solari, L. (2013). Ecomorphodynamic evolution of salt marshes: Experimental observations of bank retreat processes. Geomorphology, 195, 53–65. doi:10.1016/j.geomorph.2013.04.026.

Ford, H., Garbutt, A., Ladd, C., Malarkey, J., & Skow, M.W. (2016). Soil stabilization linked to plant biodiversity and environmental context in coastal wetlands. Journal of Vegetation Science, 27, 259–268. doi:10.1111/jvs.12367.

Houser, C. (2010). Relative importance of vessel-generated and wind waves to salt marsh erosion in a restricted fetch environment. Journal of Coastal Research, 26(2), 230–240. doi: 10.2112/08-1084.1.

Jankowski, K.L., Törnqvist, T.E., & Fernandes, A.M. (2017). Vulnerability of Louisiana's coastal wetlands to present-day rates of relative sea-level rise. Nature Communications, 8, 14792. doi:10.1038/ncomms14792.

Kirwan, M.L., & Megonigal, J. P., (2013). Tidal wetland stability in the face of human impacts and sea-level rise.: Nature, 504, 53–60, doi: 10.1038/nature12856.

Kirwan, M.L., Temmerman, S., Skeehan, E.E., Guntenspergen, G.R., and Fagherazzi, S., (2016). Overestimation of marsh vulnerability to sea level rise: Nature Climate Change, 6, 253–260, doi: 10.1038/nclimate2909.

Kolker, A.S., Goodbred, S.L.Jr., Hameed, S., & Cochran, J.K. (2009). High-resolution records of the response of coastal wetlands systems to long-term and short-term sea-level variability. Estuarine, Coastal and Shelf Science, 84, 493–508. doi:10.1016/j.ecss.2009.06.030.

Leonardi, N., Defne, Z., Ganju, N.K., & Fagherazzi, S. (2016a). Salt marsh erosion rate and boundary features in a shallow Bay. Journal of Geophysical Research: Earth Surface, 121, 1861–1875. doi:10.1002/2016JF003975.

Leonardi, N., Ganju, N.K., & Fagherazzi, S. (2016b). A linear relationship between wave power and erosion determines salt-marsh resilience to violent storms and hurricanes. Proceedings of the National Academy of Sciences of the United States of America, 113(1), 64–68. doi:10.1073/pnas.1510095112.

Leonardi, N., Carnacina, I., Donatelli, C., Ganju, N.K., Plater, A.J., Schuerch, M., & Temmerman, S. (2018). Dynamic interactions between coastal storms and salt marshes: A review. Geomorphology, 301, 92–107. doi:10.1016/j.geomorph.2017.11.001.

Lo, V.B., Bouma, T.J., van Belzen, J., Van Colen, C., & Airoldi, L. (2017). Interactive effects of vegetation and sediment properties on erosion of salt marshes in the Northern Adriatic Sea. Marine Environmental Research, 131, 32–42. doi:10.1016/j.marenvres.2017.09.006

Marani, M., D'Alpaos, A., Lanzoni, S., Carniello, L., and Rinaldo, A. (2007). Biologically-controlled multiple equilibria of tidal landforms and the fate of the Venice lagoon: Geophysical Research Letters, 34, L11402, doi: 10.1029/2007GL030178.

Marani, M., D'Alpaos, A., Lanzoni, S., & Santalucia, M. (2011). Understanding and predicting wave erosion of marsh edges. Geophysical Research Letters, 38, L21401. doi:10.1029/2011GL048995.

Mariotti, G. & Fagherazzi, S. (2013). Critical width of tidal flats triggers marsh collapse in the absence of sea-level rise. Proceedings of the National Academy of Sciences of the United States of America, 110(14), 5353–5356. doi:10.1073/pnas.1219600110.

Mariotti, G., Fagherazzi, S., Wiberg, P.L., McGlathery, K.J., Carniello, L., & Defina, A. (2010). Influence of storm surges and sea level on shallow tidal basin erosive processes. Journal of Geophysical Research, 115, C11012. doi:10.1029/2009JC005892.

Massari, F., Rio, D., Serandrei Barbero, R., Asioli, A., Capraro, L., Fornaciari, E., and Vergerio, P.P., (2004). The environment of Venice area in the past two million years: Palaeogeography, Palaeoclimatology, Palaeoecology, v. 202, p. 273–308, doi: 10.1016/S0031-0182(03)00640-0.

McLoughlin, S., Wiberg, P., Safak, I., & McGlathery, K. (2015). Rates and forcing of marsh edge erosion in a shallow coastal bay. Estuaries and Coasts, 38(2), 620–638. doi:10.1007/s12237-014-9841-2.

Möller, I., Kudella, M., Rupprecht, F., Spencer, T., Paul, M., van Wesenbeeck, B.K., et al. (2014). Wave attenuation over coastal salt marshes under storm surge conditions. Nature Geoscience., 7, 727–731. doi:10.1038/NGEO2251.

Roner, M., D'Alpaos, A., Ghinassi, M., Marani, M., Silvestri, S., Franceschinis, E., & Realdon, N. (2016). Spatial variation of salt-marsh organic and inorganic deposition and organic carbon accumulation: inferences from the Venice Lagoon, Italy. Advances in Water Resources, 93, 276–287. doi:10.1016/j.advwatres.2015.11.011.

Roner, M., Ghinassi, M., Fedi, M., Liccioli, L., Bellucci, L.G., Brivio, L., & D'Alpaos, A. (2017). Latest Holocene depositional history of the southern Venice Lagoon, Italy. The

Holocene, 27(11), 1731–1744. doi:10.1177/0959683617708450.

Schwimmer, R.A. (2001). Rates and processes of marsh shoreline erosion in Rehoboth Bay, Delaware, U.S.A. Journal of Coastal Research, 17(3), 672–683. doi:10.2307/4300218.

Silinski, A., Heuner, M., Schoelynck, J., Puijalon, S., Schröder, U., Fuchs, E., et al. (2015). Effects of wind waves versus ship waves on tidal marsh plants: A flume study on different life stages of Scirpus maritimus. PLoS ONE, 10(3), e0118687. doi:10.1371/journal.pone.0118687.

Silvestri, S., D'Alpaos, A., Nordio, G., & Carniello, L. (2018). Anthropogenic modifications can significantly influence the local mean sea level and affect the survival of salt marshes in shallow tidal systems. Journal of Geophysical Research: Earth Surface, 123. doi:10.1029/2017JF004503.

Tonelli, M., Fagherazzi, S., & Petti, M. (2010). Modeling wave impact on salt marsh boundaries. Journal of Geophysical Research, 115, C09028. doi:10.1029/2009JC006026.

van der Wal, D., & Pye, K. (2004). Patterns, rates and possible causes of saltmarsh erosion in the Greater Thames area (UK). Geomorphology, 61, 373–391.

Wang, H., van der Wal, D., Li, X., van Belzen, J., Herman, P.M.J., Hu, Z., et al. (2017). Zooming in and out: Scale dependence of extrinsic and intrinsic factors affecting salt marsh erosion. Journal of Geophysical Research: Earth Surface, 122, 1455–1470.

Zaggia, L., Lorenzetti, G., Manfè, G., Scarpa, G.M., Molinaroli, E., Parnell, K.E., et al. (2017). Fast shoreline erosion induced by ship wakes in a coastal lagoon: Field evidence and remote sensing analysis. PLoS ONE, 12(10), e0187210. doi:10.1371/journal.pone.0187210.

Zarzuelo, C., Diéz-Minguito, M., D'Alpaos A., Carniello, L., Rosal-Salido J., Ortega-Sánchez, M. (2016). Morphodynamic response to human activities in the bay of Cádiz (2012-2015). Coastal Engineering Proceedings, ICCE 2018, 1–11. doi:10.9753/icce.v35.sediment.16.

Zecchin, M., Donda, F., and Forlin, E., (2017). Genesis of the Northern Adriatic Sea (Northern Italy) since early Pliocene: Marine and Petroleum Geology, 79, 108–130, doi: 10.1016/j.marpetgeo.2016.11.009.